ҚАЗАҚСТАН РЕСПУБЛИКАСЫ
ҒЫЛЫМ ЖӘНЕ ЖОҒАРЫ БІЛІМ МИНИСТРЛІГІ

SATBAYEV UNIVERSITY
МЕТАЛЛУРГИЯ ЖӘНЕ КЕН БАЙЫТУ ИНСТИТУТЫ

ISSN 2616-6445 (Online)
ISSN 2224-5243 (Print)
DOI 10.31643/2018/166445

Минералдық шикізаттарды кешенді пайдалану

1(332)

Комплексное Использование Минерального Сырья

Complex Use of Mineral Resources

ҚАҢТАР-НАУРЫЗ 2025
JANUARY – MARCH 2025
ЯНВАРЬ-МАРТ 2025

ЖЫЛЫНА 4 РЕТ ШЫҒАДЫ
QUARTERLY JOURNAL
ВЫХОДИТ 4 РАЗА В ГОД

ЖУРНАЛ 1978 ЖЫЛДАН БАСТАП ШЫҒАДЫ
JOURNAL HAS BEEN PUBLISHING SINCE 1978
ЖУРНАЛ ИЗДАЕТСЯ С 1978 ГОДА

АЛМАТЫ - 2025

Редакция мекен жайы:
Металлургия және кен байыту институты
050010, Қазақстан Республикасы, Алматы қ., Шевченко к-сі, Уәлиханов к-нің қиылысы, 29/133,
Fax. +7 (727) 298-45-03, Tel. +7-(727) 298-45-02, +7 (727) 298-45-19
E mail: journal@kims-imio.kz, product-service@kims-imio.kz
http://kims-imio.com/index.php/main

«Минералдық шикізаттарды кешенді пайдалану» журналы ғылыми жұмыстардың негізгі нәтижелерін жариялау үшін Қазақстан Республикасы Білім және ғылым министірлігінің Білім және ғылым сапасын қамтамасыз ету комитеті ұсынған ғылыми басылымдар тізіміне енгізілген.
Меншік иесі: «Металлургия және кен байыту институты» АҚ

Журнал Қазақстан Республикасының Ақпарат және коммуникация министрлігінің Байланыс, ақпараттандыру және бұқаралық ақпарат құралдары саласындағы мемлекеттік бақылау комитетінде қайта тіркелген

2016 ж. 18 қазандағы № 16180-Ж Куәлігі

Address:
Institute of Metallurgy and Ore Beneficiation
29/133 Shevchenko Street, corner of Ch. Valikhanov Street, Almaty, 050010, Kazakhstan
Fax. +7 (727) 298-45-03, Tel. +7-(727) 298-45-02, +7 (727) 298-45-19
E mail: journal@kims-imio.kz, product-service@kims-imio.kz
http://kims-imio.com/index.php/main

The Journal "Complex Use of Mineral Resources" is included in the List of publications recommended by the Committee for Control in the Sphere of Education and Science of the Ministry of Education and Science of the Republic of Kazakhstan for the publication of the main results of scientific activities.
Owner: "Institute of Metallurgy and Ore Beneficiation" JSC

The Journal was re-registered by the Committee for State Control in the Sphere of Communication, Information and Mass Media of the Ministry of Information and Communication of the Republic of Kazakhstan.

Certificate № 16180-Ж since October 18, 2016

Адрес редакции:
Институт Металлургии и Обогащения
050010, Республика Казахстан, г. Алматы, ул. Шевченко, уг. ул. Валиханова, 29/133,
Fax. +7 (727) 298-45-03, Tel. +7 (727) 298-45-02, +7 (727) 298-45-19
E mail: journal@kims-imio.kz, product-service@kims-imio.kz
http://kims-imio.com/index.php/main

Журнал «Комплексное использование минерального сырья» включен в Перечень изданий, рекомендуемых Комитетом по контролю в сфере образования и науки Министерства образования и науки Республики Казахстан для публикации основных результатов научной деятельности.
Собственник: АО «Институт металлургии и обогащения»

Журнал перерегистрирован в Комитете государственного контроля в области связи, информатизации и средств массовой информации
Министерства информации и коммуникации Республики Казахстан
Свидетельство № 16180-Ж от 18 октября 2016 г.

Crossref
DOI: 10.31643/2025/6445.01
Engineering and technology

Assessment of the physical and mechanical characteristics of sand for the production of foam concrete using the two-stage foam injection method

[1]Lukpanov R.E., [1]Dyussembinov D.S., [1,2]Altynbekova A.D., [1]Yenkebayev S.B., [3]Talal Awwad

[1] Solid Research Group LLP, Astana, Kazakhstan
[2] L.N. Gumilyov Eurasian National University, Astana, Kazakhstan
[3]Department of Geotechnical Engineering, Damascus University, Damascus, Syria

** Corresponding author email: kleo-14@mail.ru*

Received: *October 23, 2023*
Peer-reviewed: *November 23, 2023*
Accepted: *February 5, 2024*

ABSTRACT

The article presents the results of experimental studies of the properties of quarry sand to assess their suitability for use in the production of foam concrete. The sites of quarry sand extraction in the territory of the Akmola region are analyzed and their physical and mechanical characteristics are characterized. Evaluation of the physical and mechanical characteristics of sand was made for four types of sand. The main evaluation parameters were: particle size distribution, homogeneity, shrinkage, density and moisture content of sands. The results of the study showed that the physical characteristics of sands vary depending on their type, which indicates the differences in the natural composition and properties of these materials. Evaluation of the homogeneity of the different types of sands confirms the significant differences between the types. The highest homogeneity (x_{max}=77.45; x_{max-1}=14.98; Cc=73.5%) was observed in type 1 sand, while type 4 sand shows the minimum degree of homogeneity (x_{max}=47.30; x_{max-1}=42.28; Cc=8.7%). According to the test results, the maximum values of both densities in type 2 are: ρ_d=1.519 g/cm^2, ρ_w=1.951 g/cm^2, and the minimum values of both densities in type 4 are: ρ_d=1.438 g/cm^2, ρ_w=1.894 g/cm^2. The maximum natural moisture content in Type 1 samples is vn=9.5%, while the minimum values are 7.6% and 7.2% (Type 2 and 4). The obtained private density values have a high degree of convergence because the coefficients of variation have very low values: for Type 1 sands are 0.1-0.3%; for Type 2 sands are 0.7-0.8%; for Type 3 sands are 0.5-0.7%; for Type 4 sands are 0.4-0.6% (variation of private density values of dry and wet sands, respectively). Analysis of the results of tests on the shrinkage of samples showed that the maximum shrinkage is observed for sands of type 1 equal to 15.63%, while the minimum shrinkage is characteristic of samples of type 3 and 4 (11.25% and 11.88%). Taking into account the suitability of sand for the production of foam concrete, the most preferable is Type 1 sand mined in the Eltok building sand deposit.

Keywords: sand, foam concrete, physical and mechanical characteristics, shrinkage, particle size distribution, degree of homogeneity.

Information about authors:

Lukpanov Rauan Ermagambetovich — *PhD, Professor, Scientific Supervisor, Solid Research Group LLP, Astana, Kazakhstan. Email: rauan_82@mail.ru*

Dyussembinov Duman Serikovich — *C.t.s., Associate Professor, Senior Researcher, Solid Research Group LLP, Astana, Kazakhstan. Email: dusembinov@mail.ru*

Altynbekova Aliya Doszhankyzy — *Senior lecturer, Department of Technology of Industrial and Civil Construction, L.N. Gumilyov Eurasian National University, Astana, Kazakhstan. Researcher, Solid Research Group LLP, Astana, Kazakhstan. Email: kleo-14@mail.ru*

Yenkebayev Serik Beisengalievich — *C.t.s., Associate Professor, Senior Researcher, Solid Research Group LLP, Astana, Kazakhstan. Email: yenkebayev-serik@mail.ru*

Talal Awwad — *Professor of Department of Geotechnical Engineering, Damascus University, Damascus, Syria. Department of Soils and Foundations, Civil Engineering faculty, Emperor Alexander I St. Petersburg State Transport University, Russia. E-mail: dr.awwad.gfce@gmail.com*

Introduction

In the context of the rapid development of the construction industry, a variety of building materials have appeared, and one of the most interesting and promising of them is foam concrete [[1], [2], [3]]. The relevance of this study is due to the high demand for foam concrete in the modern construction market. Foamed concrete is characterized by a variety of physical and mechanical characteristics, ease of production, relative economy and small mass of blocks, which makes it very attractive for use in construction [[4], [5], [6]]. Special interest in this material is caused by its unique properties, such as density, thermal conductivity and features of the cellular structure.

One of the main characteristics of foam concrete is its porous structure [7], which makes it an ideal material for a wide range of construction applications.

Foamed concrete belongs to promising building materials and has several significant functional properties that favorably distinguish it from heavy and lightweight concrete: low thermal conductivity, good vapor permeability, low energy costs for its production, good sound insulation, environmental friendliness, durability, and fire safety. In recent years, foam concrete has been widely used in construction as a heat-insulating and structural-insulating material.

In modern conditions, there are a variety of raw materials that can be used in the production of foam concrete. The process of making foam concrete consists of the integration of ready-made foam into the cement-sand mixture, which contributes to the creation of a closed pore system [[8], [9]]. It is important to note that the quality and characteristics of the components used are critical to ensure the required strength of foam concrete. Even minor use of low-quality aggregates can lead to a decrease in the strength of foam concrete structures [[10], [11], [12]]. Therefore, the selection and quality of raw materials play a crucial role in the production of foam concrete.

An important aspect is the durability of cellular concrete, the basis of which is cement binder and fine aggregate [13]. One of the key factors determining the quality of sand is the ratio of different fractions of its grains [[14], [15]]. In the production of foamed concrete, fine and very fine sand is used, and sometimes this sand may contain harmful impurities such as sulfur and sulfuric acid compounds, mica, and amorphous modifications of silica. The latter is especially dangerous, as they can interact with alkalis and cause destruction of the cement matrix. Therefore, control of sand quality and its composition is important to ensure the durability and reliability of foam concrete structures [[16], [17], [18], [19], [20]].

The purpose of this study is to conduct a comparative analysis of the physical and mechanical characteristics of quarry sand to assess its suitability for further use in the production of foam concrete.

Experimental technique

Based on the results of the analysis of the market of non-metallic building materials (sand) in Astana city, samples of raw materials were selected for testing. The list of selected samples includes the following quarries:

Type 1. Eltok sand deposit is located in Arshalyn district of Akmola region near Volgodonovka village, 44 km southeast of Astana city.

Type 2. Aryktynskoe sand deposit is located in Korgalzhyn district of Akmola region 1.5 km north of Arykty village, 40 km east of Korgalzhyno village, 100 km south-west of Astana city.

Type 3: Sensembay sand deposit is located in Arshalyn district of Akmola region, 1.5 km north-west of Volgodonovka village.

Type 4. Zhana-Zhol sand deposit is located in the Tselinograd district of Akmola region, 1.0 km southwest of Karazhar village and 30 km southwest of Astana city.

The main research indicator of sand is the evaluation of its particle size distribution, exactly the determination of clay particles in its composition, possible dust-like impurities and inclusions affecting the quality of the manufactured product - foam concrete. The tests are carried out under conditions of statistical evaluation of this indicator, i.e., at least 100 kg of sand will be selected to evaluate each type, which is more than 20 samples for each of the three types of sand being compared. Subsequently, the sand sieved by particle size distribution will be used to evaluate the quality of cement, instead of polyfractional sand. The sand composition for cement evaluation will be selected based on average statistical data of granulometric analysis of the type of sand to be selected for use in production. In the end, we will get the results of the activity and setting time of cement under the conditions of its interaction with real components that will be used in the production of foam concrete.

Additional tests of sand will be unregulated shrinkage tests of sand shrinkage during soaking. The amount of shrinkage will give us an understanding of the potential change in the volume of the final product relative to the initial product, which may be useful when pouring large-scale structures (in further performance studies and possible formulation adjustments for a mobile plant).

Sand studies include the following sequence of activities:

- sampling of each of the three types of sand to be compared, weighing at least 100 kg;
- washing the sand with hot water and measuring the mass (before and after washing) using a 0.05 sieve (when draining the water);

- carrying out tests of particle size distribution according to aggregated indicators: dust particles 0-0,05 mm (residue on the pallet); fine sand 0,05-0,25 mm (residue of sieve 0,05); medium sand 0,25-0,5 (residue of sieve 0,25); coarse sand 0,5-2,0 mm (residue of sieve 0,5); gravel >2,0 (residue of sieve 2,0), according to the test method regulated by GOST 8735

- analysis of the obtained granulometric (grain) composition, with the selection of the optimal type of sand suitable for the production of foam concrete;

- evaluation of sand shrinkage, as well as evaluation of sand densities to determine the dosage: bulk density, density in dry state, wet state, etc.

The sample tests for the evaluation of natural indices were performed for selected samples, immediately after transportation. However, to determine the density in the dry and water-saturated state, a preliminary quartering was performed (Figure 1), the purpose of which was to obtain results as close as possible to the average statistical indicators with a minimum number of tests (in our case, 5 tests of each type). After quartering, 1000 ml samples were taken (for more convenient density estimation).

Sand shrinkage was assessed using the soaking method, Figure 2. The sequence of work included:

- a sampling of the compared soil types, totaling at least 15 kg for each of the sand types;

- determination of sand density at natural moisture content;

- drying the samples to a constant mass;

- determination of the density of dry sand;

- Soaking of sand with the determination of shrinkage and density in a water-saturated state.

Soaking of sand samples was carried out in a measuring container with a graduated scale until complete stabilization (constant value) of sand shrinkage, Figure 2. The weighing of samples was carried out on calibrated scales.

This methodology allowed us to conduct a subsequent comparative analysis of the qualitative characteristics of the studied sands in the context of their applicability in the production of foam concrete products.

Results and Discussion

Tabulated data of sand grain size distributions are presented in Tables 1-4, which were compiled to investigate the fractional composition of each of the studied sands in more detail.

Figure 1 - Sand tests

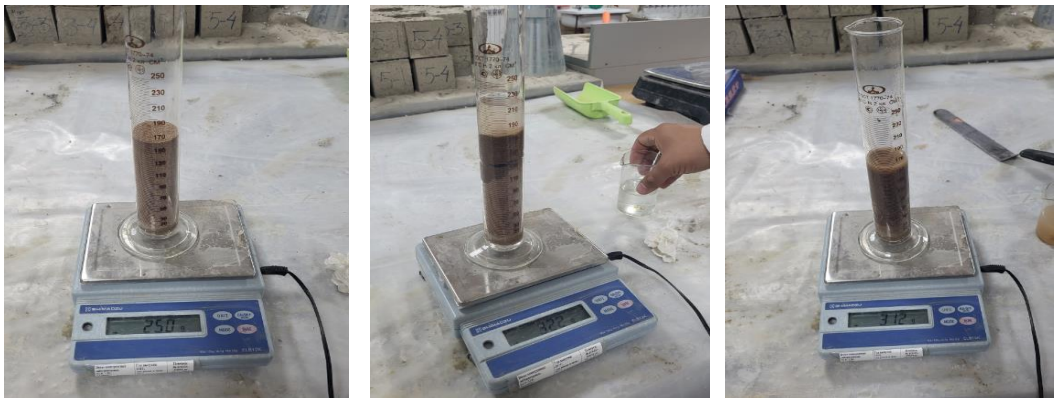

Figure 2 - Evaluation of sand shrinkage

Table 1 - Results of granulometric composition of Type 1 sands

Sample number	Weight of sand in a sieve					Sample mass		Loss, %
	Sieve 1 d=2 mm	Sieve 2 d=0.5 mm	Sieve 3 d=0.25 mm	Sieve 4 d=0.05 mm	Residue >0.05 mm	After	Before	
1	27	300	3760	919	4	5010	5010	0.000
2	30	311	4059	866	4	5270	5270	0.000
3	25	308	3917	786	3	5039	5040	0.020
4	35	297	3813	872	2	5019	5020	0.020
5	24	324	3797	854	5	5004	5005	0.020
6	21	350	3934	700	4	5009	5010	0.020
7	22	429	3805	739	5	5000	5000	0.000
8	25	358	3997	631	4	5015	5015	0.000
9	40	373	3955	646	4	5018	5020	0.040
10	25	349	3938	688	4	5004	5005	0.020
11	35	375	3942	661	4	5017	5020	0.060
12	30	398	3762	671	4	4865	4865	0.000
Average	28	348	3890	753	4	5023	5023	0.017
Deviation	6	42	99	102	1	-	-	-
Variation, %	21	12	3	14	20	-	-	-

Table 2 - Results of granulometric composition of Type 2 sands

Sample number	Weight of sand in a sieve					Sample mass		Loss, %
	Sieve 1 d=2 mm	Sieve 2 d=0.5 mm	Sieve 3 d=0.25 mm	Sieve 4 d=0.05 mm	Residue >0.05 mm	After	Before	
1	387	783	2613	1235	2	5020	5020	0.000
2	421	820	2588	1178	6	5013	5015	0.000
3	345	756	2646	1257	5	5009	5010	0.020
4	389	815	2506	1294	5	5009	5010	0.020
5	311	810	2720	1167	7	5015	5015	0.020
6	402	789	2522	1289	3	5005	5005	0.020
7	367	793	2558	1302	3	5023	5025	0.000
8	379	738	2618	1275	4	5014	5015	0.000
9	328	816	2637	1228	3	5012	5015	0.040
10	354	718	2740	1195	6	5013	5015	0.020
11	387	785	2658	1189	5	5024	5025	0.060
12	404	766	2642	1204	3	5019	5020	0.000
Average	373	782	2621	1234	4	5015	5016	0.017
Deviation	33	32	71	48	2	-	-	-
Variation, %	9	4	3	4	36	-	-	-

Table 3 - Results of granulometric composition of Type 3 sands

Sample number	Weight of sand in sieve					Sample mass		Loss, %
	Sieve 1 d=2 mm	Sieve 2 d=0.5 mm	Sieve 3 d=0.25 mm	Sieve 4 d=0.05 mm	Residue >0.05 mm	After	Before	
1	45	1782	2419	761	2	5009	5010	0.000
2	42	1653	2500	812	3	5010	5010	0.000
3	32	1735	2584	655	3	5009	5010	0.020
4	37	1758	2496	711	3	5005	5005	0.020
5	31	1733	2528	719	3	5014	5015	0.020
6	26	1672	2531	772	2	5003	5005	0.020
7	36	1645	2570	753	3	5007	5010	0.000
8	38	1812	2379	782	2	5013	5015	0.000
9	42	1741	2469	756	2	5010	5010	0.040
10	34	1795	2468	699	4	5000	5000	0.020
11	33	1776	2454	737	2	5002	5005	0.060
12	38	1649	2566	756	3	5012	5015	0.000
Average	36	1729	2497	743	3	5023	5010	0.017
Deviation	5	60	63	42	1	-	-	-
Variation, %	15	3	3	6	24	-	-	-

Table 4 - Results of granulometric composition of Type 4 sands

Sample number	Weight of sand in sieve					Sample mass		Loss, %
	Sieve 1 d=2 mm	Sieve 2 d=0.5 mm	Sieve 3 d=0.25 mm	Sieve 4 d=0.05 mm	Residue >0.05 mm	After	Before	
1	12	2134	2340	516	8	5010	5010	0.000
2	17	2009	2527	452	5	5010	5010	0.000
3	21	2067	2406	511	7	5012	5015	0.020
4	14	2178	2249	567	7	5015	5015	0.020
5	18	2113	2328	538	5	5002	5005	0.020
6	14	2016	2398	576	5	5009	5010	0.020
7	19	2231	2310	453	6	5019	5020	0.000
8	23	2166	2387	428	5	5009	5010	0.000
9	15	2095	2415	475	5	5005	5005	0.040
10	21	2154	2303	526	5	5009	5010	0.020
11	19	2183	2305	497	6	5010	5010	0.060
12	16	2075	2470	442	5	5008	5010	0.000
Average	17	2118	2370	498	6	5015	5015	0.017
Deviation	3	69	79	49	1	-	-	-
Variation, %	19	3	3	10	18	-	-	-

Analysis of the data presented in the tables allows us to make the following observations:

- The average particle size for each of the studied sand types has different characteristics. It varies from 28 to 3890 for Type 1, 373 to 2621 for Type 2, 36 to 2497 for Type 3, and 17 to 2370 for Type 4.

- The deviation from the mean particle size also varies by sand type. For Type 1, the deviation ranges from 6 to 102, for Type 2 from 32 to 71, for Type 3 from 5 to 63, and for Type 4 from 3 to 79. This indicates a considerable diversity of fractions in each type.

- The variation in the mass of the material ranges from 3 to 21%, indicating that there is considerable variability in the composition of the sand in the different types.

- The percentage of material loss during sieving is small at less than 0.1%, indicating that the sieving procedure is effective and has little effect on the total amount of material.

Tables 5-8 show the results of the percentage of particle size distribution of the compared sands.

Table 5 - Percentage of particle size distribution of Type 1 sands

Sample number	Granules percentage, %				
	Sieve 1 d=2 mm	Sieve 2 d=0.5 mm	Sieve 3 d=0.25 mm	Sieve 4 d=0.05 mm	Residue >0.05 mm
1	0.54	5.99	75.05	18.34	0.08
2	0.57	5.90	77.02	16.43	0.08
3	0.50	6.11	77.73	15.60	0.06
4	0.70	5.92	75.97	17.37	0.04
5	0.48	6.47	75.88	17.07	0.10
6	0.42	6.99	78.54	13.97	0.08
7	0.44	8.58	76.10	14.78	0.10
8	0.50	7.14	79.70	12.58	0.08
9	0.80	7.43	78.82	12.87	0.08
10	0.50	6.97	78.70	13.75	0.08
11	0.70	7.47	78.57	13.18	0.08
12	0.62	8.18	77.33	13.79	0.08
Average	00.56	6.93	77.45	14.98	0.08

Table 6 - Percentage of particle size distribution of Type 2 sands

Sample number	Granules percentage, %				
	Sieve 1 d=2 mm	Sieve 2 d=0.5 mm	Sieve 3 d=0.25 mm	Sieve 4 d=0.05 mm	Residue >0.05 mm
1	7.71	15.60	52.05	24.60	0.04
2	8.40	16.36	51.63	23.50	0.12
3	6.89	15.09	52.82	25.09	0.10
4	7.77	16.27	50.03	25.83	0.10
5	6.20	16.15	54.24	23.27	0.14
6	8.03	15.76	50.39	25.75	0.06
7	7.31	15.79	50.93	25.92	0.06
8	7.56	14.72	52.21	25.43	0.08
9	6.54	16.28	52.61	24.50	0.06
10	7.06	14.32	54.66	23.84	0.12
11	7.70	15.63	52.91	23.67	0.10
12	8.05	15.26	52.64	23.99	0.06
Average	7.43	15.60	52.26	24.62	0.09

Table 7 - Percentage of particle size distribution of Type 3 sands

Sample number	Granules percentage, %				
	Sieve 1 d=2 mm	Sieve 2 d=0.5 mm	Sieve 3 d=0.25 mm	Sieve 4 d=0.05 mm	Residue >0.05 mm
1	0.90	35.58	48.29	15.19	0.04
2	0.84	32.99	49.90	16.21	0.06
3	0.64	34.64	51.59	13.08	0.06
4	0.74	35.12	49.87	14.21	0.06
5	0.62	34.56	50.42	14.34	0.06
6	0.52	33.42	50.59	15.43	0.04
7	0.72	32.85	51.33	15.04	0.06
8	0.76	36.15	47.46	15.60	0.04
9	0.84	34.75	49.28	15.09	0.04
10	0.68	35.90	49.36	13.98	0.08
11	0.66	35.51	49.06	14.73	0.04
12	0.76	32.90	51.20	15.08	0.06
Average	0.90	35.58	48.29	15.19	0.04

Table 8 - Percentage of particle size distribution of Type 4 sands

Sample number	Granules percentage, %				
	Sieve 1 d=2 mm	Sieve 2 d=0.5 mm	Sieve 3 d=0.25 mm	Sieve 4 d=0.05 mm	Residue >0.05 mm
1	0.24	42.59	46.71	10.30	0.16
2	0.34	40.10	50.44	9.02	0.10
3	0.42	41.24	48.00	10.20	0.14
4	0.28	43.43	44.85	11.31	0.14
5	0.36	42.24	46.54	10.76	0.10
6	0.28	40.25	47.87	11.50	0.10
7	0.38	44.45	46.03	9.03	0.12
8	0.46	43.24	47.65	8.54	0.10
9	0.30	41.86	48.25	9.49	0.10
10	0.42	43.00	45.98	10.50	0.10
11	0.38	43.57	46.01	9.92	0.12
12	0.32	41.43	49.32	8.83	0.10
Average	0.35	42.28	47.30	9.95	0.11

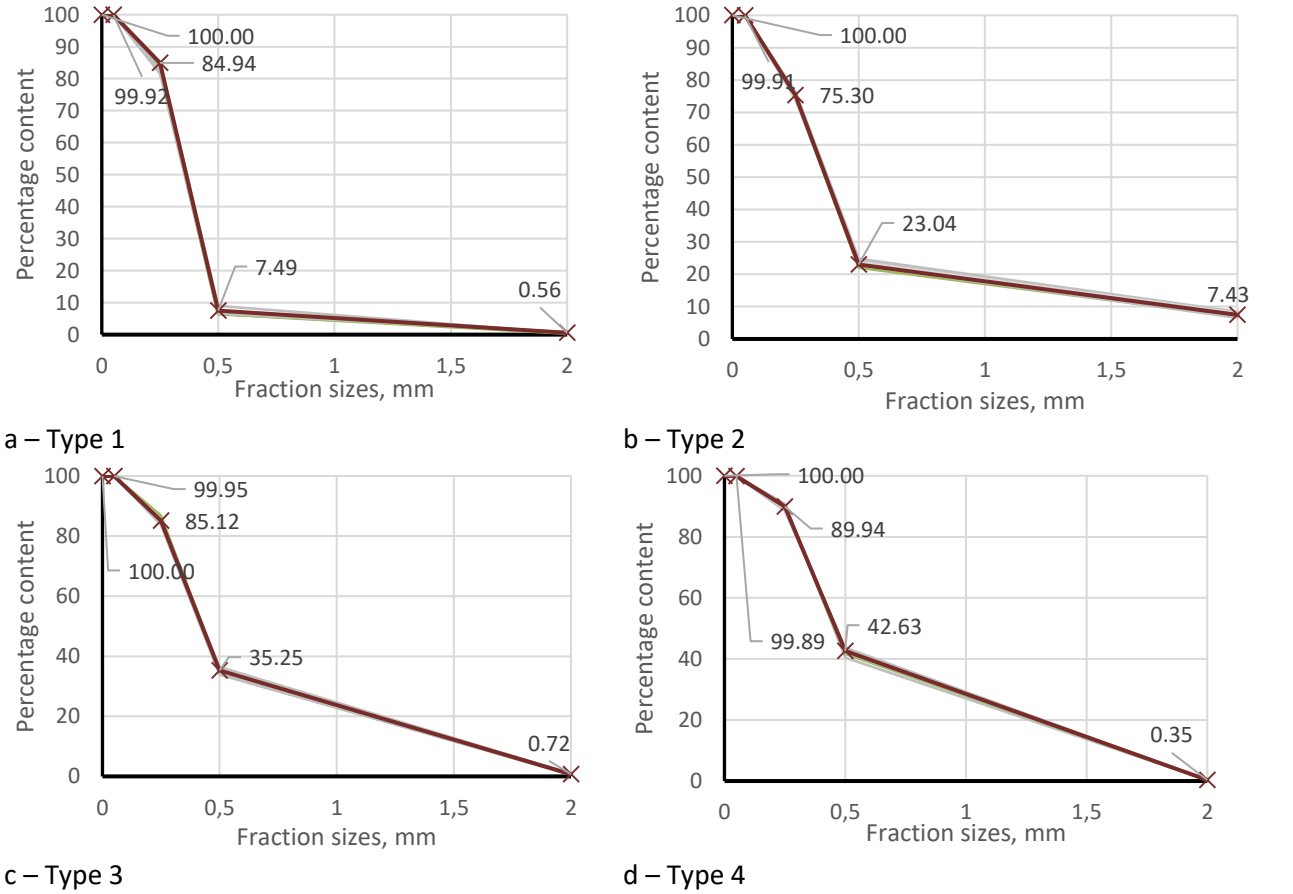

Figure 3 - Graphs of granulometric composition of sands

Figures 3a - 3d show the graphs of particle size distribution of the compared sand types. The X-axis shows the values of fraction sizes, and the Y-axis shows their percentages. In this case, the ordinate axis represents the percentage of particles whose fraction sizes are smaller than the corresponding value on the abscissa axis. That is, according to the graph of Figure 3, the fraction size is 7.49%, greater than 0.5 mm, of which 6.93% is less than 2 mm and 0.56% is greater than 2 mm (according to the summary table). It can also be interpreted that those fractions 100-7,49=92,51% with dimensions less than 0,5 mm.

According to the statistical results, all the obtained data have a close relationship with the evaluated indicators. For type 1, the coefficient of variation within the size fractions does not exceed 20%, inaccuracy lies in the range from 1.8 to 19.87 %. For type 2 this value does not exceed 35%, and for dusty fractions, the fractional content of which does not exceed 0.1% by mass of samples. For the rest, the sandy fractions in samples of type 2, the variation does not exceed 9% (from 2.55 to 8.42). A similar pattern is observed for Type 3 samples: the variation of clay particles has an unstable value of 24.45%, and within the sand fractions, the coefficient varies from 2.51 to 14.78%. For type 3, the coefficient of variation within the size fractions, just as in the case of type 1 does not exceed 20%, exactly ranges from 3.36 to 19.19%.

In general, it has been observed that maximum instability of mass ratios of fractions in the boundary ranges. That is, in the extreme ranges of sandy soils (or rather lying outside it) corresponding to the maximum (not more than 2 mm) and minimum (not less than 0.05 mm) allowable fraction for sand. For types 1 and 4, the maximum instability was detected in the range exceeding the maximum allowable value of sand fractions: fractions of size greater than 2 mm. In both cases, the mass fraction of such inclusions in the samples does not exceed 1%, which can be regarded as an error. For sand types 2 and 3, the maximum instability of the results corresponds to the lower limit of the range of sandy soils, and clay inclusions, the total content of which on average does not exceed 0.1% by mass in both cases. This low percentage can also be excluded from the particle size distribution analysis.

To assess the homogeneity of the composition, we can use the classical formula for the degree of heterogeneity of sandy soils:

$$C_c = \frac{D_{60}}{D_{10}}, \quad (1)$$

where C_c is a degree of heterogeneity of soils;

D_{60} is a particle diameter, less than which 60% of grains are in the soil;

D_{10} is a diameter of particles, less than which 10% of grains are in the soil.

The classical homogeneity assessment (Table 9) does not work, because the particle size distribution assessment is performed according to an enlarged scheme. To evaluate the particle size distribution, selected only those sieves that correspond to the boundary sizes of fractions, i.e. their limiting maximum and minimum values. If intermediate sieve values were used, the results would have been more correct, with more appropriate data regarding the estimation of homogeneity by the conditional index Cc. The homogeneity of the sands will be assessed by direct estimation of the percentage of particles of each fraction. Figure 4 shows the values of the percentage of particle content by fractions. The graph shows that most of the fractions of all four compared types of sands have a size range of 0.5-0.25 mm (not inclusive), with the maximum value of the percentage of such particle size observed in the samples of Type 1. The dependence that has developed to estimate the soil homogeneity of this particular case:

$$C_c = \left(1 - \frac{100 - x_{max}}{100 - x_{max-1}}\right) x100 \quad (2)$$

where, C_c - degree of heterogeneity;

x_{max} - percentage ratio corresponding to the maximum distribution of particles by mass;

x_{max-1} - percentage ratio corresponding to the second maximum particle mass distribution.

Table 9 – Degree of homogeneity of sands

Sample number	Sand type	Degree of homogeneity	Homogeneity criterion
1	Type 1	Cc = 0,5/0.05=10	<3 heterogeneous
2	Type 2	Cc = 0,5/0.05=10	<3 heterogeneous
3	Type 3	Cc = 0,5/0.05=10	<3 heterogeneous
4	Type 4	Cc = 2/0.05=10	<3 heterogeneous

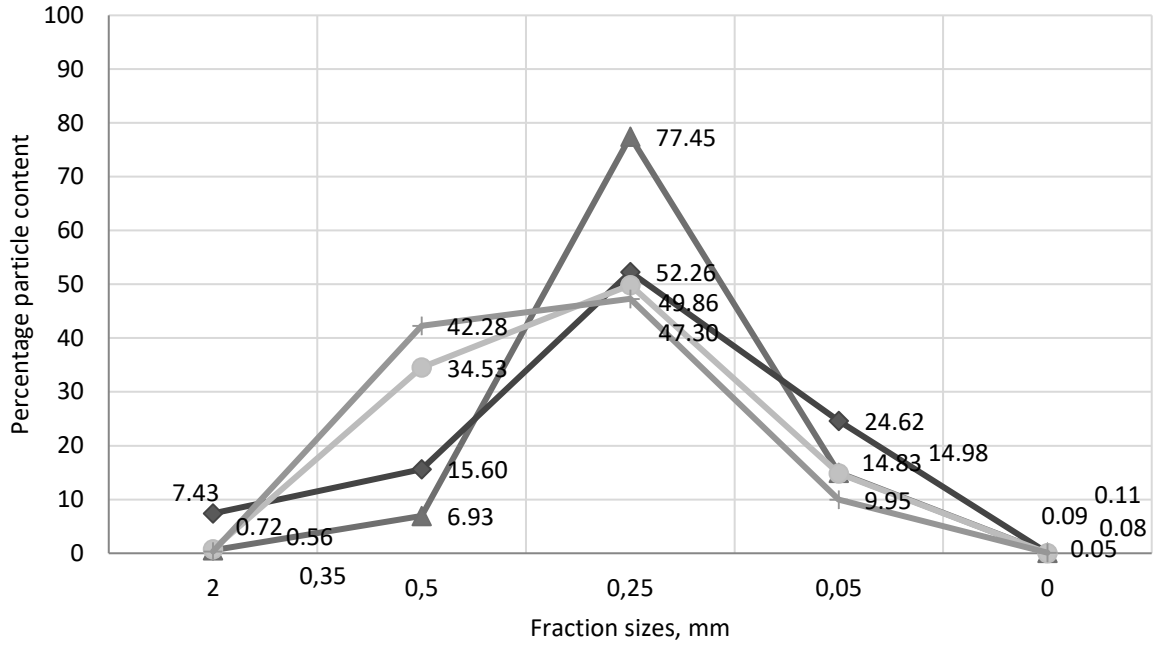

Figure 4 - Percentage distribution of fractions by weight

Table 10 – Evaluation of sand homogeneity

Type	Max	Max-1	Cc
Type 1	77.45	14.98	73.5
Type 2	52.26	24.62	36.7
Type 3	49.86	34.53	23.4
Type 4	47.30	42.28	8.7

This dependence takes into account the following evaluation conditions: the percentage of the maximum fraction relative to the total mass of the sample, as well as the criterion of relativity of the maximum fractions to the fractions immediately following the maximum value (by mass). Thus, an assessment of homogeneity is given both relative to the total mass of the sample and relative to the available difference between the percentage distribution. For a comparative (not absolute) assessment, it is sufficient to compare the percentage ratio of the maximum value of the particle mass distribution to the second value of the maximum particle distribution. The degree of heterogeneity ranges from 0 to 100%, and the interpretation of the result is summarized as follows: the larger the value of the degree, the greater the homogeneity of the sand. The results of the calculations are presented in Table 10.

According to the results, type 1 sand has maximum homogeneity and type 4 sand has minimum homogeneity. In general, the results of the heterogeneity assessment are quite logical: Type 1 has the maximum distribution index, and the difference with the second value of the mass distribution is also maximum; Types 2 and 3 have a relatively similar pattern to Type 1, but both of these indicators are inferior to Type 1; Type 4 has the lowest distribution values with the minimum difference between the maximum and second after the maximum mass distribution of fractions.

From the point of view of the suitability of sand about the prevailing size of fractions, the most preferable is the sand Type 1 deposit of building sands Eltok, located in the Arshalyn district of Akmola region near the village of Volgodonovka, 44 km southeast of Astana. This type of sand has the highest percentage of the smallest fractions, relative to other comparable types of sand. For the production of foam concrete, the grain size index is important, the smaller the size of sand fractions, the more structured the final product will be, with a more stable pore structure.

Figure 5, table 11 shows the results of weighing sand samples of 1000 grams in the dry state (after drying to constant weight) and in water-saturated state.

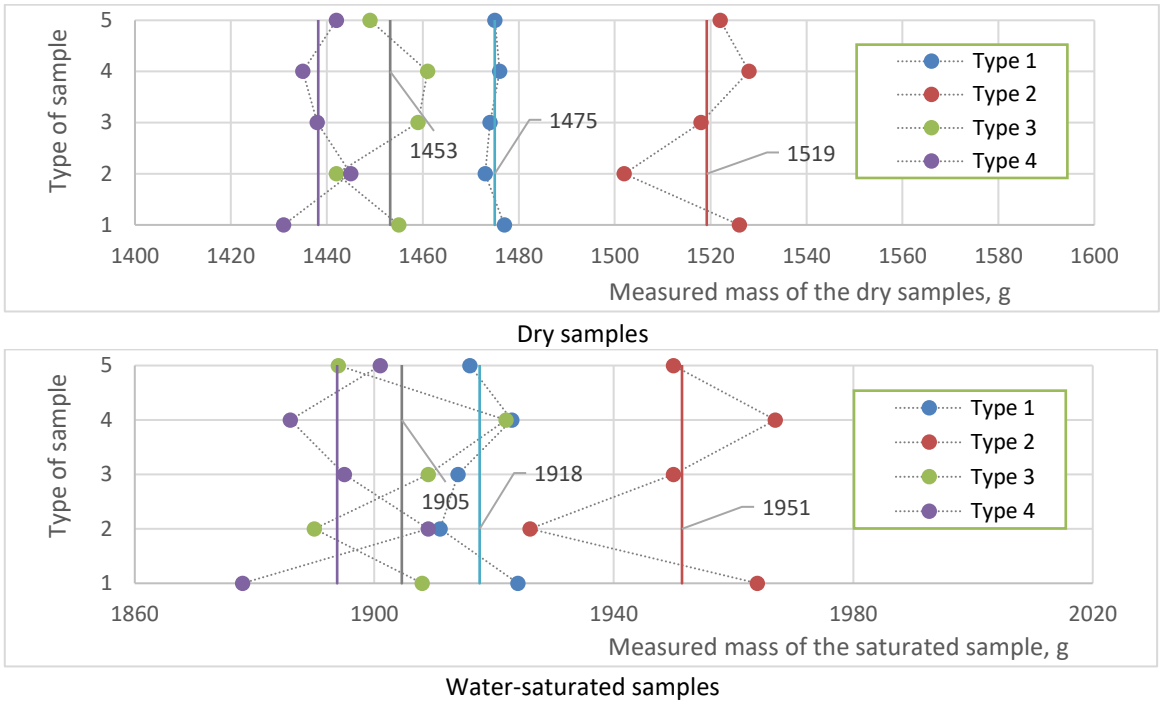

Figure 5 – Weighing results of sand samples

Table 11 – Results of density and moisture estimation of sands

Sand type	Dry sand density ρd, g/cm^2	Wet sand density, ρw, g/cm^2	Sand particle density, ρs, g/cm^2	Natural density of sand, ρn, g/cm^2	Natural humidity, vn, %	Moisture at full water saturation, vw, %
Type 1	1.475	1.918	2.648	1.615	9.5	79.5
Type 2	1.519	1.951	2.674	1.634	7.6	76.1
Type 3	1.453	1.904	2.647	1.579	8.7	82.1
Type 4	1.438	1.894	2.643	1.542	7.2	83.8

Table 12 – Results of sand shrinkage evaluation

Sand type	Dry sand volume, ml	Soaked sand volume, ml	Shrinkage volume, ml	Relative shrinkage, %	Quadratic deviation	Variation coefficient, %
Type 1	160	138	22	13.75	1.7	1.231884
Type 2	160	135	25	15.63	1.9	1.407407
Type 3	160	142	18	11.25	1.5	1.056338
Type 4	160	141	19	11.88	1.8	1.276596

In the graphs, each point corresponds to a private value of density, and the values of the central lines correspond to the average values of each of the compared types of sand. The results of density determination are shown in Table 11. The table also shows the results of calculations of the natural moisture content of sands and their moisture content after their complete water saturation.

According to the test results, the maximum density in the natural state is in type 2 sands and minimum in type 4 sands, and in both cases, the natural moisture content is a minimum of 7.6 and 7.2 % respectively. The maximum natural moisture content is observed in type 1 samples. Maximum density in dry conditions and water-saturated conditions was found in type 2 sands and minimum of both densities in type 4. A similar pattern was

found when comparing the densities of soil particles, with the only difference being that the results of densities of all the types compared are closer. The percentage of the difference between the maximum and minimum values in the case of dry soil density is +/- 5% and in the case of particle density +/- 5%.

The obtained private density values have a high degree of convergence because the coefficients of variation have very low values: for sands of type 1 are 0.1-0.3%; for sands of type 2 are 0.7-0.8%; for sands of type 3 are 0.5-0.7%; for sands of type 4 are 0.4-0.6% (variation of private density values of dry and wet sands, respectively). The low variation indices testify to the qualitative quartering performed before the tests, as well as to the high approximation of the obtained results to the average statistical values.

Table 12 shows the results of the shrinkage of samples after soaking. According to the test results, the maximum shrinkage was found in type 1 samples and the minimum shrinkage in type 3 and 4 samples. The test results can be decisive in the choice of sand for the production of foam concrete with other equal evaluation indicators. According to the analysis of statistical indicators, we also conclude that there is a sufficiently close relationship between the individual values among themselves, hence, the high reliability of the obtained averages.

Conclusion

Based on the results of the tests performed, the following generalized conclusions can be drawn:

1. The physical characteristics of sands vary from one type to another, indicating differences in their natural composition and properties.

2. The maximum density in the natural state is observed in type 2 sands while the minimum density is observed in type 4 sands. Both types of sands are characterized by low levels of natural moisture content of 7.6% and 7.2% respectively.

3. Maximum density in dry and water-saturated conditions is also found in type 2 sands while minimum density in both the states is found in type 4 sands.

4. As a result of shrinkage tests of the specimens, maximum shrinkage is found in type 1 sands while minimum shrinkage is observed in type 3 and 4 specimens.

5. From the point of view of sand suitability for the production of foam concrete, the most preferable is Type 1 sand from the construction sand deposit Eltok, located in Arshalyn district of Akmola region near Volgodonovka village, 44 km southeast of Astana. This type of sand has the highest content of the smallest fractions compared to other types of sand. For foam concrete production, the size of fractions is important, and the smaller it is, the more structured the final product will be with a more stable pore structure.

Conflict of interest. The corresponding author declares that there is no conflict of interest.

Acknowledgements. This research was funded by the science committee of the Ministry of Education and Science of Kazakhstan (Grant № AP13068424).

***Cite this article as*:** Lukpanov RE, Dyussembinov DS, Altynbekova AD, Yenkebayev SB, Talal Awwad. Assessment of the physical and mechanical characteristics of sand for the production of foam concrete using the two-stage foam injection method. Kompleksnoe Ispolzovanie Mineralnogo Syra = Complex Use of Mineral Resources. 2025; 332(1):5-18. https://doi.org/10.31643/2025/6445.01

Екі сатылы көбік енгізу әдісімен көбікбетон өндіруге арналған құмның физикалық-механикалық сипаттамаларын бағалау

[1]Лукпанов Р.Е., [1]Дюсембинов Д.С., [1,2]Алтынбекова А.Д., [1]Енкебаев С.Б., [3]Talal Awwad

[1] ЖШС «Solid Research Group», Астана, Қазақстан
[2] Л.Н. Гумилев атындағы Еуразия ұлттық университеті, Астана, Қазақстан
[3]Геотехника факультеті, Дамаск университеті, Дамаск, Сирия

Мақала келді: *23 қазан 2023*
Сараптамадан өтті: *23 қараша 2023*
Қабылданды: *5 ақпан 2024*

ТҮЙІНДЕМЕ

Мақалада көбік бетон өндірісінде қолдануға жарамдылығын бағалау мақсатында карьер құмының қасиеттеріне жүргізілген тәжірибелік зерттеулердің нәтижелері берілген. Ақмола облысы аумағындағы карьерлік құмды өндіру аймақтары талданып, олардың физика-механикалық көрсеткіштері бойынша сипаттамалары келтірілген. Құмның физика-механикалық сипаттамалары құмның төрт түрі бойынша бағаланды. Негізгі бағалау параметрлері: гранулометриялық құрамы, біркелкілігі, шөгуі, тығыздығы және құмның ылғалдылығы болды. Зерттеу нәтижелері бойынша құмдардың физикалық сипаттамалары олардың түріне байланысты өзгеретінін көрсетті, бұл осы материалдардың табиғи құрамы мен қасиеттерінде айырмашылық бар екендігін дәлелдейді. Әртүрлі типтегі құмдардың біртектілігін бағалау, түрлер арасындағы елеулі айырмашылықтарды растайды. Ең жоғары біртектілік (x_{max}=77,45; x_{max-1}=14,98; Cc=73,5%) 1-типті құмда байқалса, 4-типті құмда біртектіліктің минималды дәрежесі (x_{max}=47,30; x_{max-1}= 42,28; Cc=8,7%) байқалады. Сынақ нәтижелеріне сәйкес 2-типті құмда екі тығыздықтың да максималды мәндері: ρ_d = 1,519 г/см^2, ρ_w = 1,951 г/см^2, ал 4-тип үшін екі тығыздықтың ең төменгі мәндері: ρ_d = 1,438 г/см^2, ρ_w = 1,894 г/см^2 болады. 1-типті үлгілер үшін максималды табиғи ылғалдылық v_n=9,5%, ал ең төменгі мәндері 7,6% және 7,2% (2- және 4-типтер). Алынған жартылай тығыздық мәндері конвергенцияның жоғары дәрежесіне ие, өйткені вариация коэффициенттері өте төмен: 1-типті құмдар үшін олар 0,1-0,3% құрайды; 2-типті құмдар үшін олар 0,7-0,8%; 3-типті құмдар үшін олар 0,5-0,7%; 4-типті құмдар үшін 0,4-0,6% құрайды (сәйкесінше құрғақ және дымқыл құмның нақты тығыздықтары өзгереді). Сынамалардың шөгуі бойынша сынау нәтижелерін талдау көрсеткендей, ең жоғары шөгу 1-типті құмдарда 15,63% тең, ал ең аз шөгу 3- және 4-типті үлгілерге тән (11,25% және 11,88%). Көбік бетон өндірісіне құмның жарамдылығын ескере отырып, Елтоқ құрылыс құм кен орнында өндірілген 1-типті құм ең қолайлы болып табылады.

Түйін сөздер: құм, көбікбетон, физика-механикалық сипаттамалар, шөгу, түйіршіктік құрамы, біртектілік дәрежесі.

Авторлар туралы ақпарат:

Лукпанов Рауан Ермагамбетович — *PhD, профессор, ғылыми жетекші, «Solid Research Group» ЖШС, Астана, Қазақстан. Email: rauan_82@mail.ru*

Дюсембинов Думан Серикович — *Т.ғ.к., доцент, аға ғылыми қызметкер, «Solid Research Group» ЖШС, Астана, Қазақстан. Email: dusembinov@mail.ru*

Алтынбекова Алия Досжанкызы — *Аға оқытушы, «Өнеркәсіптік және азаматтық құрылыс технологиясы» кафедрасы, Л.Н.Гумилев атындағы ЕҰУ, Астана, Қазақстан. Ғылыми қызметкер, «Solid Research Group» ЖШС, Астана, Қазақстан. E-mail: kleo-14@mail.ru*

Енкебаев Серик Бейсенгалиевич — *Т.ғ.к., доцент, аға ғылыми қызметкер, «Solid Research Group» ЖШС, Астана, Қазақстан. Email: yenkebayev-serik@mail.ru*

Talal Awwad — *Дамас университетінің геотехника кафедрасының профессоры, Дамаск, Сирия. Топырақ және негіздер кафедрасы, құрылыс факультеті, Император Александр I Санкт-Петербург мемлекеттік көлік университеті, Ресей. E-mail: dr.awwad.gfce@gmail.com*

Оценка физико-механических характеристик песка для производства пенобетона методом двухстадийного введения пены

[1]Лукпанов Р.Е., [1]Дюсембинов Д.С., [1,2]Алтынбекова А.Д., [1]Енкебаев С.Б., [3]Talal Awwad

[1] ТОО «Solid Research Group», Астана, Казахстан
[2] Евразийский национальный университет им. Л.Н. Гумилева, Астана, Казахстан
[3]Факультет геотехники, Дамасский университет, Дамаск, Сирия

Поступила: *23 октября 2023*
Рецензирование: *23 ноября 2023*
Принята в печать: *5 февраля 2024*

АННОТАЦИЯ

В статье представлены результаты экспериментальных исследований свойств карьерного песка с целью оценки их пригодности для использования в производстве пенобетона. Проанализированы участки добычи карьерного песка на территории Акмолинской области и дана их характеристика на физико-механические показатели. Оценка физико-механических характеристик песка произведена для четырех типов песка. Основными оценочными параметрами, являлись: гранулометрический состав, однородность, усадка, плотность и влажность песков. Результаты исследования показали, что физические характеристики песков варьируются в зависимости от их типа, что свидетельствует о различиях в природном составе и свойствах этих материалов. Оценка однородности песков различных типов подтверждают значительные различия между типами. Наибольшая однородность (x_{max}=77,45; x_{max-1}=14,98; Cc=73,5%) отмечена у песка типа 1, тогда как песок

	типа 4 демонстрирует минимальную степень однородности (x_{max}=47,30; x_{max-1}=42,28; Cc=8,7%). Согласно результатам испытаний, максимальные показатели обоих плотностей у типа 2 составляет: ρ_d =1,519 г/см^2, ρ_w=1,951 г/см^2, а минимальные показатели обоих плотностей у типа 4 составляет: ρ_d=1,438 г/см^2, ρ_w=1.894 г/см2. Максимальная естественная влажность у образцов типа 1 - v_n=9,5%, тогда как минимальные значения 7,6% и 7,2% (Тип 2 и 4). Полученные частные значения плотности имеют высокую степень сходимости, поскольку коэффициенты вариации имеют очень низкие показатели: для песков типа 1 составляют 0,1-0,3%; для песков типа 2 составляют 0,7-0,8%; для песков типа 3 составляют 0,5-0,7%; для песков типа 4 составляют 0,4-0,6% (вариации частных значений плотности сухого и мокрого песков соответственно). Анализ результатов испытаний по усадке образцов показал, что максимальная усадка наблюдается у песков типа 1 равная 15,63%, в то время как минимальная усадка характерна для образцов типа 3 и 4 (11,25% и 11,88%). С учетом пригодности песка для производства пенобетона, наиболее предпочтительным является песок Типа 1, добываемый в месторождении строительных песков Ельток.
	Ключевые слова: песок, пенобетон, физико-механические характеристики, усадка, гранулометрический состав, степень однородности.
Лукпанов Рауан Ермагамбетович	***Информация об авторах:*** *PhD, профессор, научный руководитель, ТОО «Solid Research Group», Астана, Казахстан. Email: rauan_82@mail.ru*
Дюсембинов Думан Серикович	*К.т.н., доцент, старший научный сотрудник, ТОО «Solid Research Group», Астана, Казахстан. Email: dusembinov@mail.ru*
Алтынбекова Алия Досжанкызы	*Старший преподаватель, кафедра «Технология промышленного и гражданского строительства», ЕНУ им. Л.Н.Гумилева, Астана, Казахстан. Научный сотрудник, ТОО «Solid Research Group», Астана, Казахстан. E-mail: kleo-14@mail.ru*
Енкебаев Серик Бейсенгалиевич	*К.т.н., доцент, старший научный сотрудник, ТОО «Solid Research Group», Астана, Казахстан. Email: yenkebayev-serik@mail.ru*
Talal Awwad	*Профессор кафедры геотехники Дамасского университета, Дамаск, Сирия. Кафедра оснований и фундаментов Петербургского Государственного Университет Путей Сообщения Императора Александра I, Россия. E-mail: dr.awwad.gfce@gmail.com*

References

[1] Liu J, Ge T, Wu Y, Chen R. Effect of Sand-to-Cement Ratio on Mechanical Properties of Foam Concrete. Buildings. 2022; 12(11):1969. https://doi.org/10.3390/buildings12111969

[2] Liu J, Ren Y, Chen R, Wu Y, Lei W. The Effect of Pore Structure on Impact Behavior of Con-crete Hollow Brick, Autoclaved Aerated Concrete and Foamed Concrete. Materials. 2022; 15(12):4075. https://doi.org/10.3390/ma15124075

[3] Gencel O, Nodehi M, Hekimoğlu G, Ustaoğlu A, Sarı A, Kaplan G, Bayraktar OY, Sutcu M, Ozbakkaloglu T. Foam Concrete Produced with Recycled Concrete Powder and Phase Change Materials. Sustainability. 2022; 14(12):7458. https://doi.org/10.3390/su14127458

[4] Fu Y, Wang X, Wang L, Li Y. Foam Concrete: A State-of-the-Art and State-of-the-Practice Review. Advances in Materials Science and Engineering. 2020, 1-25. https://doi.org/10.1155/2020/6153602

[5] Gołaszewski J, Klemczak B, Smolana A, Gołaszewska M, Cygan G, Mankel C, Peralta I, Röser F, Koenders EAB. Effect of Foaming Agent, Binder and Density on the Compressive Strength and Thermal Conductivity of Ultra-Light Foam Concrete. Buildings. 2022; 12(8):1176. https://doi.org/10.3390/buildings12081176

[6] Zhongwei Liu, Kang Zhao, Chi Hu, Yufei Tang. Effect of Water-Cement Ratio on Pore Struc-ture and Strength of Foam Concrete, Advances in Materials Science and Engineering. 2016, 9. https://doi.org/10.1155/2016/9520294

[7] Fu Y, Wang X, Wang L, Li Y. Foam Concrete: A State-of-the-Art and State-of-the-Practice Review. Advances in Materials Science and Engineering. 2020, 1-25. https://doi.org/10.1155/2020/6153602

[8] Muhammad NZ, Keyvanfar A, Majid MZ Abd, Shafaghat A, Mirza J. Waterproof perfor-mance of concrete: A critical review on implemented approaches. Construction and Building Materials. 2015; 101(1):80-90.

[9] Plank E Sakai, Miao CW, Yu C, Hong JX. Chemical admixtures-Chemistry, applications and their impact on concrete microstructure and durability. Cement and Concrete Research. 2015; 78(1):81-99.

[10] Tian Y, Shuaifeng S, Shuguang H. Mechanical and dynamic properties of high strength con-crete modified with lightweight aggregates presaturated polymer emulsion. Construction and Building Materials. 2015; 93(1):1151-1156.

[11] Chistov YuD, Tarasov AS. Development of multi-mineral binders. Russian Chemical Journal. 2003; 4(1):12-17.

[12] Gulyaev VT, Ganik SV. Vliyaniye kachestva peska na svoystva penobetona [The influence of sand quality on the properties of foam concrete]. Vologodskiye chteniya [Vologda Readings]. 2012; 80:35-36. (in Russ.).

[13] Ruzhinskij S, Portik A, Savinyh A. Vse o penobetone [All about foam concrete]. Spb. Stroj-Beton. 2006, 632. (in Russ.).

[14] Bazhenov YUM. Betonnyye tekhnologii [Concrete Technology]. Stroyizdat [Strojizdat]. 1987, 209. (in Russ.).

[15] Altynbekova A, Lukpanov R, Dyussembinov D, Askerbekova A, Tkach E. Effect of a complex modified additive on the setting time of the cement mixture. Kompleksnoe Ispolzovanie Mineralnogo Syra = Complex Use of Mineral Resources. 2022; 325(2):29-38. https://doi.org/10.31643/2023/6445.15

[16] Altynbekova AD, Lukpanov RE, Yenkebayev SB, Dyussembinov DS, Yerzhanova NK. Bystrotverdeyushchiy rabotosposobnyy beton dlya proizvodstva buronabivnykh [Fast-hardening workable concrete for the production of bored]. Stroitel'stvo i rekonstruktsiya [Building and Reconstruction]. 2022; 2:99-111. (In Russ.). https://doi.org/10.33979/2073-7416-2022-100-2-99-111

[17] Altynbekova AD, Lukpanov RE, Dyussembinov DS, Askerbekova AM, & Gunasekaran M. Effect of a complex modified additive based on post-alcohol bard on the strength behavior of concrete. Kompleksnoe Ispolzovanie Mineralnogo Syra=Complex use of mineral resources. 2023; 327(4):5-14. https://doi.org/10.31643/2023/6445.34

[18] Lukpanov RE, Dyussembinov DS, Altynbekova AD, & Zhantlesova ZB. Research of Foam Concrete Components by Two-Stage Injection Method. In International Scientific Conference Industrial and Civil Construction Cham: Springer Nature Switzerland. 2022, 36-42.

[19] Lukpanov RE, Dyussembinov DS, Altynbekova AD, & Yenkebayev SB. Research on the Effect of Post-alcohol Bard on the Properties of the Cement-Sand Mixture. In International Scientific Conference Industrial and Civil Construction Cham: Springer Nature Switzerland. 2022, 107-113.

[20] Ngugi HN, Mutuku RN, Gariy ZA. Effects of sand quality on compressive strength of concrete: A case of Nairobi County and Its Environs, Kenya. Open Journal of Civil Engineering. 2014; 04(03):255-273. https://doi.org/10.4236/ojce.2014.43022

Crossref
DOI: 10.31643/2025/6445.02
Engineering and Technology

Overview of biodegradable polymers: synthesis, modification and application

[1]Moshera Samy, [2]Bekbayeva L., [3]Aeshah M. Mohammed, [2]Irmukhametova G., [4]Zhetpisbay D.S., [3]Noor M. Majeed, [2,5]Yermukhambetova B.B., [2,5*]Mun G.A.

[1]Polymers and Pigments Department, National Research Centre, Giza 12622, Egypt
[2]Al-Faraby Kazakh National University, Almaty, Kazakhstan
[3]University of Baghdad, Baghdad, Iraq
[4]KazNMU named S.D. Asfendiyarov, Almaty, Kazakhstan
[5]National Engineering Academy of the Republic of Kazakhstan, Almaty, Kazakhstan

**Corresponding author: mungrig@yandex.ru*

Received: *January 8, 2024*
Peer-reviewed: *February 1, 2024*
Accepted: *February 13, 2024*

ABSTRACT
Biodegradable polymeric represents a growing field. Owing to their wide-ranging properties, both synthetic and natural polymeric materials perform a vital and ubiquitous role in everyday life. Amended natural polymeric materials such as starch, cellulose, lignin, chitosan, cottonseed shell (CTS), and cotton gin trash (CGT) have enhanced properties, while synthetic Biodegradable polymeric materials such as poly (vinyl alcohol) (PVA), biodegradable plastics, biodegradable foams. Bioplastics are a kind of polymers able to be degraded by different microorganisms to small molecules (e.g., H_2O, CO_2, and CH_4). Bioplastics are observed to solve waste materials and biodegradability is just a new material to be exploited at the end of its life in specific terms. They should be used for applications that require cheap methods to dispose of items after it has fulfilled their job (e.g., for food packaging, agriculture, or medical products).

Keywords: Biodegradable polymers, starch**,** biodegradable plastics**,** biodegradable foams.

Information about authors:

Moshera Samy *Polymers and Pigments Department, National Research Centre, 33 El Buhouth St., Dokki, Giza 12622, Egypt. Moshera_samy1984@yahoo.com*

Lyazzat Bekbayeva *National Nanotechnology Open Laboratory, Al-Faraby Kazakh National University, al-Farabi av., 050040, Almaty, Republic of Kazakhstan. Email: lyazzat_bk2019@mail.ru*

Aeshah M. Mohammed *Department of Chemistry, College of Education for Pure Science (Ibn_ Alhaitham), University of Baghdad, Baghdad, Iraq. Email: aeshah.m.m@ihcoedu.uobaghda.iq*

Irmukhametova Galiya *Department of Chemistry & Technology of Organic Materials, Polymers and Natural Compounds, Al-Faraby Kazakh National University, al-Farabi av., 050040, Almaty, Republic of Kazakhstan. Email: galiya.yrmuhametova@kaznu.edu.kz*

Zhetpisbay Dinara *Department of Biochemistry, School of General Medicine-1, KazNMU named S.D.Asfendiyarov, 480012, Tole bi, 88, Almaty, Kazakhstan. Email: zhetpisbay.d@kaznmu.kz*

Noor M. Majeed *Department of Chemistry, College of Education for Bure Science, Ibn_ Alhaitham, University of Baghdad, Baghdad, Iraq. Email: noor.m.m@ihcoedu.uobaghdad.edu.iq*

Bayana B. Yermukhambetova *National Engineering Academy of the Republic of Kazakhstan, Almaty 050010, Kazakhstan. Email: baya_yerm@mail.ru*

Mun Grigory *Department of Chemistry & Technology of Organic Materials, Polymers and Natural Compounds, Al-Faraby Kazakh National University, al-Farabi av., 050040, Almaty, Republic of Kazakhstan. Email: mungrig@yandex.ru*

Introduction

Biodegradable polymers were raised as promising eco-friendly, but they are susceptible to enzymatic cleavage. Many BPs developed until now, and microorganisms capable of degrading them have been found in nature [1]. Plastic objects become part of the present society because they possess many properties [6]: light-weight, flexible and elastic, easy to shape and colour, and electric insulation. These properties are rewardingly exploited for various applications. Some include containers with hard form as well as flexible films for application packaging, sell sheets, fibres for textiles, ropes, and mattresses or most kinds of coverings surface, and assembling agents such as coatings; elastomers; sealants and adhesives. These different applications demand different combinations of properties. Particularly required applications can be reached by reinforcing polymers with glass or carbon fibres, for forming composites [2]. Biodegradable plastic degradation is caused by

bacteria as well as fungal enzymes. The biodegradability of plastic bags depends on different factors including sand, water, humidity, and temperature. Also, plastics can be degraded by organisms to CO_2, methane, water, and edible compost. Many commercial plastics are converted into compost rather than gaseous products. For plastic to be compostable, the organic matter formed should be harmless to animals or plants.

The compost can form an industrial compost at room temperature with waste food, in industrial facilities at controlled temperatures (typically 58 °C)[3]. So, classification of biodegradable polymers: Natural and biodegradable polymers

– *e.g.,* poly(saccharides), like starch, lignin, cellulose, chitosan, guar gum, collagen, albumin, etc.

Synthetic biodegradable polymers

- *e.g.,* aliphatic polyesters like polyvinyl alcohol (PVA), poly(orthoesters), poly(anhydrides), poly(phosphazenes), poly (amino acids), trimers, BDMPs, etc.

Natural Biodegradable polymeric materials (BPMs)

Starch(S)

Starch is a natural polysaccharide, and is a homopolymer of Glucopyranose units with the molecular weight $(C_6H_{10}O_5)_n$. Amylose and amylopectin are two different forms of polymer chains that make up starch. While amylopectin is a branching polymer consisting of -1,4-glycosidic with branched-chain linked by-1,6-glycosidic bonds, amylose is a straight chain -1,4-glyco-sidic links. Each of these polymers receives unique features as a result of this conformational change. For instance, the crystalline area of the granules is caused by the short branching of amylopectin at the-1,6-glycosidic linkages [4].

For example, authors studied PVA with corn starch (CS) at a 70/30 weight per cent proportion, arranged utilizing an answer projecting technique, and integrated attapulgite at different sums (0.0-1.0 grams). The review is expected to evaluate the effect of attapulgite on the biodegradability and ductile properties of the PVA/CS lattice, contrasting all outcomes and the control test (PVA/CS). The presence of attapulgite blocked the debasement cycle in enzymatic, soil, and manure entombment conditions. Water sorption content expanded with longer inundation times. The PVA/CS with 0.2 grams of attapulgite content showed the most noteworthy rigidity and stretching at break among the tried examples [5].

Another study, revised the effect of PVA and nano-SiO_2 on the enzymatic hydrolysis of thermoplastic starch (TPS) mixes utilizing α-amylase and amyloglucosidase catalysts [6]. Mixes with 5 wt.% nano-SiO_2 displayed a critical decrease in the rate and degree of starch hydrolysis, proposing communications among starch and nano-SiO_2 that obstructed enzymatic assault — the absolute solids staying following 6000 minutes diminished with expanding nano-SiO_2 content. The pace of glucose creation diminished with nano-SiO_2 expansion: 226 µg/ml h (TPS: PVA), 166 µg/ml h (TPS: PVA:1% nano-SiO_2), 122 µg/ml h (TPS: PVA:3% nano-SiO_2), and 94 µg/ml h (TPS: PVA:5% nano-SiO_2). The review laid out that nanoparticles block debasement, and the weakness to enzymatic corruption follows the request: TPS: PVA > TPS: PVA: nano-SiO_2.

, Domene-López *et al.* [7] made biodegradable coatings by dissolved blending potato starch and PVA with various centralizations of rosin. Glycerol was utilized as a plasticizer. Rosin, an inexhaustible item, went about as a handling help and support specialist because of its moderately high sub-atomic weight. The expansion of 8% rosin to starch/PVA mixes brought about films with rigidity surpassing 10 MPa and stretching at a break near 2000%. These qualities are practically identical Iskalieva *et al.* [8] united mix copolymers (PVA/S) with polyethylene glycol methyl methacrylate (PEGMA) in different proportions to concentrate on the effect on biodegradability. The mix copolymer was made out of poly (vinyl alcohol) (PVA) and starch (S). FTIR spectroscopy uncovered hydrogen bond connections between PVA, S and PEGMA. The chemical structure of the (PVA/S)-g-PEGMA obtained. TGA and SEM investigations portrayed the subsequent polymers (PVA/S/PEGMA). Mechanical properties of the mix films were fundamentally affected by PEGMA, with film corruption time expanding with higher PVA and S contents and atomic weight (MW) of PEGMA. The M8 test (PVA/S/PEGMA in a 3:1:2 proportion, separately) with an MW of 950 g/mol displayed the most minimal extension at break (67.5%), while M1 (PVA/S/PEGMA in a 1:1:1 proportion, separately) with a MW of 300 g/mol had the most noteworthy (150%). Uniting PEGMA onto the mixing polymer further developed film rigidity and stretching at the break. The glass progress temperature (T_g) and softening temperature (T_m) expanded with higher PEGMA MW, recommending that expanded chain and atomic weight be added to raised T_g and T_m in the copolymers.

Cellulose

Cellulose is a renewable polymer found in trees, bacteria, algae, plants as well as tunicates. The structure of cellulose is a linear called homopolysaccharide with highly ordered β-1.4-linked anhydro-D-glucose units, which aggregate to form cellulose fibrils. Cellulose results from the extraction of the crystalline from the amorphous portion by acid hydrolysis [9].

For instance, Ong *et al.* [10] examined PVA composite coatings with the consolidation of microcrystalline cellulose (MCC), commercial-grade cellulose nanocrystals (NCCA), and nanocellulose (NCCB) from oil palm fiber. The nanofillers showed uniform scattering in the PVA lattice, with shifting molecule sizes. The expansion of 5 wt.% microcrystalline cellulose worked on extreme elasticity (UTS) and yield strength however decreased greatest lengthening. Integrating 5 wt.% nanocellulose from oil palm fibre expanded UTS, yield strength, and flexible modulus while keeping up with the greatest prolongation. Adding business-grade cellulose nanocrystals (up to 10 wt.%) improved UTS, yield strength, and most extreme extension while keeping up with flexible modulus. Soil internment tests uncovered sped-up corruption with dampness, and the coatings were completely disintegrated following 7 days. Under controlled conditions, the heaviness of coatings remained generally unaltered following 28 days. The created PVA composite coatings displayed better mechanical execution and biodegradability looked at than a financially accessible biodegradable plastic pack (Bio-PB), recommending their true capacity as harmless to the ecosystem options.

In another study, Haque *et al.* [11]presented a financially savvy strategy for creating bio-plastic from a mix of PVA and cotton gin junk (CGT) as a possible option in contrast to non-biodegradable plastics in bundling. The effect of plasticizers (diethylene glycol, glycerol, and urea) and the covering specialist ethyl cellulose (EC) was examined. Urea displayed the best execution as a plasticizer, giving adaptability, decreased crystallinity, and further developed dampness ingestion, transmission, and warm security. The composite coatings, with properties equivalent to business LDPE, showed higher elasticity and water opposition. The expansion of EC upgraded water opposition and UV obstruction, making the coatings cloudy. The assessed cost of power and synthetic substances per gram of film creation was viewed as financially reasonable. Generally speaking, this study presents a functional strategy for delivering water-safe adaptable bioplastic with the possibility to address flow plastic contamination issues.

Lignin

Lignin is the second renewable biomass polymer and has potential as a sustainable material because of its abundance and high concentration of aromatic, complex lignin with poor chemical structure and excessive reaction sites limit its applications [12].

For instance, Su *et al.* [13] studied improving the presentation and decreasing the expense of PVA films for biodegradable mulch applications. The synergistic impact of sodium alginate and quaternary lignin was recognized as a key element. The composite coatings showed further developed water maintenance, UV obstruction, heat assortment, light transmission, mechanical properties, and soil combination. Lignin expansion guaranteed total UV obstruction, while sodium alginate synergistically improved mechanical strength and water-holding properties. The coatings exhibited better soil drooping, and their water fume porousness came to 109.2 $g/m^{2}\cdot$ day. The self-corruption properties of sodium alginate and lignin worked with film debasement, with a 55% debasement seen following 50 days. In general, the review features a promising methodology for creating practical and elite execution biodegradable coatings for mulch applications.

Synthetic biodegradable Polymeric materials

Polyvinyl alcohol (PVA)

PVA is sold form dissolved in water and biodegradable polymer which is used in various biological applications. PVA has high aqueous phase solubility and biodegradable properties due to its polymeric nature. PVA and its derivatives have demanded great recent attention [14].

For example, Belay [15] tends to the natural worries related to customary plastics and features the rise of biodegradable plastics as another option. Specifically, it centres around agar and PVA as promising biodegradable materials that don't add to deforestation or affect food supplies. Nonetheless, these materials show impediments like high water ingestion and moderate rigidity. The survey examines physicochemical change strategies utilized by scientists to upgrade the properties of biodegradable polymers, with a particular accentuation on agar and PVA. Points covered incorporate the rudiments of polymers, the science

of biodegradation, the ecological effects of biodegradable polymers, and endeavors to work on their properties for different applications.

Authors revised [16] the impacts of glycerol and sorbitol as plasticizing specialists on the properties of biodegradable polyvinyl alcohol (PVOH)/rambutan skin squander flour (RWF) films. Glycerol-plasticized films showed higher extension at break, yet lower rigidity and Young's modulus contrasted with sorbitol-plasticized films. The expansion of plasticizing specialists expanded the water fume transmission rate (WVTR), with glycerol-plasticized films showing higher WVTR, demonstrating glycerol's more prominent water partiality than sorbitol. In biodegradability tests, unplasticized PVOH/RWF films displayed lower weight reduction contrasted with glycerol-and sorbitol-plasticized films.

In another study, Li *et al.* [17]explored the effect of phytic corrosive (PhyAc) on the intermolecular hydrogen-holding, structure, chain elements, and mechanical properties of PVA in a biodegradable PVA/PhyAc composite. Sub-atomic element recreations and trial strategies were consolidated for the investigation. The quantity of PVA-PhyAc hydrogen bonds per PhyAc atom and complete hydrogen bonds show various conditions on PhyAc content. The composite with 1.9 wt% PhyAc shows diminished free volume and a more modest dissemination coefficient. The glass progress temperature (T_g) of PVA arrives at its greatest at around 1.25 wt % PhyAc. Remarkably, the expansion of 10 wt % PhyAc brings about the most elevated elasticity and great antibacterial capacity in PVA. The review gives experiences into how little atoms impact the construction and mechanical properties of polymers, extending the likely utilization of PVA/PhyAc in different businesses.

Panda *et al.* [18] in their survey centres around the new improvements in PVA and normal polymer-based films for applications in food bundling. PVA-based materials are esteemed for their biocompatibility, biodegradability, antimicrobial properties, non-harmfulness, and simplicity of film arrangement. While past writing has focused on manufactured PVA or PVA-based nanomaterials, there is a developing interest in normal polymers because of their harmless to the ecosystem nature. The survey features the utilization of PVA/regular polymer-based films in food bundling and examines the joining of bio-waste and organic product strips in composite coatings. Furthermore, research patterns in PVA films are investigated, giving bits of knowledge into the measurements of distributions in this field.

Authors researched and successfully created and analyzed environmentally friendly materials for the first time. These materials are made of a fully biodegradable substance called PVA and belong to a category known as single polymer composites (SPC) [19]. Through various tests, they demonstrated the feasibility of producing these composites within a suitable temperature range. Microscopic images showed that the desired reinforcement structure was maintained only when using high melting temperature fibres like WN8. The addition of PVOH fibres significantly enhanced the stiffness, yield properties, and Vicat softening temperature of the original PVA matrix, depending on the number of fibres added. However, as the fibre content increased, there was a decrease in the material's ability to stretch, and it became more prone to breakage. The introduction of fibres had a positive impact on the stability of the composites, leading to notable improvements in their viscoelastic properties. The storage modulus and glass transition temperature increased compared to the pure PVA, while the creep compliance values decreased significantly across all tested temperatures.

Rahman and Goswami *et al.* [20] studied the mechanical as well as barrier properties of PVA, which are useful for packaging purposes. The influence of bioactive elements added to the PVA matrix was also studied, particularly their ability to protect food from pathogens and prevent rapid expiration. Furthermore, an examination has been conducted on mitigation measures, specifically focusing on the biodegradability of industrial wastes generated by various manufacturing facilities.

Biodegradable foam (BF)

For instance, in Hendrawati *et al.* [21], the influence of PVA on the production of biodegradable foam from sago starch was determined. The production of biodegradable foam occurs at 125°C during the baking process, with a duration of one hour. The concentrations of PVOH varied from 0 to 50 wt. %. According to the results of the water absorption test, biodegradability test, and tensile test, an increase in PVOH concentration has a positive impact on water absorption, biodegradability, and tensile strength. The ideal state was achieved through the incorporation of 30% PVOH, resulting in water adsorption, biodegradability, and tensile strength values of 29.42%, 25.13%, and 2.22 MPa, respectively.

Authors studied that mixing of microfibrillated cellulose (MFC) suspension and polyvinyl alcohol results in the formation of MFC-based thin membrane-like biodegradable composites. The desired MFC content within the composites could be easily achieved by adjusting the concentration of the PVA solution [22]. To enhance the mechanical and thermal properties of the composites and render PVA partially water-insoluble, chemical crosslinking of PVA was conducted using glyoxal. Examination of the composite surfaces and fracture topographies revealed a strong bond between MFC fibrils and PVA, with uniform distribution. Infrared spectroscopy demonstrated the formation of acetal linkages in the MFC–PVA composites through glyoxal crosslinking.

Chemically altered waxy corn starch is a promising substance for creating biodegradable bioplastics. Yahia *et al.* [23] have studied the performance of films made from chemically modified waxy corn starch, along with their degradation by microbial enzymes. The effects of pre-gelatinization and the addition of cardanol oil as a mixed plasticizer with sorbitol were investigated. Biodegradable films were produced by blending waxy maize acetylated di-starch adipate (WADA) and waxy maize pregelatinized acetylated di-starch adipate (PWADA) with polyvinyl alcohol polymer using sorbitol and cardanol oil as plasticizers. The biodegradability of the films was studied through enzyme mixture testing and soil burial tests. The results showed that PWADA had a weight loss of 96% and a degradation percentage of 95.5%, which were significantly lower than WADA. The degradation was also evident from an increase in osmolality and the physical appearance of the film after 21 days. Various techniques were used to analyze the film's morphology, chemical structure, crystallinity, transparency, and thermal stability. Under an electron microscope, PWADA films had a more uniform surface. The film’s infrared spectra indicated similar chemical structures. The X-ray diffraction analysis revealed that WADA had an A-type crystalline structure, while after thermoplasticization, PWADA showed a V-type crystal pattern. The addition of cardanol oil resulted in UV absorber films. Furthermore, thermal stability was improved with the addition of cardanol oil. The water uptake rate and water vapor permeability increased after the pre-gelatinization of WADA films but slightly decreased after the addition of cardanol oil. Additionally, pre-gelatinization decreased the film's elongation but increased its strength. Overall, the chemically modified waxy maize starch film has the potential to be a biodegradable, thermally stable, and UV absorber film for packaging materials.

Liu *et al.* [24] explored how different amounts of polyvinyl alcohol (PVA) and its hydrolysis degree could improve the properties of the foams. By diving into the complex relationship between melt viscoelasticity and foam characteristics, we discovered some intriguing results. Increasing the hydrolysis degree of PVA had a significant impact on the foams, making them more suitable for various applications. The improvements observed in their foaming behaviors, viscoelastic properties, thermal stabilities, and mechanical performances were all linked to the interactions between starch and PVA chains, like hydrogen bonding and intermolecular entanglements. Additionally, incorporating PVA led to an impressive reduction in water absorption capacity. The foam that comprised 20% PVA with a hydrolysis degree of 98% demonstrated exceptional properties, including minimal water absorption, low density, excellent foaming ratio, and remarkable porosity. These qualities were on par with those of commercially available expanded polystyrene (EPS). Moreover, the addition of 20% PVA resulted in the highest compressive strength and recovery, hinting at its great potential for diverse cushioning applications. In conclusion, this research sheds light on the extensive possibilities for using starch-based foams in large-scale industrial settings, opening exciting avenues for their wider application.

There have been questions and misunderstandings surrounding the impact of liquid detergent capsules on the issue of environmental microplastics. To clarify, the film used in these detergent capsules is highly soluble in water, including cold water, as it needs to fully dissolve during the washing process. The film is typically made from water-soluble grades of polyvinyl alcohol, which is a recognized biodegradable material. Byrne *et al.* [25] conducted tests to confirm the biodegradability of various polyvinyl alcohol films commonly used in detergent capsules. The results showed that these films are readily biodegradable. Moreover, their high water solubility means that these detergent capsule films do not fall within the category of microplastics. Additionally, their biodegradability ensures that there are no concerns regarding persistence or accumulation in the environment.

In the world of packaging, there is a growing need for biodegradable composite plastics that can outperform synthetic polymer materials. Su *et al.*

[26] studied the use of a solvent-casting method to create different combinations of composite plastics using polyvinyl alcohol (PVA), esterified starch, and gliadin. Comparing these to pure PVA plastics, we found that the PVA/starch/gliadin composites exhibited lower hydrophilicity, superior tensile properties, and higher biodegradability. Although the elongation at break was lower, these composites showed promising characteristics. Through various analytical techniques, such as scanning electron microscopy, atomic force microscopy, X-ray diffraction, Fourier infrared spectra, and light transmittance measurements, we observed that the PVA/starch/gliadin plastics exhibited good compatibility due to hydrogen bonding. Interestingly, the different ratios of components in the plastics led to varying colours. Additionally, as the content of esterified starch increased, the melting and crystallization enthalpies of the composite plastics increased. Notably, at a ratio of 25% PVA and 75% starch/gliadin, the composite plastics had the lowest hydrophilicity, surpassing that of pure PVA plastics. When PVA comprised 50% and the ratio of starch to gliadin was 75%/25%, the ternary composite plastics demonstrated the highest tensile properties. Furthermore, when PVA accounted for 75% and starch accounted for 25%, the elastic modulus of the PVA/starch plastics reached its peak. Moreover, composite plastics showed higher biodegradability compared to pure PVA plastics. These environmentally friendly PVA/starch/gliadin plastics, with their versatile composition ratios, have great potential for various applications, including packaging water-sensitive goods and bearing heavy objects in real-world production scenarios.

To combat the pollution caused by mishandling petroleum-based plastics, there has been a significant interest in green composites that utilize biodegradable plastics and biomass waste. However, there is still a challenge in finding the right balance between mechanical performance and biodegradability. Tian *et al.* [27] proposed a novel concept for water-soluble composite materials using PVA and biomass waste. Unlike conventional degradation into small molecules, the PVA matrix in our composites can dissolve in water when in contact with soil. To enhance the mechanical and thermal properties, we utilized solid-state shearing milling (S3M) technology to composite PVA with waste cottonseed shell (CTS). This resulted in impressive performance, with the PVA/CTS composites achieving a maximum tensile strength of 10.3 MPa and a degradation temperature of approximately 250 °C. Furthermore, our soil burial test demonstrated that even if the PVA matrix does not degrade in the environment in the short term, its water-soluble nature ensures environmental friendliness. Within just 10 days, the PVA matrix dissolves in the soil without causing any adverse effects on plants (specifically wheat) or animals (particularly earthworms). This research not only presents the development of a range of eco-friendly PVA/biomass composites but also contributes new insights into the environmental compatibility of PVA-based materials.

Starch-based biodegradable films (S-BFs)

S-BFs are not ideal for food packaging due to their weak mechanical strength and limited barrier properties. However, by combining two or more polymers, there is a possibility to create innovative materials with enhanced functionality. Gómez-Aldapa *et al.* [28] explored various proportions (ranging from 0% to 60%) of polyvinyl alcohol (PVOH) in potato starch films to examine the impact on water absorption, water vapour permeability (WVP), mechanical properties (elongation at break and tensile strength), and thermal properties (Tg). Throughout all the formulations, the two polymers demonstrated excellent compatibility during processing and in the resulting material. The inclusion of PVA significantly improved the functional properties, gas permeability, and mechanical strength of the potato starch films. Notably, the formulation containing 60% PVA (S4P6) showcased the greatest resistance to water vapour, lower density, enhanced solubility, and superior mechanical performance. PVA proved to be a valuable addition to potato starch films, rendering them suitable for potential use in food packaging and as an eco-friendly alternative to synthetic packaging materials.

In response to increased environmental awareness and regulations, the plastic industry has been making efforts to develop environmentally friendly products and processes. For example, authors [29] make an overview of the advancements made in thermoplastic starch, polyvinyl alcohol blends, and nanocomposites. These materials offer a wide range of physical properties and other benefits, all at an acceptable cost and rate of biodegradation, making them suitable for various applications. To further enhance their properties, such as mechanical strength and moisture resistance, innovative techniques like cross-linking and the incorporation of new nanoparticles have

been explored. These advancements have enabled the creation of materials with diverse property profiles that can even rival synthetic polymers in terms of both price and performance in different applications.

Authors [30] conducted a study to analyze how additives affect the properties of biodegradable films composed of PVA and tapioca starch. Three additives, specifically glycerol (GLY), polyethene glycol (PEG), and glutaraldehyde (GLU), were utilized in the research. The PVA/tapioca starch blend films were produced through a mixing process followed by casting. Higher levels of GLY and PEG resulted in increased elongation at break for the blend film. However, the tensile strength decreased therefore. Additionally, the inclusion of a plasticizer improved the blend film's biodegradability, water absorption, and water vapour transmission. Interestingly, contrasting outcomes were observed when GLU was incorporated into the blend film.

Patil *et al.* [31] aimed to enhance the properties of starch-based biodegradable films through polymer blending. To achieve this, composite films were created by incorporating different proportions of PVA (ranging from 10% to 90% of starch weight) using the solvent casting method. Several aspects, including mechanical behaviour, barrier properties, water solubility, water contact angle, and biodegradability, were examined for all the films. The addition of PVA to the starch polymer had a significant positive impact ($p < 0.05$) on the mechanical and barrier properties of the composite films. Notably, the highest improvement in mechanical behaviour was observed in the SP90 composite film, which contained a higher percentage of PVA. This film demonstrated a remarkable 1.93-fold increase in tensile strength (TS), a 3.74-fold increase in elongation (E), and a 1.72-fold increase in breaking strength (BS) compared to the pure starch film. In terms of barrier properties, the maximum incorporation of PVA resulted in a 52% decrease in water vapour permeability (WVP) and a 57% decrease in oxygen permeability (OP) in the composite films, making them effective barriers against moisture and oxygen gas. The Fourier-transform infrared spectroscopy and scanning electron microscopy analysis of the films confirmed the excellent compatibility between starch and PVA polymers. Interestingly, these composite films degraded rapidly when subjected to moistened soil, with complete degradation occurring within three weeks of burial. The biodegradability study revealed the promising potential of starch-PVA composite films as environmentally friendly materials for food packaging applications.

Alonso-López *et al.* [32] examined the potential impact of polyvinyl alcohol (PVA)-based polymers upon release into the marine environment, focusing on biodegradation in seawater (evaluated by the percentage of Theoretical Oxygen Demand, or % ThOD, for each compound) and aquatic toxicity using the standard toxicity test with Paracentrotus lividus larvae. Three materials were tested, including two PVA-based ones with glycerol and another made from pure PVA. The biodegradation of PVA under marine conditions without an acclimated inoculum appears negligible, but it shows a slight improvement when combined with glycerol, achieving 5.3% and 8.4% ThOD after 28 days. The toxicity of pure PVA is also minimal (<1 toxic unit, TU), but it increases slightly when glycerol is included in the material (2.2 and 2.3 TU). These findings contribute to a more comprehensive understanding of the behaviour of PVA-based polymers in marine environments. Despite the low biodegradation rates observed, further research is necessary to develop PVA polymers that are genuinely degradable in real marine scenarios.

Pérez-Blanco *et al.* [33] prepared blends using ethylene-vinyl alcohol samples containing 27% and 38% ethylene, incorporating 30% and 50% thermoplastic starch (TPS) plasticized with glycerol. The biodegradability and cytotoxicity of these blends were examined using various techniques (XRD, DSC, TGA, CA, ATR-FTIR, SEM). The presence of TPS had a notable impact on copolymer behaviour, evidenced by the emergence of O-H IR bands at 1000–1170 cm^{-1} and an overall reduction in ethylene-vinyl alcohol crystallinity, melting point, thermal stability, and hydrophobicity. Biodegradation was more effective in the presence of TPS, leading to the formation of a resilient biofilm by a consortium of three bacteria.

Lower ethylene content facilitated biodegradation, rendering the material more easily metabolizable. Mineralization percentages reached up to 66% (EVOH- 27/TPS 50:50) after a 40-day bioassay at 45 °C. In vitro, cytotoxicity assays showed no cytotoxicity both before and after biodegradation. EVOH/TPS blends are proposed as a potential environmentally friendly substitute for pure synthetic polymers.

Julinová *et al.* [34] investigated the biodegradation of blow-molded films composed of poly(vinyl alcohol) (PVA)/protein hydrolysate (PH),

incorporating starch (S) and lignin (LI) as biodegradation enhancers. The goal was to enhance the biodegradation rate of PVA while maintaining or improving the technical and usage properties of the blends. The objective was to achieve the maximum breakdown rate, facilitating rapid disintegration of PVA at a wastewater treatment plant. Activated sludge from a municipal wastewater treatment plant was chosen as the biological material. The preparation of blends involved the use of glycerol (G) as a plasticizer, enabling successful processing but extending the lag phase of PVA breakdown and reducing its final biodegradation percentage. The influence of G, in this regard, remained unaffected by the inclusion of PH. While S and LI mitigated the impact of the plasticizer, they caused a breakdown rate comparable to PVA alone. Conversely, adapting biomass to PVA, when G was applied, resulted in a threefold increase in the PVA breakdown rate, albeit with a fivefold prolonged lag phase. However, the extended breakdown duration, surpassing the retention time of wastewater during activation, negated the positive effect. The addition of PH to the blends did not show a favourable impact. The incorporation of S led to a shorter lag phase, and the degradation rate increased by approximately 1.5 times. The combination of LI and S significantly accelerated blend degradation, but the drawback was an incomplete breakdown of the substrate, lowering the final biodegradation percentage. As a compromise, a blend of PVA/G PH S was identified, with a breakdown time half that of pure PVA and mechanically more convenient films.

Haque *et al.* [35] created a biodegradable composite plastic film by combining cotton gin trash (CGT), a promising lignocellulose resource, with poly(vinyl alcohol) (PVA). The composite film maintained a 50:50 CGT/PVA ratio, utilizing both coarse and fine CGT powder particles. The study investigated the impact of particle size on various properties such as morphology, crystallinity, tensile strength, optical transmittance, thermal stability, and biodegradability. The scanning electron microscope (SEM) image revealed a uniform distribution of CGT in the PVA matrix, especially with the fine powders (~5.7 µm). The incorporation of CGT improved tensile strength, biodegradability, and thermal stability, and provided complete UV protection. Although the flexibility of the composite film decreased, the tensile strength increased by 10% and 20% with the coarse and fine CGT powders, respectively, compared to the pure PVA film. Considering the estimated fabrication cost in the study, findings suggest that CGT has significant potential as a cost-effective reinforcement material for PVA in the production of biodegradable plastic.

Song *et al.* [36] enhanced the toughness of poly (vinyl alcohol)-cryogens (PVA-CGs) by adjusting three key parameters: PVA concentration (7.5%–12.5%), freezing–thawing cycles (1–5 FTCs), and the inclusion of 0%–10% glycerol as a cryoprotectant. This research explored the impact of shear stress-induced destruction (SSID) on mechanical strength, achieved by inducing rapid erosion through high frictional force. The tolerance to SSID (Tol-SSID) demonstrated varying sensitivities and trends based on the fabrication parameters. The assessed Tol-SSID displayed consistent and inconsistent correlations with tensile strength and swelling, respectively. The evaluation of Tol- SSID provides valuable insights into the practical mechanical strength of PVA- CGs against intense friction, simulating extreme shear stress in a bioreactor. A PVA-CG with a 10% PVA concentration and two FTCs showed Tol-SSID and tensile strength of 88.3% and 0.59 kPa, respectively. Additionally, 5% glycerol was added to maintain bacterial respiration activity for immobilized nitrifiers, resulting in a survival rate of 88.6% and an oxygen consumption rate of 0.097 mg-O_2/g-VSS·min. In continuous nitrification mode using the optimized PVA-CG for 10 days, an ammonia removal rate of 0.2173 kg-N/m^3·d was achieved, representing an improvement compared to cases without glycerol addition (0.1426 and 0.1472 kg-N/m^3·d for PVA-CGs in two and three FTCs, respectively).

Pan, Y. *et al.* [37] studied wastewater containing poly(vinyl alcohol) (PVA) can have a dissolved organic carbon concentration of up to 10,000 mg/L, leading to significant chemical oxygen demand (COD) issues, especially in industries like textiles and chemicals. To address this, we propose a two-stage treatment method involving Fenton pre-oxidation and Ca-induced coagulation to reduce PVA and COD levels. Optimal concentrations of FeSO4 and CaCl2 per gram of PVA were found to be 0.8 g/g- PVA and 4.0 g/g-PVA, respectively—considerably lower than reported in other treatments. Successful oxidation broke down the long chains of PVA molecules, partially converting hydroxyl (OH) groups to carboxyl (COOH) groups. In the coagulation stage, Ca^{2+} is effectively bound to the pre-oxidized PVA products, forming insoluble compounds. Applying this two-stage process to wastewater with initial COD and PVA concentrations of 20,450 and 10,000 mg/L, respectively, resulted in the removal of up to 81.3% COD and 96.0% PVA. Additionally, the sludge residue demonstrated a capacity to adsorb Sb (III) from the

wastewater, achieving an adsorption capacity of 16.0 mg/g. This study offers valuable insights into an economical and efficient approach for treating high-concentration PVA- PVA-containing wastewater.

Lan *et al.*[38] created active biodegradable packaging films using a combination of polyvinyl alcohol (PVA), chitosan (CS), and d-Limonene (DL). The study systematically investigated the impact of varying DL content levels (0%, 2.5%, 5%, 7.5%, and 10% w/w) on the structural, mechanical, biodegradable, and antimicrobial properties of PVA/CS films. Fourier transforms infrared (FTIR) spectroscopy and scanning electron microscopy (SEM) revealed the favorable compatibility between DL and PVA/CS, as well as a more uniform continuous, flat, and smooth surface. The incorporation of DL significantly enhanced the antibacterial, mechanical, and barrier properties of PVA/CS films, contributing to their substantial biodegradability. However, excessive DL loading was found to weaken the hydrogen bonds between polymer chains, negatively impacting the physical performance of the film. Notably, the PVA/CS/DL-5% film exhibited the highest water contact angle and transmittance value. Moreover, it effectively preserved packaged mango fruits over a 10-day storage period at 20 ± 2°C, as evidenced by assessments of fruit weight loss, decay rate, firmness, titratable acidity, soluble solids, and ascorbic acid. In conclusion, DL/PVA/CS composite films show promise as environmentally friendly packaging materials for food preservation.

Bian *et al.* [39] investigated that bacteria capable of degrading polyvinyl alcohol (PVA) were identified through screening sludge samples, where PVA served as the sole carbon source. A new bacterial strain, identified as Bacillus 9iacin, was isolated based on partial 16S rDNA nucleotide sequencing and morphological analysis. The PVA-degrading enzyme (PVAase) from Bacillus 9iacin was then immobilized as cross-linked enzyme aggregates (CLEAs) through a process involving ammonium sulfate precipitation followed by glutaraldehyde cross-linking. The impacts of precipitation and cross-linking on PVAase-CLEAs activity were studied and characterized. Precipitation with 70% ammonium sulfate and a 1.5% glutaraldehyde cross-linking reaction over 1 hour resulted in approximately 90% activity recovery for PVAase-CLEAs, indicating the potential for extended use without additional purification steps. Immobilization did not significantly alter the optimal pH and temperature values of the PVAase. The PVAase-CLEAs exhibited a spherical morphology and demonstrated improved efficiency in degrading PVA compared to the free PVAase in solution. Additionally, the PVAase-CLEAs displayed outstanding thermal stability, pH stability, and storage stability when compared to the free PVAase. After four usage cycles, the PVAase-CLEAs retained approximately 75% of their initial activity, suggesting their potential applicability for PVA degradation in industrial settings.

Biodegradable plastics (BP)

BP has emerged as a viable alternative to traditional plastics [[40], [41], [42], [43], [44], [45]]. This research employed the solvent casting method to create ternary plastics using varying proportions of octenyl succinic anhydride (OSA) esterified potato starch, gliadin, and polyvinyl alcohol (PVA), with subsequent characterization of their structural, physicochemical, and degradable attributes. The findings indicated that the composite plastic exhibited higher elastic modulus (EM), water resistance, and degradability compared to pure PVA. Optimal compatibility was achieved when the ratio of OSA potato starch to gliadin was 1:1, and PVA replacement was at 25%. Notably, with PVA constituting 75% of the total plastic composition, the composite plastics displayed larger values for Tm, ΔHc, and ΔHm compared to pure PVA plastics. This implies that the addition of OSA potato starch and gliadin enhances the biodegradability of PVA plastics, making them effective as food packaging materials with improved properties.

Authors [46] examined the impact of PVA molecular weight on the biodegradable properties of PVA/starch blends by blending PVAs of different molecular weights with varying compositions of cross-linked starch (CLS). A PVA exhibiting superior biodegradability was identified from the PVA/starch blends with higher biodegradability. Subsequently, this selected PVA was blended with acid-modified starch (AMS) to systematically investigate the effects of starch modification on the biodegradable characteristics of the PVA/starch blends. Higher molecular weight PVA demonstrated greater biodegradability across all PVA/starch blends. The biodegradability of PVA/modified-starch blends increased with higher modified starch contents, with PVA blended with 1N AMS showing superior biodegradability. Bio-reaction kinetics experiments indicated the decomposition tendencies of the PVA/starch blends under ambient conditions. According to the first-order reaction kinetic model, it is estimated that PVABF- 17/starch blends with

20% and 40% CLS would take approximately 16.20 years and 12.47 years, respectively, to degrade by 70%. In contrast, the specimen meets the biodegradable material criteria of the Environmental Protection Administration (EPA) of Taiwan. Overall, PVA/AMS specimens exhibit better decomposition potential than PVA/CLS specimens [[43], [47]].

Conclusion

Eco-friendly plastic materials become an interesting area due to their safety in industries such as packaging materials for the food industry, and applications in the medical and agricultural fields Novel biodegradable packages based on the percentage of biodegradablility of materials in different conditions and atmosphere attention. The produced biodegradable composite exhibits excellent tensile strength, outstanding thermal stability, pH stability, storage stability and environmentally friendly materials, making them effective barriers against moisture and oxygen gas

Prospects. The processes of development of biodegradable polymers are still in progress and to be simple with special recyle and cost-effective Also, many processes of development of biodegradable composites are expected soon as these new biodegradable polymers may possess effective and important properties such as excellent tensile strength, outstanding thermal stability, and environmentally friendly materials.

Declaration of Competing Interest

The authors declare that they have no known competing financial interests or personal relationships that could have appeared to influence the work reported in this paper.

Acknowledgements. The work was financially supported by the Ministry of Science and Education of the Republic of Kazakhstan, program-targeted financing out of competitive procedures for 2023–2025. Project No. (BR21882289), entitled “Development and implementation of technological aspects of the production and industrial application of functional carbon-silicon fillers”.

Conflicts of interest. The authors declare no conflict of interest.

Cite this article as: Moshera Samy, Bekbayeva L, Aeshah M Mohammed, Irmukhametova G, Zhetpisbay DS, Noor M Majeed, Yermukhambetova BB, Mun GA. Overview of biodegradable polymers: synthesis, modification and application. Kompleksnoe Ispolzovanie Mineralnogo Syra = Complex Use of Mineral Resources. 2025; 332(1):19-31. https://doi.org/10.31643/2025/6445.02

Биологиялық ыдырайтын полимерлерге шолу: синтезі, модификациясы және қолданылуы

[1]Moshera Samy, [2]Бекбаева Л., [3]Aeshah M. Mohammed, [2]Ирмухаметова Г., [4]Жетпісбай Д.С., [3]Noor M. Majeed, [2,5] Ермұхамбетова Б.Б., [2,5*]Mun G.A.

[1]Ұлттық зерттеу орталығы, Гиза 12622, Египет
[2]Әл-Фараби атындағы ҚазҰУ, Алматы, Қазақстан
[3]Буретану білім беру колледжі, Бағдад университеті, Бағдад, Ирак
[4]С.Д. Асфендияров атындағы ҚазҰМУ, Алматы, Қазақстан
[5]Қазақстан Республикасының Ұлттық инженерлік академиясы, Алматы, Қазақстан

Мақала келді: *8 қаңтар 2024*
Сараптамадан өтті: *1 ақпан 2024*
Қабылданды: *13 ақпан 2024*

ТҮЙІНДЕМЕ

Биологиялық ыдырайтын полимерлер бұл дамып келе жатқан жаңа сала. Кең ауқымды қасиеттерінің арқасында синтетикалық және табиғи полимерлі материалдар күнделікті өмірде маңызды және барлық жерде қолданылады. Крахмал, целлюлоза, лигнин, хитозан, мақта қабығы (CTS) және мақта тазартатын машинадан шығатын қоқыс (CGT) сияқты түрленген табиғи полимерлік материалдар жақсы қасиеттерге ие. Поливинил спирті (ПВА), биологиялық ыдырайтын пластиктер, биологиялық ыдырайтын көбіктер синтетикалық био-ыдырайтын полимерлі материалдар. Биопластика - бұл әртүрлі микроорганизмдердің

	арқасында шағын молекулаларға (мысалы, H_2O, CO_2 және CH_4) дейін ыдырайтын полимерлердің бір түрі. Биопластика қалдықтарды ерітеді, ал биологиялық ыдырайтындығының арқасында белгілі бір жағдайларда қызметінің соңына дейін пайдалануға болатын жаңа қасиет. Биопластиктер өз жұмыстарын орындағаннан кейін заттарды кәдеге жаратудың арзан әдістерін қажет ететін қолданбалар үшін қолданылуы керек (мысалы, азық-түлік орауыштары, ауыл шаруашылығы немесе медициналық бұйымдар).
	Түйін сөздер: Биологиялық ыдырайтын полимерлер, крахмал, биологиялық ыдырайтын пластмассалар, биологиялық ыдырайтын көбіктер.
Мошера Сами	***Авторлар туралы ақпарат:*** *Полимерлер және Пигменттер, Ұлттық Зерттеу Орталығы, Египет, Эль Бухут көш., 33, Докки, Гиза 12622. Email: moshera_samy1984@yahoo.com*
Бекбаева Ляззат Кайратовна	*Ашық Түрдегі Нанотехнологиялық Зертхана, әл-Фараби атындағы Қаз¥У 71, әл-Фараби даңғылы, 050040, Алматы, Қазақстан. Email: lyazzat_bk2019@mail.ru*
Айша М. Мұхаммед	*Химия бөлімі, Буре ғылымы бойынша білім беру колледжі (Ибн-Алхайсам), Бағдад университеті, Бағдад, Ирак. Email: aeshah.m.m@ihcoedu.uobaghda.iq*
Ирмухаметова Галия Серикбаевна	*Химия және химиялық технология факультеті, әл-Фараби атындағы Қаз¥У 71, әл-Фараби даңғылы, 050040, Алматы, Қазақстан. Email: galiya.yrmuhametova@kaznu.edu.kz*
Жетписбай Динара	*Биохимия кафедрасы, Жалпы Медицина Мектебі 1, С.Ж. Асфендияров атындағы Қаз¥МУ, 480012, Төле би көшесі, 88, Алматы, Қазақстан. Email: zhetpisbay.d@kaznmu.kz*
Нур М. Маджид	*Химия бөлімі, Буре ғылымы бойынша білім беру колледжі, Ибн-Алхайтам, Бағдад университеті, Бағдад, Ирак. Email: noor.m.m@ihcoedu.uobaghdad.edu.iq*
Баяна Б.Ермұхамбетова	*атындағы Қазақстан Республикасының Ұлттық инженерлік академиясы, Алматы 050010, Қазақстан. Email: baya_yerm@mail.ru*
Мун Григорий Алексеевич	*Химия және химиялық технология факультеті, әл-Фараби атындағы Қаз¥У 71, әл-Фараби даңғылы, 050040, Алматы, Қазақстан. Email: mungrig@yandex.ru*

Обзор биоразлагаемых полимеров: синтез, модификация и применение

[1]Moshera Samy, [2]Бекбаева Л., [3]Aeshah M. Mohammed, [2]Ирмухаметова Г., [4]Жетпісбай Д.С., [3]Noor M. Majeed, [2,5]Ермұхамбетова Б.Б., [2,5]Mun G.A.

[1]Отдел полимеров и пигментов, Национальный исследовательский центр, Гиза 12622, Египет
[2] КазНУ им. Аль-Фараби, Алматы, Казахстан
[3] Педагогический колледж бурых наук, Багдадский университет, Багдад, Ирак
[4]КазНМУ им. С.Д. Асфендиярова, Алматы, Казахстан
[5]Национальная инженерная академия Республики Казахстан, Алматы, Казахстан

Поступила: *8 января 2024*
Рецензирование: *1 февраля 2024*
Принята в печать*: 13 февраля 2024*

Аннотация
Биоразлагаемые полимеры представляют собой развивающуюся область. Благодаря своим разнообразным свойствам как синтетические, так и природные полимерные материалы играют жизненно важную и повсеместную роль в повседневной жизни. Модифицированные природные полимерные материалы, такие как крахмал, целлюлоза, лигнин, хитозан, оболочка хлопкового семени (CTS) и мусор хлопкоочистительной машины (CGT), обладают улучшенными свойствами. Поливиниловый спирт (ПВС), биоразлагаемые пластмассы, биоразлагаемые пены - синтетические биоразлагаемые полимерные материалы. Биопластики — это разновидность полимеров, которые могут разлагаться различными микроорганизмами до небольших молекул (например, H_2O, CO_2 и CH_4). Замечено, что биопластики растворяют отходы, а биоразлагаемость — это всего лишь новое свойство, которое можно использовать в конце его срока службы в определенных условиях. Их следует использовать для применений, требующих дешевых методов утилизации предметов после того, как они выполнили свою работу (например, для упаковки пищевых продуктов, продуктов сельского хозяйства или медицинских товаров).

Ключевые слова: Биоразлагаемые полимеры, крахмал, биоразлагаемые пластики, биоразлагаемые пенопласты.

Мошера Сами	***Информация об авторах:*** *Факультет Полимеров и Пигментов, Национальный Исследовательский Центр, Египет, ул. Эль Бухут, 33, Докки, Гиза 12622. Email: moshera_samy1984@yahoo.com*
Бекбаева Ляззат Кайратовна	*Национальная Нанотехнологическая Лаборатория Открытого Типа, Казахский Национальный Университет Имени Аль-Фараби, Казахстан, Алматы, 050013, проспект Аль Фараби, 71. Email: lyazzat_bk2019@mail.ru*
Аиша М. Мохаммед	*Факультет химии, Педагогический колледж для естественных наук (Ибн Альхайсам), Багдадский университет, Багдад, Ирак. Email: aeshah.m.m@ihcoedu.uobaghda.iq*

Ирмухаметова Галия Серикбаевна	*Кафедра Химии и Технологии Органических Веществ, Природных Соединений и Полимеров, Химии и Химической Технологии, Казахский Национальный Университет Имени Аль-Фараби, Казахстан, Алматы, 050013, проспект Аль Фараби, 71. Email: galiya.yrmuhametova@kaznu.edu.kz*
Жетписбай Динара	*Кафедра биохимии, Школа Общей Медицины 1, КазНМУ имени С.Д. Асфендиярова, 480012, ул. Толе би, 88, Алматы, Казахстан. Email: zhetpisbay.d@kaznmu.kz*
Нур М. Маджид	*Факультет химии, Педагогический колледж для естественных наук, Ибн Альхайсам, Багдадский университет, Багдад, Ирак. Email: noor.m.m@ihcoedu.uobaghdad.edu.iq*
Баяна Б.Ермұхамбетова	*Национальная инженерная академия Республики Казахстан, Алматы 050010, Казахстан. Email: baya_yerm@mail.ru*
Мун Григорий Алексеевич	*Кафедра Химии и Технологии Органических Веществ, Природных Соединений и Полимеров, Химии и Химической Технологии, Казахский Национальный Университет Имени Аль-Фараби, Казахстан, Алматы, 050013, проспект Аль Фараби, 71. Email: mungrig@yandex.ru*

References

[1] Alhanish A, Ali GAM. Biodegradable Polymers. In: Ali GAM, Makhlouf ASH, editors. Handbook of Biodegradable Materials. Cham: Springer International Publishing. 2023, 263-291.

[2] Mukherjee C, Varghese D, Krishna J, Boominathan T, Rakeshkumar R, Dineshkumar S, et al. Recent Advances in Biodegradable Polymers–Properties, Applications and Future Prospects. European Polymer Journal 2023:112068.

[3] Filiciotto L, Rothenberg G. Biodegradable plastics: Standards, policies, and impacts. ChemSusChem 2021; 14:56-72.

[4] Abd El-Ghany NA, Elella MHA, Abdallah HM, Mostafa MS, Samy M. Recent Advances in Various Starch Formulation for Wastewater Purification via Adsorption Technique: A Review. Journal of Polymers and the Environment. 2023:1-34.

[5] Azahari NA, Othman N, Ismail H. Effect of attapulgite clay on biodegradability and tensile properties of polyvinyl alcohol/corn starch blend film. International Journal of Polymeric Materials. 2012; 61:1065-1078.

[6] Abbasi Z. Water resistance, weight loss and enzymatic degradation of blends starch/polyvinyl alcohol containing SiO2 nanoparticle. Journal of the Taiwan Institute of Chemical Engineers. 2012; 43:264-268.

[7] Domene-López D, Guillén M, Martin-Gullon I, García-Quesada JC, Montalbán MG. Study of the behavior of biodegradable starch/polyvinyl alcohol/rosin blends. Carbohydrate polymers. 2018; 202:299-305.

[8] Iskalieva A, Yesmurat M, Al Azzam KM, Ainakulova D, Yerbolat Y, Negim E-S, et al. Effect of Polyethylene Glycol Methyl Ether Methacrylate on the Biodegradability of Polyvinyl Alcohol/Starch Blend Films. Polymers. 2023; 15:3165.

[9] Ferreira F, Dufresne A, Pinheiro I, Souza D, Gouveia R, Mei L, et al. How do cellulose nanocrystals affect the overall properties of biodegradable polymer nanocomposites: A comprehensive review. European polymer journal. 2018; 108:274-285.

[10] Ong T, Tshai K, Choo H, Khiew P, Chung S. Mechanical performance and biodegradability of polyvinyl alcohol nanocomposite films. Materialwissenschaft und Werkstofftechnikю 2020; 51:740-749.

[11] Haque ANMA, Naebe M. Flexible water-resistant semi-transparent cotton gin trash/poly (vinyl alcohol) bio-plastic for packaging application: Effect of plasticisers on physicochemical properties. Journal of Cleaner Production. 2021; 303:126983.

[12] Kim S, Chung H. Fully biomass-based biodegradable polymers from lignin and raw castor oil: lignin-graft-castor oil. Polymer Chemistry. 2023; 14:4126-4137.

[13] Su W, Yang Z, Wang H, Fang J, Li C, Lyu G, et al. Synergistic Effect of Sodium Alginate and Lignin on the Properties of Biodegradable Poly (vinyl alcohol) Mulch Films. ACS Sustainable Chemistry & Engineering. 2022; 10:11800-11814.

[14] Verma C, Quraishi M. Polyvinyl alcohol (PVA) as a biodegradable polymeric anticorrosive material: A review on present advancements and future directions. Corrosion Engineering, Science and Technology. 2022; 57:796-812.

[15] Belay M. Review on Physicochemical Modification of Biodegradable Plastic: Focus on Agar and Polyvinyl Alcohol (PVA). Advances in Materials Science and Engineering 2023; 2023:4056020.

[16] Ooi ZX, Ismail H, Bakar AA, Aziz NAA. The comparison effect of sorbitol and glycerol as plasticizing agents on the properties of biodegradable polyvinyl alcohol/rambutan skin waste flour blends. Polymer-Plastics Technology and Engineering. 2012; 51:432-437.

[17] Li L, Xu X, Wang B, Song P, Cao Q, Yang Y, et al. Structure, chain dynamics and mechanical properties of poly (vinyl alcohol)/phytic acid composites. Composites Communications. 2021; 28:100970.

[18] Panda PK, Sadeghi K, Seo J. Recent advances in poly (vinyl alcohol)/natural polymer based films for food packaging applications: A review. Food Packaging and Shelf Life. 2022; 33:100904.

[19] Dorigato A, Pegoretti A. Biodegradable single-polymer composites from polyvinyl alcohol. Colloid and Polymer science. 2012; 290:359-370.

[20] Rahman L, Goswami J. Poly (Vinyl Alcohol) as Sustainable and Eco-Friendly Packaging: A Review. Journal of Packaging Technology and Research. 2023; 7:1-10.

[21] Hendrawati N, Sa'diyah K, Novika E, Wibowo AA. The effect of polyvinyl alcohol (PVOH) addition on biodegradable foam production from sago starch. AIP Conference Proceedings: AIP Publishing. 2020.

[22] Qiu K, Netravali AN. Fabrication and characterization of biodegradable composites based on microfibrillated cellulose and polyvinyl alcohol. Composites Science and Technology. 2012; 72:1588-1594.

[23] Yahia R, Owda ME, Abou-Zeid RE, Abdelhai F, El-Gamil HY, Abdo AM, et al. Biodegradable, UV absorber and thermal stable bioplastic films from waxy corn starch/polyvinyl alcohol blends. Biomass Conversion and Biorefinery. 2023, 1-18.

[24] Liu F, Zhang Y, Xiao X, Cao Y, Jiao W, Bai H, et al. Effects of polyvinyl alcohol content and hydrolysis degree on the structure and properties of extruded starch-based foams. Chemical Engineering Journal. 2023; 472:144959.

[25] Byrne D, Boeije G, Croft I, Hüttmann G, Luijkx G, Meier F, et al. Biodegradability of Polyvinyl Alcohol Based Film Used for Liquid Detergent Capsules: Biologische Abbaubarkeit der für Flüssigwaschmittelkapseln verwendeten Folie auf Polyvinylalkoholbasis. Tenside Surfactants Detergents. 2021; 58:88-96.

[26] Su C, Zhang X, Ge X, Shen H, Zhang Q, Lu Y, et al. Structural, physical and degradation characteristics of polyvinyl alcohol/esterified mung bean starch/gliadin ternary composite plastic. Industrial Crops and Products. 2022; 176:114365.

[27] Tian G, Li L, Li Y, Wang Q. Water-Soluble Poly (vinyl alcohol)/Biomass Waste Composites: A New Route toward Ecofriendly Materials. ACS omega. 2022; 7:42515-42523.

[28] Gómez-Aldapa CA, Velazquez G, Gutierrez MC, Rangel-Vargas E, Castro-Rosas J, Aguirre-Loredo RY. Effect of polyvinyl alcohol on the physicochemical properties of biodegradable starch films. Materials Chemistry and Physics. 2020; 239:122027.

[29] Tang X, Alavi S. Recent advances in starch, polyvinyl alcohol based polymer blends, nanocomposites and their biodegradability. Carbohydrate polymers. 2011; 85:7-16.

[30] Ismail H, Zaaba N. Effect of additives on properties of polyvinyl alcohol (PVA)/tapioca starch biodegradable films. Polymer-Plastics Technology and Engineering. 2011; 50:1214-1219.

[31] Patil S, Bharimalla AK, Mahapatra A, Dhakane-Lad J, Arputharaj A, Kumar M, et al. Effect of polymer blending on mechanical and barrier properties of starch-polyvinyl alcohol based biodegradable composite films. Food Bioscience. 2021; 44:101352.

[32] Alonso-López O, López-Ibáñez S, Beiras R. Assessment of toxicity and biodegradability of poly (vinyl alcohol)-based materials in marine water. Polymers. 2021; 13:3742.

[33] Pérez-Blanco C, Huang-Lin E, Abrusci C. Characterization, biodegradation and cytotoxicity of thermoplastic starch and ethylene-vinyl alcohol copolymer blends. Carbohydrate Polymers. 2022; 298:120085.

[34] Julinová M, Kupec J, Alexy P, Hoffmann J, Sedlařík V, Vojtek T, et al. Lignin and starch as potential inductors for biodegradation of films based on poly (vinyl alcohol) and protein hydrolysate. Polymer Degradation and Stability. 2010; 95:225-233.

[35] Haque ANMA, Remadevi R, Wang X, Naebe M. Biodegradable cotton gin trash/poly (vinyl alcohol) composite plastic: Effect of particle size on physicochemical properties. Powder Technology. 2020; 375:1-10.

[36] Song M, Park J, Jeon J, Ha Y-G, Cho Y-R, Koo H-J, et al. Application of poly (vinyl alcohol)-cryogels to immobilizing nitrifiers: Enhanced tolerance to shear stress-induced destruction and viability control. Science of The Total Environment. 2023; 855:158835.

[37] Pan Y, Liu Y, Wu D, Shen C, Ma C, Li F, et al. Application of Fenton pre-oxidation, Ca-induced coagulation, and sludge reclamation for enhanced treatment of ultra-high concentration poly (vinyl alcohol) wastewater. Journal of hazardous materials. 2020; 389:121866.

[38] Lan W, Wang S, Chen M, Sameen DE, Lee K, Liu Y. Developing poly (vinyl alcohol)/chitosan films incorporate with d-limonene: Study of structural, antibacterial, and fruit preservation properties. International journal of biological macromolecules. 2020; 145:722-732.

[39] Bian H, Cao M, Wen H, Tan Z, Jia S, Cui J. Biodegradation of polyvinyl alcohol using cross-linked enzyme aggregates of degrading enzymes from Bacillus niacini. International journal of biological macromolecules. 2019; 124:10-16.

[40] Ibzhanova A, Niyazbekova R, Al Azzam K, Negim E, Akibekov O. Biodegradability of Non-wood Packaging Paper. Egyptian Journal of Chemistry. 2022; 65(10):131-139.

[41] Zheng J, Hu Y, Su C, Liang W, Liu X, Zhao W, et al. Structural, physicochemical and biodegradable properties of composite plastics prepared with polyvinyl alcohol (PVA), OSA potato starch and gliadin. Journal of Food Engineering. 2023; 339:111278.

[42] Yan J, Li M, Wang H, Lian X, Fan Y, Xie Z, et al. Preparation and property studies of chitosan-PVA biodegradable antibacterial multilayer films doped with Cu2O and nano-chitosan composites. Food Control. 2021; 126:108049.

[43] Rag SA, Dhamodharan D, Selvakumar M, Bhat S, De S, Byun H-S. Impedance spectroscopic study of biodegradable PVA/PVP doped TBAI ionic liquid polymer electrolyte. Journal of Industrial and Engineering Chemistry. 2022; 111:43-50.

[44] Negim ESM, Rakhmetullayeva RK, Yeligbayeva GZh, Urkimbaeva PI, Primzharova ST, Kaldybekov DB, Khatib JM, Mun GA, Craig W. Improving biodegradability of polyvinyl alcohol/starch blend films for packaging applications. International Journal of Basic and Applied Sciences. 2014; 3(3):263-273.

[45] Chai W-L, Chow J-D, Chen C-C. Effects of modified starch and different molecular weight polyvinyl alcohols on biodegradable characteristics of polyvinyl alcohol/starch blends. Journal of Polymers and the Environment. 2012; 20:550-564.

[46] Iskalieva A, Orazalin Z, Yeligbayeva G, Irmukhametova G, Taburova S, & Toktar T. Synthesis of Biodegradable Polymer-Based on Starch for Packaging Films: A Review. Kompleksnoe Ispolzovanie Mineralnogo Syra = Complex Use of Mineral Resources. 2024; 329(2):110-130.

[47] Shulen R, & Kazybayeva D. Synthesis and characterization of new biodegradable gels based on 2,2 ’-(ethylenedioxy) diethanethiol and pentaerythritol triacrylate. Kompleksnoe Ispolzovanie Mineralnogo Syra = Complex Use of Mineral Resources. 2021; 320(1):25-31.

Crossref
DOI: 10.31643/2025/6445.03
Engineering and Technology

Incorporation of neodymium, holmium, erbium, and samarium (oxides) in zinc-borotellurite glass: Physical and optical comparative analysis

[1]Azlina Y., [1*]Azlan M.N., [1]Suriani A.B., [1]Shaari H.R., [2]Naif Mohammed Al-Hada, [3]Umar S.A., [4]Kenzhaliyev B.K., [5]Zaid, M.H.M., [6]Hisam R., [7]Iskandar S.M., [7]Yusof N.N., [8]Abdul Hafidz Yusoff

[1]University Pendidikan Sultan Idris, 35900 Tanjong Malim, Perak, Malaysia
[2]Institute of Biophysics, Dezhou University, Dezhou 253023, China
[3]Federal University Lafia, Lafia, Nasarawa State, Nigeria
[4]Institute of Metallurgy and Ore Beneficiation, Satbayev University, Almaty, Kazakhstan
[5] Universiti Putra Malaysia, 43400, Serdang, Selangor, Malaysia
[6]Universiti Teknologi MARA, 40450 Shah Alam, Selangor, Malaysia;
[7]School of Physics, Universiti Sains Malaysia, 11800 USM, Penang, Malaysia;
[8]Universiti Malaysia Kelantan, Jeli 17600, Kelantan, Malaysia

[*]Corresponding author: azlanmn@fsmt.upsi.edu.my

Received: *December 13, 2023*
Peer-reviewed: *January 23, 2024*
Accepted: *February 22, 2024*

ABSTRACT

Investigating the effect of different types of rare-earth oxides on zinc borotellurite glass is important to determine the potential application in optical devices. The addition of rare-earth oxides in zinc borotellurite glass is well-known to enhance the optical properties due to the effects of 4f-4f transitions. In this work, we aim to compare the effect of different rare-earth oxides on zinc borotellurite glass denoted as ZBTNd, ZBTHo, ZBTEr and ZBTSm. The glass samples were successfully fabricated via the melt-quenched technique. The physical investigation of the glasses has been done by measuring the density and molar volume. It was found that ZBTNd glass has the lowest density than the other glasses due to the small atomic radius in neodymium oxide. High-density value for ZBTHo glass shows potential to be used as radiation shielding properties. The high value of molar volume for ZBTNd glass is advantageous for fiber optics as ZBTNd glass has good performance in elasticity. It was found that ZBTEr has a lower refractive index than the other glasses due to low dispersion characteristics. However, ZBTEr glass has good performance to be used in optical communication applications. It was found that the optical absorption shifts to a longer wavelength beginning from ZBTEr > ZBTHo > ZBTNd > ZBTSm. The optical band gap energy for ZBTEr glass is higher than the other glasses due to the Coulomb repulsion energy for erbium which is greater than neodymium and samarium and slightly higher than holmium. The pattern of electronic polarizability for all glasses was found as follows ZBTSm>ZBTNd>ZBTEr>ZBTHo. The optical basicity for ZBTEr was found highest which indicates a higher acidity, meanwhile, the ZBTNd glass has the lowest value which corresponds to a higher basicity.

Keywords: tellurite glass, rare-earth oxides, optical properties

	Information about authors:
Azlina Y.	*Physics Department, Faculty of Science and Mathematics, University Pendidikan Sultan Idris, 35900 Tanjong Malim, Perak, Malaysia*
Azlan M.N.	*Dr., Physics Department, Faculty of Science and Mathematics, Universiti Pendidikan Sultan Idris, Tanjung Malim, Perak, 35900, Malaysia. Email: azlanmn@fsmt.upsi.edu.my*
Suriani A.B	*Physics Department, Faculty of Science and Mathematics, University Pendidikan Sultan Idris, 35900 Tanjong Malim, Perak, Malaysia*
Shaari H.R.	*Physics Department, Faculty of Science and Mathematics, University Pendidikan Sultan Idris, 35900 Tanjong Malim, Perak, Malaysia*
Naif Mohammed Al-Hada	*Shandong Key Laboratory of Biophysics, Institute of Biophysics, Dezhou University, Dezhou 253023, China*
Umar S.A.	*Department of Physics, Faculty of Science, Federal University Lafia, Lafia, Nasarawa State, Nigeria*
Kenzhaliyev Bagdaulet Kenzhaliyevich	*Professor, Dr. Sci. Tech., Institute of Metallurgy and Ore Beneficiation, Satbayev University, Almaty, Kazakhstan. Email: bagdaulet_k@satbayev.university*
Zaid M.H.M.	*Department of Physics, Faculty of Science, Universiti Putra Malaysia, 43400, Serdang, Selangor, Malaysia*
Hisam R.	*Faculty of Applied Sciences, Universiti Teknologi MARA, 40450 Shah Alam, Selangor, Malaysia*
Iskandar S.M.	*School of Physics, Universiti Sains Malaysia, 11800 USM, Penang, Malaysia*
Yusof N.N.	*School of Physics, Universiti Sains Malaysia, 11800 USM, Penang, Malaysia*
Abdul Hafidz Yusoff	*Gold Rare Earth and Material Technopreneurship Centre (GREAT), Faculty of Bioengineering and Technology, Universiti Malaysia Kelantan, Kelantan, Jeli 17600, Kelantan, Malaysia*

Introduction

There is no denying the extensive ongoing investigations on glass science and technology, which discuss discoveries in photonics and optical applications [1]. Rapid development and innovation in telecommunications enhance the production of new materials for optical fiber and laser [2]. A wide range of glass materials has often been produced to manufacture optical devices. Silicate-based glass is widely utilized as the primary core of the optical fiber. However, silicate-based glass has more than 1500 ^{0}C melting point, moderate absorbency and high signal loss [3]. The high quality of optical glass is essential for the advancement of current optoelectronic devices. Whilst tellurite-based glass is the best choice for high-quality glass materials [4].

Tellurite oxide is comprised of double triangular bipyramids which are surrounded by four oxygen atoms in the tellurite glass network. Four oxygen atoms are located at a distance of 1.95 Å from the tellurite ion [5]. Hence, the tellurite ion is located in an intermediate state between four oxygen atoms. Pure TeO_2 glass is not stable and exists in a crystal state with four coordination numbers as Te^{4+}. The addition of modifier ion in tellurite oxide, TeO_2 may lead to the formation of the glassy state and hence vitrified TeO_2. The tellurite ion in the glass network is more stable in four coordination numbers than in six coordination numbers. This trend is due to the shrinking distance between tellurite and oxide atoms, Te–O as the valence electrons increase in the glass network. Besides that, if the modifier ions have the same coordination number and size as TeO_6, the six-atom coordination state of Te^{4+} might be stable [6].

Erbium oxide is a well-known material to be used in fiber amplifiers such as erbium-doped fiber amplifier (EDFA) devices [7]. In previous research, holmium oxide has been used extensively in telecommunication and solid-state lasers [8]. Moreover, samarium oxide is one of the best lanthanide compounds to be utilized as an optical amplifier and fiber [9]. Meanwhile, neodymium oxide has the greatest interest in the area of optical materials due to its near-infrared lasing properties at around 1.06 µm [10]. Hence, the inclusion of these rare-earth oxides is beneficial to improve the optical properties of the current zinc borotellurite glass. Extensive studies have been done to incorporate these rare-earth oxides in tellurite glass. However, the detailed comparative analysis between these rare-earth oxides is rarely documented.

This study aims to compare the role of holmium, erbium, neodymium and samarium oxides on the physical and optical performance of zinc-borotellurite glass. The objectives of this study are to determine the physical properties of the glasses such as density and molar volume. The optical analysis such as optical absorption, optical band gap energy, Urbach energy, electronic polarizability, optical basicity and metallization criterion is investigated. The outcomes of this study will provide a detailed comparative analysis between rare-earth oxide inclusions in zinc borotellurite glass. These reports will be useful to manufacture novel materials to be used in optoelectronic applications.

Methodology

A conventional melt-quenching method was used in the chemical formula of $\{\{[(TeO_2)_{0.70}(B_2O_3)_{0.30}]_{0.7}(ZnO)_{0.3}\}_y(RE_2O_3)_{1-y}$, RE= Ho_2O_3, Er_2O_3, Nd_2O_3 and= 0.005, 0,01, 0,02, 0.03, 0.04, 0.05). High-purity chemical powder (99 per cent purity grade) of erbium oxide, Er_2O_3 (Reacton, Alfa Aesar), holmium oxide, Ho_2O_3 (Reacton, Alfa Aesar), neodymium oxide, Nd_2O_3 (Reacton, Alfa Aesar), samarium oxide, Sm_2O_3 (Reacton, Alfa Aesar), tellurite oxide, TeO_2 (Reacton, Alfa Aesar), boron oxide, B_2O_3 (Reacton, Alfa Aesar) and zinc oxide, ZnO (Reacton, Alfa Aesar) were collected and used. The raw materials were measured with a ±0,0001 g accuracy and carefully mixed to produce 13 g of mixed powder by using an electrical balance.

The mixture was placed in the alumina crucible and preheated by an electric furnace at 400 0C for 1 hour. The aim of the preheating process is that the excess hydrogen molecules are removed from the mixture. The mixture in the alumina crucible was then melted in the second electric furnace at a temperature of 900 0C for 2 hours. During this process, the molten mixture was formed. The molten was then transferred to the cylindrical stainless-steel mold which was preheated for 1 hour at 400 0C. During the quenching process, the glass sample was formed. For the annealing process, the glass sample in a cylindrical stainless-steel mold was heated for 1 hour at 400 0C. The aim is to increase mechanical strength and remove stress during the cooling process. The glass sample was then cooled down at around 5 hours at room temperature. By using Isomet Buehler high precision low-speed saw machine, the obtained glass sample was cut to a thickness of about 2 mm. The sample was polished to get a smooth surface on either side of the sample with a various sandpaper grade (1000 grid, 1.500

grid and 2.000 grid). Shimadzu-1650PCUV-Vis spectrophotometer was used to analyze the absorption band of the glass sample.

Results and discussions

Physical comparative analysis

The density of the glass system has a significant effect on the elastic properties, the refractive index and the mechanical strength [11]. High high-density glass matrix is known to be beneficial for increasing the refractive index. In contrast, a low dense glass matrix has an excellent contribution to the elastic and mechanical properties of the glass matrix.

The density calculation can be made using the following formula:

$$\rho = \rho_t \frac{W_a}{W_a - W_t} \quad (1)$$

where ρ_t is the density of water W_a and W_t are the weight of the sample in the air and water respectively.

The change in density may be due to several factors, such as the softening or compactness of the structure, the type of doping, the coordination number and the atomic radii of the components [12]. The results of density for different types of rare-earth doping are shown in Figure 1. Figure 1 shows that neodymium oxide doping has the lowest density among doping, while holmium oxide has the highest value. Several factors may explain the large differences in density between ZBTNd and ZBTHo. The first factor is the atomic radius of the dopant, which is higher in holmium oxide than in neodymium oxide.

The high degree of atomic radius may significantly contribute to an increase over free space in the glass matrix [13]. As a result, the compactness of the glass matrix will be reduced due to an increase in free space. In addition, the bond length between the rare earth atom and oxygen has a significant effect on the oxygen packing density in the glass matrix [14]. Table 1 shows that neodymium oxide has a higher bond length than holmium oxide, which reduces the oxygen packing density. The density of ZBTEr and ZBTSm glasses shows small differences in number compared to ZBTNd glasses. However, erbium oxide has a similar atomic radius with holmium oxide and small differences in bond length. The small degree of density of erbium oxide compared to holmium oxide can be explained by the change in the number of polyhedral coordination after the formation of the glass system [15]. Holmium oxide has a higher number of polyhedral coordination than erbium oxide, which in turn increases the density [16]. In addition, the properties of radiation shielding are highly dependent on the density value. High glass density contributes to excellent shielding properties. ZBTHo glasses therefore have a high potential to be used as shielding properties due to their high-density value.

The investigation of the molar volume of the glass system is important for the analysis of the spatial distribution of oxygen in the glass matrix [17]. The molar volume is directly affected by the density of the glass system through the compaction and expansion of the glass structure [18]. In addition, the result of molar volume is more significant in the analysis of structural changes in the glass network, except mass (m) from density, and the inclusion of equal particles for comparison between samples. The molar volume can be calculated by the following formula:

$$V_m = \sum_i \frac{x_i M_i}{\rho} = \frac{M}{\rho} \quad (2)$$

where x_i and M_i denote the molar fraction and molecular weight of the respective component and M is the total molecular weight of the composition. The obtained values for molar volume are listed in Table 1 and plotted in Figure 2. It is noted from Figure 2 that the molar volume is higher in ZBTNd than in the glasses. The interatomic spacing between the atoms may influence the molar volume in the glass network [19]. The high bond length in neodymium oxide may lead to the increase in interatomic spacing which in turn increase the molar volume. Moreover, the high number in ionic radius may increase the tendency of free expansion in the glass matrix [20]. The low number of molar volume values is obtained in ZBTHo glasses which represent the reciprocal value of density. Bulk modulus has a high dependency on molar volume which determines the elasticity of optical fiber. Based on the obtained molar volume data, ZBTHo glasses have a lower performance in elasticity than ZBTNd glasses. Hence, ZBTNd glasses is more preferable to be used for optical fiber than ZBTHo glasses.

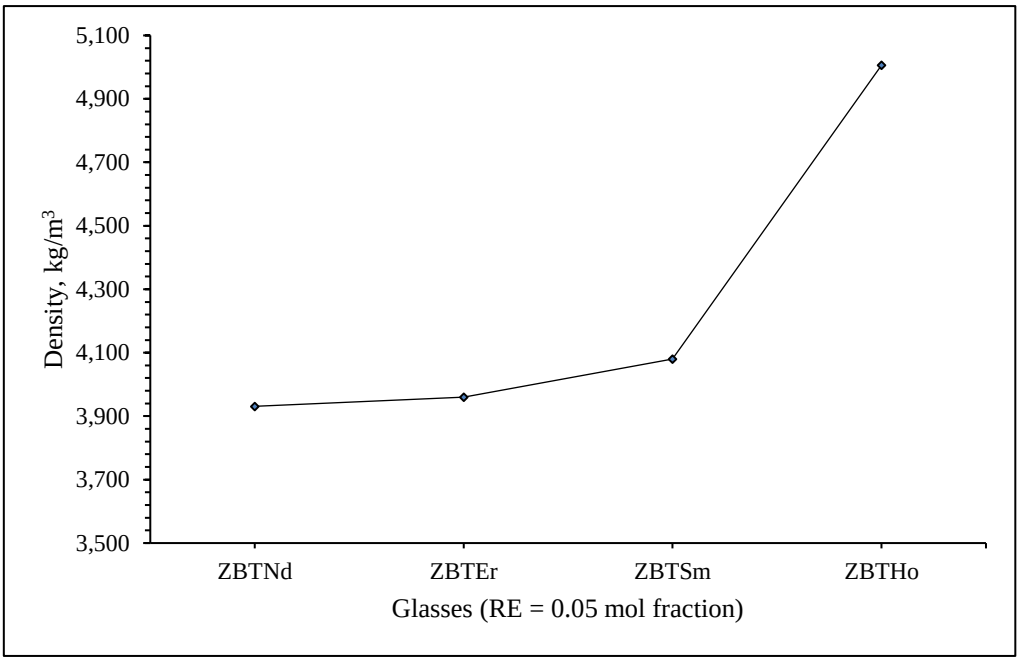

Figure 1 - Density of ZBTNd, ZBTEr, ZBTSm and ZBTHo glasses

Table 1 - Density of ZBTNd, ZBTEr, ZBTSm and ZBTHo doped tellurite glass

Glasses	Density (kg/m^3)	Molar Volume (m^3/mol)	Atomic radius (pm)	Bond length	Ionic radius
ZBTNd	3.931	128.200	-	-	-
ZBTHo	5.006	26.043	-	-	-
ZBTEr	3.960	32.955	-	-	-
ZBTSm	4.080	31.570	-	-	-
Single constituents					
TeO_2	-	-	140	1.974	2.210
B_2O_3	-	-	85	1.236	0.230
ZnO	-	-	135	1.975	0.740
Nd_2O_3	-	-	185	2.559	0.983
Ho_2O_3	-	-	175	2.385	0.901
Er_2O_3	-	-	175	2.310	0.890
Sm_2O_3	-	-	185	2.509	0.958

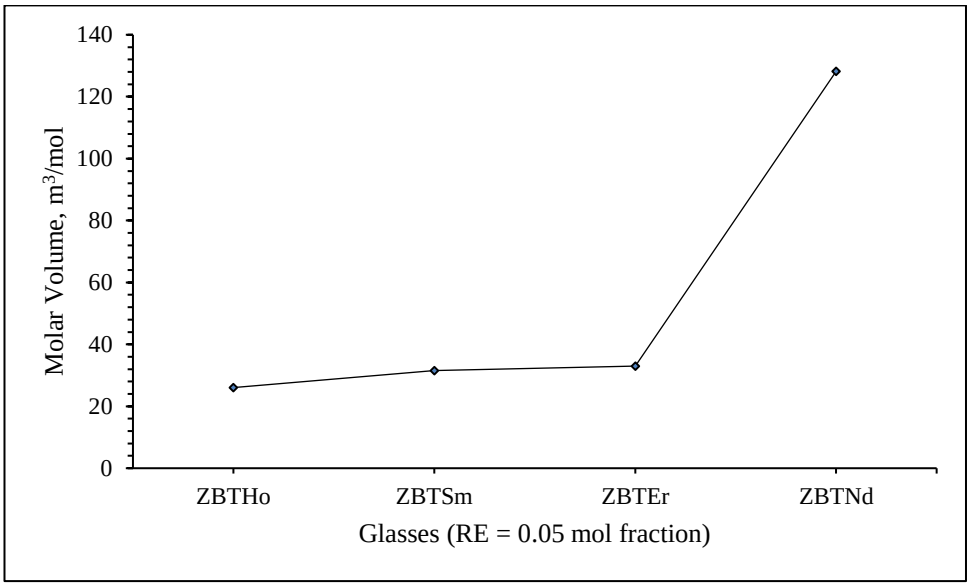

Figure 2 - Molar volume of ZBTHo, ZBTSm, ZBTEr and ZBTNd glasses

Refractive index

The refractive index is an important parameter to be used in a variety of applications such as smart glass, lenses, optical fiber and electronic displays [21]. The structure of an amorphous glass network is closely associated with the amount of non-bridging oxygen in the glass network. The existence of non-bridging oxygen will contribute to improving the polarization of materials which, in turn, may impact the value of refractive indexes. There are two effects of polarization on the transmission of light in a medium;

1. Some light transmission may be absorbed,
2. The delay in the velocity of light waves passes through the medium.

The large polarizability of the glass system minimizes the velocity of light propagation in a medium which, in turn, generates a high refractive index. The results of the refractive index are shown in Table 2 and shown in Figure 3. Figure 3 shows that the highest refractive index is the ZBTSm glasses.

Factors that affect the value of the refractive index are the characteristics of dispersion, doping coordination number, non-bridging oxygen, electronic cloud density, polarization and density [22]. Based on previous data, the density of the ZBTHo glasses is higher than that of the ZBTSm glasses. It is therefore presumed that the refractive index of the ZBTHo glasses must be higher than the rest of the series of glasses. However, the density of the glass system is not the only factor affecting the value of the refractive index.

Cation polarization values for single samarium oxide and holmium oxide are 1.16 Å and 0.91 Å respectively**.** The high number of cation polarizability can therefore contribute to the increase in the refractive index value. The high value of the refractive index is beneficial to produce fiber optics as it widens the angle of reflection by increasing the critical angle. The lowest refractive index value is found in the ZBTEr glasses due to the low cation polarization (0.89 Å) compared to the other dopants. Another possibility is that ZBTEr glasses may have low dispersion characteristics compared to other dopants as one of the important parameters for optical communication is the dispersion characteristic.

High-dispersion characteristics may reduce the performance of optical fiber by increasing the optical pulse and limiting the information-carrying capacity of the fiber. It can therefore be justified that ZBTEr glasses are also a good choice to produce fiber optics, particularly as a core material. In addition, the amount of non-bridging oxygen may contribute to the variation of the refractive index as the existence of lone-pair electrons is high in non–bridging oxygen. Based on the trend of the refractive index, the ZBTSm glasses produce high levels of non-bridging oxygen compared to ZBTHo, ZBTNd and ZBTEr glasses.

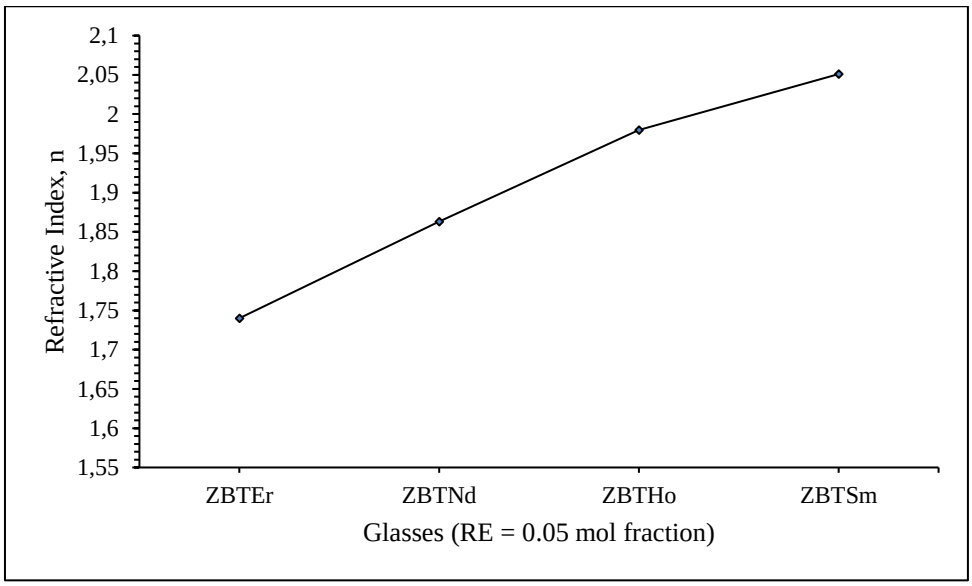

Figure 3 - Refractive index of ZBTEr, ZBTNd, ZBTHo and ZBTSm glasses

Table 2 - Refractive index of ZBTEr, ZBTNd, ZBTHo and ZBTSm glasses

Glasses	Refractive index
ZBTEr	1.740
ZBTNd	1.863
ZBTHo	1.980
ZBTSm	2.051

Optical absorption and band gap energy

Optical absorption spectra have a significant role in determining the properties of the electronic structure of non-crystalline solids. The optical absorption in glass materials can occur by two mechanisms which are electronic polarization and the excitation of an electron from the valence band to the conduction band [23]. The occurrence of optical absorption by electronic polarization only depends on the light frequency in the constituent atoms. Meanwhile, the process of optical absorption during the transition of an electron from valence to conduction band depends on the electronic band structure of semiconducting materials.

The promotion of an electron from the valence band to the conduction band is due to the absorption of photon energy from the electron. Figure 4 shows the optical absorption spectra for ZBTSm, ZBTNd, ZBTHo and ZBTEr glasses. It can be seen from the figure that the optical absorption shifts to a longer wavelength beginning from ZBTEr > ZBTHo > ZBTNd > ZBTSm. In comparison, the absorbance is higher at the lower wavelength and lower at the higher wavelength for all glasses indicating an increase in the absorption factor.

Sharp peaks are observed in the absorption spectra of all dopants leading to the excitation of electrons from the ground to the excitation state. This trend can be explained by the type of orbital in rare–earth oxide. It is well established that rare earth oxides have 4f orbital, which are localized due to their strong intra-atomic Coulomb association [24]. The 4f-4f orbital in rare earth materials leads to a strong magnetic dipole and an electric dipole force which, in turn, produces sharp peaks in the absorption spectra [25].

The investigation of the optical band gap is important, as the tendency of glass materials to be more applicable in semiconductor devices is expected. Optical absorption in glass materials may arise through two different mechanisms, e.g. electronic polarization and electron excitation from the valence band to the conduction band. The occurrence of optical absorption by electronic polarization relies only on the frequency of light in the constituent atoms. Meanwhile, the process of optical absorption during the transition from valence to conduction band depends on the electronic band structure of semiconductor materials. The promotion of the electron from the

valence band to the conductive band is due to the absorption of photon energy from the electron.

There are two types of optical band gaps that work in both crystalline and amorphous structures that are direct and indirect optical band gaps. In the case of glass materials, the indirect optical band gap is more accurate in describing the behavior of electronic transitions due to the long-range structural disorder in the glass matrix.

The absorption coefficients near the absorption edge of the glass samples are calculated by:

$$\alpha(\lambda)=2.303\frac{A}{d} \quad (3)$$

Where A applies to absorption and d refers to the thickness of the glass samples. The absorbance of the glass materials often impacts the absorption coefficient with a directly proportional behavior to the absorption coefficient value. More evidence of the electronic states of the glass system is given by the higher energy components of the spectral region corresponding with the electronic transition. Electrons are excited through photon absorption from a filled band to an empty band. The following formula can be used to measure photon energy

$$\hbar\omega=\frac{\hbar}{2\pi}(2\pi f) = hf = \frac{\hbar c}{\lambda} \quad (4)$$

where c=2.9979 x 108 m/s and ħ = 4.14 x 10-15 eVs. As a result of the electron transitions, the absorption coefficient α(to) increases significantly. The relationship between α (a), the photon energy of the incident radiation, and the absorption coefficient, can be written as follows:

$$\alpha(\omega)=\frac{B(\hbar\omega-E_{0pt})^n}{\hbar\omega} \quad (5)$$

Where the tailing parameter is denoted as B, Eopt is the optical bandgap energy, n is the type of transition where n=2 in the indirect transition, n=1/2 in the forbidden indirect transition, n=1/3 in the prohibited direct transition, and n=1/3 in the forbidden direct transition. Electromagnetic waves interact with electrons in the valence band, which are raised across a fundamental gap in the conductive band in direct and indirect transition cases [25].

The absorption coefficient is calculated near the absorption edge of all the different glass samples. Amorphous materials are well known to fit equation (3) where n = 2 which is an indirect transition. The equation (3.8) is therefore converted to the following equation:

$$((\alpha\hbar\omega)^2=B(\hbar\omega-E_{opt}) \quad (6)$$

The optical band gap can be used to provide insight into the state of solid-state materials. The Urbach energy (ΔE) be computed by the plot of the logarithm of the absorption coefficient (a(v)) as a function of the photon energy of the amorphous material as given below:

$$\alpha(\upsilon)=ßexp(\frac{\hbar\upsilon}{\Delta E}) \quad (7)$$

Where ß is a constant, h is the plank constant, v is the frequency of the photon, and ΔE is the Urbach energy (Maheshvaran et al., 2013).

Figure 5 shows the optical band gap pattern for ZBTSm, ZBTNd, ZBTHo and ZBTEr glasses and the data are listed in Table 3. It can be seen from Figure 5 that the ZBTEr glass has the highest number of optical band gaps than the other glasses. The variations in optical band gap can be explained by the Coulomb repulsion energy between the glasses. The Coulomb repulsion energy for rare-earth is shown in Figure 6. It is noted that the Coulomb repulsion energy for erbium is greater than neodymium and samarium and slightly higher than holmium.

Coulomb repulsion energy confines the electron in orbital which affects the mobility of electrons to be excited from the ground state to the excited state [26]. Hence, it can be justified that the higher number in the optical band gap may be due to the Coulomb repulsion energy which is greater in erbium. ZBTSm glass has the lowest number of optical band gaps which reflects the lower number in Coloumb repulsion energy. Besides that, the 4f states for rare-earth may affect the excitation of electrons to the conduction band. The unoccupied 4f orbitals may experience the energetic up-shift to the conduction band which improves the optical band gap for ZBTSm [27]. The highest optical band gap value for ZBTEr reflects the lower number of unoccupied 4f orbitals. However, all glasses fall in the range of semiconductor energy gap which is compatible to be used in semiconductor applications.

Figure 7 and Table 3 depicted and listed the values of Urbach energy for the glasses. The exponential area in the absorption coefficient and near to the optical band edge is called as Urbach tail.

The appearance of the Urbach tail is due to the localized states in the amorphous structure which is extended in the band gap. The localized states are associated with the disorders of structure which gives the information of defects in the glass system. The high number of Urbach energy indicates the higher tendency of the weak bond in the glass structure to be converted to defects. It can be seen from Figure 7 that the ZBTSm glass has the highest number of Urbach energy which reflects the fragility of the glass structure. The lower value of Urbach energy in ZBTEr glass shows that the glass structure is less likely to convert the weak bond into defects. Hence, ZBTEr is more stable than the other glasses.

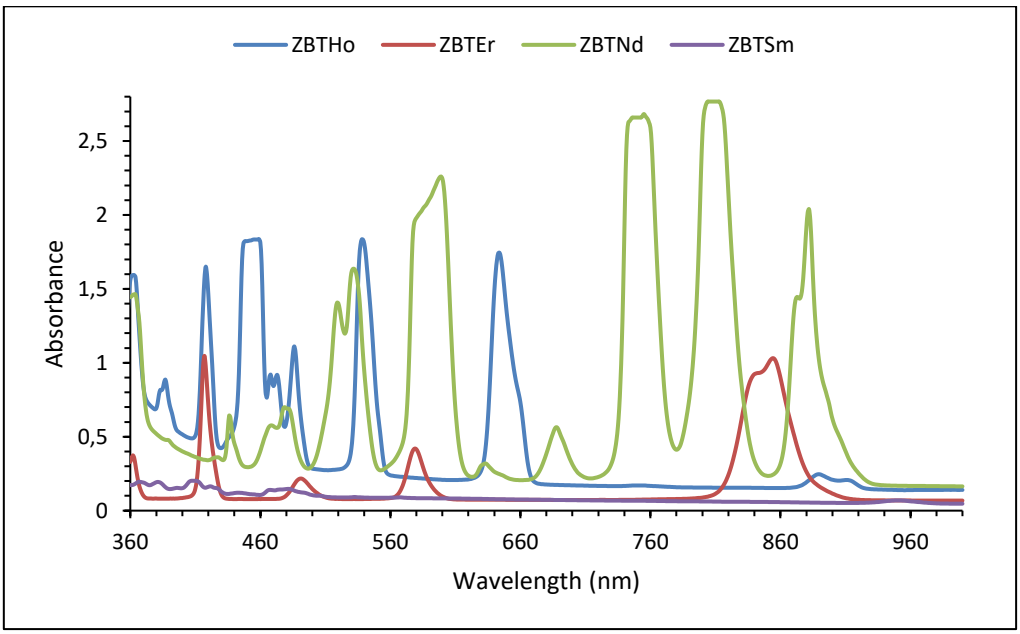

Figure 4 - Optical absorption of ZBTHo, ZBTEr, ZBTNd and ZBTSm glasses

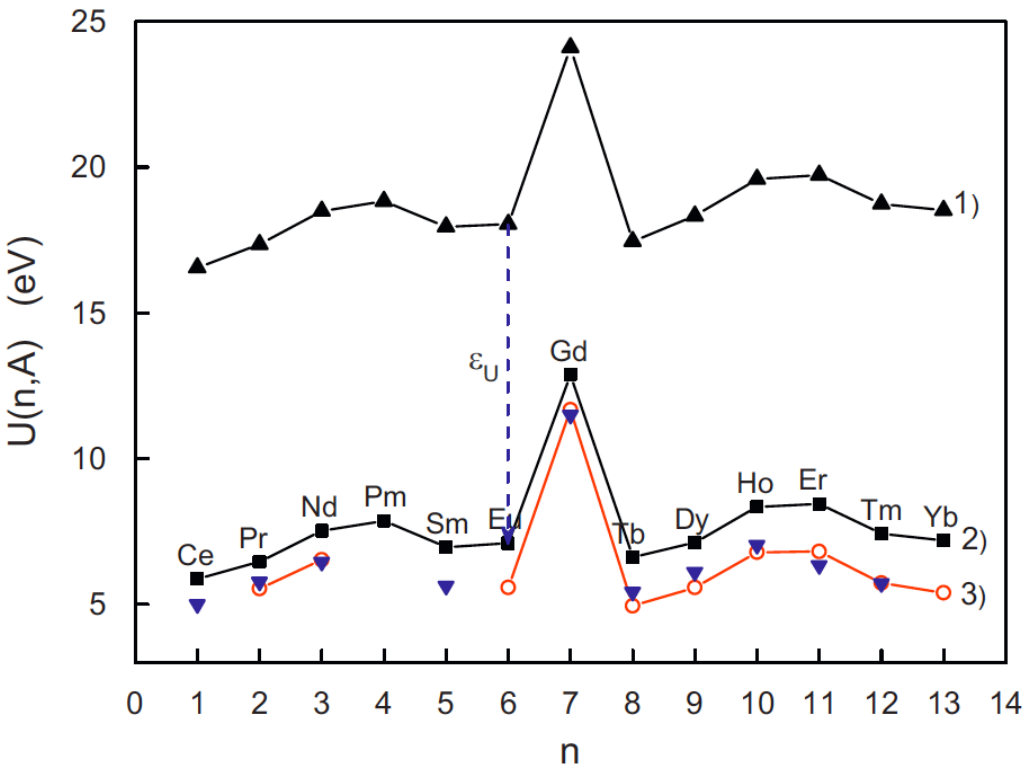

Figure 6 - Coulomb repulsion energy for rare-earth. Reproduced figure from **[27]**

Figure 5 - Optical band gap energy of ZBTSm, ZBTNd, ZBTHo and ZBTEr glasses

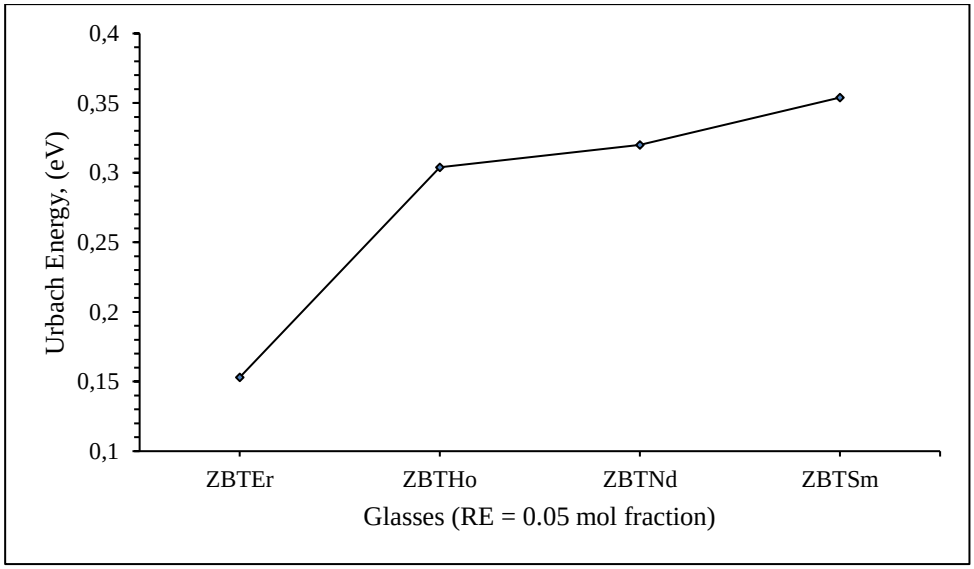

Figure 7 - Urbach energy of ZBTEr, ZBTHo, ZBTNd and ZBTSm glasses

Table 3 - Optical band gap and Urbach energy of ZBTEr, ZBTHo, ZBTNd and ZBTSm glasses

Sample (0.05)	Optical band gap	Urbach Energy
Samarium	2.980	0.660
Neodymium	3.151	0.320
Holmium	3.268	0.432
Erbium	3.380	0.153

Electronic polarizability and oxide ion polarizability

Electronic polarization was used to describe the deformation of electron clouds by applying an electromagnetic field. Electronic polarization affects inter-ionic interaction, refractive index, conductivity, optical basicity and non–linear optical properties. The early study of polarization in the field of glass materials was carried out by Fajans and Kriedl in 1948 [28]. Polarizability values have been

determined for three types of oxide glasses which are; 1. Acid oxides, 2. Ionic oxide, 3. High ion oxides.

The Lorentz-Lorenz equation explains the relationship between the refractive index and the molar volume as shown below:

$$R_m = \frac{(n_0^2 - 1)}{(n_0^2 + 2)} V_m \quad (8)$$

When Rm represents molar refraction, n0 signifies linear refractive index, and Vm implies molar volume. The Lorentz-Lorenz equation represents the average molar refraction for isotropic substances that are liquids, glasses and cubic crystals. The average electronic polarizability can be computed from the Lorentz-Lorenz equation by applying the number of the Avogadro to the given equation:

$$\alpha_m = \frac{3}{4\pi N_A} R_m \quad (9)$$

Where NA defines the Avogadro's number corresponding to the number of polarizable ions per mole. The value 4π/3 is known as a constant in the Lorentz function. Electronic polarization provides the magnitude of the electron response by incorporating the electromagnetic field into the electron clouds. With the α_m in (Å3), equation (3) can be altered into the given formulas:

$$\alpha_m = \frac{R_m}{2.52} \quad (10)$$

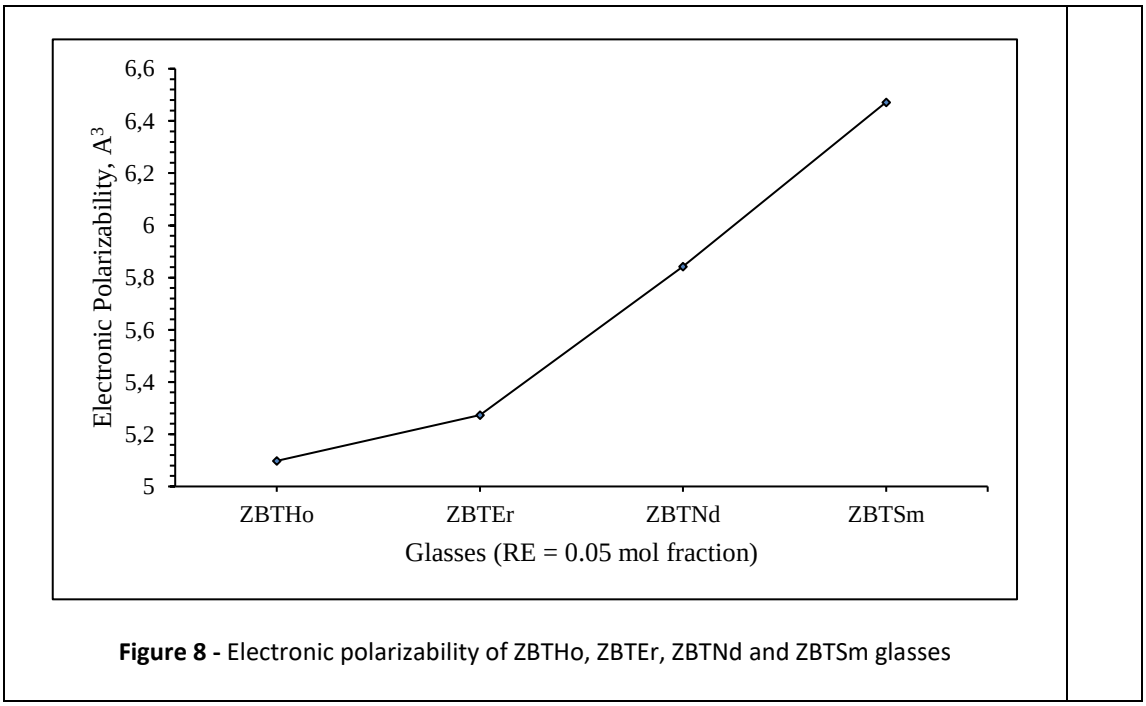

Figure 8 - Electronic polarizability of ZBTHo, ZBTEr, ZBTNd and ZBTSm glasses

Table 4 - Electronic polarizability, oxide ion polarizability, optical basicity and metallization criterion of ZBTHo, ZBTEr, ZBTNd and ZBTSm glasses

Glasses (0.05)	Electronic Polarizability			Metallization Criterion
		Oxide ion polarizability	Optical Basicity	
ZBTHo	5.098	2.361	1.151	0.404
ZBTEr	5.274	3.216	1.165	0.411
ZBTNd	5.843	3.306	1.173	0.483
ZBTSm	6.472	3.516	1.195	0.549

The obtained values of electronic polarizability for all glasses are depicted in Figure 8 and listed in Table 4. The pattern of electronic polarizability for all glasses is as follows ZBTSm>ZBTNd>ZBTEr>ZBTHo. This pattern shows that the ZBTSm glass has a higher tendency to be more polarized than the other glasses. The variations of electronic polarizability can be explained by the attraction between electrons and the nucleus and Hooke's law of potential energy. Furthermore, the values of electronic polarizability differ with various types of compounds. In other words, the values of polarizability depend on the density of charge distribution in both negative and positive ions. Hence, the ZBTSm glass has a higher density of charge distribution than the other glasses.

Moreover, the number of non-bridging oxygen has an important role in the tendency of glass to be polarized. Non-bridging oxygen has a lone pair which is independent of the chemical bonding and high mobility. ZBTSm glass may have a higher number of non-bridging oxygen than the other glass which contributes to high electronic polarizability. According to Fajan's rule, the polarizing power of the cation increases with decreasing its size and number of filled orbitals and with increasing its positive charge [28]. It is known that the samarium has a lower number of occupied 4f orbitals than the other glass system. Hence, this effect may increase the polarizing power of the cation according to Fajan's rule. Besides that, Sm^{3+} trivalent ions have a higher positive charge which leads to higher electronic polarizability.

Previously, Dimitrov and Sakka, 1996 illustrated the computation of the polarization of oxide ions based on optical band gap energy [29]. The deformity of the oxide ion's electron cloud is wider than that of the cation. This is due to the increased tendency of the cation electron to hold onto the cationic charge. This effect will contribute to the cation's electron cloud being not particularly polarised. The correlation between $\sqrt{E_g}$ and 1-R_m/V_m was presented by Duffy and Ingram in 1991 for a large number of simple oxides as shown in the given equation:

$$E_g = 20(1 - \frac{R_m}{V_m})^2 \qquad (11)$$

The oxide ion polarizability can be obtained by the substitution of Equation (6) into Equation (4) as shown by the following formula:

$$\alpha_{O_2^-}(E_g) = \left[\frac{V_m}{2.52}\left(1 - \sqrt{\frac{E_g}{20}}\right) - \sum \alpha_i\right](N_{O_2^-})^{-1} \qquad (12)$$

This equation has been accepted to be compliant with heavy metal oxide glasses.

The obtained values of oxide ion polarizability for all glass samples are illustrated in Figure 9 and listed in Table 4. The pattern of oxide ion polarizability for all glass samples is as follows; ZBTSm>ZBTEr>ZBTHo>ZBTNd. It is noted that ZBTSm has a higher number of oxide ion polarizability which reflects the high density of non-bridging oxygen in the glass system. Samarium oxide may enhance the formation of non-bridging oxygen in the glass system than erbium oxide, holmium oxide and neodymium oxide. The free electrons of the oxides in ZBTSm glass are independent of the nuclear charge and chemical bonding which improve the oxide ion polarizability. Moreover, the existence of localized states in the forbidden gap for different compounds leads to variations of oxide ion polarizability. The low number of polarizabilities in ZBTNd glass indicates that the neodymium oxide has low tendency to form the non-bridging oxygen in the tellurite glass as compared to other constituents.

Optical basicity and metallization criterion

The deep understanding of optical basicity was described by the work of Duffy and Ingram, 1971. Duffy and Ingram, 1971 proposed the theoretical calculation of the optical basicity for the multi-component oxide glasses as given below [30]:

$$\Lambda = X_1\Lambda_1 + X_2\Lambda_2 + \ldots\ldots + X_n\Lambda_n \qquad (13)$$

Where X_1, X_2,…., X_n correspond to the equivalent fractions of each oxide which contributes to the overall material stoichiometry and Λ_1, Λ_2,….,Λ_n correspond to the optical basicity of each individual oxide in the glass system.

The obtained values for the optical basicity of all glasses are shown in Figure 10 and Table 4. The pattern of optical basicity for the glasses is as follows; ZBTNd>ZBTHo>ZBTSm>ZBTEr. The low number of optical basicity for ZBTEr glass indicates higher in acidity. Meanwhile, the high number of optical basicity for ZBTNd glass corresponds to higher in basicity. It is known that a single neodymium oxide has higher number of optical basicity Λ (1.014) than erbium oxide Λ (0.929).

Hence, it is noted that ZBTNd glass has greater number of optical basicity than ZBTEr. Meanwhile, optical basicity values for holmium and samarium oxides are Λ (0.945) and Λ (0.984), respectively. The difference in optical basicity for single oxide contributes to the variations of overall optical basicity.

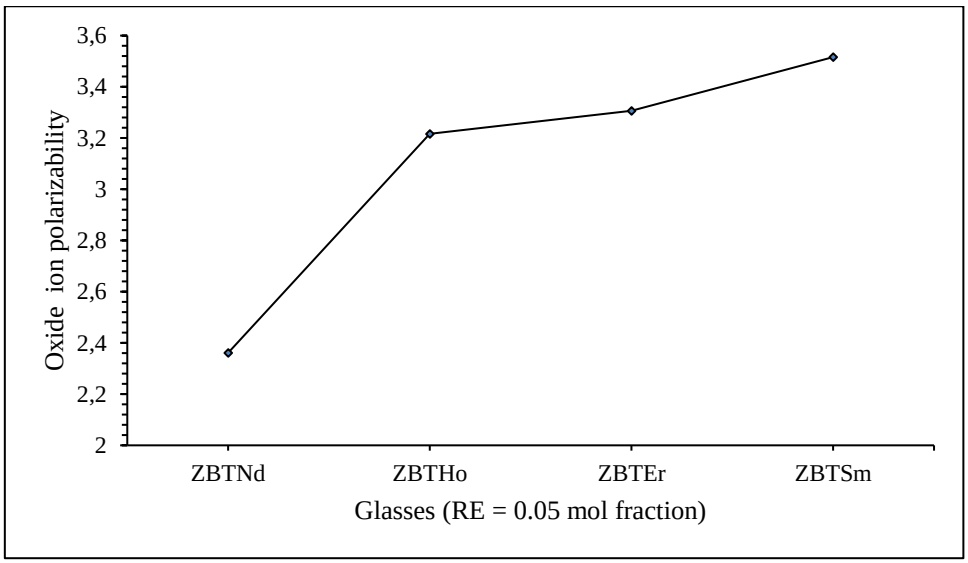

Figure 9 - Oxide ion polarizability of ZBTNd, ZBTHo, ZBTEr and ZBTSm glasses

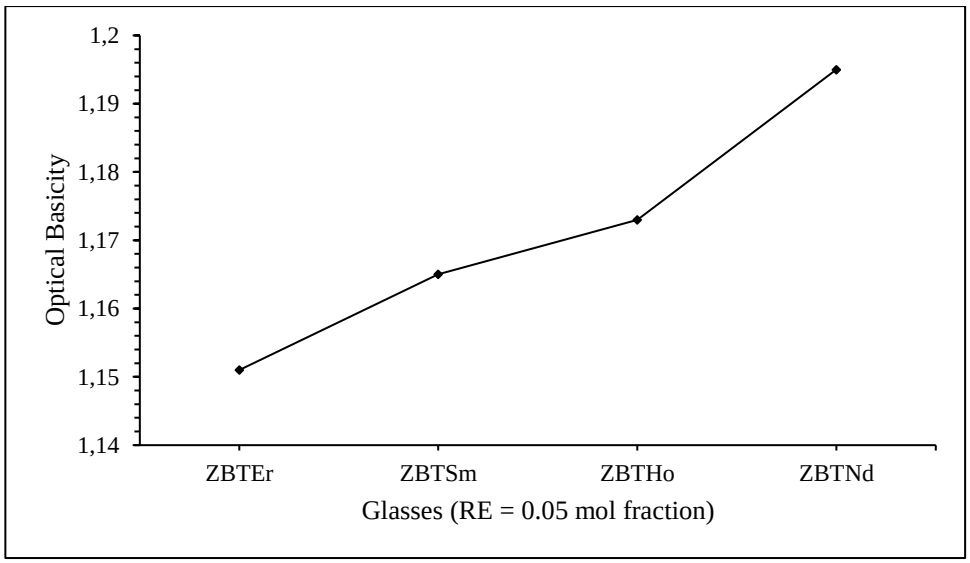

Figure 10 - Optical basicity of ZBTEr, ZBTSm, ZBTHo and ZBTNd glasses

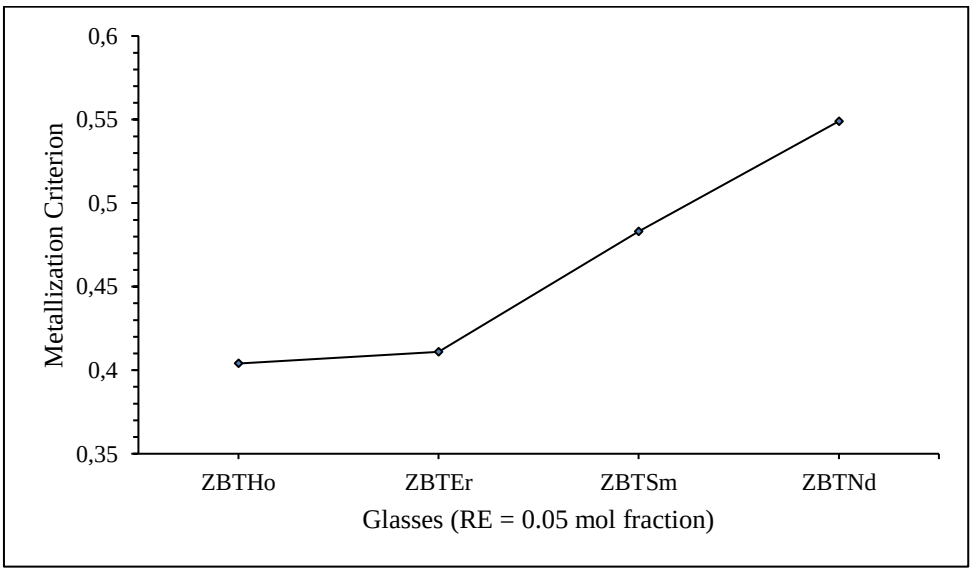

Figure 11 - Metallization criterion of ZBTHo, ZBTEr, ZBTSm and ZBTNd glasses

The concept of metallization of the condensed matter can be explained by the theory proposed by Herzfeld [31]. The condition of R_m/V_m= 1 in the Lorentz-Lorenz equation describes that the refractive index becomes infinite. This is in accordance with the metallization of covalent solid materials. In other words, the electrons become itinerant and acquires metallic status. The nature of metallic and non-metallic of oxide glasses can be predicted by the following conditions: $R_m/V_m<1$ (non-metal) and $R_m/V_m>1$ (metal). Subtracting by 1 gives the equation of metallization criterion as shown in the following expression:

$$M = 1 - \frac{R_m}{V_m} \quad (14)$$

This equation indicates that when the metallization criterion becomes zero, the transition to the metal states will occur. The metallization criterion based on refractive index and optical band gap can be calculated by transforming Equation (10) to the following expression:

$$M = 1 - \frac{(n_0^2 - 1)}{(n_0^2 + 2)} = \left(\frac{E_g}{20}\right)^{\frac{1}{2}} \quad (15)$$

The obtained values of the metallization criterion for all glasses are depicted in Figure 11 and tabulated in Table 4. The pattern of metallization criterion for the glasses is as follows; ZBTNd>ZBTSm>ZBTEr>ZBTHo. It is noted that all glasses are non-metallic and have a relatively large refractive index. The lower number of metallization criteria for ZBTHo indicates that the glass containing holmium oxide tends to be more metallic than neodymium oxide. Meanwhile, the high number of metallization criteria for ZBTNd shows the tendency of glass to be more insulator. The high metallization criterion reflects the widen of the forbidden gap and reduction in overlapping electronic transition. However, all glasses are poor conductive materials and good for semiconductor devices.

Conclusions

The glass series identified as ZBTSm, ZBTHo, ZBTEr, and ZBTNd were fabricated using the conventional melt-quenching method, leading to distinct physical and optical properties among them. The density of these glasses showed a pattern of ZBTHo>ZBTSm>ZBTEr>ZBTNd, with ZBTHo glass being highlighted as an ideal material for radiation shielding. In terms of refractive index, the order was ZBTSm>ZBTHo>ZBTNd>ZBTEr, positioning ZBTEr glass as a promising candidate for optical communication applications due to its low dispersion. Optical absorption trends indicated a shift to longer wavelengths in the order of ZBTEr > ZBTHo > ZBTNd > ZBTSm. Additionally, the optical band gap followed the sequence ZBTEr>ZBTHo>ZBTNd>ZBTSm, influenced by Coulomb repulsion energy in rare-earth oxides. The electronic polarizability adhered to the pattern of ZBTSm>ZBTNd>ZBTEr>ZBTHo, with ZBTSm glass exhibiting a higher charge distribution density, enhancing its electronic polarizability. These findings underscore the exceptional optical characteristics of the selected rare-earth oxides, underscoring their utility in optical communications applications.

Acknowledgements

This research was financially supported by Skim Geran Penyelidikan Fundamental (FRGS) Fasa 1/2018 (Grant code: 2019–0006–102–02). The authors would like to thank the following institutions for equipment support: Faculty of Science and Mathematics, Universiti Pendidikan Sultan Idris and Faculty of Science and Universiti Putra Malaysia.

Cite this article as: Azlina Y, Azlan MN, Suriani AB, Shaari HR, Naif Mohammed Al-Hada, Umar SA, Kenzhaliyev BK, Zaid MHM, Hisam R, Iskandar SM, Yusof NN, Abdul Hafidz Yusoff. Incorporation of neodymium, holmium, erbium, and samarium (oxides) in zinc-borotellurite glass: Physical and optical comparative analysis. Kompleksnoe Ispolzovanie Mineralnogo Syra = Complex Use of Mineral Resources. 2025; 332(1):32-48. https://doi.org/10.31643/2025/6445.03

Мырыш-боротеллурит шынысына неодим, гольмий, эрбий және самарий оксидтерін енгізу, физикалық және оптикалық салыстырмалы талдау

[1]Azlina Y., [1*]Azlan M.N., [1]Suriani A.B., [1]Shaari H.R., [2]Naif Mohammed Al-Hada, [3]Umar S.A., [4]Kenzhaliyev B.K., [5]Zaid, M.H.M., [6]Hisam R., [7]Iskandar S.M., [7]Yusof N.N., [8]Abdul Hafidz Yusoff

[1]Пендикан Сұлтан Идрис университеті, 35900 Tanjong Malim, Перак, Малайзия
[2]Биофизика Институты, Дечжоу университеті, Дечжоу 253023, Қытай
[3]Лафия федералдық университеті, Лафия, Насарава штаты, Нигерия
[4]Металлургия және кен байыту институты, Сәтбаев университеті, Алматы, Қазақстан
[5]Университет Путра Малайзия, 43400, Серданг, Селангор, Малайзия
[6]MARA технологиялық университеті, 40450 Шах Алам, Селангор, Малайзия
[7]Физика мектебі, Universiti Sains Malaysia, 11800 USM, Пенанг, Малайзия;
[8] Малайзия Келантан университеті, Джели 17600, Келантан, Малайзия

Мақала келді: *13 желтоқсан 2023*
Сараптамадан өтті: *23 қаңтар 2024*
Қабылданды: *22 ақпан 2024*

ТҮЙІНДЕМЕ

Сирек жер элементтері оксидтерінің әртүрлі типтерінің мырыш боротеллурит шынысына әсерін зерттеу оптикалық құрылғыларда әлеуетті қолдану мүмкіндігін анықтау үшін маңызды. Мырыш боротеллуритті шыныға сирек жер элементтері оксидтерін қосу 4f-4f ауысуларының әсерінен оптикалық қасиеттерді жақсартатыны белгілі. Бұл жұмыста ZBTNd, ZBTHo, ZBTEr және ZBTSm деп белгіленген мырыштың боротеллурит шынысына әртүрлі сирек жер элементтері оксидтерінің әсерін салыстыру мақсат етілген. Шыны үлгілері балқыту әдісімен дайындалды. Шыныларға физикалық зерттеу тығыздық пен молярлық көлемді өлшеу арқылы жасалды. Неодим оксидіндегі атомдық радиус аз болғандықтан, ZBTNd шынысының басқа шыныларға қарағанда ең төмен тығыздығы бар екені анықталды. ZBTHo шынысының жоғары тығыздығы оның радиациядан қорғау ретінде пайдалану мүмкіндігін көрсетеді. ZBTNd шыны үшін молярлық көлемнің жоғары мәні тиімді талшықты оптика болып табылады, өйткені ZBTNd шыны серпімділік бойынша жақсы көрсеткішке ие. ZBTEr төмен дисперсиялық сипаттамаларға ие болғандықтан басқа әйнектерге қарағанда сыну көрсеткіші төмен екені анықталды. Дегенмен, ZBTEr әйнегі оптикалық байланыс қолданбалары ретінде пайдалану үшін жақсы көрсеткішке ие. Оптикалық сіңіру ZBTEr > ZBTHo > ZBTNd > ZBTSm бастап ұзағырақ толқын ұзындығына ауысатыны анықталды. ZBTEr шынысының оптикалық диапазондық энергиясы эрбийдің кулондық тебілу энергиясына байланысты басқа шыныларға қарағанда жоғары, ол неодим мен самарийден үлкен және гольмиден сәл жоғары. Барлық шынылардың электрондық поляризациялық үлгісі келесідей ZBTSm>ZBTNd>ZBTER>ZBTHo болады. ZBTEr үшін оптикалық негізділік ең жоғары болды, бұл қышқылдықтың жоғары екенін көрсетеді, ал ZBTNd шынысының қышқылдығы төмен, бұл негізділіктің жоғарырақ мәніне сәйкес келеді..

Түйін сөздер: теллуритті шыны, сирек жер элементтері оксидтері, оптикалық қасиеттер.

Авторлар туралы ақпарат:

Azlina Y.	*Физика кафедрасы, ғылым және математика факультеті, Пендикан Сұлтан Идрис университеті, 35900 Танджонг Малим, Перак, Малайзия*
Azlan M.N.	*Доктор, физика кафедрасы, ғылым және математика факультеті, Пендикан Сұлтан Идрис университеті, 35900 Танджонг Малим, Перак, Малайзия*
Suriani A.B	*Физика кафедрасы, ғылым және математика факультеті, Пендикан Сұлтан Идрис университеті, 35900 Танджонг Малим, Перак, Малайзия*
Shaari H.R.	*Физика кафедрасы, ғылым және математика факультеті, Пендикан Сұлтан Идрис университеті, 35900 Танджонг Малим, Перак, Малайзия*
Naif Mohammed Al-Hada	*Шандонг биофизикасының негізгі зертханасы, Биофизика институты, Дечжоу университеті, Дечжоу 253023, Қытай*
Umar S.A.	*Физика кафедрасы, ғылым факультеті, Лафия федералдық университеті, Лафия, Насарава штаты, Нигерия*
Кенжалиев Багдаулет Кенжалиевич	*Профессор, т.ғ.д., Металлургия және кен байыту институты, Сәтбаев Университеті, Алматы, Қазақстан*
Zaid M.H.M.	*Физика департаменті, ғылым факультеті, Университет Путра Малайзия, 43400, Серданг, Селангор, Малайзия*
Hisam R.	*Қолданбалы ғылымдар факультеті, MARA технологиялық университеті, 40450 Шах Алам, Селангор, Малайзия*
Iskandar S.M.	*Физика мектебі, Сайнс Малайзия Университеті, 11800 USM, Пенанг, Малайзия*
Yusof N.N.	*Физика мектебі, Сайнс Малайзия Университеті, 11800 USM, Пенанг, Малайзия*
Abdul Hafidz Yusoff	*«Алтын сирек жер және материалды өңдеу» орталығы (GREAT), биоинженерия және технологиялар факультеті, Малайзия Келантан университеті, Джели 17600, Келантан, Малайзия*

Внедрение неодима, гольмия, эрбия и самария (оксидов) в цинкборотеллуритное стекло: физический и оптический сравнительный анализ

[1]Azlina Y., [1*]Azlan M.N., [1]Suriani A.B., [1]Shaari H.R., [2]Naif Mohammed Al-Hada, [3]Umar S.A., [4]Kenzhaliyev B.K., [5]Zaid, M.H.M., [6]Hisam R., [7]Iskandar S.M., [7]Yusof N.N., [8]Abdul Hafidz Yusoff

[1]Университет Пендидикан Султан Идрис, 35900 Танджонг Малим, Перак, Малайзия
[2] Институт биофизики, Университет Дэчжоу, Дэчжоу 253023, Китай
[3] Федеральный университет Лафии, Лафия, штат Насарава, Нигерия
[4]Институт металлургии и обогащения, Сатбаев Университет, Алматы, Казахстан
[5] Университет Путра Малайзия, 43400, Серданг, Селангор, Малайзия
[6] Технологический университет MARA, 40450 Шах Алам, Селангор, Малайзия
[7]Школа физики, Университет Сайнс Малайзия, 11800 USM, Пенанг, Малайзия
[8] Университет Малайзии Келантан, Джели 17600, Келантан, Малайзия

Поступила: *13 декабря 2023*
Рецензирование: *23 января 2024*
Принята в печать: *22 февраля 2024*

АННОТАЦИЯ

Исследование влияния различных типов оксидов редкоземельных элементов на цинкборотеллуритное стекло важно для определения потенциального применения в оптических устройствах. Известно, что добавление оксидов редкоземельных элементов в цинкборотеллуритное стекло улучшает оптические свойства за счет эффектов 4f-4f-переходов. В данной работе мы стремимся сравнить влияние различных оксидов редкоземельных элементов на цинкборотеллуритное стекло, обозначенное как ZBTNd, ZBTHo, ZBTEr и ZBTSm. Образцы стекла были успешно изготовлены методом закалки в расплаве. Физическое исследование стекол было проведено путем измерения плотности и молярного объема. Установлено, что стекло ZBTNd имеет самую низкую плотность по сравнению с другими стеклами из-за малого атомного радиуса оксида неодима. Высокая плотность стекла ZBTHo указывает на его потенциал для использования в качестве защиты от радиации. Высокое значение молярного объема стекла ZBTNd является преимуществом оптоволокна, поскольку стекло ZBTNd имеет хорошие показатели эластичности. Установлено, что ZBTER имеет более низкий показатель преломления, чем другие стекла, из-за низких дисперсионных характеристик. Тем не менее, стекло ZBTER имеет хорошие характеристики для использования в приложениях оптической связи. Обнаружено, что оптическое поглощение смещается в длинноволновую область, начиная с ZBTEr > ZBTHo > ZBTNd > ZBTSm. Энергия оптической запрещенной зоны у стекла ZBTER выше, чем у других стекол, из-за энергии кулоновского отталкивания эрбия, которая больше, чем у неодима и самария, и немного выше, чем у гольмия. Характер электронной поляризуемости для всех стекол был найден следующим образом: ZBTSm>ZBTNd>ZBTER>ZBTHo. Оптическая основность ZBTEr оказалась самой высокой, что указывает на более высокую кислотность, в то время как стекло ZBTNd имеет самое низкое значение, соответствующее более высокой основности.

***Ключевые слова*:** теллуритное стекло, оксиды редкоземельных элементов, оптические свойства

Информация об авторах:

Azlina Y.	*Факультет физики, факультет естественных наук и математики, Университет Пендидикан Султан Идрис, 35900 Танджонг Малим, Перак, Малайзия*
Azlan M.N.	*Доктор, Факультет физики, факультет естественных наук и математики, Университет Пендидикан Султан Идрис, 35900 Танджонг Малим, Перак, Малайзия*
Suriani A.B	*Факультет физики, факультет естественных наук и математики, Университет Пендидикан Султан Идрис, 35900 Танджонг Малим, Перак, Малайзия*
Shaari H.R.	*Факультет физики, факультет естественных наук и математики, Университет Пендидикан Султан Идрис, 35900 Танджонг Малим, Перак, Малайзия*
Naif Mohammed Al-Hada	*Ключевая лаборатория биофизики Шаньдуна, Институт биофизики, Университет Дэчжоу, Дэчжоу 253023, Китай*
Umar S.A.	*Кафедра физики, факультет естественных наук, Федеральный университет Лафии, Лафия, штат Насарава, Нигерия*
Кенжалиев Багдаулет Кенжалиевич	*Профессор, д.т.н., Институт Металлургии и Обогащения, Satbayev University, Алматы, Казахстан*
Zaid M.H.M.	*Кафедра физики, факультет естественных наук, Университет Путра Малайзия, 43400, Серданг, Селангор, Малайзия*
Hisam R.	*Факультет прикладных наук Технологического университета MARA, 40450 Шах Алам, Селангор, Малайзия*
Iskandar S.M.	*Школа физики, Университет Сайнс Малайзия, 11800 USM, Пенанг, Малайзия*
Yusof N.N.	*Школа физики, Университет Сайнс Малайзия, 11800 USM, Пенанг, Малайзия*
Abdul Hafidz Yusoff	*Центр технопредпринимательства золотых редкоземельных и материалов (GREAT), факультет биоинженерии и технологии, Университет Малайзии Келантан, Джели 17600, Келантан, Малайзия*

References

[1] Abdel Wahab EA, Koubisy MSI, Sayyed MI, Mahmoud KA, Zatsepin AF, Sayed A Makhlouf, Shaaban KhS. Novel borosilicate glass system: Na2B4O7-SiO2-MnO2: Synthesis, average electronics polarizability, optical basicity, and gamma-ray shielding features, Journal of Non-Crystalline Solids. 2020.

[2] Hong Luo, Jianwu Yu, Haiqin Lou, Kaifeng Huang, Junzhi Hu, Binchao Xu, Thermal/tribological effects of superimposed ultrasonic vibration on viscoelastic responses and mold-filling capacity of optical glass: A comparative study, Ultrasonics. 2020; 108.

[3] Nazrin SN, Halimah MK, Muhammad FD, Latif AA, Iskandar SM, Asyikin AS. Experimental and theoretical models of elastic properties of erbium-doped zinc tellurite glass system for potential fiber optic application, Materials Chemistry and Physics. 2021; 259.

[4] Azlina Y, Azlan MN, Suriani AB, Halimah MK, Umar SA. Optical properties of graphene oxide-coated tellurite glass for potential fiber optics, Journal of Non-Crystalline Solids. 2020; 536.

[5] El Yuwei Wu, Chunhui Niu, Lei Wang, Mingqing Yang, Shiyu Zhang. Structural, luminescence, and temperature sensing properties of the Er3+-doped germanate-tellurite glass by excitation at different wavelengths, Journal of Luminescence. 2024; 266.

[6] Azlina Y, Azlan MN, Halimah MK, Umar SA, El-Mallawany R, Najmi G. Optical performance of neodymium nanoparticles doped tellurite glasses, Physica B: Condensed Matter. 2020; 577.

[7] Azlan MN, Halimah MK, Sidek HAA. Linear and nonlinear optical properties of erbium doped zinc borotellurite glass system, Journal of Luminescence. 2017; 181:400-406.

[8] Vani P, Vinitha G, Praveena R, Durairaj M, Sabari Girisun TC, Manikandan N. Influence of holmium ions on the structural and optical properties of barium tellurite glasses, Optical Materials. 2023; 136.

[9] Hemlata Kumari, Ghizal F Ansari, Mahajan SK, Sk Rezaul K, Sukhdev Bairagi. Study of visible upconversion luminescence in Er3+ and Er3+/Yb3+ doped tungsten tellurite glasses, Materials Today: Proceedings. 2023.

[10] Yusof NN, Ghoshal SK, Jupri SA, Azlan MN. Synergistic effects of Nd3+ and Ag nanoparticles doping on spectroscopic attributes of phosphate glass, Optical Materials. 2020; 110.

[11] Umar SA, & Ibrahim GG. Theoretical Elastic Moduli of TeO2 – B2O3 – SiO2 Glasses. EDUCATUM Journal of Science, Mathematics and Technology. 2020; 7(2):18-30.

[12] Tekin HO, Kassab LRP, Shams AM Issa, Camila Dias da Silva Bordon, M.S. Al-Buriahi, Filipe de Oliviera Pereira Delboni, Gokhan Kilic, Evellyn Santos Magalhaes, Structural and physical characterization study on synthesized tellurite (TeO2) and germanate (GeO2) glass shields using XRD, Raman spectroscopy, FLUKA and PHITS, Optical Materials. 2020; 110:110533.

[13] Kawa M Kaky, Sayyed MI, Mhareb MHA, Alyaa H Abdalsalam, Mahmoud KA, Baki SO, Mahdi MA. Physical, structural, optical and gamma radiation attenuation properties of germanate-tellurite glasses for shielding applications, Journal of Non-Crystalline Solids. 2020; 545.

[14] Devaraja C, Jagadeesha Gowda GV, Keshavamurthy K, Eraiah B, Devarajulu G, Jagannath G. Physical, structural and photo luminescence properties of lead boro-tellurite glasses doped with Eu3+ ions, Vacuum. 2020; 177:109426.

[15] Murali Krishna V, Mahamuda Sk, Rekha Rani P, Swapna K, Venkateswarlu M, Rao AS. Effect of samarium ions concentration on physical, optical and photoluminescence properties of Oxy-Fluoro Boro Tellurite glasses, Optical Materials. 2020; 109:110368.

[16] Ravi Prakash M, Neelima G, Venkata Krishnaiah Kummara, Ravi N, Dwaraka Viswanath CS, Subba Rao T, Mahaboob Jilani S. Holmium doped bismuth-germanate glasses for green lighting applications: A spectroscopic study, Optical Materials. 2019; 94:436-443.

[17] Katarzyna Pach-Zawada, Magdalena Leśniak, Katarzyna Filipecka, Edmund Golis, El Sayed Yousef, Piotr Pawlik, Dominik Dorosz, Maciej Sitarz, Jacek Filipecki, Structural studies of tellurite glasses from the 70TeO2-5XO-10P2O5–10ZnO–5PbF2 system (X = Ba, W, Sr, Cd) doped with erbium ions, Journal of Molecular Structure. 2021; 1224:128787.

[18] Naseer KA, Marimuthu K, Al-Buriahi MS, Amani Alalawi, Tekin HO. Influence of Bi2O3 concentration on barium-telluro-borate glasses: Physical, structural and radiation-shielding properties, Ceramics International. 2021; 47(1):329-340.

[19] Halimah MK, Umar SA, Chan KT, Latif AA, Azlan MN, Abubakar AI, Hamza AM. Study of rice husk silicate effects on the elastic, physical and structural properties of borotellurite glasses, Materials Chemistry and Physics. 2019; 238:121891.

[20] Azlan MN, Halimah MK. Role of Nd3+ nanoparticles on enhanced optical efficiency in borotellurite glass for optical fiber, Results in Physics. 2018; 11:58-64.

[21] Yusof NN, Ghoshal SK, Azlan MN. Optical properties of titania nanoparticles embedded Er3+-doped tellurite glass: Judd-Ofelt analysis, Journal of Alloys and Compounds. 2017; 724:1083-1092.

[22] Halimah MK, Faznny MF, Azlan MN, Sidek HAA. Optical basicity and electronic polarizability of zinc borotellurite glass doped La3+ ions, Results in Physics. 2017; 7:581-589.

[23] Mariselvam K, Juncheng Liu. A novel Er3+ ions doped zirconium magnesium borate glass with very high quantum efficiency for green laser and optical amplifier applications, Solid State Sciences. 2021; 111.

[24] Swetha BN, Devarajulu G, Keshavamurthy K, Jagannath G, Deepa HR. Enhanced 1.53 μm emission of Er3+ in nano-Ag embedded sodium-boro-lanthanate glasses, Journal of Alloys and Compounds. 2021; 856:158212.

[25] Madhu A, Srinatha N. Structural and spectroscopic studies on the concentration dependent erbium doped lithium bismuth boro tellurite glasses for optical fiber applications, Infrared Physics & Technology. 2020; 107:103300.

[26] Alaska Subedi, First-principles study of the electronic structure and magnetism of CaIrO3, Phys. 2012; 85(2):020408.

[27] Pieter Dorenbos, Lanthanide 4f-electron binding energies and the nephelauxetic effect in wide band gap compounds, Journal of Luminescence. 2013; 136:122-129.

[28] Fajans K, & Kreidl NJ. Stability of lead glasses and polarization of ions, Journal of the American Ceramic Society. 1948; 31(4):105-114.

[29] Dimitrov V, and Sakka S. Electronic Oxide Polarizability and Optical Basicity of Simple Oxide. Journal of Applied Physics. 1996; 79:1736-1740.

[30] Duffy JA, Ingram MD. Establishment of an optical scale for Lewis basicity in inorganic oxyacids, molten salts, and glasses, J. Am. Chem. Soc. 1971; 93:6448.

[31] Dimitrov V, Komatsu T. An interpretation of optical properties of oxides and oxides glasses in term of electronic polarizability and average single bond strength, J. Univ. Chem. Technol. Metal. 2010; 45: 219-225.

Crossref
DOI: 10.31643/2025/6445.04
Earth Sciences

Nature of ree accumulation in clayey interlayers and coals in Karaganda coal basin

Kopobayeva A.N., Baydauletova I.V., *Amangeldikyzy A., Askarova N.S., Blyalova G.G.

Abylkas Saginov Karaganda Technical University, Karaganda, Kazakhstan

** Corresponding author email: amangeldykyzy@inbox.ru*

Received: *November 17, 2023*
Peer-reviewed: *December 21, 2023*
Accepted: *February 23, 2024*

ABSTRACT
It is the first completed complex mineralogical and geological research of REE (Y, La, Ce, Pr, Nd, Sm, Eu, Gd, Tb, Dy, Ho, Er, Tm, Yb, Lu) in the coals of Karaganda coal basin in Central Kazakhstan. This paper presents the results of the research of REE (from lanthanum to lutetium and Y) distribution in 85 samples of coal and clayey interlayers of stratum k7 of Karaganda coal basin in the faces of Saranskaya, T.Kuzembayev, Aktasskaya mines. The ultimate composition of clayey interlayer and coal samples was analyzed by the methods of inductively coupled plasma optical emission spectroscopy and inductively coupled plasma mass spectrometry (ICP-OES and ICP-MS). Research of the lateral and vertical discontinuity of the total REE concentration has indicated the presence of mixed types of REE distribution in coals, which supposes various forms of REE migration and different mobility of heavy and light lanthanides within the hypergenesis zone. The established lanthanum-ytterbium (La/Yb) ratio in the coal, which is normalized to UCC and equals La/Yb<1, relates to the coals with H type of REE distribution, and the one that equals La/Yb>1 and normalized to chondrite belongs to the coals with L type of REE distribution, which allows making conclusions on the presence of independent sources and different mechanisms of REE accumulation in the sediments of Karaganda coal basin. It is also established that the La/Yb ratio grows from coals to clayey interlayers, which indicates a predominantly clastogenic mechanism of REE input to the coals. The prevailing mineral form of the REE in the coal and clayey interlayer samples from the Karaganda coal basin is light lanthanide phosphates. Sparry crystals with CeLaNdPO composition were found in the coal and clayey interlayer samples. It was established that xenotime is the main deportment for Y in many coals.

Keywords: coal, clayey interlayer, Central Kazakhstan, Karaganda coal basin, rare earth elements, average content.

Information about authors:

Kopobayeva Aiman Nygmetovna — *PhD, acting associate professor of the Geology and Exploration MD Department of Abylkas Saginov Karaganda Technical University. 100000, Karaganda, Republic of Kazakhstan. E-mail: kopobayeva@inbox.ru*

Baidauletova Irina Vladimirovna — *Master's student of the Geology and Exploration MD Department of Abylkas Saginov Karaganda Technical University, Mining faculty, Karaganda, 100026, Republic of Kazakhstan. E-mail: ira-sara@bk.ru*

Amangeldikyzy Altynay — *PhD, acting associate professor of the Geology and Exploration MD Department of Abylkas Saginov Karaganda Technical University. 100000, Karaganda, Republic of Kazakhstan. E-mail: amangeldykyzy@inbox.ru*

Askarova Nazym Srazhadinkyzy — *PhD, lecturer of Geology and ExplorationI MD department of Abylkas Saginov Karaganda Technical University. E-mail: srajadin-nazym@mail.ru*

Blyalova Gulim Galymzhanovna — *Doctoral student of Abylkas Saginov Karaganda Technical University, Master of Technical Sciences in Geology and Exploration MD department of Abylkas Saginov Karaganda Technical University. 100000, Karaganda, Republic of Kazakhstan. E-mail: gulim_blyalova@mail.ru*

Introduction

The growing demand for rare earth elements in the global market encourages many countries to search for alternative REE sources. In such countries as the USA, China and a range of other countries, the average content of all rare earth elements has already been estimated in the world coals [[1], [2]]. Coal and coal processing products have become an alternative for finding and extracting REE.

The main sources of REE are granite weathering crusts, carbonatite deposits and coastal-marine placers. In addition to traditional raw materials sources of lanthanides, metalliferous coals are also considered potentially promising [[3], [4]]. The factor of synchronous volcanism has a significant impact on the formation of the geochemical

background of rare elements and impurities in coals (Finkelman, 1993). Volcanogenic material is found in coal seams mainly in the form of low–power clay interlayers - tonsteins. Volcanic pyroclastic, which forms tonsteins, serves as a source of accumulation of valuable metals and abnormal concentrations of impurity elements in coals. In areas with thick seams, the accumulation levels of these impurity elements in coals can reach industrially significant values (Seredin, 1994; Spears, 1999, Arbuzov et al., 2003, 2005, 2019).

The first references to the abnormal content of REE in coals were noted in 1933 by V.M. Goldschmidt and C. Peters. In the 1980s, V.V. Seredin for the first time described rare earth mineralization with commercial content of REE in coals. After publication in 1991 by V.V. Seredin, different research groups started to publish papers on abnormally rare earth coals in other deposits [Seredin, 2001, 2005; Seredin et al., 2011, 2012, 2013; Dai et al., 2007, 2008, 2010, 2011, 2016c; Arbuzov et al., 1997, 2003, 2007a; Hower et al., 1999; Mardon, Hower, 2004; Chekryzhov et al., 2016b; Dai et al., 2016c], which had lead to an increased interest to studying lanthanide geochemistry in coal deposits. It is known [[3], [5]], that REE content in all coals is lower than in UCC (upper continental crust). Countries with developed economies (USA, Europe, Australia, China) have partially estimated REE composition in the organic matter, and it is published in many publications, which show that coals and coal ashes can also contain high, in some cases commercial concentrations of REE. For the efficiency of REE extraction from coals, it is necessary to understand the mechanism of concentration, nature of accumulation, and deportments of REE in coals. In this regard, attention to geochemical research in coal deposits has increased dramatically, and coal deposits are considered potential sources of REE [[3], [5]].

However, despite comprehensive geochemical research of coal deposits in the world, the issues related to the conditions of accumulation, migration and fractionating of lanthanides in coals, their departments, and factors controlling the formation of rare earth metal-bearing coals remain open and require additional research [[4], [6]].

For the Republic of Kazakhstan, the industry of which is focused on the extraction, processing and consumption of mineral raw materials, the state of the mineral resource base is of key importance. The Karaganda coal basin is one of the largest and most promising basins in Kazakhstan. In his Message to the people of Kazakhstan [7], President of the Republic of Kazakhstan Kassym-Zhomart Tokayev on 01.03.2023 noted the high significance of studying and researching rare and rare earth metals: “One of priority tasks must be development of deposits of rare and rare earth metals that essentially have become a “new oil”. Countries that will be able to implement their potential in this sphere will define the vector of the technological progress for the whole world”, said the President of the Republic of Kazakhstan. The President's words once again confirm the relevance of research on the REE geochemistry in coal as an additional source of REE.

A comprehensive assessment of the contents of critical elements in coal is extremely important for understanding the geological processes affecting their enrichment with elements, which allows the full use of coal in an economical and environmentally friendly way. A reliable estimation of the average content of rare earth elements in coal for the majority of coal basins and deposits of Kazakhstan needs to be clarified using modern research methods. An analysis of the nature of the lateral distribution showed that the k7 coal seam can serve as a potential raw material for complex processing and utilization of many impurity elements. The restoration of economically valuable REE and critical elements that can contribute to the national economy, the introduction of advanced environmentally friendly technologies and the reduction of the risk of coal leaks in warehouses will limit disposal costs, as well as reduce the environmental impact, which should be taken into account and implemented by coal mining companies.

Deposit Characteristics. A distinctive feature of the Paleozoic coal accumulation in Central Kazakhstan, as a result of which the Karaganda coal basin was formed, is a significant influence on the carbon formation process of volcanic activity. This was reflected in the enrichment of coals with lithophilic, including moderate and weakly carbon fiber elements such as Hf, REE, Sr, Ta, Th and U [[5], [8]]. Their anomalies in Paleozoic coals are associated with the horizons of tonsteins, modified tuffites and scattered pyroclastic material, which were described above.

The Karaganda coal basin in the west is framed by the large meridional Tekten fault. In the east, its border is considered to be part of the synclinorium, where it abruptly turns into a narrow and shallow synclinal fold (Achshisu synclinorium), which comprises coal-bearing sediments with commercial

strata. Beyond the basin, this synclinorium extends to the east along the valley of the Achshisu River for 200 km.

Within the Karaganda basin, three large synclinoria are distinguished (from west to east): Churubay-Nura, Karaganda and Upper-Sokur, which are divided by respectfully Alabas anticlinal fold and Maykuduk upheaval [9] (see Fig. 1).

This paper presents the results of the complex mineralogical and geochemical research of the stratum k7 of the Karaganda district of Karaganda coal basin in the faces of “Saranskaya”, “Aktasskaya”, Kuzembayev mines.

The listed mines belong to the Karaganda coal province. Today, all three mines are joined into the Saran field of Karaganda coal province. The field of T. Kuzembayev mine is located in the eastern part of Saran field. The fields of Saranskaya and Aktasskaya mines belong to the central and southwest parts of the Saran field of Karaganda coal province.

The Karaganda synclinorium, within which the Karaganda coal province is located, occupies the central part of the Karaganda basin. The northwestern wing of the synclinorium, where the T. Kuzembayev, Saranskaya and Aktasskaya mines are located features a comparatively simple structure and persistent east-north-eastern trending. The northwest flat dipping wing of the synclinorium has a general northeast trend with a pitch towards the southeast under the angle of 10-150. In the northeastern, part of the site in the area of synclinorium closure, the trending of the coal-bearing strata gradually changes from north-eastern to eastern. Pitch angles at outcrops are respectfully grown from 10-15 to 700. The southeastern wing of the synclinorium unlike the northwestern one has more upridging of strata.

Discontinuous faults are widely developed on the southeastern wing of the Karaganda synclinorium, and there are few of them on the northwestern flat dipping wing and this area is tectonically simple. The geological structure of the region comprises sediments of Carbonic, Jurassic, Neocene and Quaternary periods [9].

According to M.G. Chernovyants (1992), a high saturation of coal seams with tosteins has been established. Among them, coarse and crystalline varieties predominate, their thickness ranges from fractions of millimetres to 2 cm. It was also found that the k1 formation at the mine named after Gorbachev has up to 20 tonstein interlayers, and the k7 formation has 6 Tonstein horizons. In this regard, samples were taken in three operating mines, where the k7 formation is currently being worked out, these are directly in the bottom – the Saranskaya, Aktasskaya and Kuzembaev mines for a more detailed study of geochemical features and understanding of the mechanisms of accumulation of impurity elements in the coal-bearing deposits of the Karaganda syncline.

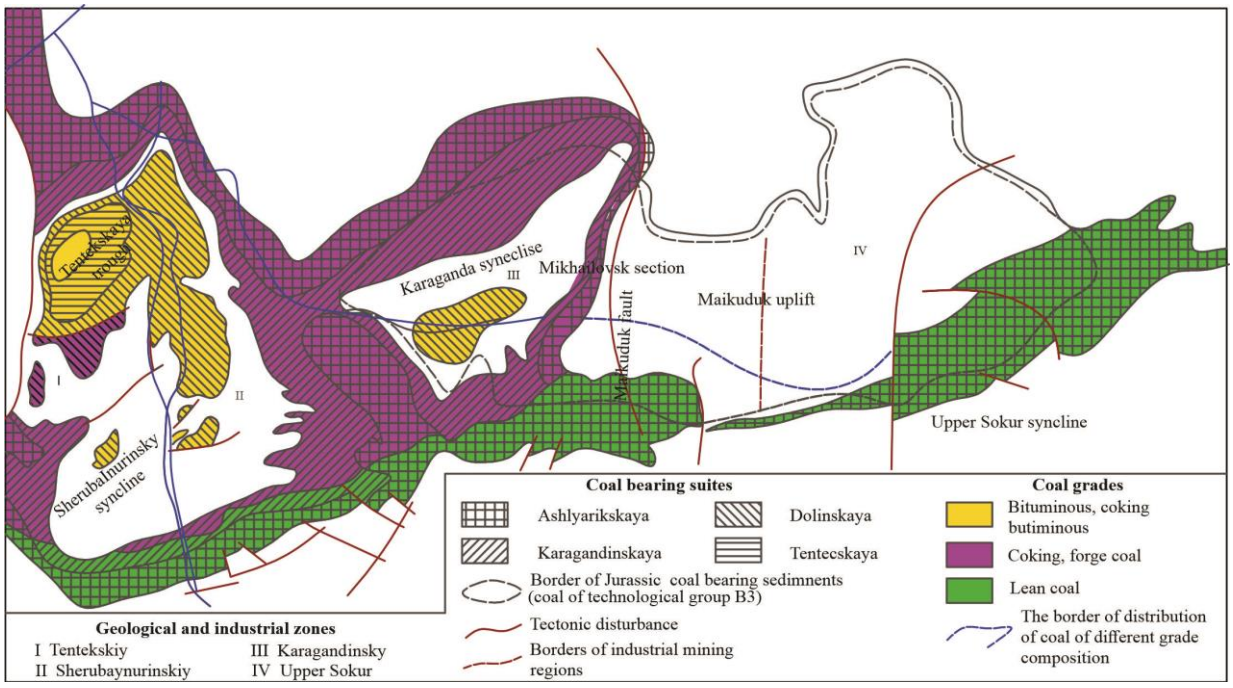

Figure 1 – Geological and Industrial Zoning of Karaganda Coal Basin

Research Methods

The grounds for this article are complex geochemical and mineralogical research of coals and clayey interlayers of stratum k_7 of the Karaganda coal basin. Coal strata sampling was performed by the channel method with differentiated sampling in the faces of Saranskaya, T. Kuzembayev, and Aktasskaya mines. 85 samples of coals and hosting rocks have been taken in vertical sections. In each section, 5 samples were taken to trace the lateral and vertical variation in the mineralogical and geochemical features of stratum k_7: coals – UC (upper coal – upper part of the section) and BC (bottom coal – bottom part of the section); clayey interlayers – CI and contact zones of coal and clayey interlayers – UCn (upper contact in the upper part of the section) and of clayey interlayer with coal – BCn (bottom contact in the bottom part of the section). The length of the sampling interval was chosen depending on the thickness and complexity of the stratum structure; it on average varied from 10 m to 200 m. The depth of the sampling points varies at the three mines, the depth of the formation varies from 600 to 650 m.

All samples were subjected to sample preparation, laboratory and analytical tests in accredited, leading laboratories that specialize in coal research. The ultimate composition of clayey interlayer and coal samples was analyzed by the methods of inductively coupled plasma optical emission spectroscopy and inductively coupled plasma mass spectrometry (ICP-OES and ICP-MS). To study the distribution of the minerals, their form, and morphological features in the coals and clayey interlayers, analytical scanning electron microscopy along with energy-dispersive X-ray spectroscopy (SEM-EDS) were used. All researches were performed in the Federal State Budget Enterprise of Science Far East Geological Institute of the Far Eastern Branch of the Russian Academy of Sciences (FEGI FEB RAS).

Discussion of the results 85 coal samples were studied: 25 coal samples at Saranskaya mine, 40 coal samples from Kuzembayev mine, 20 coal samples at Aktasskaya mine; total content of REE (Y, La, Ce, Pr, Nd, Sm, Eu, Gd, Tb, Dy, Ho, Er, Tm, Yb, Lu) are presented in Table 1, Table 2, and Table 3.

Based on these data, the total amount of REE in clayey interlayers and contact zones varies within the range of ∑REE = 53.18-102.53 g/t. And their total content in the coal is within the range ∑REE = 28.48-65.78 g/t. These data on REE amounts in the coals and clayey interlayers indicate that increased content of REE relates to the clayey interlayers and contact zones of the coal-clayey interlayer.

Table 1 – Results on the REE Contents for Saranskaya Mine

Saranskaya Mine					
	Sampling Point No. 1				
	UC	UCn	CI	BCn	BC
$\sum_{REE}$	65.78	68.01	104.89	75.81	35.86
	Sampling Point No. 2				
$\sum_{REE}$	62.44	57.34	107.18	62.19	41.04
	Sampling Point No. 3				
$\sum_{REE}$	35.52	64.52	96.19	60.61	46.8
	Sampling Point No. 4				
$\sum_{REE}$	60.52	47.99	90.45	36.26	30.59
	Sampling Point No. 5				
$\sum_{REE}$	33.07	58.46	89.04	49.59	30.34

Table 2 – Results on the REE Contents for T. Kuzembayev

Mine Aktasskaya Mine					
	Sampling Point No. 1				
	UC	UCn	CI	BCn	BC
$\sum_{REE}$	38.89	56.29	92.72	63.2	41.35
	Sampling Point No. 2				
$\sum_{REE}$	36.23	44.69	89.11	49.06	33.1
	Sampling Point No. 3				
$\sum_{REE}$	46.5	47.15	86.82	51.63	29.47
	Sampling Point No. 4				
$\sum_{REE}$	38.37	64.62	89.3	51.73	35.47

Table 3 – Results on the REE Contents for Aktasskaya

Mine Kuzembayev Mine					
	Sampling Point No. 1				
	UC	UCn	CI	BCn	BC
$\sum_{REE}$	29.99	48.46	90.46	62.17	48.59
	Sampling Point No. 2				
$\sum_{REE}$	65.31	67.69	89.04	54.87	42.41
	Sampling Point No. 3				
$\sum_{REE}$	55.9	57.15	97.67	68.1	38.74
	Sampling Point No. 4				
$\sum_{REE}$	59.32	63.22	112.45	87.2	35.67
	Sampling Point No. 5				
$\sum_{REE}$	47.11	75.7	107.01	64.03	36.26
	Sampling Point No. 6				
$\sum_{REE}$	51.42	78.99	106.66	69.23	28.48
	Sampling Point No. 7				
$\sum_{REE}$	43.36	76.46	107.99	79.19	31.09
	Sampling Point No. 8				
$\sum_{REE}$	47.71	64.65	108.94	66.36	42.72

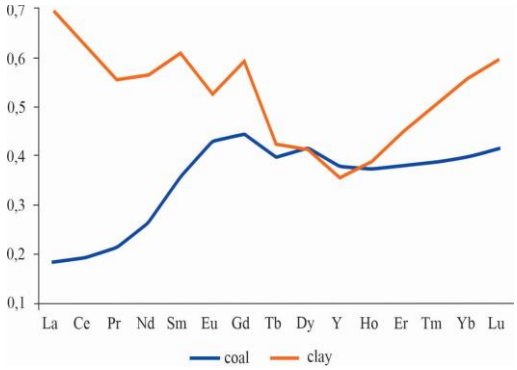

a) normalized to UCC

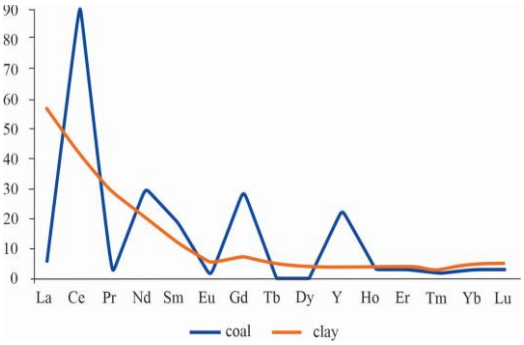

b) normalized to chondrite

Figure 2 – Rare Earth Elements Distribution in Coals and Clayey Interlayers of Karaganda Coal Basin

Seredin and Dai [4] divided REY (REE) in coal into light (LREY: La, Ce, Pr, Nd and Sm), medium (MREY: Eu, Gd, Tb, Dy and Y) and heavy (HREY: Ho, Er, Tm, Yb and Lu) groups. This classification is more convenient than other classifications for describing REE distribution in coals. When interpreting the obtained results, REE contents were considered as normalized to the chondrite composition [10] and normalized to UCC [10], and the following criteria for lanthanide estimation were used:

$$Eu_{an} = Eu/Eu^* = Eu_N/(Sm_N + Gd_N) \times 0.5 \quad (1)$$

$$Ce_{an} = Ce/Ce^* = Ce_N/(La_N + Pr_N) \times 0.5 \quad (2)$$

The distribution curve normalized to UCC in clay shows depletion of medium lanthanides and predominance of light lanthanides over heavy ones, and vice versa enrichment of medium lanthanides and predominance of heavy lanthanides over light ones in coal (Fig. 2). Estimated Eu - and Ce - anomalies in the coal and clay showed negative europium and cerium anomalies (0.24 and 0.26, respectively). This type of REE distribution is characteristic of clayey interlayers formed with the participation of ash material of acidic composition. Four main types of REE distribution are characteristic of the world coals: N–type (normal for earth crust), L –, M – and H – types feature an accumulation of light, medium and heavy lanthanides [[11], [12]]. It is considered that coals with N- and L-type distributions are formed when most of REE were introduced with terrigenous material and coals with M- and H-type distributions are formed when most REE were introduced with water solutions [[11], [12], [13]].

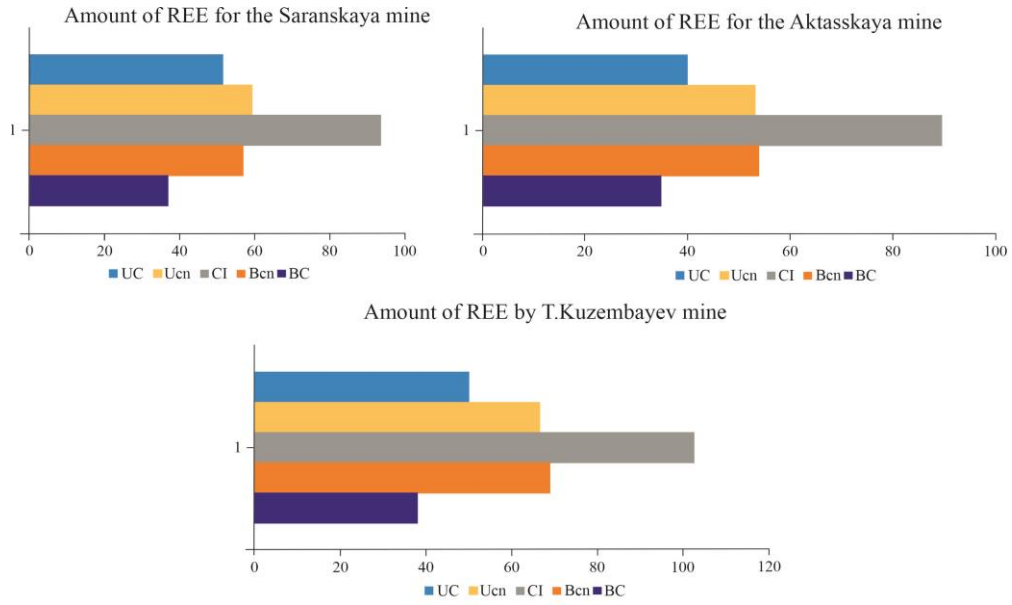

Figure 3 – Vertical Distribution of rare Earth Elements in Clayey Interlayers CI, Contacts of CI and Coal in Karaganda Coal

Basin Note. UC – upper coals, UCn – upper contact of coal and clayey interlayer, CI – clayey interlayer, BCn – bottom contact of clayey interlayer and coal, BC – bottom coals.

The indicative ratio is the lanthanum-ytterbium (La/Yb) ratio. The estimated lanthanum-ytterbium (La/Yb) ratio in coal, which is equal to La/Yb<1, allows referring the coals to H-type distribution coals, indicating the participation of water-soluble forms of lanthanides in REE accumulation in coals. Lanthanum-ytterbium ratio in clay equal to La/Yb>1 allows the conclusion of the existence of independent sources and different mechanisms of REE accumulation in the sediments of the Karaganda coal basin. For the Karaganda coal basin, the main supplier of debris material during different periods of basin formation was the mountain structures located to the south of the basin. A smaller volume of material (thinner one) came from the hilly uplands to the north (Ishina T.A., 1954).

Lanthanide normalization to chondrite differs significantly from UCC normalization: in clays, it shows a predominance of light lanthanides over heavy ones, the concentration ratio decreases from lanthanum (57.3) to ytterbium (4.9). The estimated Eu - and Ce - anomalies showed negative europium and cerium anomalies (0.1 and 0.2, respectively); there are more light lanthanides in the coal, with a positive cerium (5.6) anomaly and a negative europium anomaly (0.01) present. The lanthanum-ytterbium ratio in clay and coal equal to La/Yb>1 allows attributing coals to L-type REE distribution coals, which allows the conclusion that in the formation of L-type coals of the Karaganda coal basin with near-clark REE contents, a clayey matter of terrigenous ash as a carrier of REE prevailed [[12], [13], [14]].

According to [[15], [16]], the presence of mixed types of REE distribution implies different forms of REE migration and different mobility of heavy and light lanthanides in the hypergenesis zone. It is necessary to be cautious in interpreting these data for hard coals, since in the process of coal formation, intra-stratum migration of significant masses of excess moisture occurs, temperatures reach 200^0 C and higher, and stratal waters are also saturated with organic matter and carbon dioxide. Jointly these factors facilitate the migration of lanthanides and, consequently, can lead to significant redistribution and even their removal outside the coal stratum.

Complex processes of REE distribution in coals are indicated by the results of detailed geochemical research of the coal stratum k_7. Analysis of vertical REE distribution in stratum k_7 of the Karaganda coal basin (Fig.3) showed that the highest concentrations of all REE are characteristic of clayey interlayers and zones of coal and clayey interlayer contact.

Fig. 3 shows that lanthanides are equally enriched in the contact zones between coal and clayey interlayer. Detailed research of the coal stratum will make it possible to identify and evaluate the role of the main factors of REE accumulation in coal.

In terms of REE content in coal, the increase is seen in the REE content from the bottom (BC) towards the top (UC). La/Yb ratio in this case also grows from coals (6.31) to clayey interlayers (17.06), which indicates a predominantly clastogenic mechanism of REE input to the coals.

Distribution of lanthanum and ytterbium in coal showed that the La/Yb ratio in the stratum bottom (BC) decreases from west to northeast, and in the stratum top (UC) on the contrary increases from west to northeast. A sharp decrease in the lanthanum-ytterbium ratio indicates the participation of water-soluble forms of lanthanides in REE accumulation in the coals [[16], [17], [18]]. At the same time, the increase in the lanthanum-ytterbium ratio indicates a predominantly clastogenic mechanism of REE ingress into the coals [[19], [20]]. The La/Yb ratio from bottom to top decreases in the two mines, and towards the northeast the La/Yb ratio from BC to UC increases (Fig. 4). The latter is conditioned by the heterogeneous composition of the alimentation zones of individual regions of the basin. The nature of this phenomenon is multifactorial and requires special analysis.

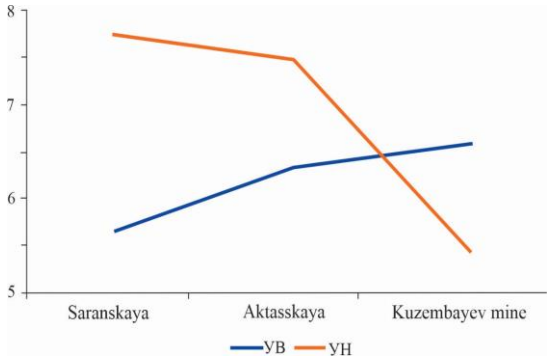

Figure 4 - Distribution of Lanthanum and Ytterbium in the Coal of Karaganda Coal Basin

Analysis of REE distribution showed increased total concentrations of light and medium lanthanides in the Karaganda coal basin, which

represents an interest in researching the nature of their accumulation in the coals (Table 4).

Analysis of REE distribution showed increased total concentrations of light and medium lanthanides in the Karaganda coal basin, which represents an interest in researching the nature of their accumulation in the coals (Table 4).

Assessment of lateral variability of element concentrations makes it possible to reveal the influence of rocks in the source area on the accumulation of abnormal REE concentrations in the coals. Within a single coal stratum, the distribution of lanthanides is often very uneven and is conditioned by the role of various factors responsible for REE accumulation in the coal.

Table 4 – Total REE Content in Coals for the Three Mines

Group	Element	∑coal Saranskaya Mine	∑coal Aktasskaya Mine	∑coal T. Kuzembayev Mine	Total Amount
Light	La	56.341	37.10	95.43	188.87
	Ce	123.522	85.24	212.59	421.35
	Pr	15.050	10.73	25.96	51.74
	Nd	69.973	49.74	115.35	235.06
	Sm	16.662	12.15	26.26	55.07
Medium	Eu	3.941	2.87	6.12	12.93
	Gd	18.083	12.65	27.05	57.78
	Tb	2.667	1.88	4.15	8.70
	Dy	15.856	10.26	23.73	49.85
	Y	95.809	61.49	127.37	284.67
Heavy	Ho	3.190	2.11	4.92	10.21
	Er	9.151	6.05	14.78	29.99
	Tm	1.349	0.85	2.18	4.37
	Yb	8.677	5.42	15.80	29.90
	Lu	1.388	0.84	2.31	4.54

Rare earth elements are distributed rather unevenly in the Karaganda coal basin. An increase in REE elements from the west (at Saranskaya mine) to the northeast (at T. Kuzembayev mine) is observed, with the minimum REE content found at the Aktasskaya mine (Fig. 5).

To explain the reduced REE content at the Aktasskaya mine, it is recommended to research the tectonic situation of stratum k_7 at the sites of these mines.

In all three mines, the Lu - Tm and Er - Yb contents are similar and range from 0.84-2.31 up to 5.42-15.80 g/t, respectively. The highest values of REE content in the coal are observed in the northeast of the Karaganda synclinorium at the T. Kuzembayev mine.

A high total content of Se, Y, Nd and La should be noted in all three mines (Table 4).

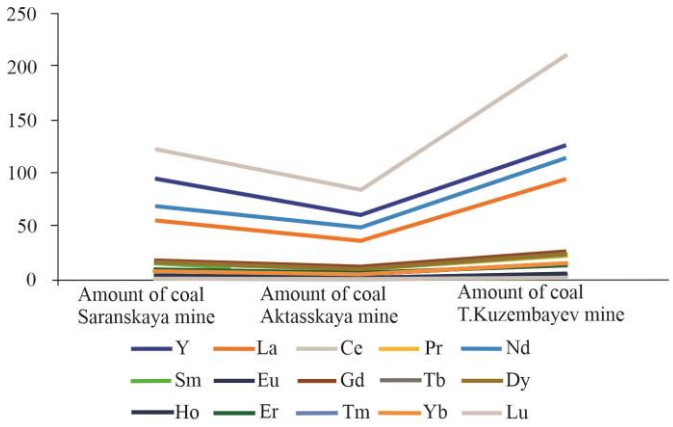

Figure 5 - Lateral Heterogeneity of REE Amount at Saranskaya, Aktasskaya, T. Kuzembayev Mines

Correlation analysis showed positive correlations of Y with light and medium lanthanides, and correlation with Y increases with light elements - La, Ce, Pr, Nd, Sm, the strongest correlation is with medium elements - Eu, Gd, Tb, Dy, and it decreases for heavy elements - No, Er, Tm, Yb, La. The correlation of cerium with light lanthanides is very strong and decreases towards heavy ones (Fig. 6).

To define trace mineral deportments of impurity elements in the rocks of the Karaganda coal basin, researches were performed using the highly local method of analytical scanning electron microscopy along with energy-dispersive X-ray spectroscopy (SEM-EDS), automated search for mineral phases with the set characteristics was performed using the AZtecFeature program modules.

By SEM-EDS method, 13 samples of coals, clayey interlayers and samples taken at the contact of the coal and host rocks were studied, and dispersion spectra were obtained for the composition using an X-ray spectrometer.

According to the research results, trace mineral inclusions of REE were found. Also, with a single occurrence, yttrium (Y) inclusions were found in the samples of coal, and argillite, and also in the samples taken at the contact of coal and clayey rocks.

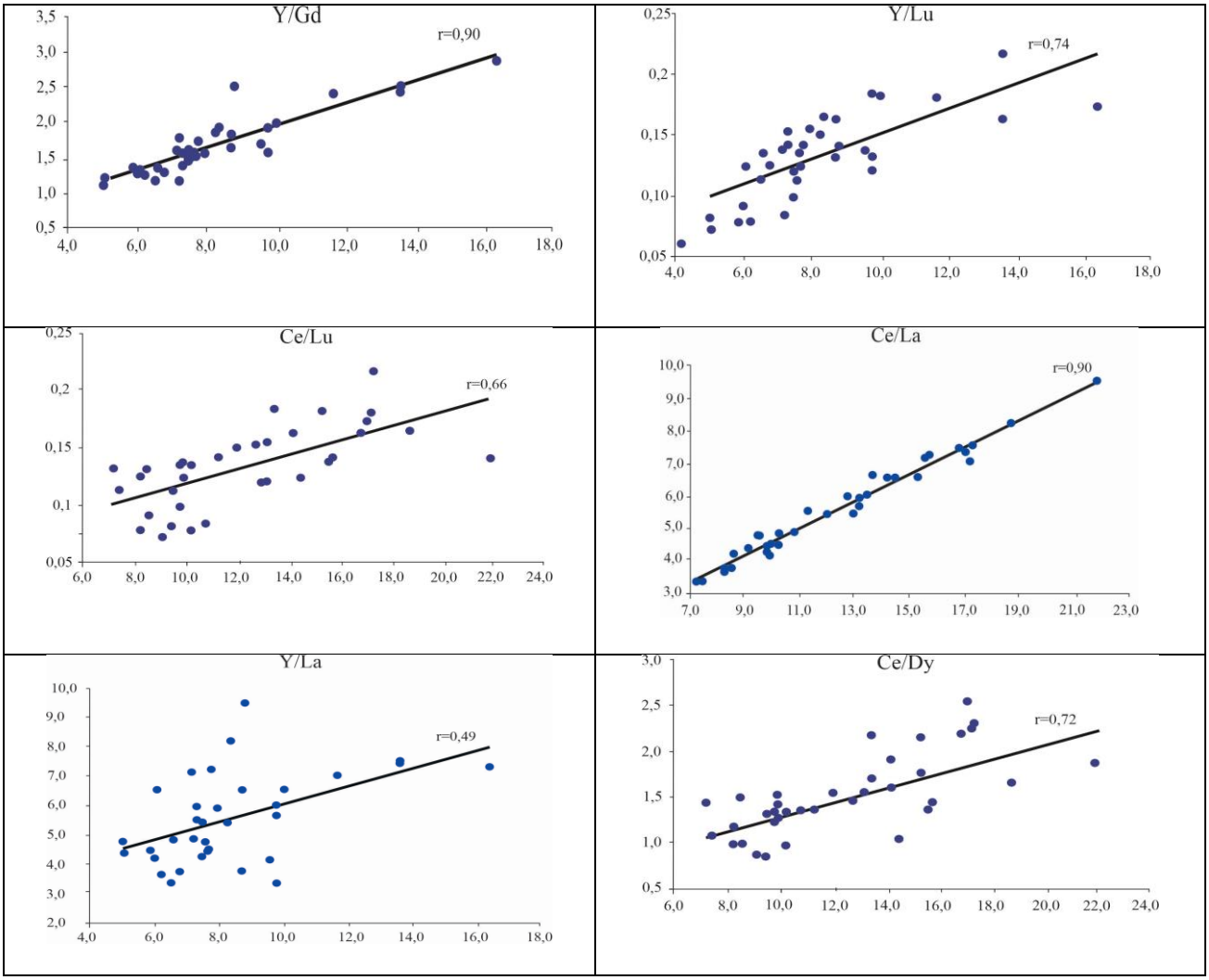

Figure 6 - Correlation Diagrams of Y and Ce and REE in the Coals of Karaganda Coal Basin

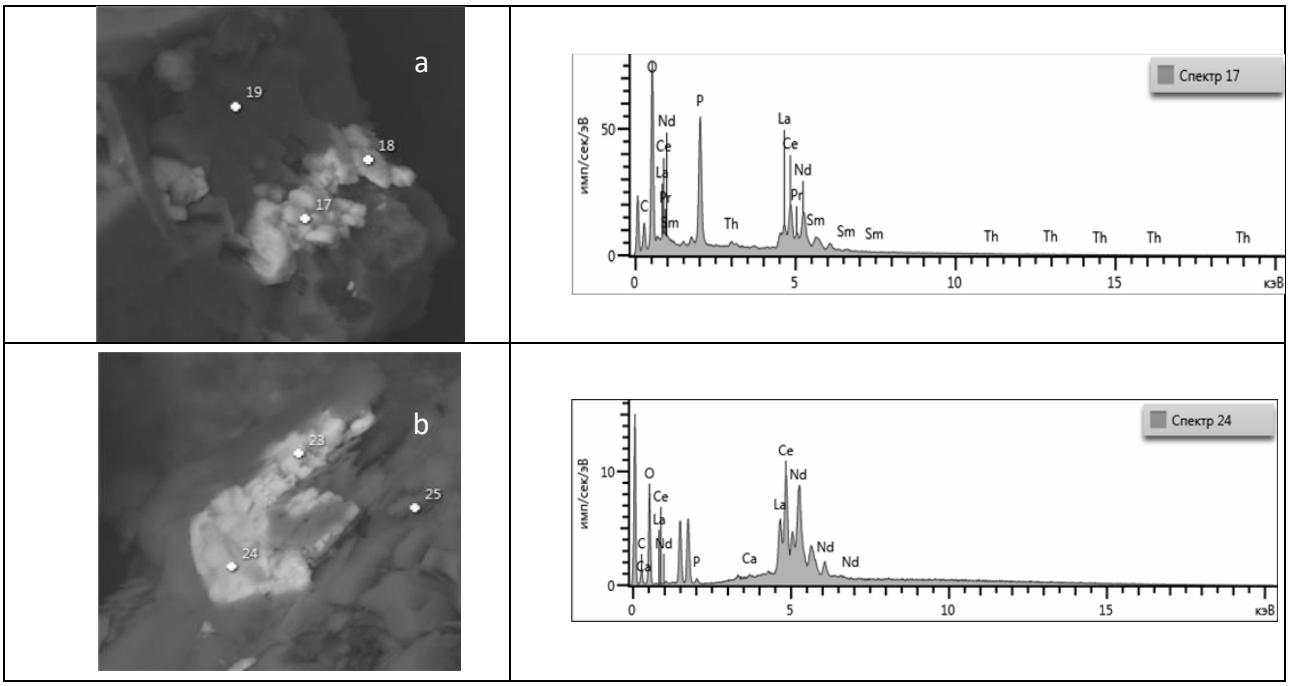

Figure 7 – Mineral Inclusions of CeLaNdPO Composition in Coals (a) and Clayey Interlayers (b) of Karaganda Coal Basin

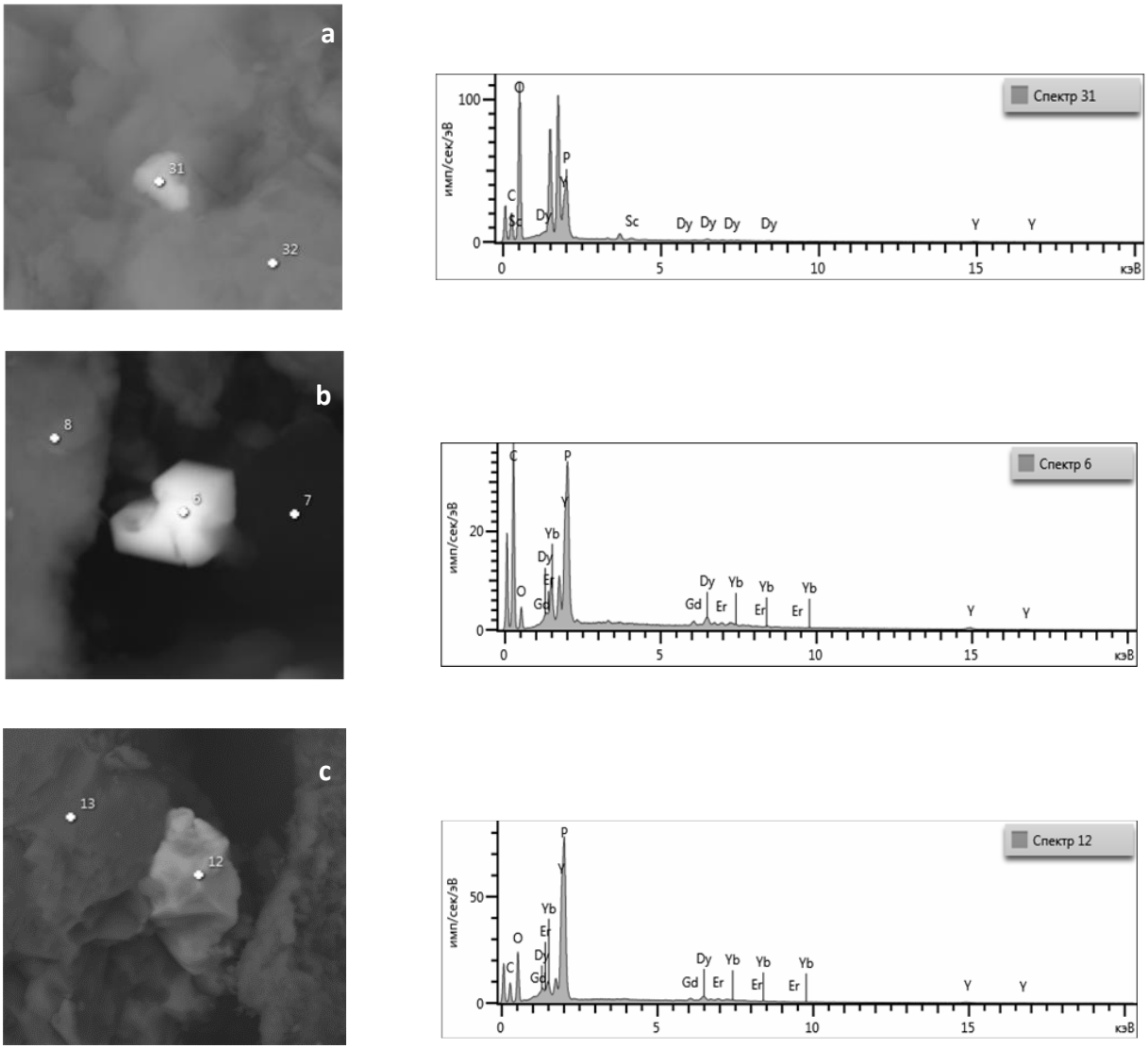

Figure 8 – Grain YPO of the Composition (xenotime?) in Coal (a), and Contact(b) Samples, in Argillite (c)

The REE deportments in coal are quite diverse; the most common ones are phosphates, aluminophosphates and carbonates. High carbonification of REE suggests an important role of organic matter in their concentration in the coals. Autigene mineral forms of REE that are sharply predominant in hard coals, including phosphates, are formed during the destruction of organic complexes in the process of organic matter transformation during the coal formation process [[21], [22]]. In coal and clay samples from the Karaganda coal basin, the predominant mineral form of REE is light lanthanide phosphates. Sparry crystals of CeLaNdPO composition (Fig. 7) were found in coal (Fig. 7a) and clayey interlayer samples (Fig. 7b).

The first data on Y contents in the coal appeared in 1931: 4 g/t of Y were found in the ashes of two samples of Silesian and English coal (Goldschmidt, 1931). It is known [20] that by its chemical properties, Y is very close to lanthanides, in particular, it is an almost complete geochemical analogue of the heavy lanthanoids Yb. According to [20], the carbonification coefficient of Y that exceeds one, as well as its high concentrations in coal inclusion ashes, indicate the presence of antigens yttrium impurity of organic form in the coals (Y_{org}), as well as the probable mineral form of antigens phosphates (Y_{phos}). In addition, the mineral yttrium (Y_{min}) can be present in clastogenic ash, in the composition of accessor minerals and clay matter. However, it should be noted that during

the thermal metamorphism and/or hypergenic oxidation of coals, the yttrium deportment can change, which leads to its migration, ingress or removal from the coals.

Using the SEM-EDS method, in the coal samples (Fig. 8a), on the contacts (Fig. 8b), as well as in host rocks (Fig. 8c) of Karaganda coal basin trace ineral inclusions of different sizes, mainly of YPO (*xenotime?)* composition were found. According to previously published results (R. Finkelman,1980) that were obtained using the combined SEM + EDS method, substantial amounts of yttrium in many coals were found in the form of abundant xenotime particles. According to (D. Swain,1990), this gives a good basis for the statement that fine-grained xenotime is the major deportment of Y in many coals.

Conclusion

This is the first comprehensive mineralogical and geochemical research of clayey interlayers and coals of the Karaganda coal basin. The research showed that increased REE contents relate to the clayey interlayers and contact zones of the coal-clay interlayer. In terms of REE content in coal, the increase is seen in the REE content from the bottom towards the top of the stratum. The lanthanum-ytterbium (La/Yb) ratio in coal that was normalized to UCC and the La/Yb ratio in coal normalized to chondrite, indicated the presence of mixed types of REE distribution in coals, which supposes various forms of REE migration and different mobility of heavy and light lanthanides within the hypergenesis zone. La/Yb ratio in this case also grows from coals to clayey interlayers, which indicates a predominantly clastogene mechanism of REE input to the coals. An increase was established in REE content from the west (at Saranskaya mine) to the northeast (at T. Kuzembayev mine), with the minimum REE content found at the Aktasskaya mine. To establish such a distribution, additional research is required for these sites of the mines.

Calculated Eu - and Ce - anomalies in the coals and clays, which are normalized by chondrite and UCC, showed negative europium and cerium anomalies, which are characteristic of clayey interlayers formed with the participation of ash material of acidic composition. Analysis of REE distribution showed increased total concentrations of light and medium lanthanides in the Karaganda coal basin. A high total content of Se, Y, Nd and La was noted in all three mines. Correlation analyses of Y and Ce showed positive correlations with light and medium lanthanides.

To define trace mineral deportments of REE in the coals of the Karaganda coal basin, researches were performed using the highly local method of analytical scanning electron microscopy along with energy-dispersive X-ray spectroscopy (SEM-EDS), automated search for mineral phases with the set characteristics was performed using the AZtecFeature program modules. Using this method, it was found that the predominant mineral form of REE was light lanthanide phosphates. Sparry crystals with CeLaNdPO composition were found in the coal and clayey interlayer samples. Y inclusions in the form of abundant xenotime particles in the coal and clayey interlayer samples, as well as in samples taken at the contact of coal and clayey interlayers were revealed for the first time.

Conflict of interest. On behalf of all the authors, the correspondent author declares that there is no conflict of interest.

Acknowledgements. This research has been funded by Science Committee of the Ministry of Science and Higher Education of the Republic of Kazakhstan (grant No. AP13067779).

Cite this article as: Kopobayeva AN, Baydauletova IV, Amangeldikyzy A, Askarova NS, Blyalova GG. Nature Of Ree Accumulation In Clayey Interlayers And Coals In Karaganda Coal Basin. Kompleksnoe Ispolzovanie Mineralnogo Syra = Complex Use of Mineral Resources. 2025; 332(1):49-61. https://doi.org/10.31643/2025/6445.04

ҚАРАҒАНДЫ КӨМІР БАССЕЙНІНІҢ САЗДЫ ҚАБАТТАРЫ МЕН КӨМІРЛЕРІНДЕ СИРЕК ЖЕР ЭЛЕМЕНТТЕРІНІҢ (СЖЭ) ЖИНАҚТАЛУ ТАБИҒАТЫ

Копобаева А.Н., Байдаулетова И.В., Амангелдіқызы А., Асқарова Н.С., Блялова Г.Г.

Әбілқас Сағынов атындағы Қарағанды техникалық университеті, Қарағанды, Қазақстан

Мақала келді: *17 қараша 2023*
Сараптамадан өтті: *21 желтоқсан 2023*
Қабылданды: *23 ақпан 2024*

ТҮЙІНДЕМЕ

Орталық Қазақстанның Қарағанды көмір бассейнінің көмірінде алғаш рет сирек жер элементтеріне (СЖЭ) (Y, La, Ce, Pr, Nd, Sm, Eu, Gd, Tb, Dy, Ho, Er, Tm, Yb, Lu) кешенді минералдық-геохимиялық зерттеу жасалды. Жұмыста Қарағанды көмір бассейнінің Саран, Т.Күзембаев, Ақтас шахта кенжарларында 85 көмір сынамасында және к7 сазды қабаттарында СЖЭ (лантаннан лютецийге дейін және Y) таралуын зерттеу нәтижелері ұсынылған. Саз қабаттары мен көмірлер сынамаларының элементтік құрамы индуктивті байланысқан плазмалық атомдық эмиссиялық спектрометрия және индуктивті байланысқан плазмалық масс-спектрометрия (ICP-OES және ICP-MS) әдістерімен зерттелді. СЖЭ элементтерінің жиынтық концентрациясының латералдық және тік өзгергіштігін зерттеу көмірде СЖЭ таралуының аралас түрлерінің болатынын көрсетті, бұл СЖЭ жылжуының әртүрлі формаларын және гипергенез аймағында ауыр және жеңіл лантаноидтардың әртүрлі қозғалғыштығын білдіреді. UCC-ге нормаланған және La/Yb<1-ге тең көмірдегі лантан-итерби (La / Yb) қатынасы СЖЭ таралуының H типі бар көмірге, сондай-ақ хондритпен нормаланған La/Yb>1-ге тең, СЖЭ таралуының L типі бар көмірге жатады, яғни бұл Қарағанды көмір бассейнінің шөгінділерінде тәуелсіз көздердің және СЖЭ жинақталуының әртүрлі тетіктерінің болуы туралы қорытынды жасауға мүмкіндік береді. Сондай-ақ, La/Yb қатынасы көмірден сазды қабаттарға дейін жоғарылайтыны анықталды, бұл көмірде СЖЭ таралуының негізінен кластогендік механизмін көрсетеді. Жыныстардағы сирек жер элементтерінің микроминералды формаларын анықтау үшін көмірдің негізгі жыныстармен жанасу аймағынан алынған көмірдің, сазды қабаттардың 13 сынамасы зерттелді және рентгендік спектрометр көмегімен құрамның дисперсиялық спектрлері алынды. Қарағанды көмір бассейнінің көмір үлгілері мен сазды қабаттарындағы СЖЭ-нің басым минералды түрі жеңіл лантаноидты фосфаттар болады. Көмір және саз қабаттарының үлгілерінде CeLaNdPO құрамының бағаналы кристалдары табылды. Көптеген көмірде Y негізінен ксенотим түрінде болатыны анықталды.

Түйін сөздер: көмір, сазды қабаттар, Орталық Қазақстан, Қарағанды көмір бассейні, сирек жер элементтері, орташа құрамы.

Авторлар туралы ақпарат:

Копобаева Айман Ныгметовна — *PhD докторы, «Геология және пайдалы қазбалар кен орындарын барлау» кафедрасының доценті міндетін атқарушы, Әбілқас Сағынов атындағы Қарағанды техникалық университеті, 100000, Қарағанды, Қазақстан. E-mail: aiman_25.87@mail.ru*

Байдаулетова Ирина Владимировна — *Әбілқас Сағынов атындағы Қарағанды техникалық университетінің «Геология және пайдалы қазбалар кен орындарын барлау» кафедрасының магистранты, 100000, Қарағанды, Қазақстан. E-mail: ira-sara@bk.ru*

Амангелдіқызы Алтынай — *PhD докторы, «Геология және пайдалы қазбалар кен орындарын барлау» кафедрасының доцент міндетін атқарушы, Әбілқас Сағынов атындағы Қарағанды техникалық университеті, 100000, Қарағанды, Қазақстан. E-mail: amangeldykyzy@inbox.ru*

Асқарова Назым Сражадинқызы — *PhD докторы, «Геология және пайдалы қазба кен орындарын барлау» кафедрасының оқытушысы, Әбілқас Сағынов атындағы Қарағанды мемлекеттік техникалық университеті, 100000, Қарағанды, Қазақстан. E-mail: srajadin-nazym@mail.ru*

Блялова Гулим Галымжановна — *Докторант, «Геология және пайдалы қазба кен орындарын барлау» мамандығы бойынша техника ғылымдарының магистрі, Әбілқас Сағынов атындағы Қарағанды мемлекеттік техникалық университеті, 100000, Қарағанды, Қазақстан. E-mail: gulim_blyalova@mail.ru*

ПРИРОДА НАКОПЛЕНИЯ РЗЭ В ГЛИНИСТЫХ ПРОСЛОЯХ И УГЛЯХ В КАРАГАНДИНСКОМ УГОЛЬНОМ БАССЕЙНЕ

Копобаева А.Н., Байдаулетова И.В., Амангелдіқызы А., Асқарова Н.С., Блялова Г.Г.

Карагандинский технический университет имени Абылкаса Сагинова, Караганда, Казахстан

Поступила: *17 ноября 2023*
Рецензирование: *21 декабря 2023*
Принята в печать: *23 февраля 2024*

АННОТАЦИЯ

Впервые выполнено комплексное минералого-геохимическое исследование РЗЭ (Y, La, Ce, Pr, Nd, Sm, Eu, Gd, Tb, Dy, Ho, Er, Tm, Yb, Lu) в углях Карагандинского угольного бассейна Центрального Казахстана. В работе представлены результаты по изучению распределения РЗЭ (от лантана до лютеция и Y) в 85 пробах угля и глинистых прослоях пласта к7 Карагандинского угольного бассейна на забоях шахт – Саранская, им. Т. Кузембаева, Актасская. Элементный состав проб глинистых прослоев и углей проводился методами атомно-эмиссионной спектрометрии с индуктивно-связанной плазмой и масс-спектрометрии с индуктивно-связанной плазмой (ICP-OES и ICP-MS).

Исследование латеральной и вертикальной изменчивости суммарной концентрации элементов РЗЭ показало на присутствие смешанных типов распределения РЗЭ в углях, что подразумевает различные формы миграции РЗЭ и различную подвижность тяжелых и легких лантаноидов в зоне гипергенеза. Установленное лантан-итербиевое (La/Yb) отношение в угле, которое нормированно к UCC и равное La/Yb<1, относится к углям с H-типом распределения РЗЭ, а также равное La/Yb>1, нормированное по хондриту, относится к углям с L-типом распределения РЗЭ, что позволяет сделать выводы о существовании независимых источников и различных механизмов накопления РЗЭ в отложениях Карагандинского угольного бассейна. Так же установлено, что La/Yb отношение возрастает от углей до глинистых прослоев, указывая на преимущественно кластогенный механизм поступления РЗЭ в угли. Для определения микроминеральных форм нахождения РЗЭ в породах исследованы 13 проб угля, глинистых прослоев и проб, отобранных на контакте угля с вмещающими породами и получены дисперсионные спектры состава с использованием рентгеноспектрометра. Преобладающей минеральной формой РЗЭ в образцах углей и глинистых прослоях Карагандинского угольного бассейна являются фосфаты легких лантаноидов. Обнаружены шестоватые кристаллы CeLaNdPO состава в образцах угля и глинистых прослоев. Установлено, что ксенотим является главной формой нахождения Y во многих углях.

Ключевые слова: уголь, глинистые прослои, Центральный Казахстан, Карагандинский угольный бассейн, редкоземельные элементы, среднее содержание

Информация об авторах:

Копобаева Айман Ныгметовна — *Доктор PhD, и.о. доцента кафедры «Геология и разведка МПИ» Карагандинского технического университета имени Абылкаса Сагинова, 100000, Караганда, Казахстан. E-mail: aiman_25.87@mail.ru*

Байдаулетова Ирина Владимировна — *Магистрант кафедры Геология и разведка МПИ Карагандинского технического университета имени Абылкаса Сагинова, Горный факультет, 100000, Караганда, Казахстан. E-mail: ira-sara@bk.ru*

Амангелдіқызы Алтынай — *Доктор PhD, и.о.доцента кафедры «Геология и разведка МПИ» Карагандинского технического университета имени Абылкаса Сагинова, 100000, Караганда, Казахстан. E-mail: amangeldykyzy@inbox.ru*

Асқарова Назым Сражадинқызы — *Доктор PhD, преподаватель кафедры «Геология и разведка МПИ» Карагандинского технического университета имени Абылкаса Сагинова, 100000, Караганда, Казахстан. e-mail: srajadin-nazym@mail.ru*

Блялова Гулим Галымжановна — *Докторант Карагандинского государственного технического университета имени Абылкаса Сагинова, магистр технических наук по специальности Геология и разведка МПИ, 100000, Караганда, Казахстан. E-mail: gulim_blyalova@mail.ru*

References

[1] Ketris MP, Yudovich YaE. Estimations of Clarkes for carbonaceous biolithes: world average for trace element contents in black shales and coals. International Journal of Coal Geology. 2009, 135-148. https://doi.org/10.1016/j.coal.2009.01.002

[2] Kalmykov DE, Malikova AD. Zagnannyye v ugol. Obzor ugledobycha i ugolnaya energogeneratsiya v Kazakhstane. Sostoyaniye i perspektivy [Driven into the Coal. Review of Coal Mining and Coal Energy Generation in Kazakhstan. Current State and Trends]. Karaganda. 2017. (in Russ.). https://bankwatch.org/wp-content/uploads/2018/01/KZ-Coal_RU.pdf

[3] Jian-qiang XUE, Jian-xin LIU and others. Sources of rare earth elements REE+Y (REY) in Bayili Coal Mine from Wensu County of Xinjiang, China. 2021, 3105-3115. https://doi.org/10.1016/S1003-6326(21)65719-9

[4] Seredin VV, Dai S. Coal deposits as potential alternative sources for lanthanides and yttrium. International Journal of Coal Geology. 2012, 67-93. https://doi.org/10.1016/j.coal.2011.11.001

[5] Seredin VV. Osnovnyye zakonomernosti raspredeleniya redkozemelnykh elementov v uglyakh. Doklady Akademii nauk [The Main Patterns of Rare Earth Elements Distribution in Coals. Doklady Akademii nauk]. 2001; 4:6-27. (in Russ.). https://repository.geologyscience.ru/bitstream/handle/123456789/40855/Arbu_17.pdf?sequence=1

[6] Balaram V. Rare earth elements: A review of applications, occurrence, exploration, analysis, recycling, and environmental impact, Geoscience Frontiers. 2019, 1285-1303. https://doi.org/10.1016/j.gsf.2018.12.005

[7] Poslaniye Glavy gosudarstva Kasym-Zhomarta Tokayeva narodu Kazakhstana ot 01.03.2023g [Message of the Head of the State Kassym-Zhomart Tokayev to the People of Kazakhstan dated 01.03.2023]. (in Russ.). https://www.akorda.kz/ru/poslanie-glavy-gosudarstva-kasym-zhomarta-tokaeva-narodu-kazahstana-181130

[8] Amangeldikyzy A, Kopobayeva AN, Blyalova GG, Askarova NS. Geochemical speciation of coals in the Karaganda coal Basin. The Mining Journal of Kazakhstan. 2023; 7. https://doi.org/10.48498/minmag.2023.219.7.008

[9] Bekman VM, Seydalin OA, Zinova RA. Geologiya Karagandinskogo ugolnogo basseyna. Kollektiv avtorov [Karaganda Coal Basin. Joint Authorship]. Moscow: Nedra. 1972, 415. (in Russ.). https://rusneb.ru/catalog/000016_000021_CHONB-RU_%D0%A7%D0%B5%D0%BB%D1%8F%D0%B1%D0%B8%D0%BD%D1%81%D0%BA%D0%B0%D1%8F+%D0%9E%D0%A3%D0%9D%D0%91_IBIS_553.94%28574.31%29-094514/

[10] Taylor SR, McLennan SM. The Continental Crust: Its Composition and Evolution. Blackwell, Oxford, Geological Magazine, November. 1985, 673-674. https://doi.org/10.1017/S0016756800032167

[11] Khasanov VV, Gafurov ShZ. Redkozemelnyye elementy v vizeyskikh ugolnykh plastakh Volgo-Uralskogo regiona. Uchenyye zapiski Kazanskogo Universiteta [Rare earth elements in Visean coal seams of the Volga-Ural region. Scientific notes of Kazan University]. 2010; 154(4). (in Russ.). https://cyberleninka.ru/article/n/redkozemelnye-elementy-v-vizeyskih-ugolnyh-plastah-volgo-uralskogo-regiona/viewer

[12] Arbuzov SI, Chekryzhov IYu. Redkozemelnyye elementy (La. Ce. Sm. Eu. Tb. Yb. Lu) v uglyakh Severnoy Azii (Sibir. Rossiyskiy Dalniy Vostok. Severnyy Kitay. Mongoliya. Kazakhstan). Geosfernyye issledovaniya [Rare Earth Elements (La, Ce, Sm, Eu, Tb, Yb, Lu) in the Coals of Northern Asia (Siberia, Russian Far East, Northern China, Mongolia, Kazakhstan). Geosferniye issledovaniya]. 2017; 4:6-27. (in Russ.). https://doi.org/10.17223/25421379/5/1

[13] Seredin VV. Osnovnyye zakonomernosti raspredeleniya redkozemelnykh elementov v uglyakh. Doklady Akademii nauk [Basic patterns of distribution of rare earth elements in coals. Reports of the Academy of Sciences]. 2001. (in Russ.). https://www.mathnet.ru/rus/dan17231

[14] Arbuzov SI. and others. Redkozemelnyye elementy v pozdnepaleozoyskikh uglyakh Severnoy Azii (Sibir. Severnyy Kitay. Mongoliya. Kazakhstan). Izvestiya Tomskogo politekhnicheskogo universiteta [Rare Earth Elements in Late Paleozoic Coals of Northern Asia, Bulletin of the Tomsk Polytechnic University]. 2016; 327(8):74-88. (in Russ.). https://repository.geologyscience.ru/handle/123456789/3217

[15] Arbuzov SI, Ershov VV. Geochemistry and rare-metal potential of coals of the Sakhalin coal basin, Sakhalin island, Russia, International Journal of Coal Geology. 2019; 113:103073. https://doi.org/10.1016/j.oregeorev.2019.103073

[16] Arbuzov SI, Maslov SG, Finkelman RB, Mezhibor AM, Ilenok SS, Blokhin MG, Peregudina EV. Modes of occurrence of Rare earth elements in peat from Western Siberia. Journal of Geochemical Exploration. 2018, 40-48. https://doi.org/10.1016/j.gexplo.2017.10.012

[17] Ayupova NR, Maslennikov VV, Herrington RE. Geohimiya redkozemel'nyh elementov v metallonosnyh diagenitah Uzel'ginskogo kolchedanonosnogo polya (Yuzhnyj Ural). Rossijskaya Akademiya Nauk. Ural'skoe Otdelenie. Ural'skij Mineralogicheskij Sbornik [Geohimiya redkozemel'nyh elementov v metallonosnyh diagenitah Uzel'ginskogo kolchedanonosnogo polya (Yuzhnyj Ural). Russian Academy of Sciences Ural Branch]. 2002; 12. (in Russ.). https://repository.geologyscience.ru/bitstream/handle/123456789/29970/Aupo_02.pdf?sequence=1&isAllowed=y

[18] Arbuzov SI, Ershov VV. Geokhimiya redkikh elementov v uglyakh Sibiri [Geochemistry of Rare Elements in the Coals of Siberia]. Tomsk: D-Print. 2007, 468. (in Russ.). https://cyberleninka.ru/article/n/geohimicheskie-issledovaniya-ugley-v-sibiri

[19] Yudovich YaE, Ketris MP. Toksichnyye elementy primesi v iskopayemykh uglyakh. Ekaterinburg [Toxic Impurity Elements in Mineral Coals, Yekaterinburg]. 2005, 648. (in Russ.). https://www.geokniga.org/books/10695

[20] Yudovich YaE, Ketris MP. Tsennyye elementy-primesi v uglyakh. Ekaterinburg: Izd-vo UrO RAN [Valuable Impurity Elements in Coals. Yekaterinburg]. Pub/House UrO RAN. 2006, 538. (in Russ.). https://www.geokniga.org/books/8321

[21] Finkelman RB, Dai Sh, French D. The importance of minerals in coal as the hosts of chemical elements: A review. International Journal of Coal Geology. 2019; 212. https://doi.org/10.1016/j.coal.2019.103251

[22] Ilyenok SS, Arbuzov SI. Mineralnyye formy redkikh elementov v uglyakh i zolakh ugley Azeyskogo mestorozhdeniya Irkutskogo ugolnogo basseyna. Izvestiya Tomskogo politekhnicheskogo universiteta [Mineral Forms of rare Elements in Coals and Coal Ashes of Azeyskoye Deposit of Irkutsk Coal Basin. Bulletin of the Tomsk Polytechnic University]. 2016, 6-20. (in Russ.). https://cyberleninka.ru/article/n/mineralnye-formy-redkih-elementov-v-uglyah-i-zolah-ugley-azeyskogo-mestorozhdeniya-irkutskogo-ugolnogo-basseyna/viewer

Crossref

DOI: 10.31643/2025/6445.05
Earth sciences

Review of the current state of knowledge in forecasting and searching for gold deposits in the North-Western Balkhash region

[1]Umirova G.K., [2]Zakariya M.K., [3*]Abdullina A.K.

[1]Geology and Oil-gas Business Institute named after K. Turyssov, Satbayev University, Almaty, Kazakhstan
[2]LLP «Nomad Geo Service», Almaty, Kazakhstan
[3]Karaganda Technical University named after Abylkas Saginov, Karaganda, Kazakhstan

** Corresponding author email: abdullinakrg@gmail.com*

Received: *December 20, 2023*
Peer-reviewed: *January 18, 2024*
Accepted: *February 28, 2024*

ABSTRACT

The article provides an assessment of the degree of knowledge of the North-Western Balkhash region based on a priori information from the previously conducted complex of geological and geophysical studies. Today, much is known about the geological, tectonic structure of the North-Eastern Balkhash region, the metallogeny of the region, the main structural elements have been identified; there are characteristics of intrusive formations, the age of the main rock complexes has been determined, several mineralization points, ore occurrences and deposits have been discovered. Based on the results of the earlier work, the Dolinnoye, Pustynnoye, and Karyernoye deposits were discovered. They are characterized by promising gold reserves. The determining role when carrying out prospecting geophysical work is played by the degree of exploration of deposits, which makes it possible to formulate an optimal technology for detecting mineralization points and ore deposits and to reduce the risks of erroneous selection of production facilities to the minimum. The article analyzes the level and provides cartograms of the exploration of the North-Western Balkhash region territory by geological surveying, mining operations, sampling and geophysical methods. The geological and geophysical history of research in the territory of the Dolinnoye, Pustynnoye, and Karyernoye deposits was considered. Conclusions were drawn about the level of exploration of the research area and the need for further geophysical work in this territory, due to the high productivity of the area for copper mineralization.

Keywords: North-Western Balkhash region; geological survey; geophysical studies; degree of knowledge; copper-pyrite and gold mineralization.

Information about authors:

Umirova Gulzada Kubashevna — *PhD, Associate Professor of the Department of Geophysics and Seismology, Satbayev University, Satpaev str., 22a, 050013, Almaty, Kazakhstan, Email: g.umirova@satbayev.university*

Zakariya Maksat — *Technical Director, LLP «Nomad Geo Service», Kopernik str., 124B, 050010, Almaty, Kazakhstan, Email: zakariya.maksat@gmail.com*

Abdullina Aigerim Kairzhanovna — *Senior Lecturer of the Department of Development of Mineral Deposits, Karaganda Technical University named after Abylkas Saginov, Ave N. Nazarbayev,56, 100027, Karaganda, Kazakhstan, Email: abdullinakrg@gmail.com*

Introduction

The purpose of the studies presented in the article is to determine the level of knowledge of the North-Western Balkhash region based on the collection, analysis and synthesis of a priori data and to justify the need for further study of the territory based on the use of geophysical methods. To achieve this goal, the following tasks were solved:

1) studying the exploration of the study area with the use of geological methods;

2) the degree of studying the study area by aerial gamma spectrometry, electrical prospecting, gravity prospecting and magnetic prospecting;

3) the effectiveness of geophysical prospecting and justification for the need to continue geophysical studies in searching for gold and copper formations in the North-Western Balkhash region.

The territory of the central part of the North-Western Balkhash region is characterized as inaccessible, which was the reason for the slow study of its geological structure [[1], [2], [3]]. The beginning of extensive geological studies in this area was the

discovery and further establishment of the industrial significance of the Kounrad copper deposit. The studies in 30-40s served as the basis for geological work in subsequent years. Thus, in 1930, N.I. Nakovnik discovered the Shointas magnesite deposit, where geologist F. Dybkov (CNIGRI, 1936) conducted preliminary exploration for magnesite. In the same 1930, N.I. Nakovnik made assumptions about the presence of nickel and platinum in the Kopa tract [[4], [5], [6]].

In 1937-1938, geologists of the Kazakh branch of the USSR Academy of Sciences (Sergievsky V.N., Dmitrievsky V.S., Vakhromeyev V.A., Lignevskaya S.I., Loginova L.I., Novokhatsky N.N.) carried out a huge amount of work to compile a geological map of the entire North-Eastern Balkhash region on a scale of 1:500,000. A wide range of materials was collected, summarized and analyzed, based on which in the North-Eastern Balkhash region it was possible to stratify the marine Devonian, represented by a full set of departments. The research results were ambiguous, therefore, as new material was accumulated, the opinions of scientists underwent significant changes. Among the works of those years, there should be noted the works by V.A. Vakhromeyev, who described in detail the conditionally Lower Silurian (Ordovician) age and divided the jasper-diabase complex into 2 formations: the lower (porphyry) and the upper (jasper-quartzite). He stratified the sandy sequence covering the jasper-quartzite sequence as Gotland.

In 1939, N.L. Bublichenko paid great attention to studying the Silurian and Devonian deposits. Observations were mainly carried out in the Kopa tract and on both sides of the Kenterlau Valley. Generalization of the collected material in 1945 resulted in the compilation of a geological map of sheet D-2-B, as a result of which the geological structure of the territory was significantly corrected. The stratigraphic scheme of the Paleozoic of the North-Eastern Balkhash region compiled by N.L. Bublichenko, remains correct to this day. He conventionally attributed the sequence of basic volcanic rocks and jaspers to the Cambrian. He combined the deposits lying between the Cambrian and terrigenous tellurium sediments into the Diamanshuruk Formation of the Ordovician age. Terrigenous green-coloured formations were dissected by him, distinguishing the Llandoverian, Wenlock-Ludlovian and Dauconian stages of the Silurian and the Zhudinsky, Sardzhal, Kazakh and Aidarlinian stages of the Silurian to the Devonian [7].

The ultrabasic intrusions of Kazakhstan (Itmurundy, Tyuretai, Tesiktas massifs) were studied in the publication by I.F. Trusova in 1948. The article was based on her 1937-1940 studies. She defined the age of all the ultrabasic rocks in Kazakhstan as Caledonian.

The studies of the Andasai expedition that were carried out from 1949 to 1951, were dealing with the diamond potential of loose sediments of Lake Balkhash (North Coast). Almost at the same time, Mikhailov N.P. and Moskaleva V.N. began studying the basic and ultrabasic intrusions of this territory. The integration of the studies included a geological and geomorphological report and a geological map on a scale of 1:200,000 (authors Kostenko N.N. and Mastryukova A.A.). Based on the results of these works, the jasper-diabase complex of Kostenko N.N. was attributed to the Upper Proterozoic.

A geological survey on a scale of 1:200,000 in the area of sheet D-2-104 with the participation of Koshkin V.Ya., Nikelev Yu.V. and Aniyatova P.A. was carried out by the North Balkhash SKSU PSP in 1953. That project was accompanied by paleontological studies carried out by palaeontologists Kaplun L.I. and Rukovishnikova T.B (SKSU), as a result of which Silurian deposits without division were stratified as undivided Gotlandian.

Editing sheet D-2-104B began in 1956 by V.Ya. Koshkin. As a result of research, the rocks of the jasper-diabase complex were divided into the Itmurunda, Kazyk and Tyuretai formations. The Itmurunda and Kazyk formations were conditionally assigned to the Sinian deposits, and the Tyuretai formation was stratified as Cambrian. The deposits lying on the rocks of the jasper-diabase complex are dissected to highlight the Dzhamanshuruk Formation of the Llandoil-Ludlovian Stage. The new edition established a gradual transition from the Upper Silurian to the Devonian, in which stage division was carried out. Rocks of the Carboniferous age were stratified by deposits of the Tournaisian stage and the Sayak formation of the Lower Devonian. In 1958, Koshkin V.Ya. divided the Sayak formation into the Karkala, Keregetas and Arharlin formations [8].

In 1960, when carrying out geological survey work on a scale of 1:50,000, V.Ya. Koshkin for the first-time established gold mineralization in the area of the Pustynnoye deposit. At this time, increased gold contents had already been identified in the local areas of Zapadny, Karierny, and Kopshoky. In 1960-63, the Khantau and North-Balkhash SKSU PSP had a small number of ditches made in these areas. Geologists discovered that elevated gold contents

were confined to zones of intensely pyritized and silicified rocks [9].

In the territory of the Northern Balkhash region, generalization of the data on geology, metallogeny and the implementation of several regional forecasting and metallogenic works to search and explore areas promising for minerals, including gold, were carried out in 1960-1965 by teams of the Ministry of Scientific Research of the Academy of Sciences of the Kazakh SSR and Central Kyiv State University (Shcherba G.N., Alperovich E.V., Kolesnikov V.V.). So, in the intervals of 1961-1962 and 1962-1966, geological surveys of sheets D-45 and D-413 on a scale of 1:50,000 were carried out by V.Ya. Koshkin and Antonyuk R.M., respectively [10].

In April 1981, a new stage of geological survey work began, when, in addition to the Moscow Research Institute of the Academy of Sciences of the Kazakh SSR and the Central Kyiv State University, the Kenterlau Research Station of the Balkhash Geological Survey (Bezuglykh I.V., Akshalov T.).

As a result, geological surveys of a large scale were carried out in the study area. Today, researchers have in their hands the information on the geological, and tectonic structure of the North-Eastern Balkhash region, the metallogeny of the region, and the main structural elements were identified. There are characteristics of intrusive formations, the age of the main rock complexes was determined, several points of mineralization, ore occurrences and deposits were discovered and their genetic relationship with the Late Hercynian magmatism was determined [11].

The stage of studying the Northern Balkhash region by geophysical methods began in 1949. One of the first geophysical methods that were used by employees of the All-Union Aerogeological Trust in 1951 (Yefremova N.N., Preobrazhensky N.A.) was an aeromagnetic survey. It is clear that the results of that survey are practically not used in present-day studies, since the sensitivity of the instruments of that time was low, the survey results were characterized as substandard. An aeromagnetic survey on a scale of 1:25,000 was carried out in the area of sheet D-2-104 by the Volkov expedition in 1955. From 1975 to 1985, the area was actively studied by KAGGE (Zhunussov R.K., Komarov A.M., et al.), ASGE PGO "Kazgeofizika" (Kozlenko O.M., Kuznetsova N.P.). A cartogram of knowledge of sheet L-43 using airborne geophysical methods is presented in Figure 1.

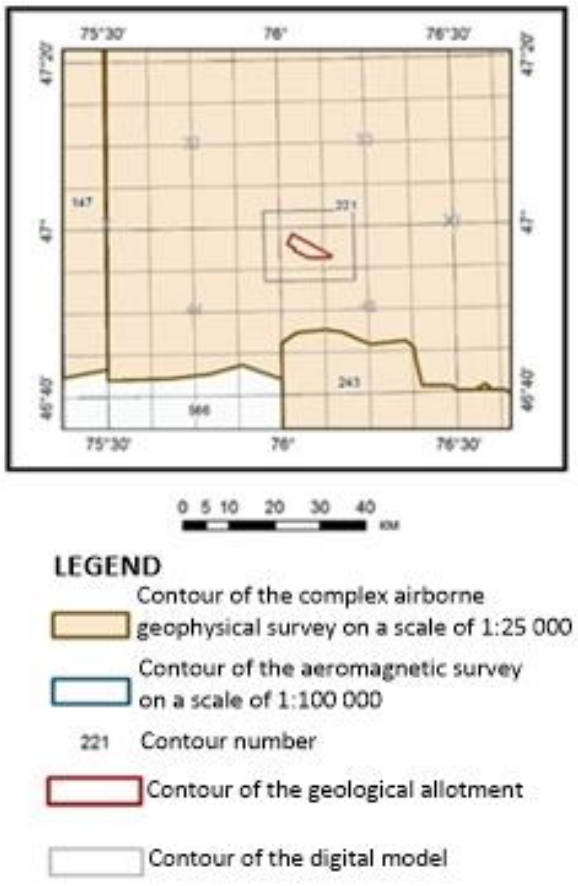

Figure 1 – Airborne geophysical knowledge of sheet L-43

The first magnetic prospecting studies on a scale of 1:50,000 were carried out together with metallometry on the area of sheet D-2-104 in 1952-1954 (the Katbar party of AGFE, Serebryakova I.S.). This territory is confined to the zones of development of ancient strata. Metallometry discovered scattering halos of copper, chromium, nickel, titanium, manganese, and molybdenum here; however, the results of these works also had a significant drawback due to a low sensitivity of spectral analysis and a limited number of elements being determined. In the area of sheets D-410, -413, -412, -415 on a scale of 1:50,000, metallometry was carried out by the Katbar GFP AGFE (Miller S.D., Zhukov M.I.) in 1957. As a result of these works, there was revealed several local scattering halos of Ni, Co, and C_2 that were associated by researchers with hypermafic intrusions.

Promising zones and nodes for sulfide and rare metal mineralization were identified based on a comprehensive interpretation of gravimetric and metallometric research data. On the other hand, gravimetric data made it possible to clarify the

structural and tectonic features of the North-Western Balkhash region [[12], [13], [14]].

When detailing and assessing the copper halos identified during metallometry in 1940-50, in 1961, the employees of the Balkhash State Geographical Enterprise AGFE (Baluta S.V.) discovered the Tesiktas copper pyrite deposit, and in 1962 the Balkhash State Geographic Exploration Company began exploration work. At the same time, the Balkhash State Exploration Survey carried out a metallometric survey on a scale of 1:20,000 of a large area that along its strike covered almost the entire territory of the Tesiktas fault zone. The prospects of several copper halos identified from the results of those studies were assessed by subsequent works as unpromising.

On sheets D-413-B, G, -414-A, B, -415-A, B in the interval of 1968-1969, Yu.P. Moskalev, V.P. Kalinin, V.V. Murashkin carried out a gravimetric survey on a scale of 1:50,000. The purpose of the survey was to trace promising structures for copper mineralization and to clarify the patterns of association of copper mineralization with the deep structures of the area. Detailing the identified gravity anomalies and determining the possibilities of high-precision areal gravity exploration at copper-pyrite deposits in 1967 at the Tesiktas deposit were carried out based on a gravimetric survey on a scale of 1:10,000 (KazKIRG, Gulnitsky V.L., Gubanov M.) [15].

Positive results were not obtained when assessing copper and arsenic copper halos by mining and drilling that were carried out in 1969-1970 at the North-West Tesiktas, East Tesiktas, Tesiktas and Ikkuduk BGRE sites (Safiyulin B.N., et al.). Therefore, in 1972, exploration work was completed due to the unprofitability of areas for industrial development, and the Tesiktas field was mothballed [9].

Deep searches for copper within the Suzyzkara zone (Western Kazyk and Eastern Tesiktas sections) also turned out to be fruitless. The work was carried out in conjunction with VP-SG, VES, MPP (Kashkarskaya GFP, Pokusayev A.V.). Based on the results of the work, it turned out that the IP anomalies were petrogenic, and the identified copper halos and points of visible mineralization were not of practical interest due to the low concentrations and low thickness of the mineralization zones [10].

Thus, the study area was covered by airborne spectrometry (AGS) and gravimetric surveys at 1:100,000 and 1:25,000 scales. A cartogram of gravity exploration knowledge is presented in Figure 2.

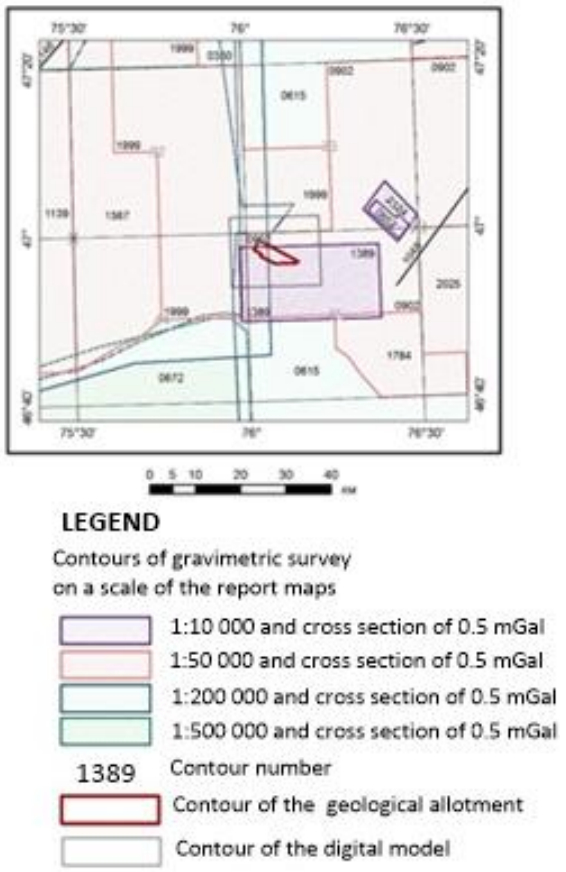

Figure 2 - Gravity exploration knowledge of sheet L-43

Let's consider the level of knowledge of the gold exploration area. In the 1960s, V.Ya. Koshkin discovered several gold-bearing areas (Zapadny, Karierny, etc.). It served as an impetus for prospecting for gold. The gold content and prospects of the listed areas were confirmed by prospecting and assessment work (Karazhalskaya PSP YuKPK, Altybayev A.A., et al.). At the same time, in the area of the Itkuduk group of manifestations, Grazhdantsev N.G. studied the gold content of the Northern Balkhash region.

In 1967, the Balkhash expedition of the Central Committee of State University began to engage in gold prospecting. From 1967 to 1968, the Ulken party of the Balkhash Exploration Expedition (Bukurov G.Yu., Voloshin V.V.) carried out prospecting and assessment work in the area of the Baktai site and the Itkuduk group of manifestations. Based on the results of work at the Baktai site, three ore areas with gold content from 1 g/t to 12 g/t were identified among the linearly elongated zone of vein silicification of sandstones. Three promising areas were identified in the Itkuduk group: Zapadny with a gold content of up to 26.6 g/t; Karyerny (two zones are identified with a content of 2.3 and 2.4 g/t with a layer thickness of 4 and 1 m, respectively); Severny

(a subzone with the content of 2.4 g/t at the thickness of 2 m and several subzones with the content of 1-1.2 g/t were identified). In those areas, work was continued by the Ulken party (Flikop R.M.) in 1970-1973. As a result of mining and testing work at the Baktai ore occurrence, two ore-bearing blocks were identified, and excavation of deep pits with cuts revealed the nest-like and uneven nature of the distribution of metal. In some samples, the gold concentration was up to 80 g/t.

In 1972-1973, specialized prospecting work was carried out (Voloshin V.V.), as a result of which several gold-bearing points were identified in the area of the Itkuduk-Baktay zone, but no industrially interesting objects were identified. Prospecting for gold in the Batykyzyl and Zhalpakkain areas carried out in 1970-1972 by the Akshokinsky party of the Balkhash KGGE (Flikop R.M., Skripchenko A.F.), also turned out to be unsuccessful. At the Batykyzyl site, four IP anomalous zones were identified that were mainly mapping the zones of pyritization of Famennian sandstones. Verification of the anomalies by drilling and testing did not yield positive results for gold and the other elements. At the same time, the Kashkar GFP (Pokusayev A.V., Katrysheva E.I.) carried out prospecting work for copper in the Itbas site, where the prospects for the area in terms of copper gave a negative assessment. Nevertheless, a series of IP anomalies were identified, coinciding with arsenic halos from 0.01 to 0.04% and gravitating towards silicified sandstones and skarn zones at the contact of sedimentary rocks of the Keregetas Formation with the gabbro-granodiorite intrusion. In the exocontact of the intrusions, gold contents of 9.6 g/t were established based on skarns.

Using the data obtained in 1963-1970, comprehensive detailed geological and geophysical prospecting work was carried out in the Zapadny, Karyerny and Kopshoky areas. The complex included excavation of surface and underground mine operations, drilling single wells, magnetic prospecting and electrical prospecting of IP on a scale of 1:10,000 (Altybayev A.A., Permyakov G.N., Flikon R.M.). As a result, in the Zapadny and Karyerny areas, a series of lens-shaped ore bodies, not consistent along the strike, up to a few tens of meters in length, with a thickness of 1.5-10.0 m with a gold content of 3 or more grams per ton, was contoured [16].

In the period from 1972 to 1979, in the area of the ore field and within the Baktai-Itkuduk zone, geological and geophysical work was continued by the Batykyzyl PRP with areal geological and geophysical work on a scale of 1:50,000 and detailed searches on a scale of 1:10,000 within the Zapadny, Kopshoky and Karyerny areas. As a result, gold-bearing zones were also identified outside the Zapadny, Karyerny and Kopshoky areas. The area under consideration was combined into a field called Pustynnoye [10].

In the Zapadny, Karyerny and Kopshoki sections, the network of ditches was thickened to 10-20 m, old ditches were cleared and retested. As a result, within the Zapadny area, seven ore bodies with gold contents above 2.0 g/t are delineated, extending from 40 to 180 m with a thickness of 1.5 to 75.5 m. The depth of the ore zones was assessed by two wells (C-12, 13) to depths of 200-300 m. Metal reserves - up to 10 tons. In the Karyerny and Kopshoky areas, ditches revealed similar zones of pyritization and silicification but with lower gold contents than those in the Zapadny area. The predicted geological reserves of the field were in general estimated at several tens of tons [17].

In the interval of 1979-1983, detailed prospecting work to study the prospective assessment was carried out by the Itkuduk EP at the Pustynnoye field. Within this period, inter-core drilling, mechanical trenching, manual trenching, drilling pits with a cross-section of 4 m^2, horizontal workings with a cross-section of 5.1 m^2, horizontal workings with a cross-section of 2.7 m^2, core sampling, furrow sampling, magnetic prospecting, electrical prospecting, topographic work, spectral analysis, assay analysis for gold, making thin sections, geophysical research in wells.

From 1973 to the present, the North Balkhash EP and the Eastern GFP specialized for gold, are carrying out geological and geophysical studies in the Baktai-Itkuduk zone [[18], [19], [20]].

Conclusion

The analysis of materials in the geological and geophysical study of the considered area made it possible to draw the following conclusions:

1. The territory of the North-Western Balkhash region was systematically studied through geological survey work from the late 30s of the last century. As a result of carrying out conditional surveys, both of small and large scales, the geology of the area was obtained, the main structural elements were identified, the characteristics of the volcanic activity of the area were given, the age of the main varieties of rocks was clarified, the number of points of mineralization, ore occurrences and deposits were

discovered, as well as their genetic connection with the Late Hercynian magmatism.

2. The entire territory of sheet L-43 is covered by the network of aerial spectrometric, magnetometric, electrical prospecting and gravimetric surveys on a scale of 1:200,000 and larger. What is common to all the studies is that the surveys were carried out in the 50s-80s of the last century using equipment of low sensitivity, quality and accuracy. Due to the low sensitivity of airborne gamma spectrometry instruments, the survey results are characterized as poor quality and now are practically not used.

3. Electrical prospecting work using a complex of VES, IP-MG, MPP, ZSB, and INFAZ-IP methods was carried out to clarify the geological structure and deep searches for copper and gold, without providing a significant increase in information on the structure of the studied areas. Thus, electrical exploration knowledge of the study area is extremely low. At the same time, the results of electrical exploration work and sufficient differentiation of the electrical properties of rocks show the effectiveness of using the IP method both for mapping purposes and for searching for zones of hydrothermal development and associated occurrences of minerals.

4. In general, the magnetic survey materials are of good quality; on their basis, standard maps of the anomalous magnetic field were compiled.

5. Gravimetric studies in the work area were carried out from the late 50s of the last century. Work on a scale of 1:200,000 and larger was carried out in the territory of sheet L-43. It can be considered that the considered area is characterized by satisfactory gravimetric study, but the results of these surveys are morally outdated. Therefore, based on the use of gravimetric results from larger surveys carried out with updated, high-tech equipment of the latest generation, the task is to detail the structural and tectonic features of the study area.

6. Based on the results of prospecting and assessment work for gold on a scale of 1:50,000, several aureole-anomalous zones were identified, coinciding with both known occurrences of gold (Baktai Yuzhny, Karyerny, Zapadny, Ortosay, etc.), and previously unknown ones. Thus, an areal halo of gold dispersion was recorded in the area of anomaly 4 of the Itbas site, within which the Dolinnoye quartz-vein deposit was identified. It was assessed as a promising one, with significant gold reserves.

7. 20 km west of the Dolinnoye deposit, in recent years there was revealed the Pustynnoye gold deposit of the quartz-gold-pyrite type, which is assessed as a large one based on predicted reserves. Exploration, evaluation, geological and geophysical work in the field began in 1980.

The obtained materials indicate the sufficient effectiveness of the geological and geophysical work performed and the high prospects of the Itkuduk-Baktay zone for searching for large industrial gold deposits. In general, the available airborne geophysical, gravity and magnetometric materials are quite sufficient to solve the problem of developing a modern geophysical basis, but the collected geological and geophysical information needs to be generalized, linked, analyzed and interpreted in light of present-day stratigraphic, geodynamic, metallogenic and the other concepts. Taking into account the high prospectivity of the area, in particular for copper mineralization, this trend is one of the priority tasks of regional research. In certain areas of detailing, it is necessary to state updated high-precision studying methods.

Conflict of interest. On behalf of all the authors, the corresponding author declares that there is no conflict of interest.

Cite this article as: Umirova GK, Zakariya MK, Abdullina AK. Review of the current state of knowledge in forecasting and searching for gold deposits in the North-Western Balkhash region. Kompleksnoe Ispolzovanie Mineralnogo Syra = Complex Use of Mineral Resources. 2025; 332(1):62-69. https://doi.org/10.31643/2025/6445.05

Солтүстік-Батыс Балқаш аймағындағы алтын кендерін болжау және іздеу кезіндегі зерттеудің қазіргі жағдайына шолу

[1]Умирова Г.К., [2]Закария М.К., [3]Абдуллина А.К.

[1]Қ. Тұрысов атындағы Геология және мұнай-газ ісі институты, Satbayev University, Алматы, Қазақстан
[2]ТОО «Nomad Geo Service», Алматы, Қазақстан
[3]Әбілқас Сағынов атындағы Қарағанды техникалық университеті, Қарағанды, Қазақстан

Мақала келді: *20 желтоқсан 2023*
Сараптамадан өтті: *18 қаңтар 2024*
Қабылданды: *28 ақпан 2024*

ТҮЙІНДЕМЕ
Мақалада бұрын жүргізілген геологиялық-геофизикалық зерттеулер кешені бойынша априорлық ақпарат негізінде Солтүстік-Батыс Балқаш аймағының зерттелу дәрежесіне баға берілген. Бүгінгі таңда Солтүстік-Шығыс Балқаш аймағының геологиялық, тектоникалық құрылымы, металлогенезі туралы көп нәрсе белгілі, негізгі құрылымдық элементтер оқшауланған, интрузивті түзілімдердің сипаттамасы бар, тау жыныстарының негізгі кешендерінің жасы анықталған, бірқатар минералдану нүктелері, кенашылымдар мен кен орындары табылған. Бұрын жүргізілген жұмыстардың нәтижелері бойынша перспективалы алтын қорымен сипатталатын Долинное, Пустынное, Карьерное кен орындары ашылды. Іздеу геофизикалық жұмыстарды жүргізуде кен орындарын зерттеу дәрежесі шешуші рөл атқарады, бұл минералдану нүктелерін, кен орындарын анықтаудың оңтайлы технологиясын қалыптастыруға және пайдалану объектілерін қате таңдау қаупін минимумға дейін төмендетуге мүмкіндік береді. Мақалада геологиялық түсірілім, тау-кен жұмыстары, сынау және геофизикалық әдістер арқылы Солтүстік-Батыс Балқаш аумағын зерттеу деңгейі талданып, картограммалар келтірілген. Долинное, Пустынное, Карьерное кен орындарының аумағындағы зерттеулердің геологиялық-геофизикалық тарихы қарастырылды. Зерттеу ауданын зерделеу деңгейі және ауданның мыспен кенденуіне жоғары іздестіру перспективасына байланысты осы аумақта одан әрі геофизикалық жұмыстарды жүргізу қажеттілігі туралы қорытындылар жасалды.

Түйінді сөздер: Солтүстік-Батыс Балқаш өңірі; геологиялық барлау; геофизикалық зерттеулер; зерделену дәрежесі; мыс колчеданды мен алтынды кендену.

Умирова Гульзада Кубашевна
Авторлар туралы ақпарат:
PhD, Геофизика және сейсмология кафедрасының қауымдастырылған профессоры, Satbayev University, Сәтбаев к., 22а, 050013, Алматы, Қазақстан. Email: g.umirova@satbayev.university

Зақария Мақсат
ТОО «Nomad Geo Service» техникалық директоры, Коперник к., 124В, 050010, Алматы, Қазақстан. Email: zakariya.maksat@gmail.com

Абдуллина Айгерим Каиржановна
Пайдалы кен орындарын қазып өндіру кафедрасының аға оқутышысы, Әбілқас Сағынов атындағы Қарағанды техникалық университеті, Н.Назарбаев д., 56, 100027, Қарағанды, Қазақстан. Email: abdullinakrg@gmail.com

Обзор современного состояния изученности при прогнозировании и поисках золоторудных месторождений Северо-Западного Прибалхашья

[1]Умирова Г.К., [2]Закария М.К., [3]Абдуллина А.К.

[1] Институт геологии и нефтегазового дела им. К. Турысова, Satbayev University, Алматы, Казахстан
[2]ТОО «Nomad Geo Service», Алматы, Казахстан
[3]Карагандинский технический университет имени Абылкаса Сагинова, Караганда, Казахстан

Поступила: *20 декабря 2023*
Рецензирование: *18 января 2024*
Принята в печать: *28 февраля 2024*

АННОТАЦИЯ
В статье дана оценка степени изученности Северо-Западного Прибалхашья на базе априорной информации по ранее проведенному комплексу геолого - геофизических исследований. На сегодняшний день известно многое о геологическом, тектоническом строении Северо-Восточного Прибалхашья, металлогении района, выделены основные структурные элементы, имеется характеристика интрузивных образований, определен возраст основных комплексов горных пород, обнаружен целый ряд точек минерализации, рудопроявлений и месторождений. По результатам проведенных ранее работ были открыты месторождения Долинное, Пустынное, Карьерное, которые характеризуются перспективными запасами золота. Определяющую роль при проведении поисковых геофизических работ играет степень изученности месторождений, которая позволяет сформировать оптимальную технологию обнаружения точек минерализации, рудных залежей, и свести риски ошибочного выбора эксплуатационных объектов до минимума. В статье проанализирован уровень и приведены картограммы изученности территории Северо-Западного Прибалхашья геологической съемкой, горнопроходческими работами, опробованием и геофизическими методами. Рассмотрена геолого-геофизическая история исследований на территории месторождений Долинное, Пустынное, Карьерное. Сделаны выводы об уровне изученности района исследований и необходимости проведения на этой территории дальнейших геофизических работ, в связи с высокой поисковой перспективностью района на медное оруденение.

Ключевые слова: Северо-Западное Прибалхашье; геологическая съемка; геофизические исследования; степень изученности; медно-колчеданное и золотое оруденение.

Умирова Гульзада Кубашевна	***Информация об авторах:*** *PhD, Ассоциированный профессор кафедры Геофизики и сейсмологии, Satbayev University, у. Сатпаева, 22а, 050013, Алматы, Казахстан. Email: g.umirova@satbayev.university*
Закария Максат	*Технический директор, ТОО «Nomad Geo Service», ул.Коперника, 124В, 050010, Алматы, Казахстан. Email: zakariya.maksat@gmail.com*
Абдуллина Айгерим Каиржановна	*Старший преподаватель кафедры Разработки месторождений полезных ископаемых, Карагандинский технический университет имени Абылкаса Сагинова, пр. Н.Назарбаева, 56, 100027, Караганда, Казахстан. Email: abdullinakrg@gmail.com*

References

[1] Shherba IG. Gercinskaja struktura severnogo Pribalhash'ja [Hercynian structure of the northern Balkhash region]. Moscow: Science. 1973, 21. (in Russ).

[2] Li Ch, Hong Di, Qing Yu, Chu XK, Seitmuratova E. Comparison of natures of barren and fertile intrusions in the Kounrad ore district, Kazakhstan and its implication for mineralization. Acta Petrologica Sinica 2023; 39(11): 3263-3283. https://doi.org/10.18654/1000-0569/2023.11.04

[3] Rafailovich MS. Zoloto nedr Kazakhstana: geologiya, metallogeniya, prognoznyye i poiskovyye modeli [Gold of the Bowels of Kazakhstan: Geology, Metallogeny, Predictive and Search Models]. Book Print: Almaty, Kazakhstan. 2009 (in Russ).

[4] Nakovnik NI. Mestorozhdenie Kounrad, ego gornye porody i mineraly [Kounrad deposit, its rocks and minerals]. Moscow; Leningrad: Acad. Sciences of the USSR. 1937. (in Russ).

[5] Cao Ch, Shen P, Pan H, Li Ch, Seitmuratova E. Fluid evolution and mineralization mechanism of the East Kounrad porphyry Mo-W deposit in the Balkhash metallogenic belt, Central Kazakhstan. Journal of Asian Earth Sciences 2018; 165:175-191. https://doi.org/10.1016/j.jseaes.2018.07.013

[6] Li GM, Cao MJ, Kezhang Q, Pete H, Evans NJ, Seitmuratova E. Petrogenesis of ore-forming and pre/post-ore granitoids from the Kounrad, Borly and Sayak porphyry/skarn Cu deposits, Central Kazakhstan. Gondwana Research 2016; 37:408-425. https://doi.org/10.1016/j.gr.2015.10.005

[7] Nikitin IF. Ordovik Kazahstana. [Ordovician of Kazakhstan]. Alma-Ata: Science. 1972. (in Russ).

[8] Li Ch, Shen P, Pan H, Seitmuratova E. Control on the size of porphyry copper reserves in the North Balkhash–West Junggar Metallogenic Belt. Lithos 2019; 328-329:244-261. https://doi.org/10.1016/j.lithos.2019.01.030

[9] Bespaev XA, Aubekerov BZh, Abishev VM, Zhautikov TM, Stepanenko NI, Gus'kova AI, Zhakupova ShA. Rossypi zolota Kazahstana. Spravochnik. [Placers of gold in Kazakhstan. Directory]. Almaty. 1999. (in Russ).

[10] Rafailovich MS. Epitermalnye mestorozhdeniya zolota Kazakhstana. Geol. Razved. Nedr Kaz. [Epithermal gold deposits of Kazakhstan. Geol. Expl. of subsoil in Kaz.]. Almaty. 1997; 5-6:12-18. (in Russ).

[11] Rakhmanova SN, Umirova GK, Ablessenova ZN. Study of the Greater Karatau's South-West by range of geophysical surveys in search of the crust-karst type polymetallic mineralization. News of the National Academy of Sciences of the Republic of Kazakhstan, Series of Geology and Technical Sciences. 2022; 1(451):76-82. https://doi.org/10.32014/2022.2518-170X.143

[12] Seitmuratova EY, Goryaeva VS, Shaidasheva FF, Arshamov YaK et all. The Current State of Research on Secondary Quartzites of the Northern Segment of the Jungar-Balkhash Folded System and Their Au Mineralization (Central Kazakhstan). Minerals 2023; 13(6):813. https://doi.org/10.3390/min13060813

[13] Zeinedinov DT, Zhonys NB, Umirova GK. Fundamentals of rational integration of geophysics methods to improve their geological efficiency in forecasting, prospecting and further study of polymetal deposits in central Kazakhstan. 17th Conference and Exhibition Engineering and Mining Geophysics, April. 2021, 1-11. https://doi.org/10.3997/2214-4609.202152163

[14] Jukebayev M, Umirova GK, Marinenko V. Results of Using Kazakhstan High-precision Electro-prospecting Equipment for Solving Ore Problems. European Association of Geoscientists & Engineers. Engineering and Mining Geophysics, April. 2018, 1-6. https://doi.org/10.3997/2214-4609.201800563

[15] Abdoldina FN, Nazirova AB, Dubovenko YI, Umirova GK. Solution of the gravity exploration direct problem by the simulated annealing method for data interpretation of gravity monitoring of the subsoil conditions. News of the National Academy of Sciences of the Republic of Kazakhstan, Series of Geology and Technical Science. 2021; 1(445):13-21. https://doi.org/10.32014/2021.2518-170X.2

[16] Almuhanbetov DA, Kazhkina AO. Poisk mestorozhdenij medi v Central'nom Kazahstane (geofizicheskie metody) [Search for copper deposits in Central Kazakhstan (geophysical methods)]. Alma-Ata: Science. 1982. (in Russ).

[17] Abishev VM, Bespaev XA, Globa VA, Guljaeva NJa. Mestorozhdenija zolota Kazahstana. Spravochnik [Gold deposits of Kazakhstan. Directory]. Information and Analytical Center of Geology of the Republic of Kazakhstan, Almaty. 1997. (in Russ).

[18] Seitmuratova EY, Lyapichev GF, Zhukov PK. Geological Additional Study of the Kounrad-Akchatau Ore District, Scale 1:200000, of the Territory of Sheets L-43-III, IV, IX, X. Report. Republican geological funds. Satbayev Institute of Geosciences: Almaty, Kazakhstan. 2000; 1–5:900.

[19] Seitmuratova EY, Diarov AB, Zhakupova SO, Goryaeva VS. Compilation of Large-Scale Predictive Maps of Promising Gold Ore Areas of Central Kazakhstan in Order to Select Specific Areas for Prospecting and Appraisal Work; Grant Project Report; Satbayev Institute of Geosciences: Almaty, Kazakhstan. 2014, 72.

[20] Seitmuratova EY, Baratov RT, Dautbekov DO, Zeilik BS, Arshamov YK, Berdina LE, Saidasheva AA, Kelyukhov VN. Studying the Ore Content of Volcanic Structures in Central and Southern Kazakhstan with the Identification of the Most Promising of Them for Setting Prospecting Operations; Grant Project Report; Satbayev Institute of Geosciences: Almaty, Kazakhstan. 2018–2020, 40.

Crossref
DOI: 10.31643/2025/6445.06
Earth sciences

Natural mineral raw materials as granular filtering materials in industrial and waste water treatment

[1,2*]Myrzalieva S.K., [1,2]Bagasharova J.T., [1]Akilbekova Sh.K., [1,2] Serikbaev P.

[1] RSE «National Center on complex processing of mineral raw materials of the Republic of Kazakhstan», Almaty, Kazakhstan
[2] Al-Farabi Kazakh National University, Almaty, Kazakhstan

[*]Corresponding author email: saulekerchaiz@mail.ru

Received: *October 17, 2023*
Peer-reviewed: *November 29, 2023*
Accepted: *February 29, 2024*

ABSTRACT

Analysis of currently existing methods of natural and waste water treatment from heavy metals has shown that one of the most promising is the sorption method using natural inorganic materials as sorbents: zeolite, diatomite, and vermiculite. The relevance of the topic is dictated by the need to develop an original technology of wastewater treatment and water treatment, which allows constant monitoring of the level of pollution of natural waters by industrial wastewater from metallurgical enterprises. The proposed methods of sorbent modification create a basis for studying the structure, porosity, and sorption capabilities of the mentioned natural materials. All three minerals: zeolite, diatomite, and vermiculite belong to highly porous, structured materials, promising for use as stable sorption systems in water treatment and water purification. The influence of physical and chemical characteristics of natural sorbents and the application of new promising environmentally safe materials and reagents for water treatment are considered. The sorption of copper ions on natural zeolite material before and after its modification by hydrothermal method was investigated. The activity of sorbents was estimated by the value of sorption capacity, i.e. the amount of heavy metal ions absorbed by a unit mass of sorbent based on zeolite and its modified form.

Keywords: wastewater, treatment, sorbents, zeolite, diatomite, vermiculite, clinoptilolite, waste, minerals.

Information about authors:

Myrzalieva SayLe Kerchaizovna — *Doctor of Chemical Sciences, professor, Head of the Department for Training of Scientific Personnel National Center for Complex Processing of Mineral Raw Materials of the Republic of Kazakhstan, Jandossov str, 67, 050036, Almaty, Kazakhstan. E-mail: saulekerchaiz@mail.ru*

Bagasharova Zhenisgyl Telmanovna — *Candidate of Technical Sciences, leading researcher RSE "National center for complex processing of mineral raw materials of the Republic of Kazakhstan", Jandossov str, 67, 050036, Almaty, Kazakhstan. senior lecturer at Al-Farabi Kazakh National University, 71 Al-Farabi Ave, 050040 Almaty. E-mail: zh.t_bagasharova@mail.ru*

Akilbekova Sholpan K. — *Candidate of Technical Sciences, Senior Researcher RSE "National center for Complex Processing of Mineral Raw Materials of the Republic of Kazakhstan" Jandossov str, 67, 050036, Almaty, Kazakhstan. E-mail: cadikova74@mail.ru*

Serikbaev Pyrmahanbet — *MA student at Al-Farabi Kazakh National University, 71 Al-Farabi Ave, 050040 Almaty, Kazakhstan. E-mail: serykbaev.pyrmahanbet@mail.ru*

Introduction

Today, an urgent environmental task for mineral resource complex facilities is the development of highly efficient and economical technological and technical solutions for wastewater treatment.

Of particular concern is the constant increase in contamination of water supplies with heavy metals, which are toxic to living organisms even at extremely low concentrations. Removing or reducing the total concentration of heavy metals to less than 10 mg/l is a primary objective when treating any natural and wastewater. The relevance of the issues of efficiency of purification and preparation of drinking, industrial and waste water and their cost reduction explains the existence of many purification methods. among which the most commonly used is sorption because it allows you to increase the degree of purification to almost any required concentration. For the production of environmentally friendly sorbents, the most attractive are natural organic raw materials and production waste of plant origin, therefore sorbents based on them are most compliant with environmental requirements.

Such sorbents are also promising for the extraction of ionic impurities and contaminants from solutions, natural and waste waters, liquid radioactive waste, extraction and concentration of ions of heavy and radioactive metals (uranium, cesium, arsenic, chromium, manganese, strontium, zirconium, etc.)

A promising direction for intensifying deep cleaning processes is the use of natural mineral raw materials as effective sorbents. The main advantages of natural sorbents are environmental friendliness, a wide raw material base, high hydrophobicity and sorption capacity at a relatively low cost.

When treating industrial and waste water, the practical task is to select local natural materials as raw materials that optimally combine economic profitability and effective treatment. Our research suggests minerals zeolite, diatomite, vermiculite and their modified forms. Their structure and properties have been studied, because there is little in the literature The listed minerals were studied as sorbents for solving environmental problems.

Modern highly effective and safe sorbents for wastewater treatment include zeolites, which are minerals with ion-exchange properties. Generalized formula of zeolites:

$$K_{x/n}Al_xSi_yO_2(x+y)*ZH_2O$$

where K are cations of alkali and alkaline earth metals, ammonium, etc.; n is the charge of the cation.

More than 40 types of natural zeolites are known. The most common ones are :

1. Phillipsite $K_2(Ca_{0.5}Na)_4[Al_6Si_{10}O_{32}]*12H_2O$

2.Mordenite $(Na_{2,}Ca,K_{2)}4(Al_8Si_{40)}O96•28H_2O$

3.Chabazite $(Ca,Na_{2)\ 2}[Al_4Si_8O_{72]}*28H_2O$

4.Clinoptilolite $(K_2Na_2Ca)_3[Al_6Si_{30}O_{72]}*20H_2O$

Zeolite contains approximately 70% silicon oxide, the rest is oxide compounds of titanium, iron, manganese, magnesium and several other metals, including copper. The mineral has a special mature microporous structure with pore sizes from 3 to 10 A $^{0.}$ Molecular-sized pores, like a sponge, can absorb and firmly hold a wide variety of contaminants. These include heavy metals (lead, cadmium, zinc, strontium, chromium), radionuclides, nitrates and nitrites, ammonium salts, oils, petroleum products and a whole range of chemical and biological contaminants.

The composition of zeolites can be described by the following empirical formula:

$$(Me+,Me^{2}+0.5)x...[AlxSiyO^{2}(x+y)]\ (H_2O)n, \quad (1)$$

where Me - metal cation, values x and y determine the number of atoms of silicon, aluminum, oxygen in the unit cell, x|y, depending on the type of zeolite, usually takes values from 1 to 5, n is the number of water molecules.

Thanks to the relatively high The Si / Al crystalline frame of clinoptilolite is heat-resistant (in air up to 700 ^{0} C), and is also resistant to aggressive substances and ionizing radiation (Fig. 1).

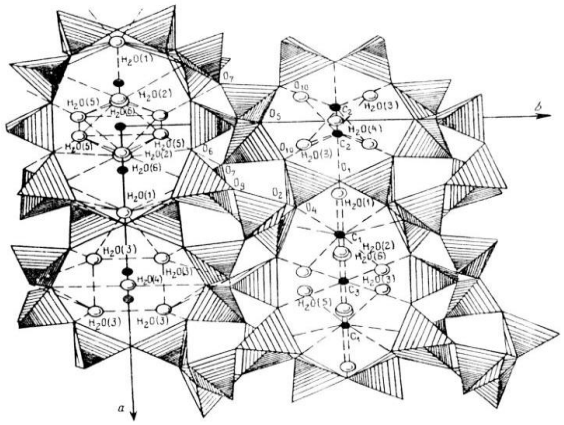

Figure 1 - Clinoptilolite frame fragment

In Kazakhstan, large deposits of zeolites are in Tayzhuzgen (Tarbagatai district of the East Kazakhstan region, approved reserves - 7 million tons, forecast - 215 million tons) and Chankanai (Kerbulak district of Almaty region, approved reserves - 5.5 million tons, forecast - 120 million tons). Zeolites from the Chankanai and Taizhuzgen deposits are medium-porous zeolites and can be used to extract pollutants from natural waters.

In Southern Kazakhstan, the Altyn- Emel (41 million tons), Karzhantau and Daubabinskoe zeolite deposits have been preliminarily assessed [1].

Modern wastewater treatment technologies include the development and implementation of technological processes that ensure:

- complex processing of mineral raw materials;
- reduction or complete elimination of environmental pollution from production waste;
-processing of production and consumption waste by obtaining commercial products;
-creation of closed systems providing recycling water supply [2].

Improvement of the main technological process, wastewater treatment methods, and disposal of resulting sediments make it possible to

create closed (drainless) water supply systems at enterprises. In this case, the main technological process and wastewater treatment are considered as a single integrated system.

Inorganic compounds of heavy metals belong to the group of highly hazardous pollutants with a wide range of toxic effects. Under natural conditions, along with surface waters, they also enter underground waters. One of the promising ways to solve this problem is the use of sorption technologies, which ensure the removal of pollutants of a wide nature to almost any residual concentration. An alternative raw material for removing toxicants from aquatic environments can be natural minerals: zeolite, diatomite, vermiculite and their modified forms. Modern enterprises are in dire need of a methodology for assessing the state of wastewater, solving problems of their treatment and prospects for the development of this area based on forecasting and management. This requires setting the problem of the need for theoretical and practical developments that ensure the implementation of organizational innovations designed to adapt the problems being solved in the field of wastewater treatment in various industries, including the metallurgical industry.

Experimental part

The need to increase the sorption capacity of filters in wastewater treatment plants leads to the search for new, cheaper and widespread materials characterized by sufficiently high mechanical strength, and chemical stability and at the same time possessing a more developed specific surface area and greater porosity. A significant indicator of the quality of filter materials is their resistance to acidic and alkaline environments. The use of natural zeolites in solving environmental problems of environmental objects is due to their adsorption properties, as well as thermal, chemical and radiation resistance. Zeolites are suitable for the sorption of amines and heavy metals from industrial wastewater. Data [3] show that long-term contact of the natural material, clinoptilolite, with a NaOH solution at 100-150 °C did not lead to any noticeable changes in the composition and structure of the zeolite, which confirms its physical and chemical stability. To test the resistance of this mineral to acids, the effect of a five-hour treatment of clinoptilolite with hydrochloric acid of various concentrations at 100-2 00^0C on the dissolution of heavy metal oxides: zinc, lead, cadmium, etc. was studied. It was established that clinoptilolite rocks meet the requirements for granular filter materials. Clinoptilolite, as mentioned earlier, is characterized by a noticeable cation exchange capacity and high selectivity to ions with a large radius: Cs^+, Rb^+, NH_4^+, Ba^{2+},Sr^{2+} [4].

Due to their unique properties: - developed internal surface, zeolites have high absorption characteristics for impurities found in the water being purified.

The advantage of sorption wastewater treatment is the ability to optimize the parameters of sorption columns, which is carried out through the use of natural sorbents, their modification and the combination of two or more granular sorbents in one adsorption column.

Table 1 shows the capacity values of clinopthiolite for cations of mono and divalent metals (Me $^{+,}$ Me $^{2+),}$ expressed both in milligram equivalents per gram of zeolite in the cationic form of the corresponding ion (E), and in milligram equivalents per gram of Na – forms of zeolite (E $^{*)}$. Capacity values in milligram equivalents per gram of zeolite in the cationic form of the corresponding ion (E) are given to show its dependence on the atomic mass of the cation, while the analysis of the results obtained was carried out using capacity values expressed in milligram equivalents per gram Na – zeolite forms, which were calculated using the formula:

$$E^* = E\, d_{kat} / d_{Na,}$$

where d_{kat} / d_{Na} are the specific gravities of the zeolite in the corresponding cationic and Na – forms.

To increase the adsorption capacity of natural zeolites about various pollutants, it is recommended to pre-grind them to particles of about 150 microns in size, due to which the specific surface area of the sorbent increases. This makes it possible to remove up to 90-95% of polluting ions from industrial wastewater.

Based on structural features, chemical composition, and physicochemical properties, three large groups of natural sorbents can be distinguished: dispersed silicas, layered and layered-tape silicates, frame silicates, and zeolites [5]. Dispersed silicas are of sedimentary origin. They are 60-95% composed of amorphous SiO_2 – silicon dioxide.

Table 1- Exchange capacity of high-silica zeolite

Cation metals	Clinoptilolite		
	E, mg eq, / g	d_{kat}/d_{Na}	E^*, mg eq, / g
Li^+	1.65	0.98	1.62
Na^+	1.95	1.00	1.95
Ag^+	1.73	1.12	1.94
K^+	1.93	1.02	1.97
NH_4^+	1.95	0.99	1.93
Rb^+	1.77	1.09	1.93
Cs^+	1.68	1.15	1.93
Ca^{2+}	1.26	0.99	1.25
Sr^{2+}	1.32	1.03	1.36
Ba^{2+}	1.42	1.06	1.51
Zn^{2+}	1.09	1.01	1.10
Cu^{2+}	1.09	1.01	1.10
Cd^{2+}	1.25	1.06	1.33
Pb^{2+}	1.45	1.11	1.61

One of the most promising filter materials in treatment facilities of metallurgical plants is the highly porous minerals zeolite, diatomite, and vermiculite, used to purify wastewater from iron, ammonium ions, heavy metals, radionuclides, organic compounds and various trace elements [6].

The sorption properties of clinoptilolite rocks, and zeolites from the Chankanai and Taizhuzgen deposits with a clinoptilolite content of at least 60-70%, were studied. The studies assessed the sorption exchange capacity (SOE, mg/g, mg-ion/g) in static mode (ion concentration 7.0±0.1 mg-ion/l, ratio of solid and liquid phases 1:10, particle size 0,8÷1.2 mm, sorption time 24 hours). Zeolite samples have significant sorption capacity not only for particularly toxic ions ($Cd^{2+,}$ $Pb^{2+)}$ but also for other heavy metals ($Cu^{2+,}$ $Zn^{2+)}$ [[7], [8], [9]].

The studies were carried out under static conditions with aqueous solutions of metal salts at a concentration of 0.1-0.5 g/l, T = 20 ^{0} C. Ion content heavy metals in powder samples and depending on time defending model solutions determined X-ray fluorescent method according to a certified methodology. The activity of sorbents was assessed by the sorption capacity, i.e., the quantity of heavy metal ions, absorbed unit mass of sorbent based on zeolite and its modified form [[10], [11], [12], [13], [14]].

Analysis of the sorption capacity showed that the sorption capacity of zeolite can be significantly increased due to its modification (Fig. 2).

In addition to zeolites, diatomites have been studied as sorbents. In Kazakhstan, the largest deposits of diatomite in the world are located in the Aktobe region. In total, the forecast resource of Kazakhstan's diatomite reserves is three billion tons. For comparison: in the United States, diatomite reserves are estimated at 500 million tons. It is a sedimentary rock, usually loose or weakly cemented. Diatomite is a good absorbent material with low heat and sound conductivity; in addition, it is refractory, acid-resistant, and non-flammable. This material is unique in that in one case it can be used as a hygroscopic material, a very strong absorbent that absorbs moisture, and in another case - as a superhydrophobic material that repels liquid. Diatomite itself is a natural nanomaterial containing up to 80% silicon dioxide. Diatomite is promising as:

- filtration material for water treatment of industrial wastewater;
- Universal sorbent for eliminating emergency spills of oil products and aggressive environments;
- filtration material for purification of food and technical liquids**.**

One of the promising materials for water treatment is also vermiculite. Vermiculite is a mineral from the group of hydromicas that have a layered structure.

Important properties of expanded vermiculite are chemical inertness, heat resistance, strength, safety, high adsorption capacity, and ion exchangeability. It is thanks to these properties that vermiculite serves as an inorganic matrix for creating a sorbent. During the expansion of vermiculite, water crystallized between mica flakes evaporates, which leads to the formation of macro- and micropores in the vermiculite particle and an increase in the specific surface area by approximately 5 times. Expanded vermiculite itself

is hydrophilic. To turn vermiculite into an effective sorbent, it must be chemically modified. In this case, macropores become hydrophobic, while micropores remain hydrophilic. Pores of different sizes and wettability characteristics give modified expanded vermiculite unique sorption and ion exchange characteristics [[15], [16], [17], [18], [19]].

Expanded vermiculite is used:

- for removing petroleum products, organic and toxic liquids from the surface of water bodies and soils;
- for localization and removal of oil in case of accidents of underwater oil pipelines and during offshore oil production;
- for wastewater treatment from oil and other contaminants.

The above-listed macroporous granular sorbents with a high exchange capacity have good kinetic characteristics for the sorption of heavy metal ions.

Results and discussion

Composition and content are given in Table 2 of model solutions of heavy metal salts.

Sorbents based on mineral raw materials and their modified forms can be used for selective or group extraction and concentration of metal ions. The kinetic laws of the cleaning process were studied to establish the optimal cleaning regime. The proposed methods for modifying sorbents create the basis for studying the structure, porosity, and sorption capabilities of these natural materials [[20], [21], [22]]. Zeolite has a significant and similar sorption capacity not only for particularly toxic ions (Hg^{2+}, Cd^{2+}, Pb^{2+}), but also for other heavy metals (Cu^{2+}, Co^{2+}, Ni^{2+}, Zn^{2+}, Ba^{2+}, Sr^{2+}), present in natural and waste waters in different quantities**.** A special role is played by the significant sorption

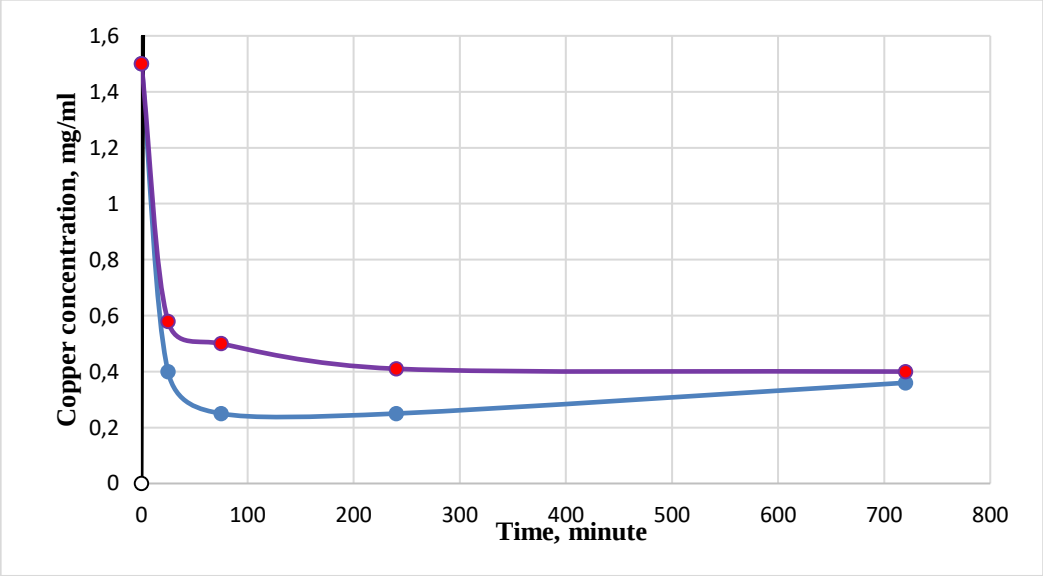

Figure 2 - Kinetics of copper ion sorption by natural sorbents
(1 - copper concentration on zeolite sorbent; 2 - on modified zeolite sorbent)

Table 2 - Composition and content of the model solution

Cation	NH_4^+	Pb^{2+}	Ba^{2+}	Sr^{2+}	Cd^{2+}	Cu^{2+}	Zn^{2+}	Co^{2+}	Ni^{2+}
Concentration (in mg/l) of metal in wastewater	40.0	2.95	3.68	1.65	2.15	2.20	2.5	2.5	1.2

capacity of the studied clinoptilolite samples for lead ion, which makes it possible to use them for wastewater treatment and soil detoxification in the adjacent territories of metallurgical enterprises**.**

Diatomite, untreated thermally, with high adsorption rates and low permeability values, can be used as an adsorbent for fine wastewater treatment in a stationary mode. The advantage of using diatomite for fine purification of wastewater from pollutants is the possibility of restoring the adsorption properties of diatomite after calcination at 300-400 ^{0} C. Diatomite used for fine purification of wastewater from heavy metal cations can also be regenerated or recycled. Calcined diatomite, which has a relatively high permeability with a fairly low adsorption value, can also be used as a filter material for rough water purification [[23], [24], [25], [26]]. It is possible to use diatomite in the form of granules of fractions 0.5-1.0, 0.8-2.0; 1.0-4.0, 2.5-5.0 mm.

Conclusions

In the EU countries and the USA, lists of priority environmental pollutants have been compiled, which for various matrices (water, soil, air, etc.) contain approximately 100-150 of the most dangerous pollutants that are constantly found in environmental objects.

In Kazakhstan, there is not yet a scientifically based (from the point of view of ecology, toxicology, hygiene and eco-analytics) list of priority pollutants for water, air and soil, which makes it difficult to periodically systematically monitor their content in various natural environments.

Therefore, it is necessary to compile a scientifically based list of priority pollutants in the natural waters of Kazakhstan.

One of the most promising filter materials are zeolite, clinoptilolite, and diatomite vermiculite, which can be used in wastewater treatment from iron, ammonium ions, heavy metals, radionuclides, organic compounds and various trace elements. The sorption properties of clinoptilolite rocks from the Chankanai and Taizhuzgen deposits with a clinoptilolite content of at least 60–70% have been studied.

Based on a detailed analysis of foreign experience in wastewater treatment technologies, research has been carried out on the possibilities of using effective adsorption methods along with traditional reagent treatment methods.

The experience of American and German scientists were studied in detail: modern methods of purification of natural and waste waters and the capabilities of new generation equipment in identifying toxic substances in natural and waste waters. The development of new and improvement of existing treatment methods, and their implementation at enterprises in Kazakhstan will allow solving the following practical problems: fundamentally new approaches to organizing energy- and resource-saving highly efficient technologies for wastewater treatment and water treatment will be developed.

Zeolite, diatomite, and vermiculite rocks for the extraction and concentration of metals in their modified forms through preliminary thermochemical treatment.

Research on the extraction of heavy metals on granular filters with zeolite, diatomite, and vermiculite loading, with a mineral content of 90-95%, fractions of 0.5-1.0 mm at a temperature of 300 ^{0} C - 400 ^{0} C, has established the almost complete extraction of large Pb cations $^{2+,}$ Fe $^{2+,}$ Ni $^{2+,}$ Mn $^{2+,}$ Zn $^{2+.}$

Zeolite exhibits sorption capacity not only for particularly toxic ions: Hg $^{2+,}$ Cd $^{2+,}$ Pb $^{2+,}$ but also for heavy metal ions Cu $^{2+,}$ Co $^{2+,}$ Ni $^{2+,}$ Zn $^{2+,}$ Ba $^{2+,}$ Sr $^{2+,}$ present in natural and waste waters in different quantities.

Thus, natural mineral raw materials (zeolites, diatomites, vermiculites, and their modified forms), the reserves of which are sufficient in Kazakhstan, can be used as a granular load for wastewater treatment and water treatment. All three minerals are highly porous, structured materials that are promising for use as stable sorption systems in water purification and water treatment.

Conflict of interest. On behalf of all the authors, the correspondent author declares that there is no conflict of interest.

Cite this article as: Myrzalieva SK, Bagasharova JT, Akilbekova ShK, Serikbaev P. Natural mineral raw materials as granular filtering materials in industrial and waste water treatment. Kompleksnoe Ispolzovanie Mineralnogo Syra = Complex Use of Mineral Resources. 2025; 332(1):70-78. https://doi.org/10.31643/2025/6445.06

Өндірістік ағынды суларды тазартуда түйіршікті сүзгі материалдары ретіндегі табиғи минералды шикізат

[1,2]Мырзалиева С.К., [1,2]Багашарова Ж.Т., [1]Акильбекова Ш.К., [1,2]Серикбаев П.К.

[1] Қазақстан Республикасының минералдық шикізатты кешенді қайта өңдеу жөніндегі ұлттық орталығы, Алматы, Қазақстан
[2]әл-Фараби атындағы Қазақ Ұлттық Университеті , Алматы, Қазақстан

Мақала келді: *17 қазан 2023*
Сараптамадан өтті: *29 қараша 2023* Қабылданды: *29 ақпан 2024*

ТҮЙІНДЕМЕ

Қазіргі уақытта табиғи және ағынды суларды ауыр металдардан тазартудың қолданыстағы әдістерін талдау сорбенттер ретінде табиғи бейорганикалық материалдарды: цеолит, диатомит, вермикулит қолданатын сорбциялық әдіс перспективалы болып табылатындығын көрсетті. Тақырыптың өзектілігі табиғи сулардың металлургиялық кәсіпорындардың өндірістік сарқынды суларымен ластану деңгейіне тұрақты мониторинг жүргізуге мүмкіндік беретін ағынды суларды тазарту мен су дайындаудың өзіндік технологиясын әзірлеу қажеттілігінен туындады. Сорбенттерді өзгертудің ұсынылған әдістері аталған табиғи материалдардың құрылымын, кеуектілігін, сорбциялық мүмкіндіктерін зерттеуге негіз болады. Аталған үш минерал: цеолит, диатомит, вермикулит жоғары кеуекті құрылымдық материалдарға жатады, оларды суды тазарту мен суды дайындауда тұрақты сорбциялық жүйелер ретінде пайдалану перспективті болып табылады. Бұл жұмыста табиғи сорбенттердің физика-химиялық сипаттамаларының әсері және су дайындау үшін жаңа перспективалы экологиялық қауіпсіз материалдар мен реагенттерді қолдану қарастырылады. Гидротермиялық әдіспен модификациялауға дейінгі және кейінгі табиғи цеолит материалында мыс иондарының сорбциясы зерттелді. Сорбенттердің белсенділігі сорбциялық сыйымдылықтың мөлшері бойынша, яғни цеолит пен оның модификацияланған түрлеріндегі сорбент массасының бірлігімен сіңірілген ауыр металл иондарының мөлшерімен бағаланды.

Түйін сөздер: ағынды сулар, сорбенттер, цеолит, диатомит, вермикулит, клиноптилолит, қалдықтар, минералды шикізат.

Авторлар туралы ақпарат:

Мырзалиева Сауле Керчаизовна — *Химия ғылымдарының докторы, профессор, Қазақстан Республикасының минералдық шикізатты кешенді қайта өңдеу жөніндегі Ұлттық орталығының Ғылыми – техникалық құзіреттілікті дамыту департаментінің білім беру қызметтері секторының меңгерушісі, Жандосова 67, 050036, Алматы, Қазақстан. Email: saulekerchaiz@mail.ru*

Бағашарова Жеңісгүл Телмановна — *Техника ғылымдарының кандидаты, Қазақстан Республикасының минералдық шикізатты кешенді қайта өңдеу жөніндегі ұлттық орталығындағы Ғылыми-техникалық құзіреттілікті дамыту департаментінің жетекші ғылыми қызметкері, Жандосова 67; әл-Фараби атындағы Қаз¥У кафедрасының аға оқытушысы, әл-Фараби даңғылы 71, 050040, Алматы, Қазақстан. Email: zh.t_bagasharova@mail.ru*

Акильбекова Шолпан Калыкуловна — *Техника ғылымдарының кандидаты, Қазақстан Республикасының минералдық шикізатты кешенді қайта өңдеу жөніндегі ұлттық орталығындағы Ғылыми – техникалық құзіреттілікті дамыту департаментінің аға ғылыми қызметкері, Жандосова 67, 050036, Алматы, Қазақстан. E-mail: cadikova74@mail.ru*

Серікбаев Пирмаханбет Қалхабадұлы — *Әл-Фараби атындағы Қаз¥У магистранты, әл-Фараби даңғылы 71, 050040, Алматы, Қазақстан. E-mail: serykbaev.pyrmahanbet@mail.ru*

Природное минеральное сырьё в качестве зернистых фильтрующих материалов при очистке природных сточных вод

[1,2]Мырзалиева С.К., [1,2]Багашарова Ж.Т., [1]Акильбекова Ш.К., [1,2] Серикбаев П.К.

[1] РГП «Национальный центр по комплексной переработке минерального сырья Республики Казахстан», Алматы, Казахстан
[2]Казахский Национальный Университет им. аль-Фараби, Алматы, Казахстан

Поступила: *17 октября 2023*
Рецензирование: *29 ноября 2023*
Принята в печать: *29 февраля 2024*

АННОТАЦИЯ

Анализ существующих в настоящее время методов очистки природных и сточных вод от тяжелых металлов показал, что одним из перспективных является сорбционный метод с использованием в качестве сорбентов природных неорганических материалов: цеолита, диатомита, вермикулита. Актуальность темы продиктованы необходимостью разработки оригинальной технологии очистки сточных вод и водоподготовки, позволяющей вести постоянный мониторинг уровня загрязнений природных вод производственными сточными водами металлургических предприятий. Предложенные способы модификации сорбентов создают основу для изучения структуры, пористости, сорбционных возможностей названных природных материалов. Все три минерала: цеолит, диатомит, вермикулит относятся к высокопористым, структурированным материалам, перспективным для использования в качестве устойчивых сорбционных систем в водоочистке и водоподготовке. Рассмотрены влияние физико-химических характеристик природных сорбентов, применение новых перспективных экологически безопасных материалов и реагентов для водоподготовки. Исследована сорбции ионов меди на природном цеолитном материале до и после его модификации гидротермальным методом. Активность сорбентов оценивали по величине сорбционной емкости, т.е. количеству ионов тяжелых металлов, поглощенных единицей массы сорбента на основе цеолита и его модифицированной формы.

Ключевые слова: сточные воды, очистка, сорбенты, цеолит, диатомит, вермикулит, клиноптилолит, отходы, минеральное сырье.

Информация об авторах

Мырзалиева Сауле Керчаизовна — *Доктор химических наук, профессор, заведующий сектором образовательных услуг департамента развития научно-технических компетенций Национального центра по комплексной переработке минерального сырья Республики Казахстан, 050036, Алматы, ул.Жандосова, 67. Email: saulekerchaiz@mail.ru*

Багашарова Женисгул Телмановна — *Кандидат технических наук, ведущий научный сотрудник департамента развития научно-технических компетенций Национального центра по комплексной переработке минерального сырья Республики Казахстан, 050036, Алматы Казахстан, ул.Жандосова, 67; старший преподователь КазНУ имени аль-Фараби, пр Аль-Фараби 71, 050040, Алматы, Казахстан. Email: zh.t_bagasharova@mail.ru*

Акильбекова Шолпан Калыкуловна — *Кандидат технических наук, старший научный сотрудник департамента развития научно-технических компетенций Национального центра по комплексной переработке минерального сырья Республики Казахстан, 050036, Алматы Казахстан, ул.Жандосова, 67. E-mail: cadikova74@mail.ru*

Серикбаев Пирмаханбет Калхабадович — *Магистрант Казахского Национального Университета им. аль-Фараби, пр Аль-Фараби 71, 050040, Алматы, Казахстан. E-mail: serykbaev.pyrmahanbet@mail.ru*

Reference

[1] Vasilyanova LS. Natural minerals at the service of ecology. Almaty: NC NTI. 2015, 90.

[2] Myrzalieva SK, GNIP Pratama, Hamidulla A.G. Wastewater treatment using natural zeolite materials. Kompleksnoe Ispolzovanie Mineralnogo Syra = Complex Use of Mineral Resources. 2021; 2(317):64-68. https://doi.org/10.31643/2021/6445.19

[3] Myrzalieva SK, Bagasharova JT. Obtaining effective sorbents from secondary plant raw materials for water purification from oil products. Journal of Oil and Gas. 2020, 162-168. http://neft-gas.kz/

[4] Myrzalieva SK. Utilization of spent activated sludge after geological treatment of oil-contaminated wastewater. Journal Bulletin of KazNITU named after K.I. Satpayev. 2018; 3:101-105. https://official.satbayev.university/ru/research/vestnik-satbayev-university

[5] AkilbekovaS, Myrzalieva S, Moldabayeva G, Turkmenbayeva M, Suleimenova B. Iinvestigation of the process of sulfide-firing of gold-antimony concentrate Journal of Chemical Technology and Metallurgy. 2021; 56(5):1051-1057. https://www.scopus.com/record/display.uri?eid=2-s2.0-85111758467&origin=resultslist&sort=plf-f

[6] Myrzalieva SK, Bagasharova JT, Akilbekova ShK. Study of the possibilities of using zeolite and diatomite in the treatment of oil-contaminated wastewater. Integrated Use of Mineral Raw Materials. 2022; 3(322).

[7] Lakhbayeva ZhA, Kurmangazhy G, Tazhibayeva SM, Artykova DM-K, Musabekov KB. Possibility of water purification from Cu^{2+}, Pb^{2+} and Cr^{3+} ions using vermiculite. Journal of Chemical Technology and Metallurgy. 2019; 3.

[8] Tattibayeva Z, Tazhibayeva S, Kujawski W, Zayadan B, Musabekov K. Peculiarities of adsorption of Cr (VI) ions on the surface of *Chlorella vulgaris ZBS1* algae cells. Heliyon. 2022; 8(9). https://doi.org/10.1016/j.heliyon.2022.e10468,SJR_{2021}=0,550

[9] Zhadra Tattibayeva, Sagdat Tazhibayeva, Wojciech Kujawski, Bolatkhan Zayadan, Kuanyshbek Musabekov. Analysis of Cr (III) ions adsorption on the surface of algae: implications for the removal of heavy metal ions from water. Eastern European Journal of Enterprise Technologies. 2021; 4(11):31-38.

[10] Yakovlev SV, Karelin JA, Laskov YM, Vorornov YuV. Treatment of industrial wastewater. Moscow: Stroyizdat. 1985, 332.

[11] Korte F, Bahadir M, Kline W, Lai JP, Parlar G, Scheunert I. Environmental Chemistry. Fundamentals and concepts. Moscow: Mir. 1997, 396.

[12] Kuznetsov AE, et al. Prikladnaya ekobiotekhnologiya. Moskva: BINOM. Laboratoriya znaniy [Applied Ecobiotechnology. Mosow: BINOM. Laboratory of knowledge]. 2012, 629. (In Russ.).

[13] Makarov AA, Rush EA. Modeling and analysis of adsorption processes of heavy metal ions on modified aluminosilicates. Modern Technologies. System analysis. Modeling. 2012; 2(34):146-152.

[14] Myrzalieva SK, Khamzina JB, Dauletbai AD. Features of the method of industrial wastewater treatment by ionic substitution of harmful heavy metals. Industry of Kazakhstan. 2011; 3:310-312.

[15] Chechevichkin AV, Samonin VV. Optimization of technological parameters of the crushing process of clinoptilolite rocks in obtaining sorption-catalytic materials. Izvestiya Sankt-Peterburgskogo Gosud.Technolog. Inst. 2015; 32(58):105-108.

[16] Vatin NI, Chechevichkin VN, Chechevichkin AV, Shilova ES. Application of clinoptilolite-type zeolites for natural water treatment. Engineering and Construction Journal. 2013; 2:81-86.

[17] Redinova AV, Grabelnykh VA, Levanova EP, Korchevin NA Extraction of heavy metal ions from aqueous solutions sulfur-containing polymeric sorbents. Bulletin of the IrGTU. 2013; 1(72):113-115.

[18] Prokofiev VY, Gordina NE, Zakharov ON, Tsvetova EV, Kolobkova AE Granulated low-modulus zeolites for extraction of cations Co.izv.vuzov. Chemistry and Chemical Technology. 2020; 63(6).

[19] Drugov S, Rodin AA. Analysis of contaminated water practical guide-M: BINOM. Laboratory of Knowledge. Methods in Chemistry. 2015, 678.

[20] Andreeva NP. Application of complex sorbents for wastewater treatment from large organic compounds and heavy metals. Author's abstract for the degree of Candidate of Technical Sciences. 2006, 155.

[21] Zubarev GI, Gurinovitch AV. Deep cleaning electroplating wastewater. Ecology and Industry of Russia. 2008, 16.

[22] Kireicheva LV, Andreeva NP. Complex sorbents for wastewater treatment from organic compounds and heavy metals ions. Water treatment, water treatment, water supply. 2009; 1:43-46.

[23] Sazonova AV, Niyazi FF, Maltseva VS. Thermodynamics and kinetics of chromium (III) ions sorption by carbonate rocks. Modern problems of science and education, Moscow. 2012; 1. http://www.science-education.ru/101-5305

[24] Dementyev SN, Drebushchak VA, Seretkin YuV. New approaches to the study of physico-chemical properties of zeolites. Novosibirsk. 1989, 102.

[25] Kolesnikova LG, Lankin SV. Ion transfer in clinoptilolite. Blagoveshensk: Publishing house of BGPU, 2007, 113.

[26] Vasilyev SI, Lapushova VM, Melkozerov VM. Ecology and rational nature management. 2016; 1(29):135-139.

Crossref
DOI: 10.31643/2025/6445.07
Earth sciences

Features of obtaining composite material from hydrophobic clay with antimicrobic properties

[1*]Ibraimova D.M-K., [2,3]Rozhkova O.V., [1]Musabekov K.B., [1]Tazhibayeva S.M., [2,4]Rozhkov V.I.,[3]Yermekov M.T.

[1]Al-Farabi Kazakh National University, Almaty, Kazakhstan
[2]Saken Seifullin Kazakh Agrotechnical University, Astana, Kazakhstan
[3]JSC Science and Technology Solutions, Almaty, Kazakhstan
[4]LLP Altai Geological and Ecological Institute, Ust-Kamenogorsk, Kazakhstan

** Corresponding author email: dana_kereevna@kaznu.kz*

Received: *September 13, 2023*
Peer-reviewed: *December 20, 2023*
Accepted: *March 5, 2024*

ABSTRACT

A method for obtaining a nanocomposite from hydrophobic clays with bactericidal properties is considered, which plays the role of a drug matrix intercalated agar-agar. Such nanocomposite materials are increasingly used in medicine as matrices for medicines and vitamins using their adsorption properties and long-term exposure. It was established using TEM analysis that halloysite particles from Beloye Glinische deposit are nanoscale and have a cylindrical shape with a length from 200 nm to 1000 nm and a diameter of nanoparticles from 50 nm to 80 nm. The first stage of the bionanocomposites manufacturing process was the treatment of halloysite nanoparticles with silver ions to impart antimicrobial properties, and hydrophobization with a cationic surfactant was carried out at the next stage. It was established by the X-ray diffraction method that the interlayer space of HNT has been expanded from 9.998 Å to 17.5 Å on the result of the cationic adsorption on the HNT. FTIR spectroscopy also proved the adsorption of surfactant molecules on halloysite by the presence of an appropriate absorption band. The adsorption of silver on a nanotube made of halloysite was revealed by the method of energy-dispersive X-ray spectroscopy. Antimicrobial properties of silver-treated and organophilic halloysite have been established and proved by *in vitro* analyses in microbiological laboratories about *Escherichia coli*. Hydrophobic samples of these organophilic clays had edge angles higher than 90° and this proves that all samples are hydrophobic. The resulting organophilic clays were intercalated into an agar-agar matrix and were thrown into a solution of calcium chloride, which gave them stability in a liquid medium. It has been practically established that the most optimal bionanocomposite microsphere is a 50% ratio of organohalloysite and agar-agar.

Keywords: bionanocomposite, halloysite nanoclay, silver clay, antimicrobial properties, oleophylization, microsphere, drug delivers.

Information about authors:

Ibraimova Dana Mykty-Kereevna — *Candidate of Chemical Sciences, Senior Lecturer, Al-Farabi Kazakh National University, 050000, al-Farabi Avenue, 71, Almaty, Kazakhstan. Email: dana_kereevna@kaznu.KZ*

Rozhkova Olga Vladimirovna — *Doctor of Chemistry, Professor of Saken Seifullin Kazakh Agrotechnical Research University, Astana, Kazakhstan, 010000, Zhenis Avenue, 62, Astana, Kazakhstan, JSC "Science and Technology Solutions", Astana, Kazakhstan, 010000, Republic Avenue, 24. Email: rozhkova.o@stsolutions.KZ*

Musabekov Kuanyshbek Bituovich — *Doctor of Chemical Sciences, Professor, Academician of the National Academy of Natural Sciences of the Republic of Kazakhstan, Al-Farabi Kazakh National University, 050000, al-Farabi Avenue, 71, Almaty, Kazakhstan. E-mail: musabekov40@mail.ru*

Tazhibayeva Sagdat Mederbekovna — *Doctor of Chemical Sciences, Professor of Al-Farabi Kazakh National University, 050000, al-Farabi Avenue, 71, Almaty, Kazakhstan. E-mail: tazhibayeva_s@mail.ru*

Rozhkov Vitaliy Igorevich — *Candidate of Technical Sciences, Saken Seifullin Kazakh Agrotechnical University, Astana, Kazakhstan; LLP "Altai Geological and Ecological Institute", Ust-Kamenogorsk, Kazakhstan. E-mail: Vitalrza1983@gmail.com*

Yermekov Marat Teginbayevich — *Director of the Project and Asset Management Department of Science and Technology Solutions JSC, 050000, Almaty, Kazakhstan. Email: yermekov.m@@stsolutions.kz*

Introduction

Academician Sh.B. Battalova described in detail the chemical and physical properties of Kazakhstani clays, she showed the possibility of using bentonites from Kazakhstani deposits as catalysts for oil refining, adsorbents of dye ions and heavy metals, as well as for cleaning vegetable oils, petroleum products and wool washing [1].

Currently, Kazakhstan's clays have been sufficiently studied by scientists from foreign and neighbouring countries, but even then they do not have a wide range of applications in production facilities within Kazakhstan, as they are transported from foreign marketplaces. As a result of the work, there will be results that will determine the scope of application of various clays in Kazakhstan [[2], [3], [4], [5], [6], [7], [8], [9], [10]].

In the domestic market, there is a growing demand for organoclays, drilling fluids and additives to building mixes. In addition, the development of nanotechnology and the production of new composite materials based on nonpolar polymers implies an expansion of the range of organoclays with differentiated surface hydrophobicity [[5], [6], [7], [8]].

The aim of this work was the synthesis of a biodegradable nanocomposite based on halloysite nanotubes (HNT), with prolonged bactericidal properties and high capacity, capable of absorbing harmful ions in the body and releasing vitamins contained in it during ion exchange.

Experimental

Materials

The halloysite clay of the White Clay deposit, which has the shape of a hollow cylinder with a length of 200-1000 nm and a diameter of 50-80 nm, was chosen as a matrix for obtaining a biodegradable nanocomposite [[4], [5]]. The mineral is characterized by a 1:1 crystal structure and a high water content. The colour is white with a hardness of 1-2.5 on the mineralogical scale and a density of 2.6 g/cm^3.

Octadecylamine (CAS No: 124-30-1, Sigma Aldrich) A solution of a cationic surfactant was used to produce organoclay [[4], [6], [11]]. The chemical formula is $C_{18}H_{39}N$, a white crystal with a molecular weight of 269,5 g/mol.

To impart bactericidal properties to halloysite nanotubes, silver nitrate (CAS: 7761-88-8, Sigma Aldrich) was used, which is a salt of the transition metal of silver and inorganic nitric acid with the formula $AgNO_3$.

Agar-agar $(C_{12}H_{18}O_9)_n$ (CAS No: 9002-18-0, Sigma Aldrich) was used as a polymer biodegradable matrix and for the absorption of drugs

Methods

For X-ray diffraction analysis, an automated Drone–3 diffractometer with CuK_α radiation and a β filter was used (U=35 kV; I=20 mA; capture θ-2θ; detector speed 2 degrees/min.). X-ray phase analysis of the diffractogram of powder samples was carried out on a semi-quantitative basis by the method of equal suspensions and artificial mixtures.

The scanning electron microscope belongs to the most modern devices for conducting research work of the highest automated processes in the direction of nanotechnology. It is an apparatus that is necessary for obtaining permissible shots of at least 2.5 nm and conducting quantitative and qualitative analyses of nanomaterial objects.

Transmission electron microscopy (TEM) was used to describe the structure of the material both in terms of sample size and surface.

Infrared spectroscopy is a method that studies the interaction of infrared light with matter.

The goniometer is a device for measuring the contact angle by the method of measuring the drop lying down.

Results and Discussion

In the process of carrying out the work, it was necessary to prepare the first halloysite, then silvered clay and after the silvered organohalloysite

Halloysite deposits in Kazakhstan are located in two places [[6], [7], [8], [9], [10], [11], [12], [13], [14], [15], [16], [17]], these are the halloysite of the Beloye Glinishche deposit near Karaganda and the Aizin-Tamara halloysite deposit in the Akmola region. The choice of halloysite from the Beloye Glinishche deposit is justified by the fineness of the mineral and the basic composition, which is represented by halloysite with chemical formula $Al_4[Si_4O_{10}][OH]_8 \cdot 4H_2O$ or $Al_2O_3 \cdot 2SiO_2 \cdot 4H_2O$. It has been proven that the mineral halloysite practically never occurs in its pure form, most often together with kaolinite and quartz or a mixture with other aluminosilicate minerals. To separate the mineral from quartz particles, Karaganda halloysite was crushed, sieved and washed by decantation in laboratory conditions. X-ray diffraction analysis was performed to confirm the resulting powder's composition.

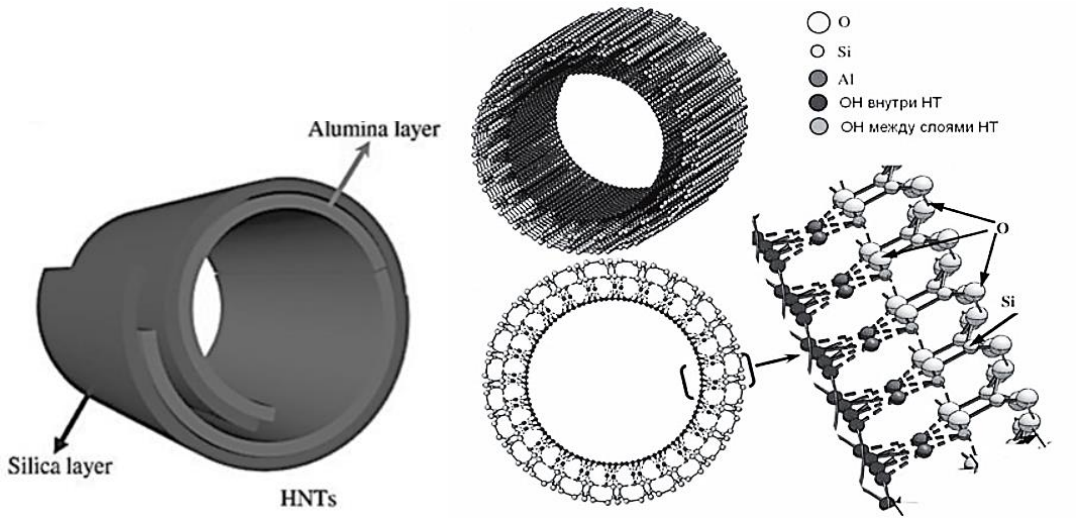

Figure 1 - 3D dimensional structure of halloysites [[4], [17]]

Table 1 below shows the mineral composition of the sample by the quantitative indications of a semi-digital X-ray phase analysis.

Table 1 - Findings of semi-digital X-ray phase analysis

1	2
Halloysite $Al_2(Si_2O_5)(OH)_4$	SiO_2 and others
81.2. %	18.8. %

The mineral halloysite has the form of rolled sheets [[4], [12]], the diagram below shows the 3D dimensional structure of the halloysite, Figure 1.

As the results of X-ray diffractometric analysis showed, the bulk of the mineral, i.e. 81.2%, is halloyisite. Two types of halloysite 10A and halloysite 7A are known in nature, since the interlayer space is 9.997 Å, it is determined that halloysite White Clay belongs to the type - halloysite 10A. In the generalization of halloysite [[7], [12]], the authors described that the studied composition of halloysite corresponds to the chemical formula $Al_2Si_2O_5(OH)_4$ nH_2O, where n=0-2. The structure of halloysite - (7Å) is described by a hexagonal unit cell with edge lengths a=5.14, b=8.9, c=17.7 A; the values of angles α=97-104, β=90-91.8, γ=90° differ slightly from different authors [[8], [13]].In tubular structures of halloysite, its long axis is often associated with the crystallographic axis. To identify halloysite-(10 A), X-ray phase analysis uses a reflex with d001, which is absent in the spectrum of several polymorphs of the kaolins. This corresponds to the sum of the thicknesses of one mineral layer of 7.14 Å and a monolayer of water of 3 Å. The authors [[4], [5], [6], [7], [8], [9], [10], [11], [12]] determined that the outer surface of aluminosilicate nanotubes consists mainly of siloxane groups (Si-O-Si). Aluminol (Al-OH) functional groups are also placed on the inner surface of the cavity and between the layers. The inner type is Al-IT is directed towards the tetrahedral silica mesh. As a result of structural defects, silanol (Si-OH) and additional Al-OH functional groups are formed on the fractures of silicate particles (Fig. 1 and 2) [12].

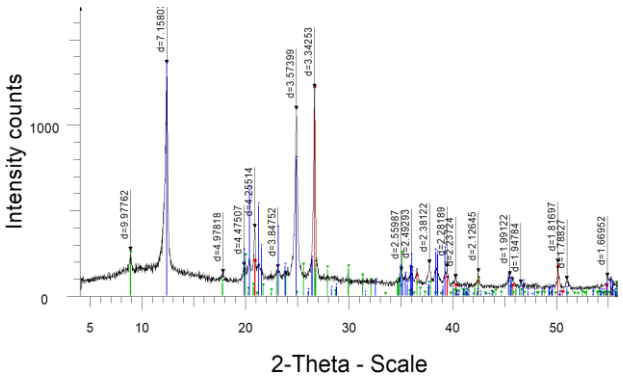

Figure 2 - Diffractogram of the halloysite (a) mineral

Also of interest is the demonstration of the presence of halloysite nanotubes determined by scanning electron microscopy (SEM), this analysis was conducted through the "National Open-type Nanotechnology Laboratory" at the Al-Farabi Kazakh National University. The results are shown in Figure 3.

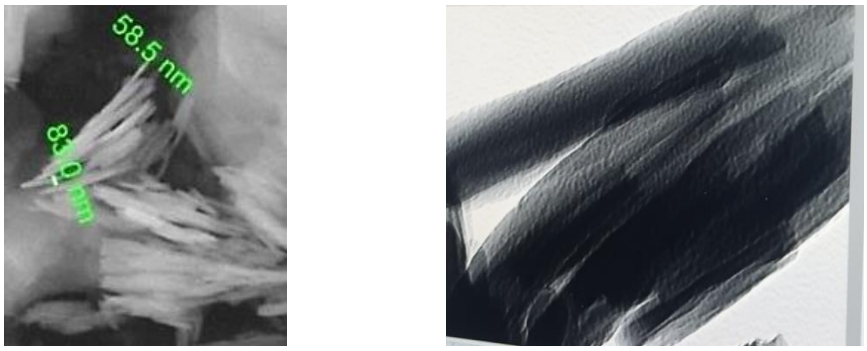

a b

Figure 3 - Morphology of mineral halloysite. a – SEM figures and b – TEM figures

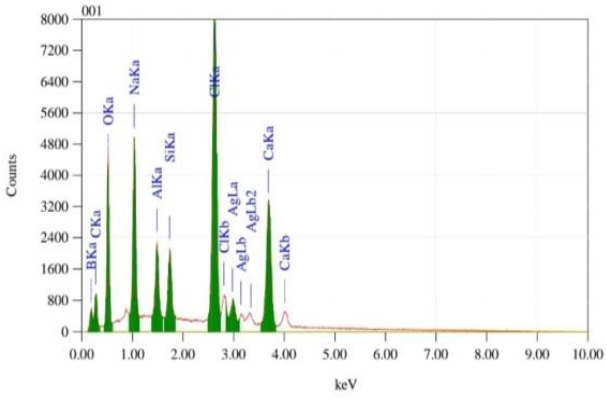

Figure 4 - Determination of silver ions by energy dispersion X-ray spectroscopy

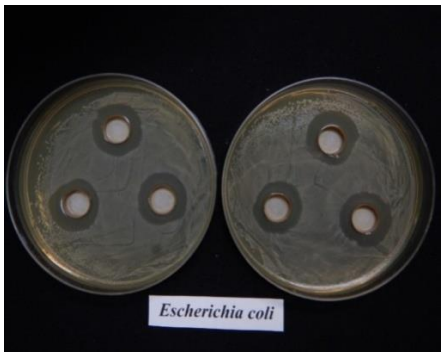

Figure 5 - Zones of inhibition of the growth of Escerichia coli shoots of silver ion planted clay (21-23mm).

Halloysite particles consist of fibrous particles, with a particle length of the order of 200-1000 nm, tube diameters range from 50-80 nm, SEM and TEM pictures (Fig. 3a and 3b). It is known that halloysite exists in the form of nanotubes, and these nanotubes are present in a hollow form [3], although due to the limitations of the SEM method, this cannot be confirmed. However, SEM analysis made it possible to determine the size of the nanotubes. In this regard, a TEM study was undertaken to verify the hollow structure of the nanotube. TEM analysis was carried out in the nanolaboratory of the Kazakh-Japanese Innovation Center of the Kazakh National Agrarian University. The obtained result is presented in Figure 3.

From Figure 3, it is evident that HNTs are in the shape of spherical tubes, with diameters ranging from 20 to 50 nm. Halloysite belongs to the colinite group and, unlike kaolinite, is located in two layers and contains a small number of water molecules. The critical grid scheme has a 1:1 ratio of clay types, one of which consists of aluminium oxide, and the other of silicon oxide [13]. The plates curl into tubes due to the sharp difference in the amount of silicon and aluminium ions. In this case, a folded tube is formed, inside of which there is a layer of aluminium oxide, and outside - a layer of silicon oxide. With different ionization of silicon by aluminium oxide, the dielectric properties are different. Aluminium oxide, if for example placed in a solution with pH = 8.5, will have a positive charge. The different charges on the outer and inner surfaces of halloysite tubes are associated with the possible filling of the inner part of the tubes with negatively charged molecules. Another attractive feature of Halloysite in comparison with other clays is that it has a large specific surface area. During the work, the halloysite was previously modified with silver ions. The bactericidal and antiseptic properties of silver ions and the ability to resist 650 types of bacteria are known [[14], [15]]. When modifying halloysite with silver ions, it was important not to change the morphological nature of the HNT, because the

introduction of a drug into the hollow part of the tube is implied.

The modification process was carried out simply, using a prepared solution of silver ions C($AgNO_3$) = 0.4 mg/l

The result of energy dispersive spectroscopy, proving that halloysite contains silver ions, is presented in Figure 4. To determine the presence of silver ions, an SEM image is first created, then by randomly placing a point on an area of the sample, an area of interest is selected (point 001 in Figure A) and the spectra of this region B. In Figure 4, the spectra coloured green are responsible for the clay mineral and silver ion. There is no need to pay attention to the content of carbon and chlorine ions revealed by the analysis since they are present in the composition of the substrate used.

Since silver ions can quickly oxidize in the sun and turn into silver oxide, all the samples obtained were stored in tinted glass containers, away from sunlight. The bactericidal properties of the resulting silver halloysite were tested. Testing of bactericidal properties was carried out by order in the microbiological laboratories INVITRO in Almaty.

The bactericidal properties were studied on the bacterium *Escherichia coli* (intestinal worm Rod), clay in an amount of 0.4 g was placed in a test tube, and then 10 ml of distilled water was added and thoroughly mixed. The test culture of *Escherichia coli* was sown in Petri dishes on top of the nutrient Agar. Then grooves were made on the agar, as shown in Figure 5, and 0.2 ml of the test suspension was poured. It was grown for 3 days in a Petri dish at 37 °C in a thermostat. As a result, the bactericidal property of the clay on which silver ions were applied was confirmed, in particular, to suppress the growth of *Escherichia coli* bacteria.

If the interlayer gallery expands, this may indicate the ingress of large molecules into it, that is, intercalation or detachment, therefore, to exclude changes in the structure of the sample under study after modification with silver, a repeated X-ray diffraction analysis was performed.

The analysis confirmed the change in the interlayer gaps from d =9.9 Å (Figure 6) to d =17.50 Å showing that octadecylamine (ODA) adsorption occurs. After organomodification with octadecylamine (ODA), the excess ODA was washed in three stages for complete removal. In this connection, ODA molecules were studied by IR spectroscopy to confirm their presence on the surface of the halloysite.

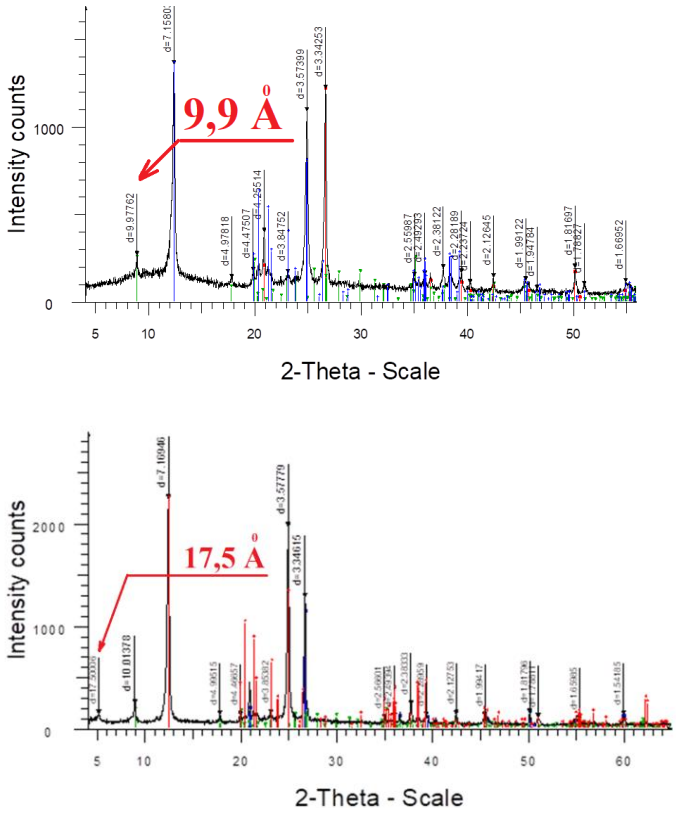

Figure 6 - Diffractogram of the halloysite (a) and organomodified halloysite (b) minerals

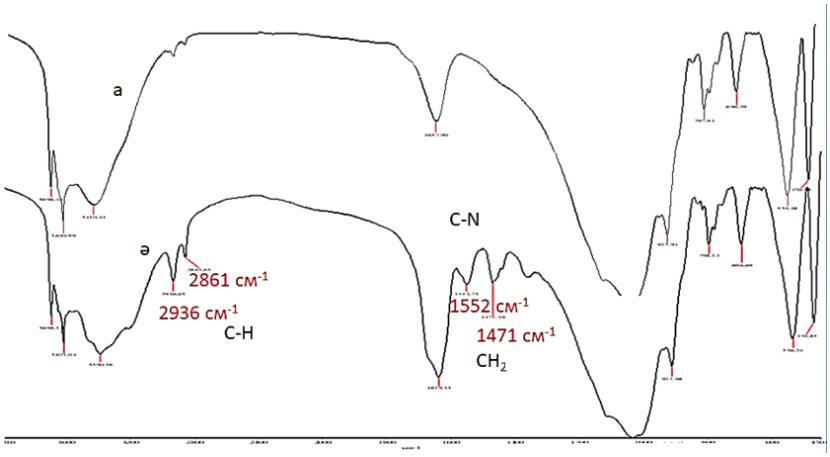

Figure 7 - IR-spectroscopic analysis results; a-halloysite; b-organohalloysite

Figure 8 shows the IR spectra of the halloysite clay of the White Clay deposit (a) and its modified ODA (b) hydrophobic clay. The values of 3699.06 cm^{-1}, 3698.64 cm^{-1}, 3696.52 cm^{-1}, and 3698.48 cm^{-1} in halloysite determine the presence of an oh group with which absorption bands are associated. The absorption of the free OH group in the spectrum of modified ODA halloysite corresponds to a frequency of 3550-3150 cm^{-1} and in the enriched natural spectrum of halloysite a short band of medium intensity 3620.99-3621.38 cm^{-1}. These bands indicate a strong association of the OH group with Halloysite. In the spectrum of modified ODA halloysite, the absorption of the trans-N-H band of the secondary amine is determined by bands 3317.80 and 3323.97 cm^{-1} with moderate intensity, and these bands manifest themselves at a very higher frequency compared to the spectrum of modified ODA (B) halloysite, whereas in halloysite these bonds manifest themselves at a lower frequency (a). The absorption of the spectrum in question in this area occurs at a very high intensity. The sample is presented in the form of a film (or tablets with KBr), and the absorption region of various symmetric C-H bonds in the spectrum of ODA-modified halloysite is observed in the regions of 2937 and 2860 cm^{-1}. Absorption bands of deformation vibrations of the hydroxyl group in the spectrum of natural halloysite and its modified form with ODA bands are manifested at frequencies 1639.33, 1639.76, and 1637.90cm^{-1}. The CH_2-group in deformation oscillations is in the region of 1500-1300cm^{-1} of the research spectrum. In this area, high-frequency components are associated with antisymmetric deformation and low-frequency components with symmetric deformation of these groups.

The absorption bands 1129 cm^{-1} and 1150 cm^{-1} of the spectra of modified ODA halloysite reflect valence vibrations of the natural and antisymmetric C-N bond associated with various particles in the molecule. This region is not observed in the spectrum of enriched natural halloysite. Thus, from the results of the IR spectra of natural halloysite and modified ODA halloysite, the following conclusion is drawn: in modified ODA halloysite, there is a significant decrease in free O-H bonds, which indicates a decrease in the number of bands in the corresponding spectral region and also indicates mixing of the remaining bands at a lower frequency. The spectrum pattern changes accordingly in the region of 1120-1000 cm^{-1}.

Organomodified halloysite can float on the surface of water, Figure 8 (the picture was taken after t=150 days). That is, organophilic halloysite is hydrophobic because it has a constant chemical composition

Figure 8 - Organoclay powder newly placed on the surface of the water after t=150 davs

Table 3 - Values of water absorption angles for samples of organoclay powders obtained at different concentrations of ODA

№	Consumption of ODA spent on modification, mole/litre	Angles of incidence, degrees	Names of organoclay of various modifications (ODA-modified and bactericidal)
1	Silvered halloysite	9°	BOMC0
2	0.000625	122°	BOMC1
3	0.00125	129°	BOMC2
4	0.0025	130°	BOMC3
5	0.005	131°	BOMC4
6	0.01	132°	BOMC5

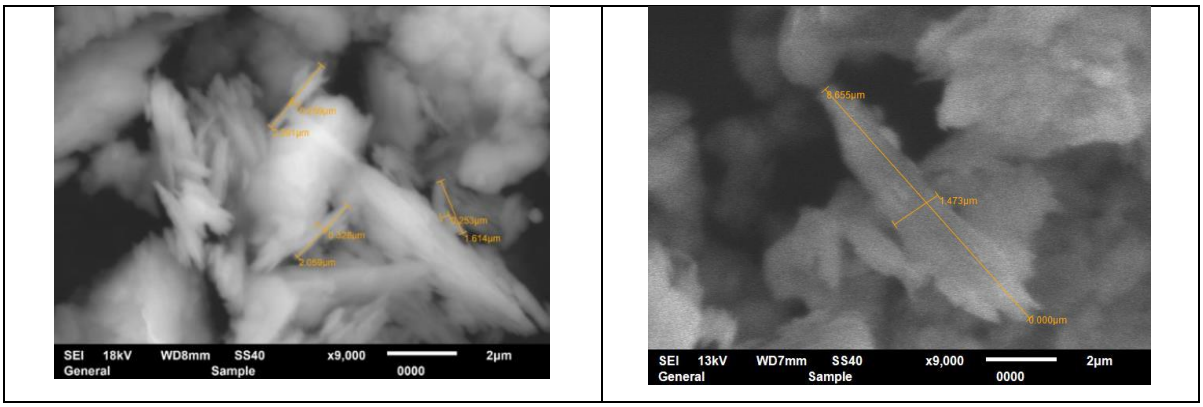

Figure 9 - SEM images of organomodified silveredhalloysite mineral

Thus, bactericidal organoclays of 6 types were obtained (Table 3) by modifying silver-plated halloysite with octadecylamine, labelled from BOMG0 to BOMG5. Since the organomodification process is carried out at a certain temperature mode of operation, it was important to make a morphological analysis of the particles of the resulting hydrophobic organohalloysite since it was necessary to preserve the organohalloysite spatially intact in the form of a nanotube during the process. For verification, an SEM picture of the organohalloysite was taken using the SEM method (Figure 9).

Using SEM analysis, the width and length of organophilic nanotubes made of halloysite were measured, it was found that the width ranges from 10 to 100 nm, and the length reaches ~1000 nm. It has been proven that this does not affect the type of rolled sheet.

At the next stage, the resulting silver sample of organophylic halloysite BOMC4 was embedded in a polymer matrix (agar-agar) to obtain samples of bionanocomposite. To create compactness, several pieces of samples were placed in a calcium solution. At the next stage, the masses, sizes and swollen and dried samples of bionanocomposite were studied. The data is shown in Table 4.

According to the data in the table, a spherical binanocomposite formed from silvered organoclay and agar-agar in a calcium shell shows water resistance and shows good swelling, although they were left in water for 72 hours to swell. This shows that this bionanocomposite with antimicrobial properties is a good enough result to be introduced into its drugs [[16], [17], [18], [19], [20]].

Table 4 - Composition of the bionanocomposite and their parameters

№№	Percentages of the composition of the OHNT in agar-agar	Mass of microparticles in swollen form, g	The mass of microparticles in dried form, g	Percentage of reduction of microparticles	The average diameter of the microparticles in the swollen form, g	The average diameter of microparticles in dried form, g	The proportion of absorbed water, dried samples, after swelling in water from its size	The "lifetime" of microspheres, the frequency of swelling / drying
1	0,1%	0.560	0.059	89.46	~2	~0.8	320%	42 time
2	1%	0.623	0.068	89.09	~2	~0.83	303%	45 time
3	10%	0.681	0.0998	85.31	~2	~0.85	273%	53 time
4	50%	0.710	0.132	81.42	~2	~0.9	233%	63 time
5	90%	0.740	0.149	79.86	~2	~1.6	143%	15 time

As can be seen from Table 4, in microspheres with an increase in the amount of organoclay, the absorption capacity of the microspheres of the bionanocomposite decreases. According to Table 4, a 50% microsphere with an oragnohalloysite nanotube (OHNT) absorbs liquid (water) almost 1.6 times worse than with their 0.1% sample, but the lifetime is better than other samples. Hence, it was concluded that the most optimal bionanocomposite microsphere is a 50% ratio of OHNT and agar-agar since it was necessary to introduce the maximum value of OHNT into these microspheres. The need to introduce OHNT into the agar-agar microsphere is that the bionanocomposite we have obtained should participate in the metabolism of nonpolar substances in the human body.

Conclusion

Thus, attention to the creation of bionanocomposites has been increasing recently. The results obtained by us significantly affect the methods of obtaining new types of medicines using clay minerals, expanding the scope of application of organomodified clays. Nanotechnology seems to be a serious scientific field capable of creating various nanobiocomposites with the expansion of their scope of application. Thanks to scientific research in this direction, the prospects for the creation and application of various types of nanoglines are significantly expanding. Research in this direction is promising and can expand the possibilities of creating various forms of medicines due to the synthesis of halloysite with oleophilic and bactericidal properties, structuring and microcapsulation of a bionanocomposite based on halloysite.

Acknowledgements

This scientific research was carried out within the framework of grant financing of the AP19674742 (IRN) project "Technology for obtaining a new organomineral composite material based on natural bentonite of East Kazakhstan" (IRN AP19674742 "Technology for obtaining a new organomineral composite material"). based on the natural bentonite of East Kazakhstan"). The source of funding is the Science Committee of the Ministry of Science and Higher Education of the Republic of Kazakhstan. The authors express their gratitude for the allocated grant funding.

Conflict of interest

The authors of this study do not cooperate with other publishers on this topic.

Cite this article as: Ibraimova D M-K, Rozhkova OV, Musabekov KB, Tazhibayeva SM, Rozhkov VI,Yermekov MT. Features of obtaining composite material from hydrophobic clay with antimicrobic properties. Kompleksnoe Ispolzovanie Mineralnogo Syra = Complex Use of Mineral Resources. 2025; 332(1):79-89. https://doi.org/10.31643/2025/6445.07

Антимикробтық қасиетке ие гидрофобты галлуазиттен композициялық материал алу ерекшеліктері

[1] Ибраимова Д.М-К., [2,3] Рожкова О.В., [1] Мұсабеков Қ.Б., [1] Тәжібаева С.М., [2,4]Рожков В.И., [3] Ермеков М.Т.

[1]Әл-Фараби атындағы Қазақ ұлттық университеті, Алматы, Қазақстан
[2]Сәкен Сейфуллин атындағы Қазақ агротехникалық зерттеу университеті, Астана, Қазақстан
[3]"Science and Technology Solutions" АҚ, Алматы, Қазақстан
[4]«Алтай геологиялық-экологиялық институты» ЖШС, Өскемен, Қазақстан

Мақала келді: *13 қыркүйек 2023*
Сараптамадан өтті: *20 желтоқсан 2023*
Қабылданды: *5 наурыз 2024*

ТҮЙІНДЕМЕ

Мақалада дәрілік матрица рөлін атқаратын бактерицидтік қасиеті бар гидрофобты саздардан бионанокомпозит алу әдісі қарастырылған. Мұндай дәрілік бионанокомпозиттік материалдар жоғары адсорбциялық қасиетке және ұзартылған әрекетке ие болғандықтан, әртүрлі дәрумендер мен дәрі-дәрмектерді тасымалдаушы матрица ретінде пайдалану үшін ұсынылады. ПЭМ талдауы арқылы Белое Глинище кенорнының галлуазиті наноөлшемді және ұзындығы 200 нм-ден 1000 нм-ге дейін цилиндр тәрізді және нанобөлшектердің диаметрі 50 нм-ден 80 нм-ге дейін болатындығы анықталған. Бионанокомпозитті өндіру процесінің бірінші кезеңінде микробқа қарсы қасиеттер беру үшін галлуазит нанобөлшектері күміс иондарымен өңделеді, ал келесі кезеңде катионды беттік белсенді затпен гидрофобталады. Катионды БАЗ адсорбциясы жүргендігі рентгендифракциялық әдіспен анықталды, мұны пакетаралық кеңістік 9,998 А-дан 17.5 А-ға дейін ығысқанынан білуге болады. Сондай-ақ, Фурье инфрақызыл спектроскопиясына сәйкес абсорбциялық жолақтардың болуы БАЗ молекулаларының галлуазитте адсорбцияланатынын дәлелдеді. Энергетикалық дисперсиялық рентгендік спектроскопияда күміс иондарының сәйкес жұту жолақтарының болуы галлуазит нанотүтікшесінде күмістің адсорбцияланатынын дәлелдейді. Күміспен өңделген және органофильді галлуазиттің микробқа қарсы қасиеттері ішек таяқшасына қарсы invitro нәтижелері бойынша микробиологиялық зертханада анықталды. Гидрофобталған органогаллуазит үлгілерінің жиек бұрыштары 90 градустан жоғары болды және бұл барлық үлгілердің гидрофобты екенін дәлелдейді. Алынған органофильді саздар агар-агар матрицасына енгізіліп, сұйық ортада тұрақтылық беретін.

Түйін сөздер: Бионанокомпозит, галлуазитті наносаз, күмістелген саз, бактерицидтік қасиет, олеофилизация, микросфера, дәрі тасымалдағыштар.

Авторлар туралы ақпарат:

Ибраимова Дана Мыкты-Кереевна — *химия ғылымдарының кандидаты, аға оқытушы, әл-Фараби атындағы Қазақ ұлттық университеті, 050000, әл-Фараби даңғылы, 71, Алматы, Қазақстан. E-mail: dana_kereevna@kaznu.kz*

Рожкова Ольга Владимировна — *химия ғылымдарының докторы, «С.Сейфуллин атындағы Қазақ агротехникалық зерттеу университеті» КЕАҚ профессоры, Астана, Қазақстан, 010000, Жеңіс даңғылы, 62, Астана қ., Қазақстан, «Science and Technology Solutions» АҚ, Астана, Қазақстан, 010000, Республика даңғылы, 24. E-mail: rozhkova.o@stsolutions.kz*

Мұсабеков Қуанышбек Битуұлы — *химия ғылымдарының докторы, профессор, Қазақстан Республикасы Ұлттық жаратылыстану ғылымдары академиясының академигі, атындағы Қазақ ұлттық университеті. әл-Фараби, 050000, әл-Фараби даңғылы, 71, Алматы, Қазақстан. E-mail: musabekov40@mail.ru*

Тәжібаева Сағдат Медербекқызы — *химия ғылымдарының докторы, әл-Фараби атындағы Қаз¥У профессоры, 050000, әл-Фараби даңғылы, 71, Алматы, Қазақстан. E-mail: tazhibayeva_s@mail.ru*

Рожков Виталий Игоревич — *т.ғ.к., «Сәкен Сейфуллин атындағы Қазақ агротехникалық университеті» ҰБ, Астана, Қазақстан; «Алтай геологиялық-экологиялық институты» ЖШС, Өскемен, Қазақстан. E-mail: Vitalrza1983@gmail.com*

Ермеков Марат Тегінбайұлы — *«Science and Technology Solutions» АҚ Жоба және активтерді басқару департаментінің директоры, 050000, Алматы, Қазақстан. E-mail: yermekov.m@stsolutions.kz*

Особенности получения композиционного материала из гидрофобного галлуазита, обладающего антимикробными свойствами

[1] Ибраимова Д.М-К., [2,3]Рожкова О.В., [1]Мусабеков К.Б., [1]Тажибаева С.М., [2,4]Рожков В.И., [3]Ермеков М.Т.

[1]Казахский национальный университет имени аль-Фараби, Алматы, Казахстан
[2]Казахский агротехнический исследовательский университет имени Сакена Сейфуллина, Астана, Казахстан
[3]АО «Science and Technology Solutions», Алматы, Казахстан
[4]ТОО «Алтайский геолого-экологический институт», Усть-Каменогорск, Казахстан

Поступила: *13 сентября 2023*
Рецензирование: *20 декабря 2023*
Принята в печать: *5 марта 2024*

АННОТАЦИЯ
Рассмотрен способ получения бионанокомпозита из гидрофобных глин с бактерицидными свойствами, который играет роль лекарственной матрицы. Такие лекарственные бионанокомпозитные материалы рекомендуются для использования в качестве носителей различных витаминов и лекарственных препаратов благодаря их высоким адсорбционным свойствам и пролонгированному действию. Установлено с помощью ПЭМ-анализа, что частицы галлуазита месторождения Белое Глинище являются наноразмерными и имеют цилиндрическую форму длиной от 200 нм до 1000 нм и диаметр наночастиц от 50 нм до 80 нм. Первой стадией процесса изготовления бионанокомпозита являлась обработка наночастиц галлуазита ионами серебра для придания антимикробных свойств, а на следующем этапе была проведена гидрофобизация катионным поверхностно-активным веществом. Рентгендифракционным методом установлена адсорбция катионным ПАВ, так как межпакетное пространство расширена с 9,998 А до 17.5 А. Также ИК-спектроскопия Фурье наличием соответствующих полос поглощения доказала адсорбцию молекул КПАВ на галлуазите. Наличие соответсвующих полос поглощения ионов серебра на энергодисперсионной рентгеновской спектроскопия доказывает адсорбцию серебра на галлуазитовой нанотрубке. Установлены антимикробные свойства обработанного серебром и органофильного галлуазита микробиологическими лабораторными результатами инвитрув по отношению кишечной палочки *Escerichia coli*. Гидрофобизированные образцы органогаллуазита имели краевые углы выше, чем 90 градусов и это доказывает, что все образцы являются гидрофобными. Полученные органофильные глины были внесены в агар-агаровую матрицу и были брошены в раствор кальция хлорида, которые придают им устойчивость в жидкой среде. Практически установлено, что наиболее оптимальной бионанокомпозитной микросферой является 50% соотношение органогаллуазита и агар-агар.

Ключевые слова: Бионанокомпозит, галлуазитовая наноглина, серебряная глина, бактерицидные свойства, олеофилизация, микросфера, носители лекарств.

Информация об авторах:

Ибраимова Дана Мыкты-Кереевна — *кандидат химических наук, старший преподаватель, КазНУ им. аль-Фараби, 050000, проспект аль-Фараби, 71, Алматы, Казахстан. E-mail: dana_kereevna@kaznu.kz*

Рожкова Ольга Владимировна — *доктор химических наук, профессор НАО «Казахский агротехнический исследовательский университет имени С.Сейфуллина», Астана, Казахстан, 010000, проспект Женис, 62, г. Астана, Казахстан, АО «Science and Technology Solutions», Астана, Казахстан, 010000, проспект Республики, 24. E-mail: rozhkova.o@stsolutions.kz*

Мусабеков Куанышбек Битуович — *доктор химических наук, профессор, академик Национальной академии естественных наук РК, КазНУ им. аль-Фараби, 050000, проспект аль-Фараби, 71, Алматы, Казахстан. E-mail: musabekov40@mail.ru*

Тажибаева Сагдат Медербековна — *доктор химических наук, профессор Казахского национального университета имени аль-Фараби, 050000, проспект аль-Фараби, 71, Алматы, Казахстан. E-mail: tazhibayeva_s@mail.ru*

Рожков Виталий Игоревич — *кандидат технических наук, НАО «Казахский агротехнический университет имени Сакена Сейфуллина», Астана, Казахстан; ТОО «Алтайский геолого-экологический институт», Усть-Каменогорск, Казахстан. E-mail: Vitalrza1983@gmail.com*

Ермеков Марат Тегинбаевич — *директор департамента Управления проектами и активами АО «Science and Technology Solutions», 050000, Алматы, Казахстан. E-mail: yermekov.m@stsolutions.kz*

References

[1] Battalova ShB. Physico-chemical bases of preparation and application of catalysts and adsorbents from bentonite. Alma-Ata. 1986, 111-137. [in Russ.].

[2] Askapova B, Musabekov K. Modification of bentonites inoculation with iron compounds to afford magnetite clays. STUDIA UBB CHEMIA, LXVII. 2022; 2:131-141. https://doi.org/10.24193/subbchem.2022.2.08

[3] Amankeldi F, Ospanova Z, Abdushukur K, Musabekov K, Miller R. Effect of bentonite clay particles on the behavior of foam stabilized by SDS-PVA SDS–PVA complexes. *Results in Surfaces and Interfaces*. 2022; 8:100073. https://doi.org/10.1016/j.rsurfi.2022.100073

[4] Musabekov KB, Artykova D M-K, Tazhibayeva SM, Oryntaeva A, Sugurbekova GK, Kulichikhin V. Surface modification of montmorillonite clay with organic molecules. Rasayan Journal of Chemistry. 2021; 14(1):635-640. https://doi.org/10.31788/RJC.2021.1416093

[5] Tyussyupova BB, Tazhibayeva SM, Musabekov K, Mussatay Y, Kokanbaev A. Effect of proteolytic enzymes on the biological degradability of gelatin-based films. International Journal of Engineering Research and Technology. 2020; 13(11):3699-3704. https://dx.doi.org/10.37624/IJERT/13.11.2020.3699-3704

[6] Johannes Chanra et al. Surface modification of montmorillonite by the use of organic cations via conventional ion exchange method. IOP Conf. Ser.: Mater. Sci. Eng. 2019; 509:012057. https://doi.org/10.1088/1757-899X/509/1/012057

[7] Alexandre, M. and Dubois, P. Polymer-layered silicate nanocomposites: preparation, properties and uses of a new class of materials Mater. Sci. Eng. R. Rep. 2000; 28:1-63. https://doi.org/10.1016/S0927-796X(00)00012-7

[8] Paul D, Zeng Q, Yu A, and Lu G. The interlayer swelling and molecular packing in organoclays J. Colloid Interface Sci. 2005; 292:462-468. https://doi.org/10.1016/j.jcis.2005.06.024

[9] Atyaksheva A, Rozhkova O, Sarsikeyev Y, Atyaksheva A, Yermekov M, Smagulov A, Ryvkina N. (2022). Determination of rational parameters for heat treatment of concrete mixture based on a hollow aluminosilicate microsphere. Eastern-European Journal of Enterprise Technologies. 2022; 1(6(115)):64-72. https://doi.org/10.15587/1729-4061.2022.251004

[10] Yermekov M, Rozhkova O, Sandibekova SG, Tolysbayev Ye T, Vetyugov A, Turbin O A, Belenko E V. Storage of the industrial waste of the mining and smelting industry of kazakhstan, landfills arrangement, efficiency and operational features. News of the National Academy of Sciences of the Republic of Kazakhstan, Series of Geology and Technical Sciences. 2020; 6(444):83-89. https://doi.org/10.32014/2020.2518-170X.134

[11] Parolo M E, Pettinari G R, Musso T B, Sánchez-Izquierdo M P, & Fernández L G. Characterization of organo-modified bentonite sorbents: The effect of modification conditions on adsorption performance. Applied Surface Science. 2014; 320: 356-363. https://doi.org/10.1016/j.apsusc.2014.09.105

[12] Musabekov K, Zhakyp B, Tazhibayeva S, Musabekov N, & Yergaliyeva A. (2020). A research of colloidal silver immobilization in bionanocomposites of natural polymers and montmorillonite. Eastern-European Journal of Enterprise Technologies. 2020; 6(6(108)):93-101. https://doi.org/10.15587/1729-4061.2020.216995

[13] Abdullayev E, Lvov Y. Halloysite Clay Nanotubes for Controlled Release of Protective Agents. J. Nanosci. Nanotech. 2011; 11:10007-10026. https://doi.org/10.1166/jnn.2011.5724

[14] Roy S, & Chakraborty C. Sub-second electrochromic switching and ultra-high coloration efficiency in halloysite nanoclay incorporated metallo-supramolecular polymer nano-hybrid based electrochromic device. Solar Energy Materials and Solar Cells. 2020; 208:110392. https://doi.org/10.1016/j.solmat.2019.110392

[15] Ahmed H B. Cluster growth adaptor for generation of bactericide Ag-Au bimetallic nanostructures: substantiation through spectral mapping data. International Journal of Biological Macromolecules. 2019; 121:774-783. https://doi.org/10.1016/j.ijbiomac.2018.10.088

[16] Ye G Yerlan, Tyussyupova B B, Tazhibayeva S M, Musabekov K B, Balabushevich N G, Kokanbayev A K. Encapsulation of Insulin in Biodegradable Polymers. Eurasian Chem.-Technol. J. 2022; 24(4):351-361. https://doi.org/10.18321/ectj1479

[17] Ibraimova D M-K, Rozhkova O V, Musabekov K B, Tazhibayeva S M, Rozhkov V I, & Yermekov M T. Development of Methods to Obtain Composite Materials from Organoclays Eurasian Journal of Chemistry. 2023; 4(112):101-111 https://doi.org/10.31489/2959-0663/4-23-14

[18] Tazhibayeva S, Tyussyupova B, Khamitova I, Musabekov K, Daribayeva G. STABILIZATION OF MELON CLOUDY JUICE WITH BIOPOLYMER AGAR. Eastern-European Journal of Enterprise Technologies. 2020; 4(11(106)):31-38. https://doi.org/10.18321/ectj1479

[19] Kenzhaliyev B, Imangalieva L, Manapova A, & Azlan M. Kaolinite clays as a source of raw materials for the aluminum industry of the Republic of Kazakhstan. Kompleksnoe Ispolzovanie Mineralnogo Syra = Complex Use of Mineral Resources. 2021; 319(4):5-12. https://doi.org/10.31643/2021/6445.34

[20] Afra, Elyas and Narchin, Parvaneh. Creating extended antimicrobial property in paper by means of Ag and nanohybrids of montmorillonite (MMT). Holzforschung. 2017; 71(5):445-454. https://doi.org/10.1515/hf-2016-0195

Crossref
DOI: 10.31643/2025/6445.08
Metallurgy

The influence of the hydrogenation process on the microstructure and properties of metallic materials

Małgorzata Rutkowska-Gorczyca, Mateusz Dziubek, Marcin Wiśniewski

Wroclaw University of Science and Technology, Wrocław, Poland

** Corresponding author email: bagdaulet_k@satbayev.university*

Received: *January 3, 2024*
Peer-reviewed: *January 9, 2024*
Accepted: *March 5, 2024*

ABSTRACT

Hydrogen, which belongs to the group of the smallest elements, can freely penetrate the structure of metallic materials and cause enormous damage. This phenomenon may occur due to various conditions and may have different effects on the properties of materials. Understanding these mechanisms is important in the era of changing to alternative energy sources. This situation may occur in combustion engines powered by hydrogen-enriched fuel. The work analyzed the impact of various hydrogenation processes on the properties of aesthetic steel, which is allergic to the formation of carbides at the grain boundaries, such a microstructure is intended to simulate the least favorable working conditions. The work was aimed at evaluating the effects of different hydrogenation methods on changes in the properties of the AISI 310s steel membrane. In the work, electrolytic hydrogenation and heat treatment procedures in a hydrogen atmosphere were used. Investigations of changes in material properties included microhardness and in-situ strength tests in a scanning electron microscope chamber. Research has shown that both processes increase the hardness of materials and change the characteristics of stretching curves.

Keywords: hydrogen process, metallic membranes, material properties

Information about authors:

Małgorzata Rutkowska-Gorczyca *PhD in Mechanics, Associate Professor, Department of Automotive Engineering, Wroclaw University of Science and Technology, Wyb. Wyspianskiego 27, 50-370 Wrocław, Poland. Email: malgorzata.rutkowska-gorczyca@pwr.edu.pl*

Mateusz Dziubek *MSc, Department of Automotive Engineering, Wroclaw University of Science and Technology, Wyb. Wyspianskiego 27, 50-370 Wrocław, Poland. Email: mateusz.dziubek@pwr.edu.pl*

Marcin Wiśniewski *Engineer, Department of Automotive Engineering, Wroclaw University of Science and Technology, Wyb. Wyspianskiego 27, 50-370 Wrocław, Poland. Email: 255206@student.pwr.edu.pl*

Introduction

The problem of hydrogen embrittlement is quite a dangerous phenomenon in the case of metals and their alloys [[1], [2]]. In technological and metal processing processes (Xi et al., 2023), the mechanical properties and corrosion resistance of materials may deteriorate due to the impact of the hydrogen environment [[4], [5], [6]]. The negative impact of hydrogen on metallic materials affects a wide range of different industries such as metallurgy, petrochemicals, aviation, and other fields. The threats of hydrogen to metals include hydrogen-induced cracking, high-temperature hydrogen corrosion [[7], [8]], hydride and hydrogen-to-martensitic transformation, etc. Research on hydrogen embrittlement has been ongoing for a long time, but the mechanism of microstructure interaction with hydrogen and damage caused by the presence of hydrogen requires numerous additional studies.

A very interesting issue related to alternative methods of reducing the negative impact of transport on exhaust emissions into the environment is the use of combustion engines powered by hydrogen-enriched fuel. Hydrogen engines open up new perspectives for the automotive sector but also pose new design problems to solve [[9], [10], [11], [12], [13]]. A major threat that may damage an engine operating in a hydrogen environment is the phenomenon of hydrogen embrittlement of metallic materials. The influence of hydrogen causes a weakening of the structure of metallic materials and an increase in susceptibility to brittle fracture. Hydrogen, which belongs to the group of the smallest elements, can freely penetrate the structure of the material. The diffusion of hydrogen into the material causes changes in the material's microstructure and

permanently reduces the strength and plastic properties of the material. The greatest threat is the creation of conditions initiating brittle cracking of materials after some time of exposure to loads.

Various materials are used to build engines, one of the groups of materials used due to their high strength and corrosion resistance is austenitic steel. AISI 310s heat-resistant steel is an austenitic chrome-nickel grade with increased nickel content, characterized by high strength, ductility, resistance to air and oxidizing atmosphere in the high-temperature range up to 1050 ℃. Steel is used for mechanically loaded parts that operate at high temperatures. Improper technological processes and working conditions at elevated temperatures may cause the formation of hard phases in austenitic steels. Depending on the chemical composition of the steel, $M_{23}C_6$ carbides may be formed, which significantly weaken the properties of this material [[12], [13]]. The work presents the influence of various methods of the hydrogenation process on the surface and properties of AISI 310s steel, which is allergic to the formation of carbides $M_{23}C_6$.

Research problem. As energy management methods change to more ecological ones, hydrogen will play a huge role in this topic. The topic of hydrogen will be considered at many levels: new mechanisms, new theories, new phenomena of hydrogen embrittlement of metal, steel or light alloy, research and development of hydrogen removal process in metal, the interaction between hydrogen, fatigue and crack growth, action laws of other hydrogen-induced failure forms, corrosion issues related to hydrogen and fatigue, fracture and failure of hydrogen charging metals. This paper presents the effect of various hydrogenation processes, on surface changes and the strength of ASIA 310s steel membranes sensitized by intergranular corrosion. The study showed the effect of this process on the strength of the material.

Material

The material in the form of commercially available AISI 310s steel was selected for the tests (jfs-steel.com). The tested steel showed a microstructure, equiaxed alloy austenite grains with precipitations of carbides forming a shell at the grain boundaries (Fig. 1.). In the delivery state, according to the supplier, the material was characterized by the chemical composition given in tab. 1. and showed the properties presented in tab. 2. Membranes for the tests were prepared in the form of plates with a thickness of 0.7 mm, dimensions shown in Fig. 2. The area of interaction with the electrolyte during electrochemical processes was about 550 mm^2 and was the same for each sample. The surface of the materials before the electrochemical process was cleaned in an ultrasonic scrubber in an acetone solution for 10 minutes.

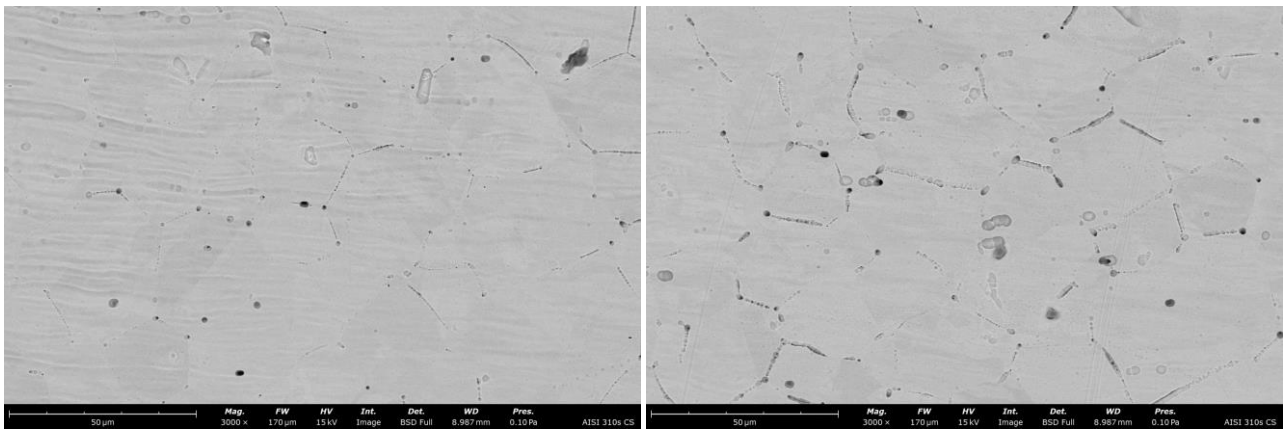

Fig. 1 - Microstructure of alloyed austenite with evolved carbons at grain boundaries in AISI 310s steel in the supply state. SEM

Table 1 - Chemical composition of steel AISI 310s

AISI 310s	C <0.2	Mn<1.5	Si<1.0	V <0.2	W <0.5
P<0.045	S<0.030	Cr 22.0-25.0	Ni 17.0-20.0	Mo <0.5	Fe rest

Table 2 - Mechanical properties of steel AISI 310s

tensile strength Rm	Elongation A	Hardness
500-700 MPa	33%	192HB

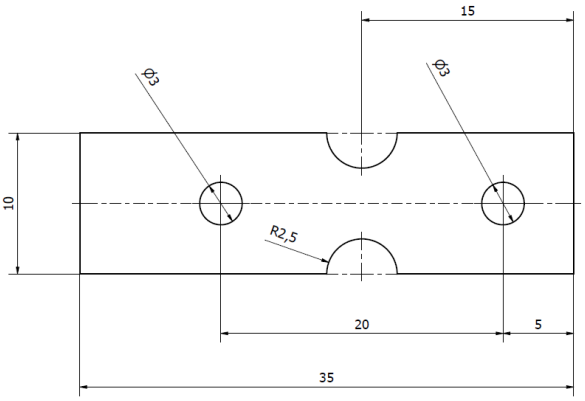

Fig. 2 - Austenitic steel membrane dimensions

Method

The hydrogen charging process was carried out using a BioLogis SP50ze potentiostat/galvanostat. Current waveforms were carried out in an electrolyte with a concentration of 0.5 M H_2SO_4 and pH 1. Voltammetry (CV measurement) was carried out in a three-electrode system, where the metallic membrane was the working electrode. The hydrogen charging process included two ranges: 25 cycles (1 hour) and 50 cycles (2 hours). The system was cyclically loaded with current between a potential of −0.200 V and −1.4 V, with a scanning rate of 20 mV/s. The measurement procedure began with a 10-minute open circuit measurement (OCV) in the electrode system used, based on which the open circuit potential Ewe was determined, which was used to determine the range of the voltammetry process. The open circuit voltage consists of the period during which no potential or current is applied to the working electrode. The cell is disconnected from the power amplifier. Potential measurements are available on the cell. Thus, the evolution of the resting potential can be recorded. This period is commonly used as a preconditioning time or to equilibrate an electrochemical cell.

CV voltammetry measurements were performed in the range below the open circuit value Ewe to eliminate the oxidation process and force the hydrogen evolution process. Cyclic voltammetry (CV) is the most widely used technique for acquiring qualitative information about electrochemical reactions. CV provides information on redox processes, heterogeneous electron-transfer reactions and adsorption processes. It offers a rapid location of the redox potential of the electroactive species. A CV consists of scanning linearly the potential of a stationary working electrode using a triangular potential waveform. During the potential sweep, the potentiated measures the current resulting from electrochemical reactions. The cyclic voltammogram is a current response as a function of the applied potential.

Heat treatment tests were carried out in resistance furnaces in an air atmosphere and a furnace with a protective atmosphere (Czelok furnace). Argon gas with a 5% hydrogen admixture was selected for testing in a hydrogen atmosphere, the flow was set at 3 dm3 per minute. The samples were heated in a hydrogen atmosphere with an oven from 20°C to a temperature of 900°C, at which the samples were kept for 2 hours. After an appropriate time, the samples were removed from the oven, cooled in water and immediately subjected to the tensile process in a Deben Microtest strain gauge holder compatible with the Phenom XL scanning electron microscope. The holder enables strength tests up to 1000N and in-situ observations in scanning microscope mode. Investigations of the surface of the material after hydrogenation were also carried out using scanning electron microscopy methods on a Phenom XL microscope. Then, microhardness measurements were carried out by the PN-EN ISO 6507-1:2018-05 standard using the Vickers method, using a Leco LM-248AT microhardness tester. The measurements were carried out with a load of 300 g, which is equivalent to a force of 2.94 N.

Research results

Electrochemical hydrogen charging of AISI 310

Voltammetry measurements CV showed in all cycles similar shape of the curves, during observations the hydrogenation process showed an increasingly intense and violet process of hydrogen evolution in the lower parts of the graph. The most intensive hydrogenation process took place in the range below 0.5 Ewe, numerous hydrogen bubbles were visible, concentrating on the surface of the metallic membrane constituting the working electrode. In subsequent hydrogenation cycles, the current values decreased in the range of -2.5mA/cm to -3.5mA/cm for 25 cycles (Fig. 3). For hydrogenation in 50 cycles, the current values were lower and oscillated from -3.0mA/cm to -6mA/cm (Fig. 4). Differences in the initial values result from differences in the closed-circuit measurement values in a given electrode system. There is a clear tendency to decrease the current values in successive hydrogenation cycles. This proves the changes taking place in the metallic membranes and the change of their electrochemical potentials about the material in the delivery state.

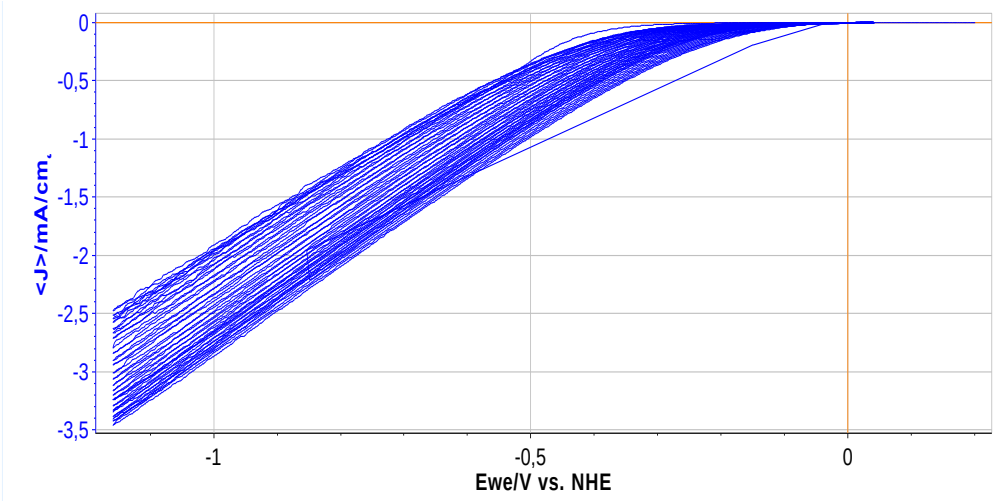

Fig. 3 - Cyclic Voltammetry curve after 25 hydrogen cycles in 0,5MH_2SO_4

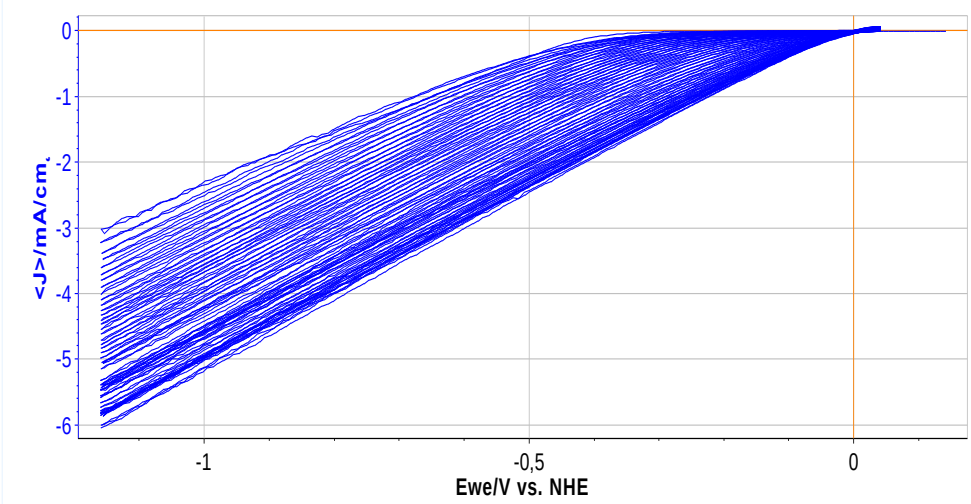

Fig. 4 - Cyclic Voltammetry curve after 50 hydrogen cycles in 0,5MH_2SO_4

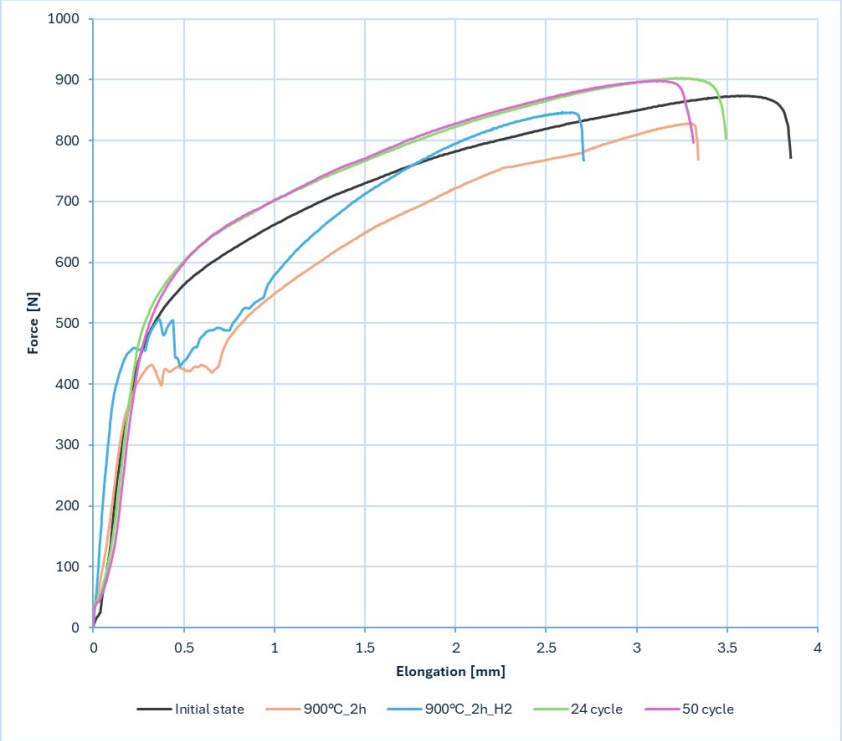

Fig. 5 - Tensile curves for delivery state and after hydrogenation proces

The samples after the hydrogenation process were subjected to axial tensile testing at a constant speed of 0.5 mm/s inside a scanning electron microscope chamber equipped with a tensile holder with a maximum measurement force of 1 kN. All the tensile tests were conducted in a single setup, creating geometric notches in the central part of the samples. As a result of the tensile testing, the maximum force and elongation were determined, which were considered as comparative values due to the identical geometry of the samples (Fig. 5). The hydrogenation process after 25 and 50 cycles resulted in a slight strengthening of the material, increasing the maximum force value by 3%, which represents a minor change. On the other hand, the elongation value underwent a significant reduction, decreasing by 9% after 25 cycles of hydrogenation and 13% after 50 cycles of hydrogenation compared to the reference state. This indicates a negative impact of the hydrogen environment on AISI 310S steel.

Microhardness tests are one of the simplest methods to determine changes in the form of strengthening in the material after the hydrogenation process. Hardness measurements were carried out on the surface of the membranes, on the undeformed elements of the sample after both the hydrogenation process. Analysis of the microhardness results showed that the H2 environment affects the surface hardening of AISI 310s steel (Fig. 6).

An increase in hardness compared to the initial state material was observed in all tested materials. Hydrogen charging in electrolytic processes resulted in an increase in hardness from 154HV0.2 to 162HV0.2. A linear increase in this parameter was observed when the number of cycles was increased to 50, where the hardness increased to 169HV0.2. The hydrogenation process at a temperature of 900°C also increased the hardness to 182HV0.2 for the membrane heated in an oxygen atmosphere and to 179HV0.2 for the environment enriched with hydrogen particles. The reduced hardness of the material after heat treatment in a hydrogen atmosphere seems puzzling, it may be related to the presence of atomic hydrogen, which only changes to a molecular form when the material is loaded and results in increased brittleness.

In the electrochemical hydrogenation process, an increase in hardness was found commensurate with the increasing number of hydrogenation cycles.

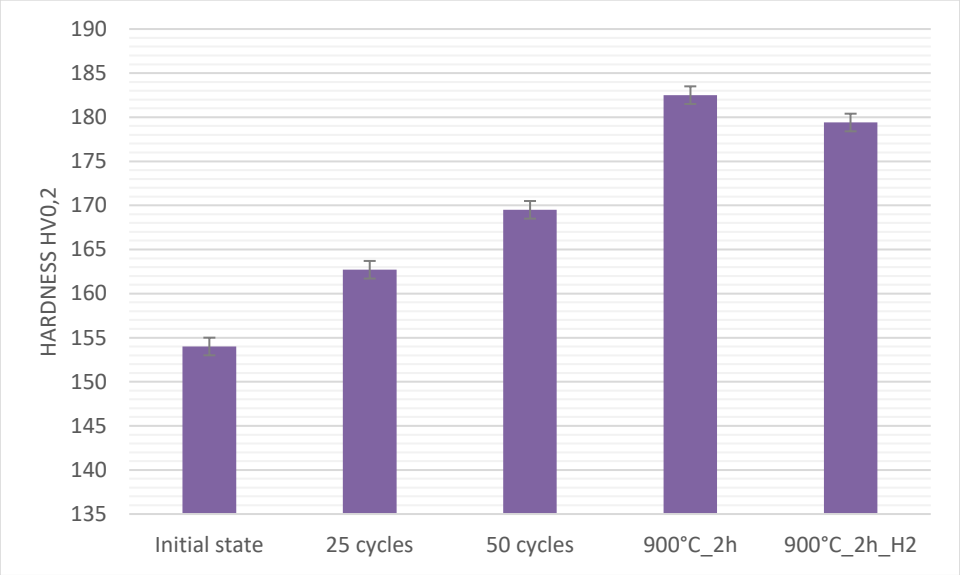

Fig. 6 - Averaged hardness measurement results for metallic membranes

Research discussion

The steel becomes brittle and more prone to cracking after both treatments, which can result in sudden and uncontrolled material fracture. This effect is most intense in the first hours of hydrogenation. In both cases, the strengthening of the material was found to result from the absorption of hydrogen into the material, independent of the hydrogenation process. This mechanism is known and described as hydrogen strengthening [[14], [15, [16], [17], [18], [19], [20], [21]].

The process of strengthening the material caused by the presence of hydrogen is visible in the stretching curves and the obtained value of the breaking force of the membrane and hardnes of the material. Heat treatment in a hydrogen atmosphere significantly increased the hardness of the material, changed the nature of the tensile curves and reduced the value of the breaking force, both for membranes processed in a hydrogen atmosphere and without.

Conclusions

Based on the conducted research, it was found that AISI 310s steel in a state sensitive to the formation of carbides at the grain boundaries is susceptible to hydrogenation processes. Both during electrochemical processes and heat treatment in a hydrogen atmosphere. This is evidenced by changes on the surface of hydrogenated metallic membranes and the impact on the hardness and strength of this material. The research has revealed very interesting relationships, the results of which leave many new questions to which we will need to know the answers soon. The era of hydrogen technologies is coming quickly.

Acknowledgements

The authors would like to thank anonymous reviewers and the conference editors for their comments on earlier versions.

Cite this article as: Małgorzata Rutkowska-Gorczyca, Mateusz Dziubek, Marcin Wiśniewski. The influence of the hydrogenation process on the microstructure and properties of metallic materials. Kompleksnoe Ispolzovanie Mineralnogo Syra = Complex Use of Mineral Resources. 2025; 332(1):90-97. https://doi.org/10.31643/2025/6445.08

Гидрлеу процесінің микроқұрылымға әсері және металл материалдардың қасиеттері

Małgorzata Rutkowska-Gorczyca, Mateusz Dziubek, Marcin Wiśniewski

Вроцлав ғылым және технология университеті, Вроцлав, Польша

Мақала келді: *2 қаңтар 2024*
Сараптамадан өтті: *9 қаңтар 2024*
Қабылданды: *5 наурыз 2024*

ТҮЙІНДЕМЕ

Ең жеңіл элементтер тобына жататын сутегі металл материалдардың құрылымына еркін еніп, орасан зор зиян келтіре алады. Бұл құбылыс әртүрлі жағдайларға байланысты болады және материалдардың қасиеттеріне әртүрлі әсер етуі мүмкін. Бұл механизмдерді түсіну баламалы энергия көздеріне көшу кезеңінде маңызды. Бұл жағдай сутегімен байытылған отынмен жұмыс істейтін ішкі жану қозғалтқыштарында болуы мүмкін. Жұмыста түйіршік шекарасында карбидтердің түзілуіне бейім болаттың қасиеттеріне әртүрлі гидрлеу процестерінің әсері талданған, мұндай микроқұрылым ең қолайлы жұмыс жағдайларын модельдеуге арналған. Жұмыс AISI 310s болат мембранасының қасиеттерінің өзгеруіне әртүрлі гидрлеу әдістерінің әсерін бағалауға бағытталған. Жұмыста сутегі атмосферасында электролиттік гидрлеу және термиялық өңдеу әдістері қолданылды. Материалдардың қасиеттеріндегі өзгерістерді зерттеуге сканерлеуші электронды микроскоп камерасында микроқаттылыққа және заттық беріктікке жасалатын сынақтар кіреді. Зерттеулер екі процестің де материалдардың қаттылығын арттыратынын және созылу қисықтарының сипаттамаларын өзгертетінін көрсетті.

Түйін сөздер: сутегі процесі, металдық мембраналар, материал қасиеттері

Авторлар туралы ақпарат:

Małgorzata Rutkowska-Gorczyca — *Механика ғылымдарының кандидаты, Вроцлав ғылым және технология университетінің автомобиль жасау кафедрасының доценті, Станислав Виспиански жағалауы 27, 50-370, Вроцлав, Польша. Email: malgorzata.rutkowska-gorczyca@pwr.edu.pl*

Mateusz Dziubek — *Магистр, Автокөлік техникасы кафедрасы, Вроцлав ғылым және технология университеті, Станислав Виспиански жағалауы 27, 50-370, Вроцлав, Польша. Email: mateusz.dziubek@pwr.edu.pl*

Marcin Wiśniewski — *Инженер, Вроцлав ғылым және технология университетінің автомобиль жасау бөлімі, Станислав Виспиански жағалауы 27, 50-370, Вроцлав, Польша. Email: 255206@student.pwr.edu.pl*

Влияние процесса гидрирования на микроструктуру и свойства металлических материалов

Małgorzata Rutkowska-Gorczyca, Mateusz Dziubek, Marcin Wiśniewski

Вроцлавский университет науки и технологий, Вроцлав, Польша

Поступила: *3 января 2024*
Рецензирование: *9 января 2024*
Принята в печать: *5 марта 2024*

АННОТАЦИЯ

Водород, относящийся к группе мельчайших элементов, может свободно проникать в структуру металлических материалов и наносить огромный вред. Это явление может возникать из-за различных условий и по-разному влиять на свойства материалов. Понимание этих механизмов важно в эпоху перехода на альтернативные источники энергии. Такая ситуация может возникнуть в двигателях внутреннего сгорания, работающих на топливе, обогащенном водородом. В работе проанализировано влияние различных процессов наводораживания на свойства стали, склонной к образованию карбидов по границам зерен. Такая микроструктура призвана моделировать наименее благоприятные условия работы. Целью работы была оценка влияния различных методов гидрирования на изменение свойств мембраны из стали AISI 310s. В работе использовались методы электролитического гидрирования и термообработки в атмосфере водорода. Исследования изменения свойств материалов включали испытания на микротвердость и натурную прочность в камере сканирующего электронного микроскопа. Исследования показали, что оба процесса повышают твердость материалов и изменяют характеристики кривых растяжения.

Ключевые слова: водородный процесс, металлические мембраны, свойства материала.

Информация об авторах:

Małgorzata Rutkowska-Gorczyca — *Кандидат механических наук, доцент кафедры автомобильной техники Вроцлавского университета науки и технологий, побережье Станислава Выспяньского 27, 50-370, Вроцлав, Польша. Email: malgorzata.rutkowska-gorczyca@pwr.edu.pl*

Mateusz Dziubek — *Магистр, кафедра автомобильной техники, Вроцлавский университет науки и технологий, побережье Станислава Выспяньского 27, 50-370 Вроцлав, Польша. Email: mateusz.dziubek@pwr.edu.pl*

Marcin Wiśniewski — *Инженер, кафедра автомобильной техники, Вроцлавский университет науки и технологий, побережье Станислава Выспяньского 27, 50-370, Вроцлав, Польша. Email: 255206@student.pwr.edu.pl*

References

[1] Hem R, Ann P. Diffusion of hydrogen in metals. 1984; 101.

[2] Lai CL, Tsay LW, Chen C. Effect of Microstructure on Hydrogen Embrittlement of Various Stainless Steels. Materials Science and Engineering: A. 2013; 584:14-20. https://doi.org/10.1016/j.msea.2013.07.004

[3] Xi X, Wu T, Tian Y, Hu J, Huang S, Xie T, Wang J, Chen L. The Role of Reverted Transformation in Hydrogen Embrittlement of a Cu-Containing Low Carbon High Strength Steel. Journal of Materials Research and Technology. 2023; 25:5990-5999. https://doi.org/10.1016/J.JMRT.2023.07.071

[4] Jaxymbetova M, Kanayev A, Akhmedyanov A, & Kirgizbayeva K. On the applicability of hardening mechanisms to low-carbon and low-alloy steels. Kompleksnoe Ispolzovanie Mineralnogo Syra = Complex Use of Mineral Resources. 2022; 321(2):47-55. https://doi.org/10.31643/2022/6445.17

[5] Karboz ZhA, Dossayeva SK. Study of Hydrogen Permeability of Membranes Coated with Various Metal Films (Review). Kompleksnoe Ispolzovanie Mineralnogo Syra = Complex Use of Mineral Resources. 2019; 310(3):48-54. https://doi.org/10.31643/2019/6445.28

[6] Panichkin AV, Mamaeva AA, Derbisalin AM, Kenzhegulov AK, Imbarova AT. The Influence of Solid Solutions Compound on the Hydrogen Permeable Membranes Characteristics from Niobium and Tantalum Applied above Films. Kompleksnoe Ispolzovanie Mineralnogo Syra = Complex Use of Mineral Resources. 2018; 307(4):130-139. https://doi.org/10.31643/2018/6445.39

[7] Khanchandani H, Gault B. Atomic Scale Understanding of the Role of Hydrogen and Oxygen Segregation in the Embrittlement of Grain Boundaries in a Twinning Induced Plasticity Steel. Scr Mater. 2023; 234:115593. https://doi.org/10.1016/J.SCRIPTAMAT.2023.115593

[8] Safyari M, Khossossi N, Meisel T, Dey P, Prohaska T, Moshtaghi M. New Insights into Hydrogen Trapping and Embrittlement in High Strength Aluminum Alloys. Corros Sci. 2023, 111453. https://doi.org/10.1016/J.CORSCI.2023.111453

[9] Equivalent Terminology Used in the Book Includes Internal Hydrogen Embrittlement (IHE) and Hydrogen Environment Embrittlement (HEE). 2012. https://doi.org/10.1016/B978-0-85709-536-7.50018-0

[10] Tomaszewski S, Grygier D, Dziubek M. Assessment of Engine Valve Materials. Combustion Engines. 2023. https://doi.org/10.19206/ce-166569

[11] Hamaad ASAA, Tawfik M, Khattab S, Newir A. Device for Using Hydrogen Gas as Environmental Friendly Fuel for Automotive Engine (GREEN & ECO H2). Procedia Environ Sci. 2017; 37:564-571. https://doi.org/10.1016/J.PROENV.2017.03.043

[12] Chen G, Rahimi R, Harwarth M, Motylenko M, Xu G, Biermann H, Mola J. Non-Cube-on-Cube Orientation Relationship between M23C6 and Austenite in an Austenitic Stainless Steel. Scr Mater. 2022, 213. https://doi.org/10.1016/j.scriptamat.2022.114597

[13] Kim HP, Park YM, Jang HM, Lim SY, Choi MJ, Kim SW, Kim DJ, Hwang SS, Lim YS. Early-Stage M23C6 Morphology at the Phase Boundary in Type 304L Austenitic Stainless Steel Containing δ Ferrite. Metals (Basel). 2022; 12(11). https://doi.org/10.3390/met12111794

[14] Khanchandani H, Gault B. Atomic scale understanding of the role of hydrogen and oxygen segregation in the embrittlement of grain boundaries in a twinning induced plasticity steel. Scr Mater. 2023 Sep 1;234:115593. https://doi.org/10.1016/j.scriptamat.2023.115593

[15] Jack TA, Moreno BD, Fazeli F, Szpunar J. Influence of Hydrogen Ingress on Residual Stress and Strain in Pipeline Steels. Mater Charact. 2024, 113654. https://doi.org/10.1016/j.matchar.2024.113654

[16] Au M. Mechanical Behavior and Fractography of 304 Stainless Steel with High Hydrogen Concentration. No WSRC-TR-2002-00558 Savannah River Site (US). 2003;(865). https://www.osti.gov/servlets/purl/807672.

[17] Bertsch KM, Nagao A, Rankouhi B, Kuehl B, Thoma DJ. Hydrogen embrittlement of additively manufactured austenitic stainless steel 316 L. Corros Sci. 2021 Nov 1;192:109790. https://doi.org/10.1016/j.corsci.2021.109790

[18] Caskey GR. Fractography of hydrogen-embrittled stainless steel. Scripta Metallurgica. 1977;11(12). https://doi.org/10.1016/0036-9748(77)90311-8

[19] Komatsu A, Fujinami M, Hatano M, Matsumoto K, Sugeoi M, Chiari L. Straining-temperature dependence of vacancy behavior in hydrogen-charged austenitic stainless steel 316L. Int J Hydrogen Energy. 2021 Feb 3;46(9):6960–9. https://doi.org/10.1016/j.ijhydene.2020.11.148

[20] Rieck RM, Atrens A, Smith IO. Stress corrosion cracking and hydrogen embrittlement of cold worked AISI type 304 austenitic stainless steel in mode I and mode III. Materials Science and Technology (United Kingdom). 1986;2(10). https://doi.org/10.1179/mst.1986.2.10.1066

[21] Saborío-González M, Rojas-Hernández I. Review: Hydrogen Embrittlement of Metals and Alloys in Combustion Engines. Revista Tecnología en Marcha. 2018;31(2). https://doi.org/10.18845/TM.V31I2.3620

Crossref
DOI: 10.31643/2025/6445.09
Metallurgy

On the influence of iron and silicon content on the phase composition of the Al-Fe-Si system

***Andreyachshenko V.A., Toleuova A.R.**

Abylkas Saginov Karaganda Technical University, Karaganda, Kazakhstan

**Corresponding author email: Vi-ta.z@mail.ru*

Received: *January 15, 2024*
Peer-reviewed: *February 18, 2024*
Accepted: *March 12, 2024*

ABSTRACT

Increasing interest in intermetallic phases of the Al-Fe-Si system is associated with their high specific strength, corrosion and wear resistance, as well as the low cost of their production. To exhibit the most successful combination of properties, it is necessary to impart a specific compact morphology to the precipitated intermetallic phases. It is important to create an alloy with a composition capable of accepting plastic deformation. The purpose of the work is to develop the composition of an Al-Fe-Si system alloy capable of withstanding plastic deformation and determining the corresponding deformation interval. Based on computer modeling, an alloy composition capable of accepting plastic deformation was developed and the corresponding deformation interval was determined. The simulation was carried out in the ThermoCalc software package, TCAL8 database. It has been revealed that alloys with a high content of both silicon and iron are not characterized by the formation of a single-phase region, however, with a certain combination of alloy components, it is possible to achieve a quasi-single-phase structure, when the content of one phase is observed to be more than 90%. The solidus temperatures for different alloy compositions and the boundary conditions for the existence of phases have been determined. The α phase is present in the system from a temperature of 770°C up to a temperature of 446°C. In composition, it is found in the range from 5 to 35% iron with an amount of silicon of 10% and from 0 to 15% silicon with an iron content of 30%. The maximum amount of α phase was obtained for the Al60-65 alloy; Fe30-32; and Si5-10%, deformation temperature range is 600-450°C. Deformation in this region will ensure processing in a quasi-single-phase region without melting.

Keywords: Al-Fe-Si, ThermoCalc software, intermetallic phases, phase diagram, α phase.

Information about authors:

Andreyachshenko Violetta Alexandrovna — *PhD, associate professor, Head of the Testing Laboratory Engineering Profile "Comprehensive Development of Mineral Resources". Abylkas Saginov Karaganda Technical University, N. Nazarbayev Ave., 56, Karaganda, Kazakhstan. E-mail: Vi-ta.z@mail.ru*

Toleuova Ainagul Rymkulovna — *PhD, associate professor, docent of the Department of Nanotechnology and Metallurgy. Abylkas Saginov Karaganda Technical University, N. Nazarbayev Ave., 56, Karaganda, Kazakhstan. Email: rymkul.ainagul@mail.ru*

Introduction

In recent years, many studies have been devoted to the processing and processing of aluminum alloys with a high iron content [1]. At the same time, it is the processing of iron-enriched alloys that claims to be a leader in the field of light metallurgy. The main problem that scientists may encounter when developing technological schemes for processing aluminum alloys is the high iron content, which significantly reduces all the properties of the alloys [2]. In works devoted to the processing of aluminum alloys, attention is paid to alloys containing an increased amount of iron, i.e. 1, 3, 5 and even 10% [[3], [4], [5], [6], [7]]. At the same time, many researchers see a promising direction in applying efforts to transform the needle-shaped β phase into the α phase, which has a more compact morphology [[8], [9], [10], [11]]. It is noted that in alloys with such an iron content, the α phase is the main strengthening phase, and a general increase in strength and thermal stability is realized due to dispersion strengthening. At the same time, there is information that the α phase has very high Vickers hardness values, including in comparison with the β phase. An effective way to suppress the α↔β transformation is also doping with transition metals such as Cr, Mn, Cu, etc., accelerated cooling and exposure to deformation [[12], [13], [14], [15], [16], [17], [18], [19], [20]].

Although Al–Si alloys are the most commonly used aluminum alloys in the foundry industry [21], it is often necessary to use specific processing methods to meet the increasing demands on the performance and properties of these alloys. One of the processing methods is injection molding methods [[22], [23]], while porosity can be successfully controlled by modifying the traditional process with the transition to Two-stage super vacuum (19 mbar) assisted high-pressure die casting (HPDC) [24] or the use of An air-cooled stirring rod (ACSR) process technology [25]. Selective laser melting makes it possible to effectively process aluminum alloys, including those containing high amounts of iron [26]. In addition, additive technologies, which have been intensively developing in recent decades, have proven themselves well. With the high variability of technological conditions, it is possible to obtain both porous and practically monolithic alloys with a wide chemical range of composition [[27, [28], [29], [30]]. Depending on the strengthening mechanism, aluminum alloys are divided into two main groups: heat-strengthening and non-heat-strengthening [31]. Depending on the group, additional post-processing is usually used to increase and stabilize the final properties of the alloy, such as [[32], [33], [34], [35], [36]] and others.

Experimental part

Numerical modeling to study the phase composition of the three-component system was carried out using ThermoCalc software. As part of the study, the Al-Fe-Si system under study was specified for calculation. An important element of the calculations is the identification and assessment of the interaction of the main components of the system. Aluminum was chosen as the base material, because its quantity in the system is maximum. ThermoCalc software version 2024a, TCAL8 database, and version v8.2 were used for modeling. The tools Phase diagram, One Axis, Scheil Solidification, and Ternary calculation were used for the calculation.

Modeling the phase composition of a system begins with the formulation of the problem. The Al-Fe-Si system containing aluminum ≥50% (by weight %) was chosen as the object of study. To build an isothermal section, we performed the following steps: My project→Ternary. Next, we selected the required elements from the table of elements: Al, Fe, Si. The temperature is set to 660°C. After setting the parameters, we moved on to setting the boundary conditions. The iron content is located along the X-axis, from 0 to 50% wt., the silicon content along the Y-axis, from 0 to 50% wt.

To construct polythermal sections, the Phase diagram tool was used: My project → Phase diagram. The required elements are also selected from the table, their quantity is specified in mass percent. When constructing phase diagrams of multicomponent systems, the number of elements other than 2 is constant for calculation. In our case, Si-const=10% and Fe-const=10%. The calculation was carried out using the following parameters: Temperature, °C – 1200°; Pressure, Pascal – 100000; Size of the system, mol – 1.

Estimation of the number of formed phases under given modeling conditions was carried out in a combination of the One Axis and Scheil Solidification tools according to the following scheme: My project → One Axis → Selection of elements and their content in weight % → setting modeling conditions (similar to the previous task) → Interpretation of results.

My project→Scheil Solidification→Selection of elements and their content in weight %→setting modeling conditions→Interpretation of results.

The choice of compositions is explained by the peculiarities of alloy production technology - the fact that the combination of iron and silicon can neutralize the negative impact on mechanical properties with the formation of intermetallic compounds of various types. Therefore, it is necessary to know which iron-containing phases will be formed during the production process. Variation of iron and silicon is necessary to better understand the crystallization intervals and phase transformation of each composition. The simulation was implemented using the ThermoCalc Software 2024a software in the Testing Laboratory Engineering Profile “Comprehensive Development of Mineral Resources” of the Abylkas Saginov Karaganda Technical University, Karaganda, Kazakhstan.

Discussion the results

The literature presents a sufficient number of casting alloys containing silicon and iron, as well as a number of wrought aluminum alloys with these elements. Increasing the level of mechanical properties, heat resistance, wear resistance and a number of other properties is achieved, as a rule, by alloying with various elements, including rare earth

ones. Another way to improve the properties of the alloy is by using heat treatment, including thermomechanical treatment. Often the desired level of properties can only be achieved through a combination of chemical alloying and exposure to temperature. At the same time, the main efforts of materials scientists are aimed at purifying the alloy from harmful iron impurities and stabilizing the composition of silicon. Alloys of the Al-Fe-Si system with equiatomic and/or quasi-equiatomic composition have not been sufficiently studied in the literature. We believe that alloys of the Al-Fe-Si system have sufficient potential for use as a structural material capable of being subjected to deformation treatments. However, to ensure the possibility of plastic deformation, a number of conditions must be met, such as:

-increased deformation temperature for transition to a single-phase region, or a region with a predominant one-phase;

- rational composition, which will ensure the formation of a phase with the most compact morphology, or a type of crystal lattice capable of accepting plastic deformation;

- the use of heat treatment, which makes it possible to consolidate or enhance the effect of plastic deformation of an alloy with a rational composition.

At this stage of the work, the authors concentrated their efforts on selecting an alloy composition capable of withstanding plastic deformation and determining the appropriate deformation interval.

Alloys of the Al-Fe-Si system are considered in this work as alloys based on aluminum, i.e. Σ Fe+Si≤50 wt%. In this system, aluminum has the lowest melting point, which is 660°C; an assessment of the phase composition under these conditions (Fig.1) shows that liquid is observed for almost any composition. First of all, crystallization begins with an iron content of more than 40% and a minimum amount of silicon with the release of the primary high-temperature phase θ, which has a monoclinic crystal lattice. This phase exists only when there is a lack of silicon, which is dissolved in the liquid phase

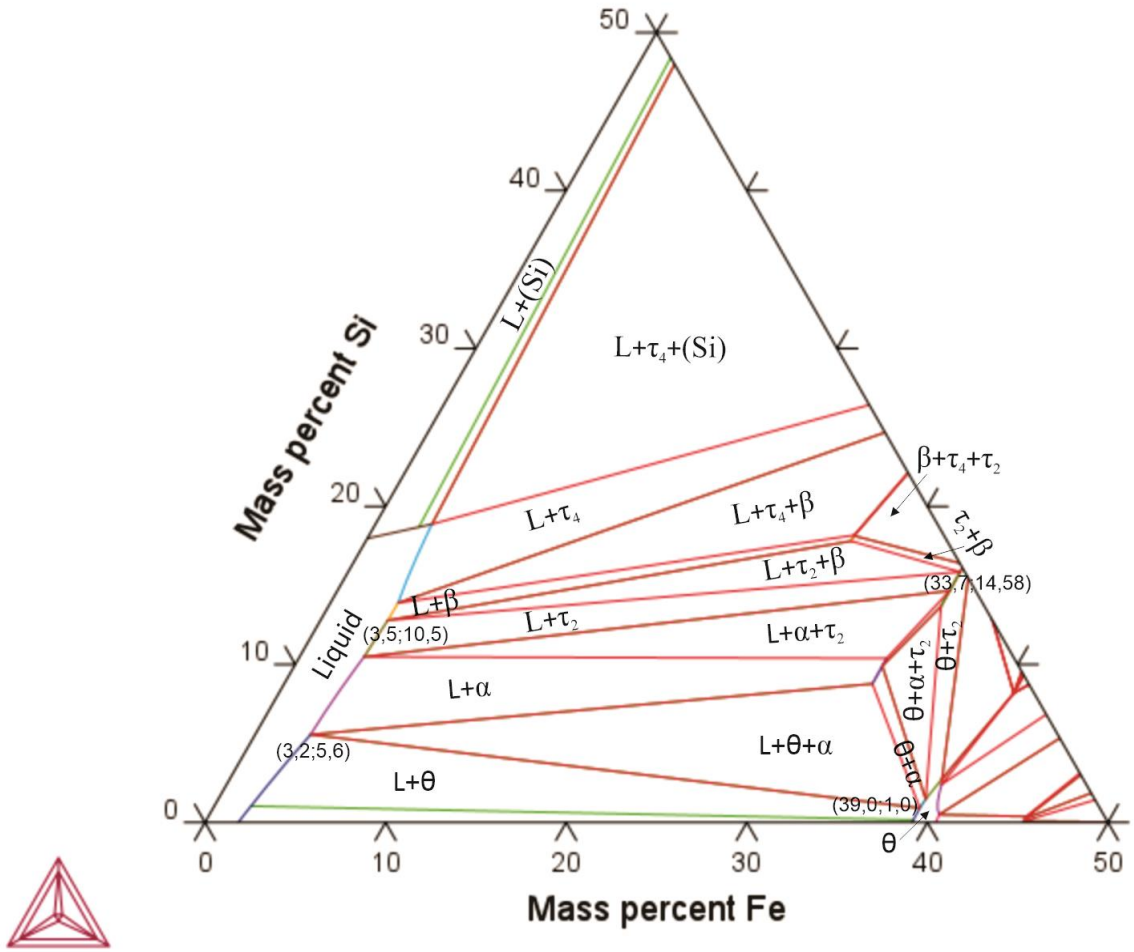

Figure 1 - Isothermal section diagram Al-Si-Fe at 660°C

and in the θ phase, while the solubility in the latter does not exceed 1.5 mol%.

As silicon increases, conditions are created for the formation of ternary intermetallic phases, such as α, then τ2, β and τ4. With an iron content of up to 5%, structurally free silicon is released directly from the melt at a silicon content of 18%. With an increase in the amount of iron, in addition to silicon, the τ4 phase is also formed, the amount of which increases with the amount of iron in the ternary system.

The range of formation of the ternary intermetallic phase α at a temperature of 660°C is limited by the content of iron and silicon as shown in Table 1.

Table 1 - The content of iron and silicon

Phase composition	Composition, wt.%	
	Fe	***Si***
L+α+θ	up 39	from 1
L+α+ τ_2	up 33.7	up 14.58
L+α	from 3.5	up 10.5
L+α+θ	from 3.2	from 5.6

In this case, the composition of the α phase remains quite constant and is Al 0.59:Fe 0.32:Si 0.09 wt%, Al 0.70:Fe 0.19:Si 0.11 at%. It is logical to assume that the maximum amount of α phase can be achieved with alloy compositions close to the composition of the α phase.

It is worth noting that the equilibrium α-phase is released only at relatively high temperatures with its further decomposition. To understand the mechanism of formation and decomposition of the α phase, phase diagrams with the base composition Al60-Fe30-Si10 were studied. Two main polythermal sections with fixed values of iron and silicon of 30 and 10%, respectively, are considered (Fig.2 and Fig.3.).

It was revealed that the α phase is present in the system from a temperature of 770°C up to a temperature of 446°C. In composition, it is found in the range from 5 to 35% iron with a fixed amount of silicon of 10% and from 0 to 15% silicon with an iron content of 30%.

Let us consider in more detail the phase transformations in the indicated composition ranges.

Alloys of the Al-Fe-Si system are very sensitive to composition, which manifests itself in a significant change in the phase composition, which, in turn, causes a change in the final properties of the metal. Alloys with a high iron content are particularly sensitive. From the point of view of the level of mechanical properties, the phases formed in a given

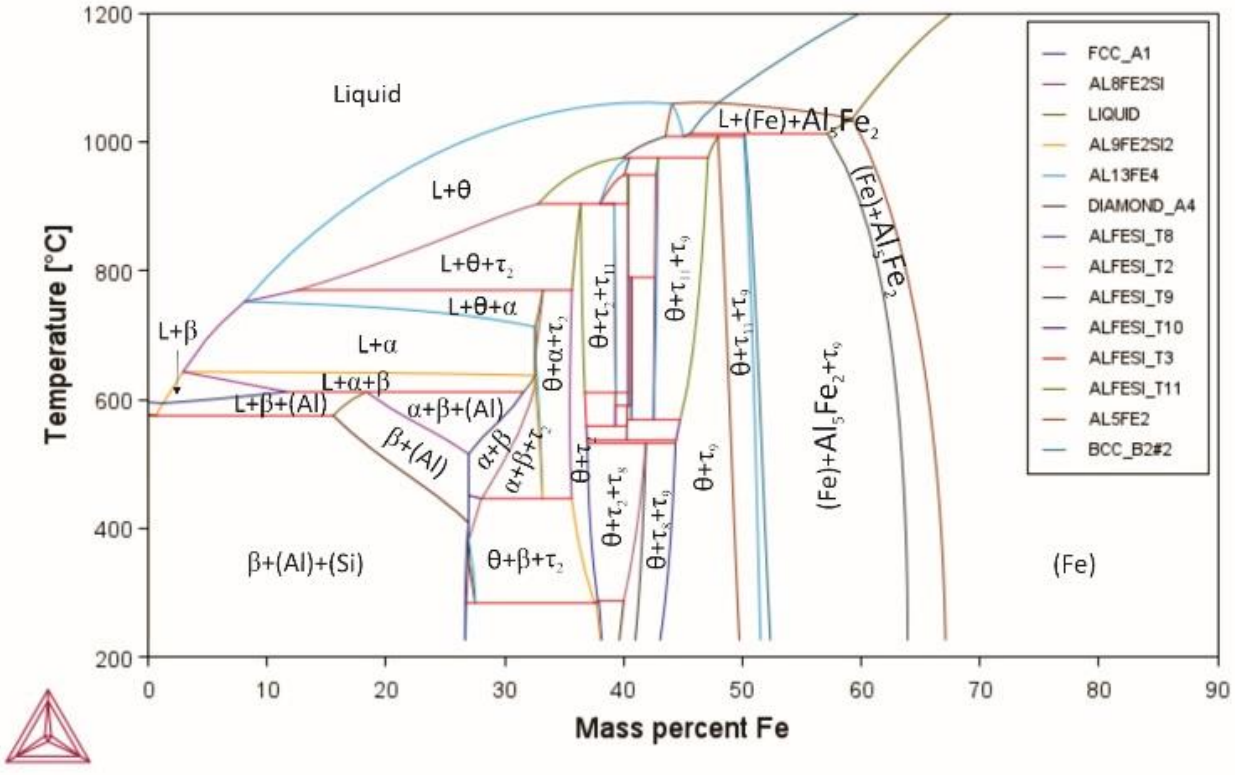

Figure 2 - Polythermal section diagram Al-Si-Fe with Si-const=10%

metal can be divided into harmful and useful. Solid solutions of silicon and iron in aluminum (indicated as (Al) in the figure), silicon and aluminum in iron (indicated as (Fe) in the figure) and the α phase, which exists only at elevated temperatures, can be considered useful. The morphology of the α phase typically has a “Chinese script” shape and is characterized by a hexagonal crystal lattice. With slow cooling, the α phase is transformed into the β phase, which is classified as “harmful” due to its morphology. The β phase is represented predominantly by tube-shaped or needle-shaped particles and is monoclinic. The remaining intermetallic compounds formed have monoclinic, triclinic and orthorhombic crystal lattices. In addition to the indicated phases, a monoclinic double phase θ and structurally free silicon are formed.

With an iron content of less than 26% and 10% silicon at room temperature, the alloy consists of a mechanical mixture of the β phase, an fcc solid solution of aluminum and excess silicon, which is present in the form of structurally free silicon precipitated as inclusions. But in this region, complex processes of dissolution and separation of individual phases are observed at higher temperatures.

When the iron content is less than 44%, the primary high-temperature phase, crystallizing at temperatures below 1065°C, is the monoclinic, iron-depleting liquid θ phase. After sufficient purification of the liquid from iron, the formation of ternary intermetallic phases becomes possible as the temperature decreases. At a high iron content, the intermetallic phase τ11 is released; for this composition, the solidus temperature is 904°C. In this case, the residual liquid after crystallization of the θ phase disintegrates simultaneously with the formation of phases τ2 and τ11, with further rectistallization of the τ11 phase into the τ8 phase. When the amount of iron decreases to 36%, only phases θ and τ2 are formed. When the iron content is 12-36%, in addition to the θ phase, the τ2 phase immediately begins to separate from the liquid, which, with a decrease in temperature and through interaction with the remaining liquid, transforms into the α phase at a temperature of 770°C. In this case, the α phase becomes dominant as the composition of the alloy approaches the composition of the α phase up to 32.5% iron. A decrease in the amount of iron leads to an increase in the proportion of fluid in this area.

For an alloy with a large amount of iron, a temperature of 770°C is the solidus temperature,

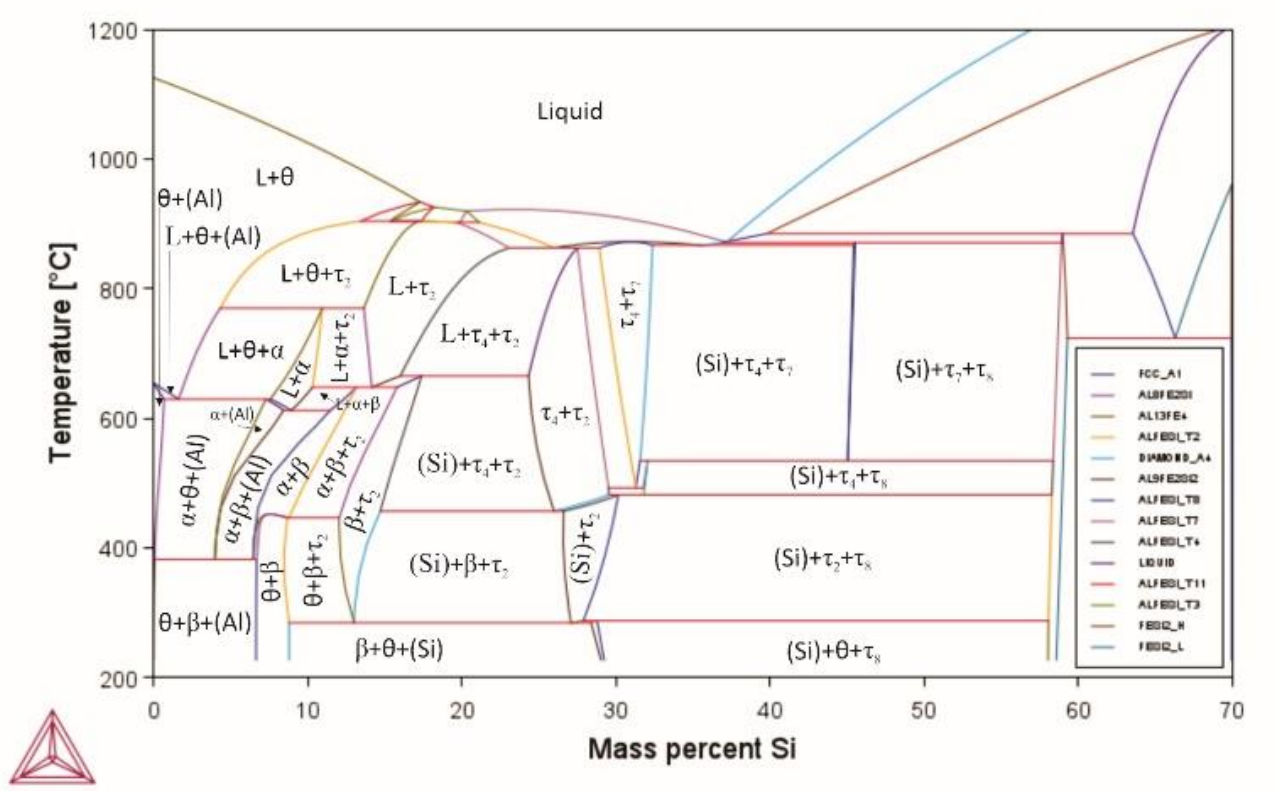

Figure 3 - Polythermal section diagram Al-Si-Fe with Fe-const=30%

and the entire liquid ends up with the composition of the α phase, into which it crystallizes. Subsequently, the α↔β transition occurs at a temperature of 446°C. This is the boundary of the existence of phase α. With iron content in the range of 8-12%, i.e. If the iron/silicon ratio = 1 is observed, phases α and θ are released directly from the liquid. For alloys with an iron content of less than 35% and temperatures below 715°C, the θ phase either does not form or completely dissolves. Alloys with an iron content of 1-3% are characterized by the release of β phase crystals directly from the liquid at temperatures below 642 ° C; with a further decrease in temperature, crystallization of the fcc solid solution of silicon and iron in aluminum begins.

An iron content of less than 1% with a silicon amount of 10% leads to the formation of a minimum melting temperature, which is 595°C, which is lower than the melting point of pure aluminum, with the crystallization of the aluminum fcc solid solution immediately. When the solubility limit of silicon in aluminum is reached with a further decrease in temperature, structurally free silicon precipitates in the form of inclusions (at temperatures below 580°C). In this case, the release of silicon particles is observed in up to 40% of iron.

When examining the phase diagram with an amount of iron of 30% (Fig.3), it is clear that structurally free silicon will be present in the microstructure of the metal already at a silicon content of 11.5%, and even at high temperatures it will not be completely dissolved. The θ phase is released when there is an excess of iron. It crystallizes from liquid primarily at iron/silicon ratios >2. As the amount of silicon increases, intermetallic compounds are formed that bind both silicon and iron. At room temperature, the θ phase is observed at silicon contents up to 11.5. The aluminum solid solution completely transforms into intermetallic compounds when the silicon content is more than 8%. The solidus temperatures were as follows: 629°C with a silicon content of 0.5-7.5, 613°C with a silicon content of 8.5-11.5%, 646°C with a silicon content of 13-16%, 665°C, with a silicon content of 17-24%, 862°C with a silicon content of 27-29% and 872°C with an iron/silicon ratio of 1:1, with 30% silicon.

The α phase is observed in the alloy containing 4.3-13.5 in the temperature range below 770°C, while the lower temperature limit of the α phase in the range of 8-12% is 446°C, and for the range of 0.06-6.7% silicon –382°C. It can be seen that the α phase for all compositions is present together with other phases, such as aluminum solid solution, β, τ2 phases and liquid.

In order to provide the alloy with the greatest ductility, it is preferable to carry out deformation in a single-phase region, or with a minimum amount of the second phase. Therefore, to optimize the composition, modeling was performed with a quantitative assessment of the phases formed when the temperature changes with varying number of alloy components. The variation was carried out with a step of 5. The variation conditions, temperature parameters and modeling results are shown in Table 2.

Analysis of the data obtained indicates that the determining factor in the formation of the phase composition is the content of elements, while a significant amount of α-phase is observed at an aluminum content of 60-65%, iron ~30%, and silicon 5-10%. It is noted that for the Al60-Fe30-Si10 composition the maximum concentration of the α phase is observed at a temperature of 662°C and reaches a concentration of 87%, and for the Al65-Fe30-Si5 composition the maximum concentration reaches 89% at a temperature of 510°C. Thus, reducing the amount of silicon to 5% while increasing aluminum leads to a decrease in the lower limit by 65° and an increase in the upper limit by 50°C.

Table 2 - Batch parameters and quantitative assessment

№	Content of main elements, %			α-phase quantity, %	Temperature conditions, °C
	Al	*Fe*	*Si*		
1	60	30	10	87	725-450
2	60	20	20	-	
3	60	10	30	-	
4	60	35	5	60	780-450
5	60	25	15	15	640-620
6	60	29	1	20	620-380
7	50	30	20	-	
8	50	20	30	-	
9	50	35	15	-	
10	50	25	15	15	640-620
11	50	35	5	65	760-450
12	55	35	10	25	780-450
13	50	35	15	-	
14	65	30	5	89	775-385
15	70	25	5	70	745-385

In this case, a further increase in aluminum concentration to 70%, on the contrary, causes a decrease in the amount of α phase.

When the silicon content exceeds 15% or more, a sharp decrease in the amount of the α phase is observed, but a decrease in silicon of less than 5% also leads to a decrease in its amount. It is worth noting that iron and silicon have a complex effect, and their amount should be close to the composition of the α phase. Oscillations of even 5% already have a significant impact on the phase relationship.

Thus, the composition of the Al60-65 alloy was adopted as the most optimal; Fe30-32; Si5-10%, deformation temperature range is 600-450°C. Deformation in this region will provide processing in a quasi-single-phase region without melting.

Conclusions

By constructing diagrams of the Al-Fe-Si system, the phase composition and kinetics of phase separation were revealed, the boundary conditions for the existence of phases were determined for a wide range of compositions, and the liquidus, solidus and solvus temperatures were identified. With an aluminum content of 60-65%, iron ~30%, and silicon 5-10%, the amount of α-phase reaches 87-89%. An increase in aluminum content to more than 70% causes a decrease in the amount of α phase in favor of an fcc solid solution of silicon and iron in aluminum. In this case, the aluminum solid solution completely transforms into intermetallic compounds with a silicon content of more than 8% in the presence of iron. A quasi-single-phase region with a phase composition that provides susceptibility to plastic deformation has been found. The temperature range of deformation is 600-450°C without melting. The most optimal composition of the alloy is Al60-65; Fe30-32; Si5-10%.

Conflict of interest. On behalf of all authors, the corresponding author declares that there is no conflict of interest.

Acknowledgements. This research is funded by the Science Committee of the Ministry of Science and Higher Education of the Republic of Kazakhstan. Grant No. AP19675471 “Development of technology for the synthesis of composite ceramic materials of the AlxFeySi system using the additive method”.

Cite this article as: Andreyachshenko VA, Toleuova AR. On the influence of iron and silicon content on the phase composition of the Al-Fe-Si system. Kompleksnoe Ispolzovanie Mineralnogo Syra = Complex Use of Mineral Resources. 2025; 332(1):98-107. https://doi.org/10.31643/2025/6445.09

Al-Fe-Si жүйесінің фазалық құрамына темір мен кремний құрамының әсері туралы

Андреященко В.А., Толеуова А.Р.

Әбілқас Сағынов атындағы Қарағанды техникалық университеті, Қарағанды, Қазақстан

Мақала келді: *15 қаңтар 2024*
Сараптамадан өтті: *18 ақпан 2024*
Қабылданды: *12 ақпан 2024*

ТҮЙІНДЕМЕ

Al-Fe-Si жүйесінің интерметалдық фазаларына қызығушылықтың артуы олардың жоғары меншікті беріктігімен, коррозияға және тозуға төзімділігімен, сондай-ақ оларды өндірудің төмен құнымен байланысты. Қасиеттердің ең сәтті комбинациясын көрсету үшін тұндырылған интерметалдық фазаларға нақты ықшам морфологияны беру қажет. Пластикалық деформацияны қабылдауға қабілетті құрамы бар қорытпаны жасау маңызды. Жұмыстың мақсаты - пластикалық деформацияға төтеп беруге қабілетті Al-Fe-Si жүйесі қорытпасының құрамын жасау және сәйкес деформация аралығын анықтау. Компьютерлік модельдеу негізінде пластикалық деформацияны қабылдауға қабілетті қорытпа композициясы әзірленді және сәйкес деформация аралығы анықталды. Модельдеу ThermoCalc бағдарламалық пакетінде, TCAL8 деректер базасында жүргізілді. Құрамында кремнийдің де, темірдің де мөлшері жоғары қорытпалар бір фазалы аймақтың түзілуімен сипатталмайтыны анықталды, алайда қорытпа компоненттерінің белгілі бір комбинациясы кезінде бір фазаның мөлшері 90% -дан жоғары болған кезде квази-бірфазалы құрылымға қол жеткізуге болады. Әртүрлі қорытпалар құрамы үшін солидус температуралары және фазалардың болуының шекаралық шарттары анықталды. α фазасы жүйеде 770°C

	температурадан 446°С температураға дейін болады. Құрамында кремний мөлшері 10% болатын 5-тен 35%-ға дейін темір және 30% темір мөлшерімен 0-15% кремний аралығында кездеседі. α фазасының максималды мөлшері Al60-65 қорытпасы үшін алынды; Fe30-32; Si5-10% қорытпаларында деформация температурасының диапазоны 600-450°С болады. Бұл аймақтағы деформация балқымай-ақ квази-бірфазалы аймақта өңдеуді қамтамасыз етеді.
	Түйін сөздер: Al-Fe-Si, ThermoCalc бағдарламалық қамтамасыз ету, металаралық фазалар, фазалық диаграмма, α фаза.
Андреященко Виолетта Александровна	***Авторлар туралы ақпарат:*** *PhD, қауымдастырылған профессор, "Минералдық шикізат қазбаларды кешенді игеру" инженерлік бейіндегі сынақ зертханасының басшысы. Әбілқас Сағынов атындағы Қарағанды техникалық университеті, Н. Назарбаев даңғылы, 56, Қарағанды, Қазақстан. Email: Vi-ta.z@mail.ru*
Толеуова Айнагуль Рымкуловна	*PhD, қауымдастырылған профессор, Нанотехнология және металлургия кафедрасының доценті, Әбілқас Сағынов атындағы Қарағанды техникалық университеті, Н.Назарбаев даңғылы, 56, Қарағанды, Қазақстан. Email: rymkul.ainagul@mail.ru*

О влиянии содержания железа и кремния на фазовый состав системы Al-Fe-Si

Андреященко В.А., Толеуова А.Р.

Карагандинский технический университет имени Абылкаса Сагинова, Караганда, Казахстан

Поступила: *15 января 2024*
Рецензирование: *18 февраля 2024*
Принята в печать: *12 марта 2024*

АННОТАЦИЯ

Возрастающий интерес к интерметаллидным фазам системы Al-Fe-Si связан с их высокой удельной прочностью, коррозионной и износостойкостью, а также низкой стоимостью их изготовления. Для проявления наиболее удачного сочетания свойств необходимо придание специфической компактной морфологии выделяющимся интерметаллидным фазам. Актуально создание сплава с составом, способным воспринимать пластическую деформацию. Цель работы разработать состав сплава системы Al-Fe-Si, способного воспринимать пластическую деформацию и определить соответствующий интервал деформирования. На основе компьютерного моделирования разработан состав сплава, способного воспринимать пластическую деформацию и определен соответствующий интервал деформирования. Моделирование осуществлялось в программном комплексе ThermoCalc, база данных TCAL8. Выявлено, что для сплавов с высоким содержанием как кремния, так и железо не характерно формирование однофазной области, однако при определенном сочетании компонентов сплава удается достичь квази однофазной структуры, когда наблюдается содержание одной фазы более чем на 90%. Определены температуры солидуса для различного состава сплава, граничные условия существования фаз. α фаза присутствует в системе с температуры 770°С вплоть до температуры 446°С. По составу она обнаруживается в диапазоне от 5 до 35 % железа при количестве кремния 10% и от 0 до 15% кремния при содержании железа 30%. Максимальное количество α фазы получено для сплава Al60-65; Fe30-32; Si5-10%, температурный интервал деформирования составляет 600-450°С. Деформирование в данной области обеспечит обработку в квазиоднофазной области без оплавления.

Ключевые слова: Al-Fe-Si, программное обеспечение ThermoCalc, интерметаллидные фазы, фазовая диаграмма, α-фаза.

Информация об авторах:

Андреященко Виолетта Александровна
PhD, ассоциированный профессор, руководитель испытательной лаборатории инженерного профиля «Комплексное освоение ресурсов минерального сырья», Карагандинский технический университет имени Абылкаса Сагинова, пр. Н. Назарбаева, 56, Караганда, Казахстан. Email: Vi-ta.z@mail.ru

Толеуова Айнагуль Рымкуловна
PhD, ассоциированный профессор, доцент каф. нанотехнологии и металлургии. Карагандинский технический университет имени Абылкаса Сагинова, пр. Н. Назарбаева, 56, Караганда, Казахстан. Email: rymkul.ainagul@mail.ru

References

[1] Shen W, Hu A, Liu S, Hu H. Al-Mn alloys for electrical applications: A review. Journal of Alloys and Metallurgical Systems 2023; 2:100008. https://doi.org/10.1016/j.jalmes.2023.100008

[2] Lan X, Kai L, Wang J, Yang M, Lu Q, Du Y. Developing Al–Fe–Si alloys with high thermal stability through tuning Fe, Si contents and cooling rates. Intermetallics. 2022; 144:107505. https://doi.org/10.1016/j.intermet.2022.107505

[3] Que Zh, Fang Ch, Mendis ChL, Wang Yu, Fan Zh. Effects of Si solution in θ-Al13Fe4 on phase transformation between Fe-containing intermetallic compounds in Al alloys. Journal of Alloys and Compounds. 2023; 932:167587. https://doi.org/10.1016/j.jallcom.2022.167587

[4] Jin L, Liu K, Chen XG. Evolution of Fe-Rich Intermetallics in Al-Si-Cu 319 Cast Alloy with Various Fe, Mo, and Mn Contents. Metall Mater Trans B. 2019; 50:1896-1907. https://doi.org/10.1007/s11663-019-01584-2

[5] Kishor M, Chopra K, Ayyagari KPR. Tackling Fe-rich Intermetallics in Al-Si Alloy: A Critical Review. Trans Indian Inst Met. 2023; 1-6. https://doi.org/10.1007/s12666-023-03205-8

[6] Song DF, Zhao YL, Wang Z et al. 3D Fe-Rich Phases Evolution and Its Effects on the Fracture Behavior of Al–7.0Si–1.2Fe Alloys by Mn Neutralization. Acta Metall. Sin. (Engl. Lett.). 2022; 35:163-175. https://doi.org/10.1007/s40195-021-01299-x

[7] Sanchez JM, Vicario I, Albizuri J, Guraya T, Garcia JC. Phase prediction, microstructure and high hardness of novel light-weight high entropy alloys. Journal of Materials Research and Technology. 2019; 8(1):795-803. https://doi.org/10.1016/j.jmrt.2018.06.010

[8] Zhang X, Wang D, Li X, Zhang H, Nagaumi H. Understanding crystal structure and morphology evolution of Fe, Mn, Cr-containing phases in Al-Si cast alloy. Intermetallics. 2021; 131:107103. https://doi.org/10.1016/j.intermet.2021.107103

[9] Orozco-González P, Castro-Román M, Muñiz-Valdez R, Luna-Álvarez S, Equihua-Guillén F, Hernández-Rodríguez A, Baltazar-Hernández VH, Alvarado-Hernández F. Formation and crystal structure of the τ phase in the Al-Fe-Mn-Si system. Materials Letters. 2016; 180:277-279. https://doi.org/10.1016/j.matlet.2016.05.139

[10] Nová K, Novák P, Průša F, Kopeček J, Čech J. Synthesis of Intermetallics in Fe-Al-Si System by Mechanical Alloying. Metals. 2019; 9:20. https://doi.org/10.3390/met9010020

[11] Fang CM, Que ZP, Fan Z. Crystal chemistry and electronic structure of the β-AlFeSi phase from first-principles. Journal of Solid State Chemistry. 2021; 299:122199. https://doi.org/10.1016/j.jssc.2021.122199

[12] Jin L, Chen XG. Evolution of dispersoids and their effects on elevated-temperature strength and creep resistance in Al-Si-Cu 319 cast alloys with Mn and Mo additions. Materials Science and Engineering: A. 2020; 770:138554. https://doi.org/10.1016/j.msea.2019.138554

[13] Jiang H, Liu YC, Wei C, Zhang YH, Gao ZM. Influence of minor Co on the formation of intermetallic phases in the Al91Fe7Si2 alloy. Journal of Alloys and Compounds. 2008; 466(1–2):92-97. https://doi.org/10.1016/j.jallcom.2007.11.019

[14] Yu JM, Wanderka N, Rack A, Daudin R, Boller E, Markötter H, Manzoni A, Vogel F, Arlt T, Manke I, Banhart J. Influence of impurities, strontium addition and cooling rate on microstructure evolution in Al-10Si-0.3Fe casting alloys. Journal of Alloys and Compounds. 2018; 766:818-827. https://doi.org/10.1016/j.jallcom.2018.06.372

[15] Wu X, Zhang H, Zhang F, Ma Zh, Jia L, Yang B, Tao T, Zhang H. Effect of cooling rate and Co content on the formation of Fe-rich intermetallics in hypoeutectic Al7Si0.3Mg alloy with 0.5%Fe. Materials Characterization. 2018; 139:116-124. https://doi.org/10.1016/j.matchar.2018.02.029

[16] Becker H, Bergh T, Vullum PE, Leineweber A, Li Y. Effect of Mn and cooling rates on α-, β-and δ-Al–Fe–Si intermetallic phase formation in a secondary Al–Si alloy. Materialia. 2019; 5:100198. https://doi.org/10.1016/j.mtla.2018.100198

[17] Yang W, Gao F, Ji Sh. Formation and sedimentation of Fe-rich intermetallics in Al–Si–Cu–Fe alloy. Transactions of Nonferrous Metals Society of China. 2015; 25(5):1704-1714. https://doi.org/10.1016/S1003-6326(15)63776-1

[18] Andreyachshenko VA. Evolution of the AA2030 alloy microstructure in the ECAP process. Kovove Materialy. 2022; 60(2):79-87. https://doi.org/10.31577/km.2022.2.79

[19] Andreyachshenko V. Evolution of Al-Si-Mn-Fe aluminum alloy microstructure in the equal-channel angular pressing with back pressure. Materials letters. 2019; 254:433-435. https://doi.org/10.1016/j.matlet.2019.07.127

[20] Zhang X, Wang D, Li X, Zhang H, Nagaumi H. Understanding crystal structure and morphology evolution of Fe, Mn, Cr-containing phases in Al-Si cast alloy. Intermetallics. 2021; 131:107103. https://doi.org/10.1016/j.intermet.2021.107103

[21] Dong X, Yang H, Zhu X, Ji Sh. High strength and ductility aluminium alloy processed by high pressure die casting. Journal of Alloys and Compounds. 2019; 773:86-96. https://doi.org/10.1016/j.jallcom.2018.09.260

[22] Outmani I, Fouilland-Paille L, Isselin J, Mansori ME. Effect of Si, Cu and processing parameters on Al-Si-Cu HPDC castings. Journal of Materials Processing Technology. 2017; 249:559-569. https://doi.org/10.1016/j.jmatprotec.2017.06.043

[23] Chen JK, Hung HY, Wang CF, Tang NK. Effects of casting and heat treatment processes on the thermal conductivity of an Al-Si-Cu-Fe-Zn alloy. International Journal of Heat and Mass Transfer. 2017; 105:189-195. https://doi.org/10.1016/j.ijheatmasstransfer.2016.09.090

[24] Dong X, Zhu X, Ji Sh. Effect of super vacuum assisted high pressure die casting on the repeatability of mechanical properties of Al-Si-Mg-Mn die-cast alloys. Journal of Materials Processing Technology. 2019; 266:105-113. https://doi.org/10.1016/j.jmatprotec.2018.10.030

[25] Qi M, Kang Y, Xu Y, Wulabieke Z, Li J. A novel rheological high pressure die-casting process for preparing large thin-walled Al–Si–Fe–Mg–Sr alloy with high heat conductivity, high plasticity and medium strength. Materials Science and Engineering: A. 2020; 776:139040. https://doi.org/10.1016/j.msea.2020.139040

[26] Bayoumy D, Schliephake D, Dietrich S, Wu XH, Zhu YM, Huang AJ. Intensive processing optimization for achieving strong and ductile Al-Mn-Mg-Sc-Zr alloy produced by selective laser melting. Materials & Design. 2021; 198:109317. https://doi.org/10.1016/j.matdes.2020.109317

[27] Queudet H, Lemonnier S, Barraud E, Guyon J, Ghanbaja J, Allain N, Gaffet E. One-step consolidation and precipitation hardening of an ultrafine-grained Al-Zn-Mg alloy powder by Spark Plasma Sintering. Materials Science and Engineering: A. 2017; 685:227-234. https://doi.org/10.1016/j.msea.2017.01.009

[28] Balasubramanian V, Lakshminarayanan AK, Varahamoorthy R, Babu S. Understanding the Parameters Controlling Plasma Transferred Arc Hardfacing Using Response Surface Methodology. Materials and Manufacturing Processes. 2008; 23:7:674-682. https://doi.org/10.1080/15560350802316744

[29] Srikarun B, Oo HZ, Petchsang S, Muangjunburee P. The effects of dilution and choice of added powder on hardfacing deposited by submerged arc welding. Wear. 2019; 424–425:246-254. https://doi.org/10.1016/j.wear.2019.02.027

[30] Zahiri R, Sundaramoorthy R, Lysz P, Subramanian C. Hardfacing using ferro-alloy powder mixtures by submerged arc welding. Surface and Coatings Technology. 2014; 260:220-229.

[31] Çam G, Koçak M. Progress in joining of advanced materials. Int Mater Rev. 1998; 43(1):1-44.

[32] Kunčická L, Kocich R, Németh G, Dvořák K, Pagáč M. Effect of post process shear straining on structure and mechanical properties of 316 L stainless steel manufactured via powder bed fusion. Additive Manufacturing. 2022; 59:103128. https://doi.org/10.1016/j.addma.2022.103128

[33] Naizabekov AB, Andreyachshenko VA. Evaluation of possible mechanical property improvement for alloy of the Al-Fe-Si-Mn system by equal-channel angular pressing. Metallurgist. 2013; 57(1-2):159-163. https://doi.org/10.1007/s11015-013-9706-0

[34] Andreyachshenko V, et al. ECAP-treated aluminium alloy AA2030: microstructure and mechanical properties. Materials & Technologies/Materiali in Tehnologije. 2019; 53(6):805–810. https://doi.org/10.17222/mit.2018.250

[35] Andreyachshenko V, Naizabekov A. The technology of equal channel angle backpressure extrusion for deformation iron and aluminium alloys. In: Proceedings of the 3rd International Conference on NANOCON. Brno, Czech Republic. sep 21-23. 2011, 246-252.

[36] Andreyachshenko VA, Naizabekov AB. Microstructural and mechanical characteristics of AlSiMnFe alloy processed by equal channel angular pressing. Metalurgija. 2016; 55(3):353-356.

Crossref
DOI: 10.31643/2025/6445.10
Metallurgy

Sequential Transportation of Different Oil Batches through the Industrial Pipeline

[1*]Ramazanova G.I., [1] Bekibayev T.T., [1]Soltanbekova K.A., [2] Aldzhambekova G.T.

[1] Satbayev University, Almaty, Kazakhstan
[2] Almaty University of Power Engineering and Telecommunications named after G. Daukeyev, Almaty, Kazakhstan

** Corresponding author email: gaukhar.ri@gmil.com*

Received: *February 28, 2024*
Peer-reviewed: *March 11, 2024*
Accepted: *March 13, 2024*

ABSTRACT

In sequential pumping, several liquids with different physical and chemical properties are pumped through one pipeline. The advantages of this method include: using one pipeline to transport different liquids; more complete pipeline loading; and reduced cost of pumping. The paper considers the sequential pumping of two batches of oil blends with different physicochemical properties through an industrial oil pipeline. This is because a batch of high-paraffin oil blend is simultaneously pumped to an oil refinery, and a batch of high-viscosity oil blend is transported further along a pipeline. The difference between the thermal-physical and rheological properties of oil batches imposes a condition on the thermal mode of operation of an industrial pipeline. A mathematical model and algorithm have been created for calculating the sequential transportation of high-paraffin and high-viscosity oil blends. Thermohydraulic calculations of the model show the distribution of hydraulic head, pressure, and temperature of the batches under the operating conditions of pumping units and heating furnaces. The verification and validation of the theoretical analysis was carried out with experimental data measured by the SCADA along the industrial pipeline length. By the thermal mode of sequential pumping, optimal heating temperatures of oil blends were found at the industrial pipeline stations.

Keywords: sequential transportation, batch of oil blends, high-paraffin oil, high-viscosity oil, heating temperature, industrial pipeline.

Information about authors:

Ramazanova Gaukhar Izbasarovna — *Candidate of physical and mathematical sciences, Leading Researcher. Research and Production Laboratory "Modeling in Energy", Satbayev University, 22 Satbayev str., 050013 Almaty, Kazakhstan. E-mail: gaukhar.ri@gmil.com*

Bekibayev Timur Talgatovich — *Master of engineering and technology, Head of section. Research and Production Laboratory "Modeling in Energy", Satbayev University, 22 Satbayev str., 050013 Almaty, Kazakhstan. E-mail: timur_bekibaev@mail.ru*

Soltanbekova Karlygash Alimkhanovna — *Master's degree in petroleum engineering, Head of section, Research and Production Laboratory "Modeling in Energy", Satbayev University, 22 Satbayev str., 050013 Almaty, Kazakhstan. E-mail: k.soltanbekova@satbayev.university*

Aldzhambekova Guldana Tleuzhanovna — *Candidate of Technical Sciences, Associate Professor, Department of Space Engineering, Almaty University of Power Engineering and Telecommunications named after G. Daukeyev, 126/1 Baytursynuli str., 050013 Almaty, Kazakhstan. E-mail: adana@bk.ru*

Introduction

The method of sequential pumping is widely used in pipeline transportation of oil and oil products [[1], [2], [3], [4], [5], [6]]. In this method at each moment, several oil blends differing in their physical and chemical properties are pumped through one pipeline. At that, each batch displaces the previous one and in turn, is displaced by the next one. Such regimes are non-stationary, as at different moments in each point of the pipe the value of parameters of the passing oil batch changes, which, having different rheological properties, cause different hydraulic losses for each point of the pipe in time.

Sequential pumping technology, or batch transportation, offers several advantages in the context of transporting oil and petroleum products through pipelines [[7], [8], [9]]:

Optimizing Pipeline Capacity. By transporting multiple types of oil in batches, pipeline operators can make the most efficient use of the available space and maximize throughput. This can be especially important in regions with limited pipeline infrastructure.

Economic Efficiency. Utilizing a single pipeline for transporting multiple products is more cost-effective than constructing separate pipelines for each product.

Flexibility and Adaptability. Sequential transportation provides flexibility to respond to changing market conditions.

Reducing Energy Consumption. Transitioning from one type of oil to another within the pipeline can be more efficient than emptying the pipeline before switching.

Efficient Resource Allocation. By transporting multiple types of oil through the same pipeline, resources such as labor, maintenance, and monitoring can be more effectively allocated, reducing overall operational costs.

An approximate theory of sequential pumping of petroleum products by direct contacting was first proposed in the paper [6].

Sequential pumping is used in the pipeline transportation of various oil blends and petroleum products, such as diesel fuel, kerosene, etc. In practice, different types of oil se-quential pumping are applied: 1) the presence of a dividing plate between different batch-es of heavy oil blends and oil products; 2) with separating plug is created by introducing drag reducing additive to the fluid; 3) direct contact methods of oil and oil products.

Most publications on this topic focus on planning the operation of a multi-product pipeline system when the pipeline is connected to multiple tank farms and local consumer markets [[10], [11], [12], [13], [14]].

The problem of mixture formation during the sequential pumping of light oil products through the same pipeline [[9], [15], [16]] is considered. It is known that when one oil product is displaced by another in the contact area of sequentially moving batches, a mixture is formed.

[3] used BFC-POD-ROM to simulate the cyclic transportation of Shengli and Oman oil batches to reduce the time cost. The paper [4] uses the gradient-type flow rate distribution model to increase the calculation accuracy in modelling sequential pumping with a non-constant flow rate. In the paper [17], a mathematical model was developed to describe the sequential pumping of cool and hot oil. It is assumed that the safety of batch-ing of cold and hot oil can be improved by reheating the cold oil ahead or increasing the capacity of the hot oil.

In Kazakhstan, the method of sequential pumping is applied on the Karazhanbas-Aktau and Uzen-Atyrau industrial oil pipelines. The Uzen - Atyrau oil pipeline facilitates the batch pumping of high-viscosity Buzachi and high-paraffin Mangyshlak oil blends. At the outlet of the main oil pumping station (MOPS) 'Uzen,' the pour point temperature of the Mangyshlak crude mixture is Tpt = +27°C, while for the Buzachinsk crude mixture, it is Tpt = -12°C. The difference in pour point temperatures between the Mangyshlak and Buzachinsk crude mixtures requires optimization of the heating temperature to ensure safe cyclic pumping. This operational process is interconnected with the concurrent transfer of a Mangyshlak oil blend batch to an oil refinery. While the batch of Buzachi oil blend is transported further along the industrial pipeline. The peculiarity of this task is that the pumping and heating of oil blends is carried out at several pumping and heating stations located along the length of the oil pipeline. Associated pumping and heating require the development of a model and an algorithm for calculating batch pumping. This paper presents the results of thermohydraulic calculations of sequential pumping of Mangyshlak and Buzachi oil blends through the Uzen - Atyrau industrial pipeline.

Sequential pumping

The longitudinal profile and diagram of the Uzen - Atyrau oil pipeline section are shown in Fig.1. The pipeline section passes through high-relief terrain, which creates static pressure in the pipeline. There are five intermediate stations along the pipeline: Sai Utes, Beineu, Opornaya, Kultumiev, and Shmanov.

Two oil batches with different physicochemical properties are pumped in sequential order through the oil pipeline section.

With this method of pumping, the changeability of the output of a batch of oil blends from the initial station occurs cyclically under a constant condition: the first batch (the first type of oil blend) goes out until it exhausts the pre-set batch volume for it, then the second batch (the second type of oil blend) also comes out until the predetermined volume is also exhausted, then the first batch comes out again with the same condition, etc. For the sequential pumping, different initial temperatures of oil blends can be set for each batch.

Sequential pumping modes are non-stationary, since at different times at each point of the pipe, the values of the parameters of the passing batch of oil change, which, having different rheological properties, causes different hydraulic losses for each point of the pipe in time.

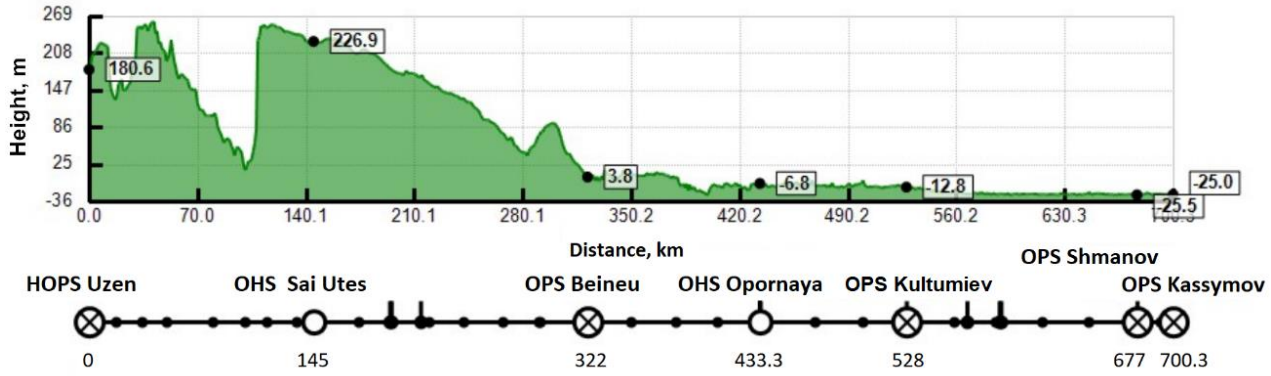

Figure 1 – The Uzen – Atyrau industrial pipeline profile and station location diagram: HOPS is the head oil pumping station; OPS is the oil pumping station; OHS is the oil heating station

Basic assumptions of the sequential pumping model. The batch pumping is considered as a non-stationary process and the following assumptions are made:

- oil is not compressible, the density of oil does not depend on the temperature and pressure;
- different batches of oil do not mix;
- the temperature of the fluid along the radius of each section of the pipe is constant.

Consider a pipeline of a length L, in which there are n operating oil pumping stations (OPS) and m operating oil heating station (OHS). Let each OPS be located in x_i^{ops} along the pipeline and, depending on the oil flow rate, crcreatedditional pressure ΔP_i^{ops} (pressure jumps). Let each OHS be located in x_j^{ohs} along the pipeline and, depending on the oil consumption, creates heating ΔT_i^{ohs} (temperature jumps) and pressure loss ΔP_i^{ops}.

It should be noted that the pressure ΔP_i^{ops} generated by OPS, oil heating ΔT_i^{ohs} in OHS and pressure loss ΔP_i^{ops} are the operating parameters and are set for the sequential pumping.

Model of mass and heat transfer

1. Mass and heat transfer in the linear part of the pipeline

The length of the oil pipeline L reaches hundreds of kilometers, and its diameter is D_1 = 1m, so the batch pumping can be considered in the framework of a one-dimensional model.

Denote the density of the first batch of oil blend as ρ_1, and the second batch as ρ_2. Then the density of the oil blend in the batch pumping can be expressed as $\rho = \rho_1\omega + \rho_2(1-\omega)$, where ω is the specific fraction of the oil blend; the variable ω takes the values ω =1 for the first batch of oil blend or ω =0 for the second batch of oil blend, since batch mixing is not allowed.

The assumption of incompressibility of the oil blend can be formulated as an equation:

$$\frac{\partial \omega}{t} + u\frac{\partial \omega}{\partial x} = 0 \qquad (1)$$

The equation of motion, considering the accepted assumptions, can be written as:

$$\rho\frac{\partial u}{\partial t} + \frac{\partial P}{\partial x} = -\zeta\frac{\rho u^2}{2D_1} - \rho g\sin\beta + \\ + \sum_{i=1}^{n}\Delta P_i^{ops}\delta(x - x_i^{ops}) - \sum_{j=1}^{m}\Delta P_j^{ohs}\ (x - x_j) \qquad (2)$$

The heat transfer equation, considering the accepted assumptions, has the form:

$$\frac{\partial T}{\partial t} + u\frac{\partial T}{\partial x} = -\frac{4K}{\rho C\ D_1}(T - T_w) + \frac{\zeta u^3}{2C_p D_1} + \\ + \sum_{j=1}^{m}\Delta T_j^{ohs}\delta(x - x_j^{ohs}) \qquad (3)$$

where T is the temperature distribution of oil blends along the pipeline; P is the pressure distribution along the pipeline; u is the linear velocity of fluid flow in the pipe; ζ is the coefficient of hydraulic resistance; g is the acceleration of gravity; D_1 is the inner diameter of the pipe; β is the angle of inclination of the pipe profile; K is the heat transfer coefficient from the oil flow to the surrounding environment; T_w is the temperature of the surrounding soil; C_p is the heat capacity of oil; *δ(x)* is the Dirac function.

The equation (1) describes changes in the distribution of batches of oil blends along the pipeline. The second equation (2) is derived from the equations of motion and continuity, considering the incompressibility of the fluid and the operation of OPS and OHS. The equation (3) is derived from the

heat balance equation considering the OHS operation along the pipeline. Equations (2) and (3) are interconnected through the coefficient of hydraulic resistance ζ, which depends on the temperature of the oil blends. There are no diffusion terms in equation (1) since the model assumes that batches of oil blends do not mix. The equation (1) is related to equations (2) and (3) via the parameters ρ, C_p, K, ζ as follows:

$$C_p = C_{p1}\omega + C_{p2}(1-\omega),\ \lambda = \lambda_1\omega + \lambda_2(1-\omega),$$
$$\mu = \mu_1\omega + \mu_2(1-\omega),\ K = K(\alpha,\lambda) \quad (4)$$

Where C_{p1}, C_{p2} are the heat capacity of batches No. 1 and No. 2, respectively; λ_1, λ_2 are the thermal conductivity of batches No. 1 and No. 2, respectively; $\mu_1(T), \mu_2(T)$ are the dependences of viscosity of batches No. 1 and No. 2 on temperature.

2. Initial and boundary conditions

The system of equations (1)–(2) has the following boundary conditions:

$$P(0,t) = P_0, P(L,t) = P_L \quad (5)$$

$$T(0,t) = T_1 \text{ by } \omega = 1,\ T(0,t) = T_2 \text{ by } \omega = 0 \quad (6)$$

$$\omega(0,t) = 1,\ \left\langle \frac{S_0 \int_0^t u dt}{V_1 + V_2} \right\rangle < \frac{V_1}{V_1\ \ V_2};$$
$$\omega(0,t) = 0,\ \left\langle \frac{S_0 \int_0^t u dt}{V_1 + V_2} \right\rangle \geq \frac{V_1}{V_1\ \ V_2}, \quad (7)$$

where P_0 is the pressure at the outlet of the tanks at the initial station; P_L is the pressure at the inlet to the final station; T_1, T_2 are the initial temperature of the oil blends for batch No. 1 and batch No. 2, respectively; S_0 is the cross-sectional area of the pipe at the outlet of the initial station; V_1, V_2 are the volumes necessary for switching for batch No. 1 and batch No. 2, respectively; $\langle\ \ \rangle$ is the operation of taking the fractional part of the number.

The boundary condition (7) was derived from the following considerations: let the volume of oil blends $V = V(t)$ that came out of the initial station be known for each moment of time t. Consider switching batches of oil blends from the start of pumping:

$V \in [0, V_1)$ - pumping of batch No. 1;

$V \in [V_1, V_1 + V_2)$ - pumping of batch No. 2;

$V \in [V_1 + V_2, 2V_1 + V_2)$ - pumping of batch No. 1;

$V \in [2V_1 + V_2, 2V_1 + 2V_2)$ - pumping of batch No. 2;

…

$V \in [k(V_1 + V_2), k(V_1 + V_2) + V_1)$ - pumping of batch No. 1

It is easy to notice that during the pumping of batch No. 1, the fractional part of the ratio $\frac{V}{V_1+V_2}$ lies in the range from 0 to $\frac{V_1}{V_1+V_2}$, i.e. $\langle\frac{V}{V_1+V_2}\rangle < \frac{V_1}{V_1+V_2}$, when pumping of batch No.2 $\langle\frac{V}{V_1+V_2}\rangle \in [\frac{V_1}{V_1+V_2}, 1]$. For each moment t, the value of V can be calculated by considering the volume pumped through the section S_0 with linear velocity u, i.e. $V = V(t) = S_0 \int_0^t u dt$.

3. Closure relations

The values of the additional pressure created on the OPS, as well as heating and pressure loss on OHS are known and depend on the flow rate of oil blends, i.e. they are predefined functions of the flow rate u:

$$\Delta P_i^{ops} = \Delta P_i^{ops}(u),\ \Delta T_j^{ohs} = \Delta T_j^{ohs}(u),$$
$$\Delta P_j^{ohs} = \Delta P_j^{ohs}(u), \quad (8)$$

In the current model, the profile of the oil pipeline and the ambient temperature are known and depend only on the location along the route, i.e. they are predefined functions of space:

$$\beta\quad \beta(x),\quad T_w = T_w(x), \quad (9)$$

The coefficient of hydraulic losses $\zeta = \zeta(u, \mu)$ in equations (2) and (3) can be calculated using well-known formulas or equations [[18], [19], [20]].

The heat transfer coefficient $K = K(\alpha, \lambda)$ from the oil flow to the environment can be found using the formulas described in detail in [[21], [22]].

Soil temperature T_w was taken from measured SCADA data. Since the ground along the considered section of the pipeline is heterogeneous, the values of ground thermal conductivity were calculated using historical actual data of oil flow rate, oil temperature and ground temperature for the given section of the pipeline [23].

The heat capacity of oil blends is described by the Krego's formula [8]:

$$C_p(T) = (53357 + 107.2 \cdot T)/\sqrt{\rho}\ \text{[J/(kg·°C)]}, \quad (10)$$

4 Setting the sequential pumping period

Since the boundary conditions (5) and (6) are cyclic, depending on the given constants V_1, V_2, the state of the pipeline will also be cyclic, i.e. after a certain time Δt_{cyc}, the values of the variables u, P, T, ω will be the same:

$$u(x,t) = u(x,t+\Delta t_{cyc}),\ P(x,t) = P(x,t+\Delta t_{cyc})$$
$$T(x,t) = T(x,t+\Delta t_{cyc}),\ \omega(x,t) = \omega(x,t+\Delta t_{cyc}) \quad (11)$$

Thus, to simulate the sequential pumping process, it is sufficient to use some initial distribution of *P*, T, ω. In the process of calculations, such a cycle start time t^0_{cyc} will be found that the conditions $t > t^0_{cyc}$ (11) will be met. Such time t^0_{cyc} can be found by storing variables u, P, T, ω for each moment t and comparing them with the values of the previous time.

In practice, it is enough to compare only the values $u(0,t)$, since this method is less computationally intensive. The condition of the pipeline $t > t^0_{cyc}$ is conditionally called the "steady state" during the sequential pumping of oil blends.

Let batch No. 1 be less viscous than batch No.2, if, with a given pumping mode (OPS and OHS operating modes), the batch pumping of two oil blends is possible, only when pumping of batch No. 1 is possible.

It is also obvious that if pumping batch No. 1 is impossible, then sequential pumping of two batches is also impossible. Therefore, as an initial distribution of P, T, ω for modeling the batch pumping, it would be correct to take the values of the batch of oil blend No. 1:

$$P(x,0) = P^{batch1}(x),\ T(x,0) = T^{batch1}(x),\ \omega(x,0) = 1, \quad (12)$$

where P^{batch1}, T^{batch1} are the distribution of oil pressure and temperature, respectively, along the pipeline for stationary pumping mode of batch No. 1. In this case, for $t < t^0_{cyc}$ a transition process from the stationary oil pumping mode No. 1 to the "steady-state" batch pumping mode will be obtained.

Figure 2 shows the time change u(0,t) for an example of calculating the batch pumping of the Mangyshlak and Buzachi oil batches though the Uzen-Atyrau pipeline section.

As can be seen from Figure 2, after a certain time (t = 55 h), the process of pumping a batch with a given initial condition (12) switches to a "steady state" sequential pumping mode.

Thus, the pumping of 2 batches is impossible if and only if the stationary mode of pumping oil blend No. 1 is impossible or when modeling with the initial condition (12), the value of u at some point in time becomes equal to 0.

So, to simulate the batch pumping of two oil blends, the system of equations (1) - (4) with boundary (5-7) and initial (12) conditions is used. The result of such modeling will be either the "steady state" of the pipe.

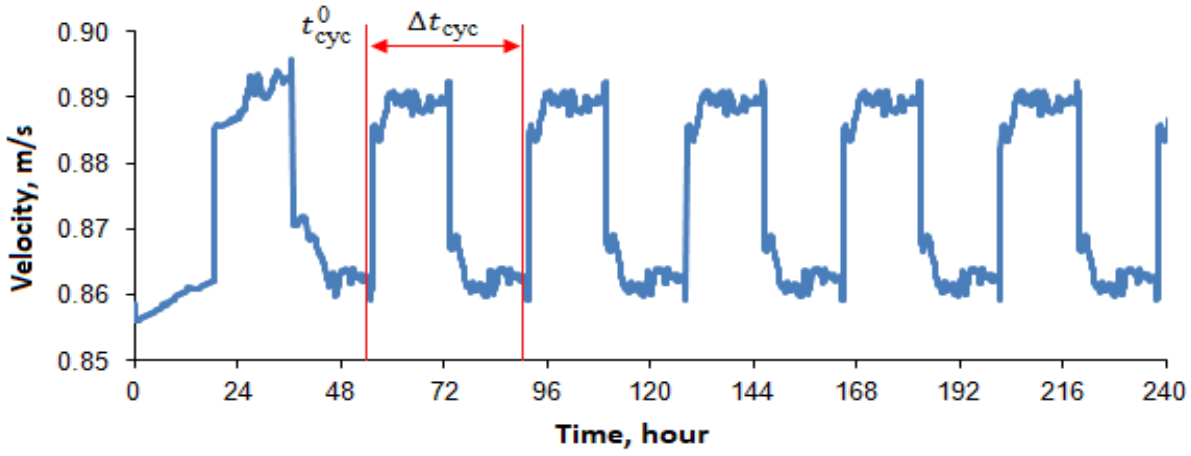

Figure 2 – An example of a change in the flow rate over time for modeling the batch pumping of the oil blends with a given initial condition for transition to the "steady state" at $t > t^0_{cyc}$

Calculation algorithm

The system of equations (1) - (4) with the initial and boundary conditions (5) - (7) and closures of relations (8) - (10) is solved by the numerical method [24]. The value of the hydraulic resistance coefficient ζ_i^n is expressed by the Altshul's formula [20], depending on the flow regime, respectively. This hydraulic resistance coefficient value is put into the momentum equation (2) and the pressure P_i^{n+1}, velocity u_i^{n+1}, temperature T_i^{n+1} values at the difference grid nodes are calculated. According to the obtained temperature distribution T_i^{n+1}, the values of the viscosity $\mu_i^{n+1}(T_i)$ and the Reynolds number Re_i^{n+1} are found. According to the found Reynolds number Re_i^{n+1}, the value of the hydraulic resistance coefficient ζ_i^{n+1} is specified.

The SmartTran software [25] conducts the thermal-hydraulic calculations by the system of equations (1)-(3) with the conditions (5)-(12) for the oil pumping modes through main oil pipelines.

Results and Discussion

For the Mangyshlak oil blend, the density is equal to $\rho_1 = 843.1$ kg/m³, and for Buzachi oil blend is $\rho_2 = 891.9$ kg/m³. The temperature dependences of the viscosity of Mangyshlak and Buzachi oil blends are shown in Fig. 3.

The temperature dependences of viscosity of Mangyshlak and Buzachi oil blends are expressed by the formulas (13) and (14):

$$\mu_1(t) = 1.6838 \cdot \exp(-0.095 \cdot T) \quad (13)$$

$$\mu_2(t) = 0.9109 \cdot \exp(-0.116 \cdot T) \quad (14)$$

The length of the Usen-Atyrau oil pipeline section is L = 700.3 km (see Fig.1), the pipe inner diameter is D_1 = 1.0 m, and the pipeline laying depth is H = 1.5 m.

The batch pumping of Buzachi and Mangyshlak oil blends takes place through the Uzen-Atyrau oil pipeline. The calculated data is based on the “steady state” sequential pumping with cycle times Δt_{cyc}.

The oil batches are pumped through the considered pipeline section by pumping units of the Uzen, Beineu, Kultumiev and Shmanov oil pumping stations. Along the pipeline section, there are the Uzen, Sai-Utes, Beineu, Opornaya, and Kultumiev oil heating points where the oil batches are heated by fired furnaces.

For the safety of batch pumping, the oil temperature in the pipeline should be 5 °C higher than the pour point of the Mangyshlak oil blend. One batch of the oil blend sequentially displaces the next along the length of the pipeline. The same heating temperature of both oil blends at the stations can provide a thermal mode of sequential pumping and reduce the hydraulic resistance of the Buzachi oil blend.

The calculated data were obtained for the mass of the batch of Mangyshlak oil blend is 20,000 tons and the mass of the batch of Buzachi oil blend is 21,000 tons. The volumetric flow rate of sequential pumping does not change along the length of the pipeline section.

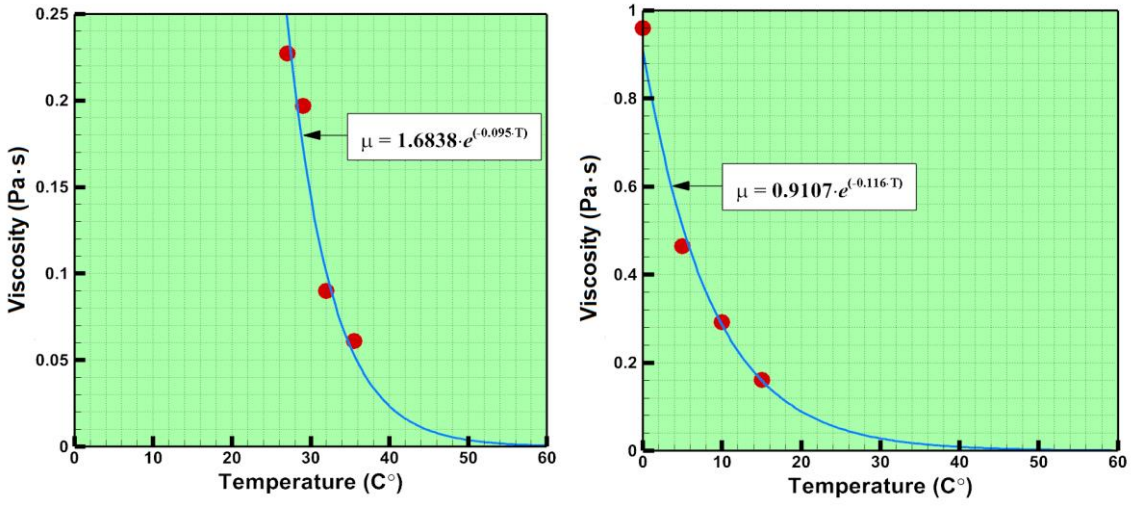

a) b)

Figure 3 – Effective viscosity dependences on temperature: (a) Magyshlak oil blend; (b) Buzachi oil blend

In Fig. 4 the batch of the Buzachi oil blend is painted in white color, and the batch of the Mangyshlak oil blend is painted in yellow. Analysis of calculations is carried out for typical periods within 24 hours.

As can be seen from Fig. 4, the calculation data describe a picture of batch pumping of Buzachi and Mangyshlak oil blends through the Uzen-Atyrau industrial pipeline. The upper diagram illustrates the distribution of hydraulic head, the middle diagram presents the pressure distribution and the lower diagram presents the temperature distribution of oil blends and soil along the route of the section.

Pumping units create pressures to overcome the hydraulic resistance of oil blends and the static pressure of the elevations of the pipeline profile. The temperature distribution shows the heating of oil blends at heating and cooling stations due to heat exchange with the surrounding cold soil.

The batch pumping is carried out by pumping units at the Uzen and Kultumiev stations (see Fig. 4). Oil blends are heated at the following stations: Uzen, Sai-Utes, Beineu, Opornaya, Kultumiev, Shmanov. Wave-like temperature change is caused by the higher heat content of the Mangyshlak oil blend compared to the Buzachi oil blend.

Fig. 5 shows the calculated data (lines) of hydraulic head, pressure and temperature in comparison with the actual data (points) of batch pumping through the Uzen-Atyrau industrial pipeline. The actual data of the hydraulic head, pressure and temperature are obtained by measuring the flow parameters of oil blends by sensors of the SCADA.

As depicted in Figure 5, the actual SCADA data points align closely with the computed values for hydraulic head, pressure, and temperature, represented by the lines.

Referring to the earlier statement, the thermal mode for batch pumping necessitates maintaining the oil blend's temperature within the pipeline at least 5°C above the pour point of Mangyshlak oil blend (Tpp = 27°C). Consequently, the selection of furnace heating temperatures at the respective stations becomes crucial to uphold the desired thermal conditions along the Uzen-Atyrau pipeline.

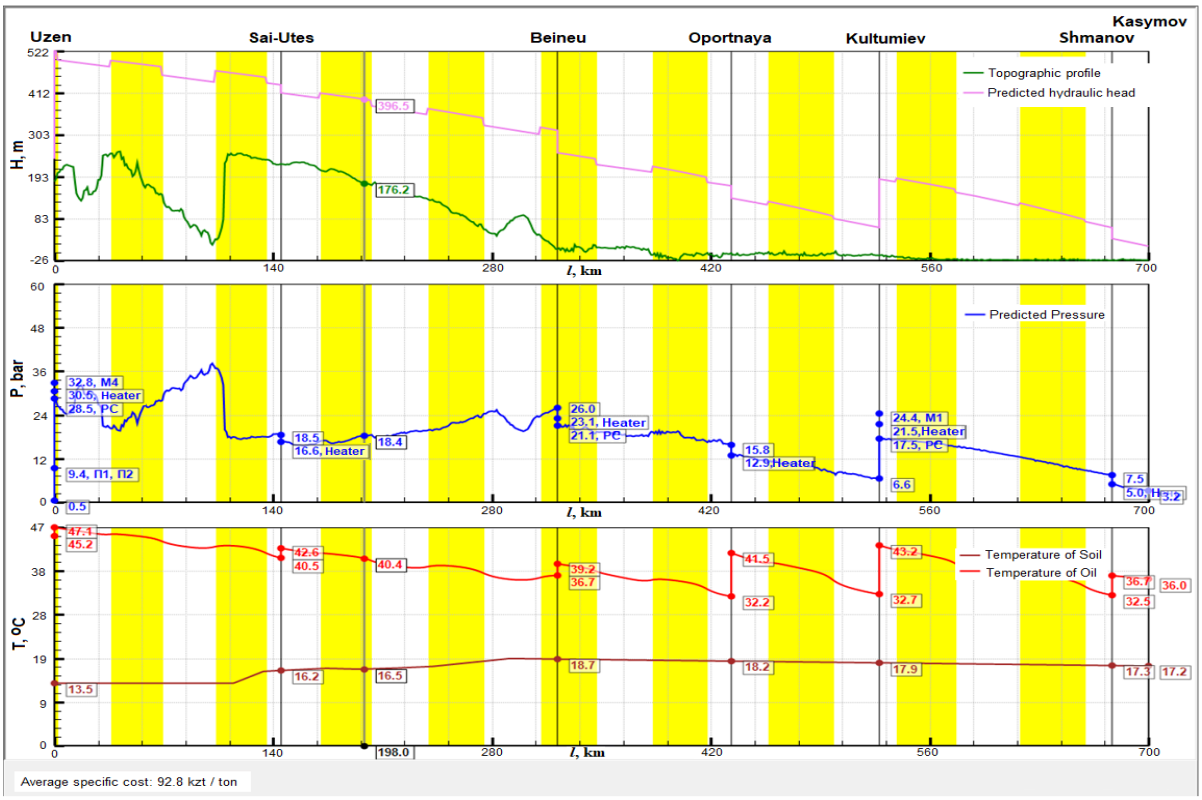

Figure 4 – The sequential pumping mode of the Buzachi and Mangyshlak oil blends

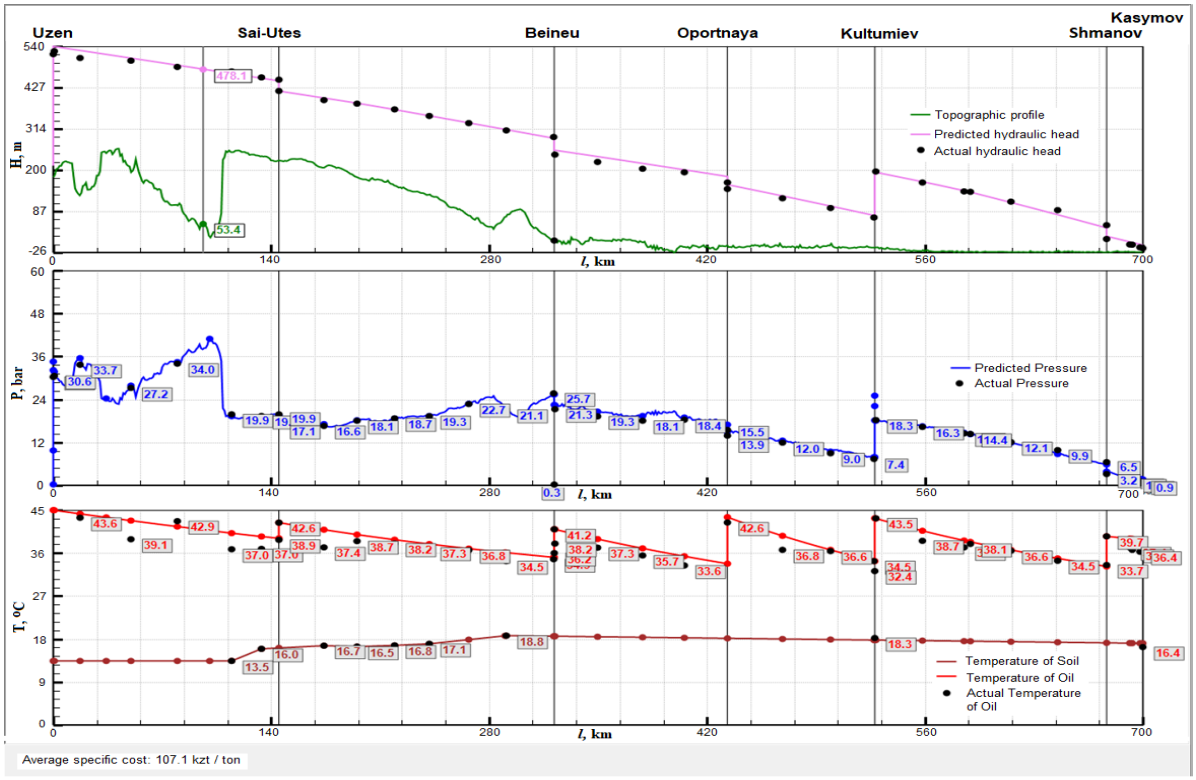

Figure 5 – Distribution of hydraulic head (upper diagram), pressure (middle diagram) and temperature (lower diagram) of the oil batch pumping

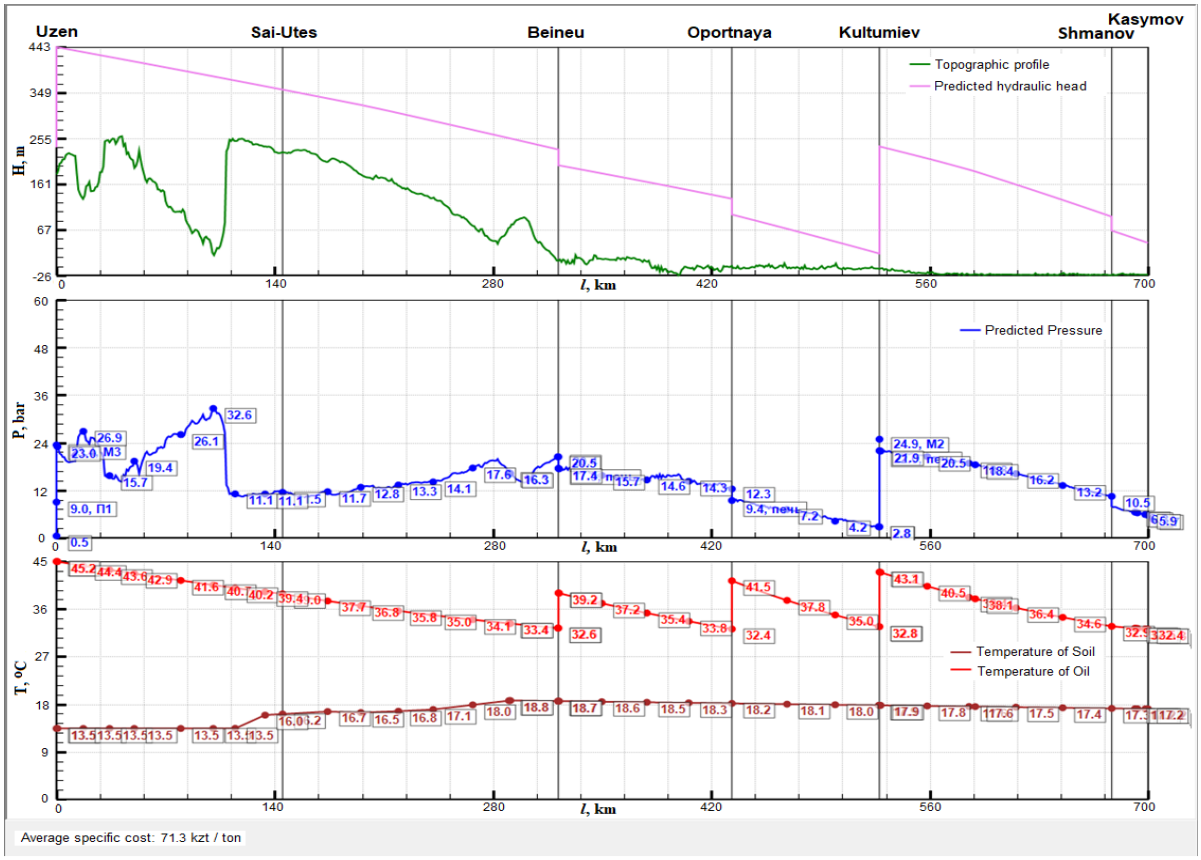

Figure 6 – Distribution of hydraulic head (upper diagram), pressure (middle diagram) and temperature (lower diagram) of batch pumping in optimal mode

According to the algorithm [25], the lower bound of the search for the heating temperature of oil blends at stations is assumed to be 32 °C. Conversely, the upper limit is determined by an optimization criterion.

Figure 6 shows the results of the search for the heating temperature of oil blends at the stations. As a result of the search, the upper limit of the heating temperature at Uzen is 45.2 °C, at Beineu is 39.2 °C, at Opornaya is 41.5 °C, and at Kultumiev is 43.1 °C (see Fig. 6).

The temperature of the oil blends within the pipeline remains consistently above 32°C, ensuring a safe thermal regime for cyclic pumping, as depicted in Figure 6.

The heating temperature decreases at the Beineu, Opornaya and Kultumiev stations, while there is no oil heating at the Sai-Utes and Shmanov stations, as shown in Figure 6. The specific cost of batch pumping decreases from $0.28 per ton (see Fig. 5) to $0.19 per ton (see Fig. 6), resulting in a savings of 32 %.

Conclusion

1. The mathematical model and algorithm for calculating the batch pumping of high-viscosity and high-pour-point oil blends through the Uzen-Atyrau industrial oil pipeline have been developed. The validity and accuracy of the mathematical model's outcomes were confirmed through rigorous validation against real-time data derived from the SCADA system.

2. The calculated data of the batch pumping through the Uzen-Atyrau industrial pipeline have been obtained:

- depending on the volume of pumped batches of Mangyshlak oil blend weighing 20,000 tons and batches of Buzachi oil blend weighing 21,000 tons;
- by searching for the optimal heating temperature of oil blends at stations with a lower limit of 32 °C and a distribution of soil temperature;

3. The identification of optimal operational conditions for the pumping units and heating furnaces has led to a noteworthy reduction of 32% in the unit costs attributed to both oil blend pumping and heating.

Conflict of interest. On behalf of all the authors, the correspondent author declares that there is no conflict of interest.

Acknowledgements. This research work was supported by the Science Committee of the Ministry of Science and Higher Education of the Republic of Kazakhstan (Grant No. AP19677859).

Cite this article as: Ramazanova GI, Bekibayev TT, Soltanbekova KA, Aldzhambekova GT. Sequential Transportation of Different Oil Batches through the Industrial Pipeline. Kompleksnoe Ispolzovanie Mineralnogo Syra = Complex Use of Mineral Resources. 2025; 332(1):108-118. https://doi.org/10.31643/2025/6445.10

Өнеркәсіптік құбыр арқылы мұнайдың әртүрлі партияларын тізбекті тасымалдау

[1*] Рамазанова Г.І., [1] Бекібаев Т.Т., [1] Солтанбекова Қ.А., [2] Алжамбекова Г.Т.

[1] Сәтбаев университеті, Алматы, Қазақстан
[2] Г.Даукеев атындағы Алматы энергетика және байланыс университеті, Алматы, Қазақстан

Мақала келді: *28 ақпан 2024*
Сараптамадан өтті: *11 наурыз 2024*
Қабылданды*: 13 наурыз 2024*

ТҮЙІНДЕМЕ

Тізбекті тасымалдау әдісінде физикалық және химиялық қасиеттері әртүрлі бірнеше сұйықтықтар бір құбыр арқылы айдалады. Мақалада өнеркәсіптік мұнай құбыры арқылы әртүрлі физикалық және химиялық қасиеттері бар мұнай қоспаларының екі партиясын тізбекті айдау қарастырылады. Жоғары парафинді мұнай партиясы бір мезгілде мұнай өңдеу зауытына айдалады, ал тұтқырлығы жоғары мұнай партиясы құбыр арқылы әрі қарай тасымалданады. Мұнай партияларының жылу физикалық және реологиялық қасиеттері арасындағы айырмашылық құбырдың жылулық жұмыс жағдайларына әсер етеді. Жоғары парафинді және жоғары тұтқыр мұнай қоспаларының кезекпен тасымалдануын есептеудің математикалық моделі мен алгоритмі құрылды. Жылу гидравликалық есептеулер айдау қондырғылары мен қыздыру пештерінің жұмыс жағдайында мұнай қоспалары

	партияларының гидравликалық қысымының, қысымының және температурасының таралуын анықтайды. Теориялық талдауды тексеру және валидациялау өнеркәсіптік құбырдың ұзындығы бойынша SCADA тәжірибелік деректерді пайдалану арқылы жүзеге асырылды. Тізбектеп айдаудың жылу режиміне сәйкес өнеркәсіптік құбыр станцияларында мұнай қоспаларын қыздыру үшін оңтайлы температуралар табылды.
	Түйін сөздер: тізбекті тасымалдау, мұнай қоспаларының партиясы, жоғары парафинді мұнай, жоғары тұтқырлы мұнай, қыздыру температурасы, өндірістік құбыр
Рамазанова Гаухар Ізбасарқызы	***Авторлар туралы ақпарат:*** *Физика-математика ғылымдарының кандидаты, жетекші ғылыми қызметкер, «Энергетикадағы модельдеу» ғылыми-өндірістік зертханасы, Сәтбаев университеті, Сәтбаев көшесі, 22 үй, 050013 Алматы, Қазақстан. E-mail: gaukhar.ri@gmil.com*
Бекібаев Тимур Талғатұлы	*Техника және технология магистрі, сектор меңгерушісі. «Энергетикадағы модельдеу» ғылыми-өндірістік зертханасы, Сәтбаев университеті, Сәтбаев көш., 22, 050013 Алматы, Қазақстан. E-mail: timur_bekibaev@mail.ru*
Солтанбекова Қарлығаш Әлімханқызы	*Мұнай және газ мамандығының магистрі. «Энергетикадағы модельдеу» ғылыми-өндірістік зертханасы, Сәтбаев университеті, Сәтбаев көш., 22, 050013 Алматы, Қазақстан. E-mail: k.soltanbekova@satbayev.university*
Алжамбекова Гүлдана Тілеужанқызы	*Техника ғылымдарының кандидат, Г.Дәукеев атындағы Алматы энергетика және байланыс университетінің ғарыштық технологиялар кафедрасының доценті, Байтұрсынов көш., 126/1, 050013 Алматы, Қазақстан. E-mail: adana@bk.ru*

Последовательная перекачка различных партий нефти по промышленному трубопроводу

[1*] Рамазанова Г.И., [1] Бекибаев Т.Т., [1]Солтанбекова К.А., [2] Алджамбекова Г.Т.

[1] Казахский национальный исследовательский технический университет им. К.И. Сатпаева , Алматы, Казахстан
[2] Алматинский университет энергетики и связи им.Г.Даукеева, Алматы, Казахстан

Поступила: *28 февраля 2024*
Рецензирование: *11 марта 2024*
Принята в печать: *13 марта 2024*

АННОТАЦИЯ

При последовательной перекачке по одному трубопроводу перекачивается несколько жидкостей с разными физико-химическими свойствами. В статье рассматривается последовательная перекачка двух партий нефтесмесей с различными физико-химическими свойствами по промышленному нефтепроводу. Это связано с тем, что партия высокопарафинистой нефтесмеси перекачивается на нефтеперерабатывающий завод, а партия высоковязкой нефтесмеси транспортируется далее по трубопроводу. Разница между теплофизическими и реологическими свойствами партий нефти накладывает условие на тепловой режим работы трубопровода. Создана математическая модель и алгоритм для расчета последовательной транспортировки высокопарафинистых и высоковязких нефтяных смесей. Теплогидравлические расчеты показывают распределение гидравлического напора, давления и температуры партий нефтесмечей в условиях работы насосных агрегатов и печей нагрева. Верификация и валидация теоретического анализа проводилась с помощью экспериментальных данных SCADA по длине промышленного трубопровода. В соответствии с тепловым режимом последовательной перекачки найдены оптимальные температуры нагрева нефтяных смесей на станциях трубопровода.

Ключевые слова: последовательная перекачка, партия нефтяных смесей, высокопарафинистая нефть, высоковязкая нефть, температура подогрева, промышленный трубопровод.

Рамазанова Гаухар Избасаровна — ***Информация об авторах:***
Кандидат физико-математических наук, ведущий научный сотрудник. Научно-производственная лаборатория "Моделирование в энергетике", КазНИТУ им. К.И. Сатпаева, ул. Сатбаева, 22, 050013 Алматы, Казахстан. E-mail: gaukhar.ri@gmail.com

Бекибаев Тимур Талгатович — *Магистр техники и технологии, заведующий сектором. Научно-производственная лаборатория "Моделирование в энергетике", КазНИТУ им. К.И. Сатпаева, ул. Сатбаева, 22, 050013 Алматы, Казахстан. E-mail: timur_bekibaev@mail.ru*

Солтанбекова Карлыгаш Алимхановна — *Магистр по специальности нефтегазовое дело, руководитель отдела. Научно-производственная лаборатория "Моделирование в энергетике", КазНИТУ им. К.И. Сатпаева, ул. Сатбаева, 22, 050013 Алматы, Казахстан. E-mail: k.soltanbekova@satbayev.university*

Алждамбекова Гульдана Тлеужановна — *Кандидат технических наук, доцент, кафедра космической техники, Алматинский университет энергетики и связи им. Г. Даукеева, ул. Байтурсынова, 126/1, 050013 Алматы, Казахстан. E-mail: adana@bk.ru*

References

[1] Cui XG, Zhang JJ. The research of heat transfer problem in process of batch transportation of cool and hot oil. Oil Gas Storage and Transportation. 2013; 23(11):15-19. http://dx.doi.org/10.3969/j.issn.1000-8241-D.2004.11.006

[2] Cui X, Dong X, Zhang Z, Sun X, Gu W, Zhang H. The application analysis of batching transportation of cool and hot crude oil for Jinhua pipeline. Journal of Petrochemical Universities. 2015; 28(6):87-92. http://dx.doi.org/10.3969/j.issn.1006-396X.2015.06.016

[3] Han D, Yu B, Wang, Y, Zhao Y, Yu G. BFC-POD-ROM Aided Fast Thermal Scheme Determination for China's Secondary Dong-Lin Crude Pipeline with Oils Batching Transportation. Energies. 2018; 11(10):2666. https://doi.org/10.3390/en11102666

[4] Yuan Q, Wu CC, Yu B, Han D, Zhang X, Cai L, Sun D. Study on the thermal characteristics of crude oil batch pipelining with differential outlet temperature and inconstant flow rate. Journal of Petroleum Science and Engineering. 2018; 160:519-530. https://doi.org/10.1016/j.petrol.2017.10.074

[5] Liang Y, Zhang N, Jiang X, Zhou J. A feasibility study of light hydrocarbon batching transportation through pipeline networks. Natural Gas Industry. 2014; 34(4):121-124. https://doi.org/10.3787/j.issn.1000-0976.2014.04.020

[6] Yablonsky VS, Yufin VA, Budarov IP. Posledovatelnaya perekachka neftei i nefteproduktov po magistralnym truboprovodam [Sequential pumping of petroleum products and oils through main pipelines]. Moscow: Gostoptekhizdat. 1959. (in Russ.).

[7] Garcia-Hernandez A. Modeling and simulation case study of a batching operation of crude oils in a pipeline system. Pipeline Simulation Interest Group Annual Meeting; 24-27 May 2011. Napa Valley, California, United States, PSIG-1111.

[8] Nechval MV, Novoselov VF, Tugunov PI. Posledovatelnaya perekachka neftei i nefteproduktov [Sequential pumping of oils and oil products through main pipelines]. Moscow: Nedra. 1976. (in Russ).

[9] Lurie MV, Timofeev FV, Sereda SV. Raskladka smesi pri posledovatelnoi perekachke nefteproduktov [Mix layout for sequential pumping of petroleum products]. Nauka i tehnologii truboprovodnogo transporta nefti i nefteproduktov = Science and technology of pipeline transport of oil and petroleum products. 2017; 7:42-47. (in Russ.).

[10] Rejowski R, Pinto JM. Scheduling of a multiproduct pipeline system. Computers & Chemical Engineering. 2003; 27(8-9): 1229-1246. https://doi.org/10.1016/S0098-1354(03)00049-8

[11] Li Zh, Liang Y, Liao Q, Zhang B, Zhang H. A review of multiproduct pipeline scheduling: from bibliometric analysis to research framework and future research directions. Journal of Pipeline Science and Engineering. 2021; 1(4):395-406. https://doi.org/10.1016/j.jpse.2021.08.001

[12] Ghenaati SH, Aghaei S. Modeling and MPC-based Method for Planning Transportation of Multiple Oil Products in Pipeline Network. 27th Iranian Conference on Electrical Engineering (ICEE); 30 April - 2 May. Yazd, Iran. 2019, 1145-1150. https://doi.org/10.1109/IranianCEE.2019.8786581

[13] Han D, Yu B, Wang Y, Zhao Y, Yu G. Fast thermal simulation of a heated crude oil pipeline with a BFC-Based POD reduced-order model. Applied Thermal Engineering. 2015; 88:217-229. https://doi.org/10.1016/j.applthermaleng.2014.10.017

[14] Herran A, de la Cruz JM, de Andres B. A mathematical model for planning transportation of multiple petroleum products in a multi-pipeline system. Computers & Chemical Engineering. 2010; 34(5):401-413. https://doi.org/10.1016/j.compchemeng.2009.11.014

[15] Serediuk MD. Methods of hydrodynamic calculation oil pipeline sequential transportation of small batches of various oil. Archives of Materials Science and Engineering. 2022; 117:25-33. https://doi.org/10.5604/01.3001.0016.1394

[16] Wang K, Zhang J-J, Yu B. Optimal heating ratio of batch pipelining of cold and hot crude oils. Journal of China University of Petroleum. (Edition of Natural Science). 2008; 32(5):102-107.

[17] Polania JN, Algarin CR, Fula JG. Predictive-cooperative control for the operation of a centrifugal pump network in a serial multiproduct pipeline system. Ingeniare. 2015; 23:38-49. http://dx.doi.org/10.4067/S0718-33052015000100005

[18] Schlikhting G. Teoriya pogranichnogo sloya [Boundary Layer Theory]. Nauka: Moscow, USSR. 1974. (in Russ.).

[19] Colebrook CF, White CM. Experiments with fluid friction in roughened pipes. Proceedings of the Royal Society of London. Series A, Mathematical and Physical Sciences. 1937; 161:367-381. https://doi.org/10.1098/rspa.1937.0150

[20] Altshul AD. Gidravlicheskie soprotivleniya [Hydraulic resistance]. Moscow: Nedra. 1982. (in Russ.).

[21] Agapkin VM, Krivoshein BL, Yufin VA. Teplovoi i gidravlicheskii raschety truboprovodov dlya nefti i nefteproduktov [Heat and hydrodynamic calculations for oil and oil products pipelines]. Moscow: Nedra. 1981. (in Russ.).

[22] Bekibayev TT, Zhapbasbayev UK, Ramazanova GI, Bossinov DZh. Oil pipeline hydraulic resistance coefficient identification. Cogent Engineering. 2021; 8:1950303. https://doi.org/10.1080/23311916.2021.1950303

[23] Anderson D, Tannehill JC, Pletcher RH. Computational Fluid Mechanics and Heat Transfer. Boca Raton: CRC Press; 2020. https://doi.org/10.1201/9781351124027

[24] Beysembetov IK, Bekibayev TT, Zhapbasbayev UK, Ramazanova GI, Panfilov M. SmartTran software for transportation of oil JSC KazTransOil. News of the National Academy of Sciences of the Republic of Kazakhstan, Series of Geology and Technical Sciences. 2020; 2(330):5-13. https://doi.org/10.32014/2020.2518-170X.25

[25] Zhapbasbayev UK, Ramazanova GI, Bossinov DZh, Kenzhaliyev BK. Flow and heat exchange calculation of waxy oil in the industrial pipeline. Case Studis Thermal Eng. 2021; 26:101007. https://doi.org/10.1016/j.csite.2021.101007

Crossref

DOI: 10.31643/2025/6445.11
Metallurgy

Mechanism and technological results of sulfidation roasting of oxidized lead compounds

[1]Chepushtanova T.A., [1*]Merkibayev Y.S., [1]Mamyrbayeva K.K., [1]Sarsenbekov T., [2]Mishra B.

[1]Satbayev University, Almaty, Kazakhstan
[2]Worcester Polytechnic Institute, Worcester, USA

** Corresponding author email: y.merkibayev@satbayev.university*

Received: *March 11, 2024*
Peer-reviewed: *April 9, 2024*
Accepted: *April 16, 2024*

ABSTRACT

The paper presents the results of a critical analysis of existing technologies for processing lead-zinc ores and industrial products; the relevance of the research lies in the development of methods aimed at additional extraction of zinc and lead in conditions of a rapid decrease in the content of lead and zinc in ores. The paper presents research on the thermodynamic justification of sulfiding roasting, the results of the development of technology for intensifying the process of processing poor, difficult-to-process complex lead-zinc ores and middlings through preliminary thermal activation by sulfiding roasting in a fluidized bed furnace. The mechanism of sulfidation of oxylated lead compounds has been established according to the scheme: PbO → PbO·PbSO4 → PbSO4 → PbS. The results of the physicochemical study of roasting products, as well as the results of magnetic enrichment of cinders, are presented. The results of magnetic separation of cinders after heat treatment of industrial products show that it is possible to separate up to 70% of iron in the form of pyrrhotite into a magnetic product, while the pyrrhotite content in the magnetic product is up to 98.2%. The paper presents a new technological scheme for processing lead-zinc industrial products from enrichment to obtain pyrrhotites with predicted properties.

Keywords: lead, lead-containing waste, refractory ores, sulfidizing roasting, fluidized bed furnaces, sulfidation, pyrite

Information about authors:

Chepushtanova Tatyana Aexandrovna — *Candidate of Technical Sciences, PhD, Head of Department "Metallurgical processes, heat engineering and technology of special materials", Associate Professor, Mining and Metallurgical Institute, Satbayev University, Almaty, Kazakhstan. Email: T.Chepushtanova@satbayev.university*

Merkibayev Yerik Serikovich — *Master's degree, head of laboratories of the JSC "Satbayev University", Mining and Metallurgical Institute, Almaty, Kazakhstan. Email: y.merkibayev@satbayev.university*

Mamyrbayeva Kulzira Kaldybekovna — *PhD, Associate Professor, Department "Metallurgical processes, heat engineering and technology of special materials", Mining and Metallurgical Institute, Satbayev University, Almaty, Kazakhstan. Email: k.mamyrbayeva@satbayev.university*

Sarsenbekov Turar — *PhD student, of the JSC "Satbayev University", Mining and Metallurgical Institute, Almaty, Kazakhstan. Email: t.sarsenbekov@satbayev.university*

Brajendra Mishra — *Professor and MPI Director of Mechanical and Materials Engineering, Worcester Polytechnic Institute, Worcester, USA. Email: bmishra@wpi.edu*

Introduction

Currently, not only in Kazakhstan but also in the world, zinc and lead are the most important metals that form modern industry, the metallurgical industry and the circular economy (circular economy) of different countries of the world (Circular Economy (CE)) [1]. The main amount of lead (over 65%) is used for the production of batteries, a significant part of which is used for the manufacture of electrical cable sheaths. Zinc is used mainly (up to 50%) as anti-corrosion coatings and for galvanizing surfaces. Also, a significant amount of zinc is consumed in the production of various types of alloys with the addition of aluminum, copper and magnesium, which have good casting properties. Innovative uses of zinc have increased by 30% since 2015 as nanomaterials in the form of zinc ferrites, zinc-ion batteries provide higher power density and longer life. The innovative use of lead is also growing by more than 10% each year through its use as

nanostructured lead electrodes to operate lead-acid batteries.

According to the content of basic metals, lead-zinc ores are classified into: rich with a lead content above 4% or with a total content of lead and zinc above 7%; medium quality (ordinary), containing from 2 to 4% lead or a total of lead and zinc from 4 to 7%; poor with a lead content of 1.2 - 2% or a total lead and zinc content of 2 - 4%. Over the past 10 years, since 2013, ores with a lead and zinc content of less than 2 - 3.5% have been used in the industry.

Zinc and lead are extracted mainly from sulfide raw materials using pyrometallurgical technologies, however, a decrease in the liquid concentration of lead and zinc in sulfide ores has been recorded in many deposits around the world. Due to the increasing consumption of natural resources in the world, primary resources will soon become insufficient to meet the demand for lead, and Pb–Zn oxide ore, typically containing 1%-5% Pb and 1%-20% Zn, may become a valuable source to meet in need of the above metals. Extracting valuable metals from refractory ores, characterized by a complex composition and high content of carbonates and silicon, seems to be the most difficult task. Lead and zinc are mainly found in the form of carbonates in the ore, and in recent years many technologies such as flotation or flotation combined with gravity separation, hydrometallurgy and pyrometallurgy have been tried to treat such refractory ore.

Difficulties in processing such raw materials arise at all stages of processing, at the flotation stage, there is a problem with the use of Na2S as a sulfidizer, the consumption is too high due to non-selective adsorption on sludge, and desliming is required before flotation, while the loss of metals in the fine fraction remains high [[2], [3]].

To solve these problems, various hydrometallurgical processes, including acid and alkaline leaching, have been introduced. Sulfuric acid leaching seems to be the most promising for zinc recovery from economic and environmental points of view. However, Pb-Zn oxide ore usually contains large amounts of silica, which can also dissolve and then gel, preventing the leach solution from separating from the residue. In addition, a significant amount of carbonate containing gangue will react with acid, resulting in high operating costs.

The mechanochemical process of processing non-ferrous metal oxides by grinding with sulfur and iron powders at room temperature turned out to be unfeasible in practice due to the high energy costs required to obtain a satisfactory degree of sulfidation [[4], [5], [6]].

Hydrothermal sulfidation has also been proposed for the treatment of zinc-containing compounds [[7], [8], [9]], but it remains a major challenge to achieve satisfactory recovery due to artificial sulfides characterized by fine crystallization.

A feature of difficult-to-process ores is the complex mineralization of valuable components, significant oxidation and mutual germination of minerals. The practice of processing plants has shown that direct processing of such ores using enrichment methods, even when selecting a reagent regime and improving enrichment schemes, does not give satisfactory results. From the analysis of literary sources and the practice of domestic and foreign enterprises, it follows that a solution to this problem must be sought in the development of combined technologies.

Of particular relevance is the use of preliminary preparation of ores for enrichment through thermal activation of non-ferrous metal minerals. Among them, the method of activating and high-temperature roasting of ore minerals has a significant effect.

Thermodynamic justification of sulfiding friction of oxidized lead compounds

The most promising technology for processing oxidized and mixed polymetallic ores is a technology that involves preliminary sulfidation of oxidized compounds of non-ferrous metals with pyrite or elemental sulfur under pyrrhotinizing roasting conditions, followed by the separation of non-ferrous metals into appropriate concentrates.

The use of partial pressure diagrams has been used by many authors, however, to substantiate the sulfidation process, it is necessary to establish data under the conditions being developed [10].

When processing oxidized lead-zinc ores, the composition is mixed, i.e. sulfide-oxide, or predominantly oxide. Middlings are also mixed and oxidized in composition: FeS_2, PbO, $PbCO_3$, PbS, $PbSiO_3$.

To study the thermodynamics of physical and chemical transformations, the HSC-5 software package developed by Outocumpu Ou was used.

Thermodynamic analysis of the behavior of complex oxygen-containing compounds of zinc and lead was performed based on calculations of ΔG^0 and logKp of possible reactions. Previous studies have established that the thermal decomposition of

pyrite begins at temperatures of about 600 0C, so we chose a temperature range of 600 - 900 0C for thermodynamic analysis.

Thermodynamic characteristics (Table 1) show that at temperatures of 600 - 900 ^{0}C, decomposition of lead zinc carbonates will occur with the formation of zinc and lead oxides, respectively. Aluminates and silicates of zinc and lead are stable at temperatures of 600 - 900 0C.

Thus, oxides, aluminates and silicates of zinc and lead will participate in high-temperature sulfidation processes.

Table 1 - Values of thermodynamic characteristics of the decomposition reactions of oxidized lead and zinc compounds

Reaction	lgKp/ΔG0 , kJ at T, 0C	
	700	900
PbCO3 = PbO+CO2	2.80/-52.3	3.396/-76.2
PbSiO3 = PbO+SiO2	-0.87/16.2	-0.85/20.4
Pb2O3 = 2PbO+1/2O2	1.19/-22.2	1.551/-34.8
PbO2 = PbO+1/2O2	2.056/-9.1	2.320/-3.7
Pb2SiO4 = 2PbO+SiO2	-2.12/39.6	-1.979/40.9

Phase transformations in the Pb-S-O system

The results of thermodynamic analysis of the Pb-S-O system are presented in Table 2 and Fig. 1. When firing pyrite, elemental sulfur is present in the gas phase and its pressure can reach 10 Pa or more. Therefore, during the thermodynamic analysis of the Pb-S-O system, calculations of logKp and ΔG0 of the reactions of the interaction of lead oxides with elemental sulfur and pyrite were performed.

In the Pb-S-O system, the stable condensed phases are PbS, PbO, Pb, PbSO4, PbO·PbSO4. Thermodynamic calculations of the potentials of the reactions of sulfidation of lead oxide with elemental sulfur, carried out using the method of reduced potentials, showed that sulfidation in the temperature range of 600-900 ^{0}C is thermodynamically possible and can proceed both with the direct production of lead sulfide and with the initial production of a number of intermediate compounds with the subsequent formation of lead sulfide. At low temperatures, the formation of intermediate oxysulfates and lead sulfate is thermodynamically more likely. When the temperature rises to 900 0C, the possibility of direct production of sulfide and the formation of intermediate metallic lead with its subsequent sulfidation increases significantly.

Table 2 - Values of thermodynamic characteristics of reactions in the Pb-S-O system

Reaction	lgKp/ΔG^0 , kJ/mol at T, ^{0}C	
	700	900
$4/3PbO+S_2=4/3PbS+2/3SO_2$	6.9/129	5.8/124
$PbSO4+S_2=PbS+2SO_2$	5.3/100	6.1/132
$2PbO+PbS=3Pb+SO_2$	0.0/0,0	1.7/38
$4PbO+S_2=4Pb+2SO_2$	6.9/129	8.0/172
$2Pb+ S_2=2PbS$	6.9/129	4.6/100
$2PbO+SO_2=PbSO_4+Pb$	1.6/30	0.23/4,9
$12/7PbO+S_2=2/7PbSO_4+10/7PbS+2/7SO_2$	7.3/138	5.6/122
$24/9PbO+S_2=12/9PbS+2/9SO_2+4/9(2PbO*PbSO_4)$	20.7/385	9.1/411
$2PbO+S_2+5/2O_2=(PbSO_4*Pb)+SO_2$	30.6/571	22.5/485
$4/7(PbO*PbSO_4)+S_2=8/7PbS+10/7SO_2$	10.7/198	10.6/229
$3PbS+2(PbSO_4*PbO)=7Pb+5SO_2$	13.3/248	21.0/452

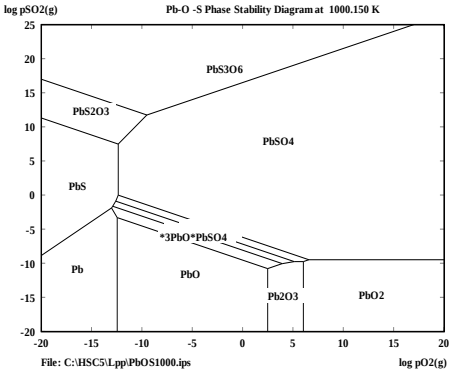

Figure 1 - Diagram of phase equilibria of the Pb-S-O system depending on temperature

Thus, sulfidation of lead oxide in a wide range of sulfur pressures in the gas phase, depending on temperature, can proceed according to the following mechanisms: PbO → PbO $PbSO_4$ → $PbSO_4$ → PbS. As the temperature increases, it is preferable to carry out direct sulfidation: PbO → PbS.

Lead-zinc tailings from the Ridder enrichment plant of Kazzinc LLP were used as feedstock. Pyrite contained in the tailings was used as a sulfidizer.

The chemical compositions of lead-zinc flotation tailings and pyrite concentrate are given in Table 3.

Table 3 - Chemical composition of lead-zinc tailings and pyrite concentrate

Name of elements	Lead-zinc tailings, %	Pyrite concentrate, %
Pb	0.169	0.719
Al	7.548	5.049
Cu	0.9	0.548
Fe	12.947	32.946
Si	49.789	22.29
Mn	0.289	1.89
P	0.69	0.39
Cu	0.09	0.48
Zn	0.52	6.49
Mg	3.3	1.702
Fe	12.88	32.89

Method of high-temperature sulfidation firing in a fluidized bed furnace

High-temperature sulfidation roasting was carried out in a fluidized bed furnace. A diagram of an enlarged laboratory installation for firing in a fluidized bed furnace is shown in Figure 2.

The installation of a fluidized bed furnace includes the following main components and mechanisms: a fluidized bed furnace reactor with an adjustable continuous system for loading the charge and unloading the cinder; a gas duct with a system for coarse and fine dust collection, condensation of sublimates and absorption of sulfur dioxide from exhaust gases, air heating units and the furnace reactor, a system for adjustable supply and control of air blast flow, a control unit and control of the temperature regime in the furnace.

The reactor of the fluidized bed furnace of rectangular cross-section with a hearth area of 120 cm^2 is made of XI8N90T stainless steel, and the hearth is made of stainless heat-resistant mesh with a hole size of up to 5 microns. The charge is loaded into the reactor from above in a non-breakthrough mode using two screw feeders driven by reversible engines of the KD-30-U4 type. The rotation speed of the screws is selected depending on the specified loading mode of the material and is regulated by changing the voltage supplied to the motors from a laboratory autotransformer.

The cinder is unloaded from the furnace into a sealed bunker by a horizontal auger located 15 cm from the hearth level. The height of the discharge window can vary depending on the material being fired and the specified operating mode of the furnace.

The exhaust gases from the reaction zone through the furnace charge enter a heated flue, equipped with three cascaded cyclone chambers for coarse and fine dust collection, a sublimation condenser and an absorber for fine dust and sulfur dioxide. Through the work program, experiments were carried out at the enlarged laboratory installation of a fluidized bed furnace to test the operating parameters of sulfiding roasting of zinc-oligonite ore from the Zhairem deposit.

The preparation of a charge of a given composition was carried out by thoroughly mixing the original ore with a particle size of 0.1-0.25 mm with pyrite concentrate with a size of 0.074 mm 90%, taken in the required proportions. The finished mixture was loaded into the furnace feed hopper.

Before starting the furnace, a “bed” of previously burned material (cinder) weighing up to 1.0-1.5 kg was laid on the hearth. The firing conditions for the “bed” and the supply of “fresh” mass of ore and pyrite concentrate remained unchanged, the addition of pyrite concentrate varied from 50 to 75%, the firing parameters were calculated based on the $NMeO/NFeS_2$ ratio, the degree of sulfidation, %, with the best indicators being the firing conditions in the temperature range 700 – 800 °C.

Simultaneously with heating the furnace to a given temperature, the air blast flow rate was set, which on average varied from 8.0 to 20 l/min. Upon reaching the specified temperature in the cinder layer, loading of the charge into the furnace began with simultaneous adjustment of the screw rotation speed, ensuring the specified productivity. After the furnace bath had reached the unloading window, the unloading screw was turned on and after 2-3 times the exchange of material in the reaction zone, the selection of burnt cinder into a sealed bunker began.

During the preparation of the furnace for operation, a vacuum was established in the flue duct and under the roof of the furnace and an alkaline solution was poured into the bubbler to neutralize the gases. Unloading of collected dust from cyclones and sublimations from the condenser was carried out after each experiment before switching to another firing mode.

The unloaded firing products (cinder, dust, sublimates) were weighed, averaged and selected

for chemical analysis for zinc, sulfur and iron. Individual samples were subjected to mineralogical and X-ray phase analyses.

The progress of the technological process was monitored according to the following parameters: blast flow rate, charge loading rate, temperature in the fluidized bed and the gas duct, and composition of roasting gases and roasting products.

During the ongoing research, the influence of temperature on the degree of sulfidation of zinc oxides in the range of 650-800ºC, the influence of the composition of the charge and the sulfur potential in the system were studied. The ratio of pyrite concentrate to ore is 1:1 and 2:1.

The change in sulfur potential, depending on the ratio of pyrite concentrate to ore, was determined by calculation depending on the amount of oxygen supplied with air blast and the amount of sulfur introduced with the charge per unit time; in this case, the blast flow rate varied from 10 to 20 l/min, and the charge loading varied from 10 to 60 g/min. By sulfur potential we mean thermodynamic conditions in the S-O system or phase equilibria in the Fe-S-O system in an aggregate, the release and concentration of sulfur (elemental sulfur) directly in the fluidized bed. The source of heat required for the dissociation of pyrite is the heat released during the oxidation of the dissociation product - elemental sulfur directly in the fluidized bed, which allows its losses to be reduced to a minimum.

Good conditions of heat and mass transfer, characteristic of a fluidized bed, allow for quite intensive dissociation of pyrite. Since the thermal effect of the oxidation of elemental sulfur significantly exceeds the thermal effect of thermal dissociation, it becomes possible to oxidize only part of the sulfur released during dissociation in the layer. In this case, 95% or more per cent of the blast oxygen is used to produce gases containing up to 20% sulfur dioxide. In addition, part of the sulfur 1-4%, depending on the firing conditions, is obtained in the form of elemental sulfur.

It has been established that at 650°C favorable conditions are created for obtaining the maximum sulfur potential in the system, associated with the kinetic laws of thermal dissociation of pyrite, oxidation and distillation of dissociated sulfur.

Enlarged laboratory installation for sulfidation firing in a fluidized bed furnace, Figure 2.

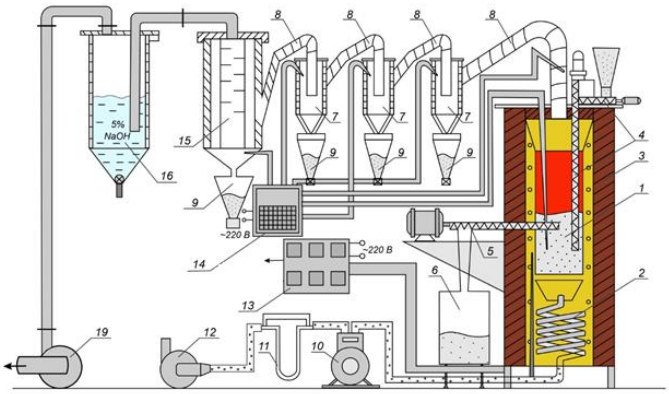

1 – reactor; 2 – air heating unit; 3 – fluidized bed furnace; 4 – loading unit; 5 – unloading unit; 6 – cinder hopper; 7 – cyclone; 8 – heated flue; 9 – dust bin; 10 – gas meter; 11 – rheometer; 12 – blower; 13 – furnace control unit; 14 – potentiometer KSP; 15 – capacitor; 16 – bubbler; 17 – valve; 18 – adjustable damper; 19 – smoke exhauster

Figure 2 - Enlarged laboratory installation for sulfidation roasting in a fluidized bed furnace

Component distribution and firing material balance

According to the balance, the cinder yield is 56-65% of the original charge, 20-21% dust yield and 15-23% loss with gases in the form of fine dust up to 3-4% and sulfur dioxide. An increase in temperature from 650 to 750°C leads to a decrease in the yield of cinder and an increase in gas formation, which is easily explained by the kinetic laws of the processes of dissociation and oxidation of pyrite, as well as a more complete decomposition of carbonate compounds. When the pyrite ore ratio is increased to 2:1, the distribution of products is similar to the 1:1 ratio.

The distribution of sulfur in the roasting products, depending on the temperature, changes in the direction of increasing sulfur oxidation with increasing temperature and its removal with gases in the form of sulfur dioxide up to 50%. In this case, the sulfur content in the cinder varies from 16.6 to 15.8% (1:1) and from 19.8 to 18.6% (2:1), and the iron content from 26 to 27% and from 31 to 33 % respectively. The inversely proportional change in the contents of sulfur and iron in the cinder is associated with the kinetic laws of thermal dissociation of pyrite, when the removal of sulfur from pyrite occurs at a very high speed and the oxidation of pyrrhotite begins.

Table 4 - Results of spectral analysis

Elements	Contents of elements, %, 10^3		
	Ore	Pyrite	Cinder
Zinc	2000	100	1000
Lead	120	60	100
Copper	6	150	150
Manganese	1000	80	200
Arsenic	10	80	30
Nickel	4	8	10
Strontium	20	-	10
Barium	100	100	400
Titanium	100	60	100
Vanadium	4	-	2
Chromium	2	-	-
Zirconium	10	-	6
Antimony	2	10	4
Tin	0.2	-	-
Cobalt	3.0	5.0	8.0
Molybdenum	0.4	2.0	3.0
Cadmium	3.0	-	3.0
Beryllium	0.2	-	-
Bismuth	-	-	0.6
Germanium	0.15	15.0	-
Gallium	0.8	0.4	1.0
Thallium	0.6	0.4	0.5
Gold	-	0.8	0.8
Silver	1.0	8.0	6.0

The distribution of zinc among the roasting products, depending on the temperature and the pyrite-ore ratio, varies slightly and lies in the range of 83-86% in cinder and 14-17% in dust. Losses of zinc in the form of sublimates and fine dust do not exceed 2-3%. The dust removed from the reactor is mainly dust from pyrite concentrate, which is finer ground than ore, as confirmed by the results of mineralogical analysis. As a result, an increase in the content of pyrite concentrate in the charge leads to an increase in the extraction of zinc and iron in the dust, which is due to the close intergrowth of zinc with pyrite in the initial concentrate.

Measurements of the composition of the gas phase showed that the oxygen content (arrived with air blast) in the exhaust gases does not exceed 0.2-0.4%, while the sulfur dioxide content varied from 8 to 18% depending on the amount of air blast supplied.

The distribution of rare and trace elements among the firing products was assessed based on the results of a full spectral analysis presented in Table. 4.

From the data obtained, we believe that part of the rare and trace elements, under certain process conditions, is concentrated in dust and roasting sublimes, which determines the practical value of separate processing of dust. This work does not involve the task of processing the resulting dust; these studies are planned to be carried out in future projects.

Characteristics of firing products and evaluation of the results obtained

Based on the results of the phase analysis of zinc compounds, the degree of sulfidation during the firing process was determined. At the same time, the extreme nature of zinc sulfidation was established at all pyrite concentrate: ore ratios depending on temperature. The maximum degree of sulfidation is 88% at a temperature of 650°C and a ratio of 2:1 - concentrate: ore. This is because at 650°C favourable conditions are created for obtaining the maximum sulfur potential in the system, associated with the kinetic laws of thermal dissociation of pyrite, oxidation and distillation of dissociated sulfur. With increasing temperature, the established proportions shift towards increasing the rate of pyrite dissociation and removal of unreacted sulfur, which leads to the interaction of blast oxygen with pyrrhotite and the resulting zinc sulfide.

Mineralogical analysis, carried out by dividing samples into light and heavy fractions, showed that in cinders of sulfiding roasting zinc is represented by sphalerite, which is present 60-70% in the form of independent grains and 30-35% in the form of small anhedral dissemination in carbonate waste rock fragments. Sphalerite inclusions in pyrrhotite are observed. An increase in the pyrite content in the charge leads to an increase in both free grains of zinc sulfide and those bound in pyrrhotite. Carbonate zinc in the fired products did not come into view, and X-ray phase analysis did not show peaks characteristic of it. Formations of zinc-containing aluminosilicates, which were probably previously present in the ore, are found in single grains. Individual grains of galena (traces) are observed in a free state and in intergrowths with pyrrhotite, but cerussite is not found.

The cinder under study under the binocular is a black sooty material, in which porosity and a cellular structure are observed and consists mainly of pyrrhotite and a fine black mass. In polished sections, pyrrhotite is presented in a wide variety of forms with intricately sinuous outlines. Myrmikitic and eutectoid types of intergrowth with sooty

material are noted. There are grains of three component compositions. When observed in immersion oil, pyrrhotite, a finely dispersed, matte gray and intermediate product with finely aggregated secondary pyrite, is identified in them. The intermediate product has less reflectivity and better seed ability from the action of concentrated nitric acid. Pyrrhotite in these grains forms peripheral rims and branching veins in the grain, the gaps which are made of fine aggregate mass.

Copper is present in the form of chalcopyrite with a film of black-blue chalcocite, which was found in the original ore. However, after heat treatment of chalcopyrite, chalcocine formations began to stand out brighter than in the original ore. Formations of the second phase, represented by cubanite, appeared and an increase in the chalcocite structure was observed.

The volume of carbonate rocks with sulfide dissemination decreases from 80% to 25% in the heavy fraction and from 95% to 25% in the light fraction for materials larger than 0.05 mm. In the heavy fraction of materials less than 0.03 mm, only sooty material with pyrrhotite (100%) was found, and in the light fraction, carbonates are represented by 50%, while in the original ore, carbonates are present in the heavy fraction by 73%, and in the light fraction by 73%. 80%.

It should be noted that after firing, sphalerite is present only in material larger than 0.05 mm. It follows from this that the newly formed zinc sulfides and the original sphalerite are enlarged to 50-60 microns.

The X-ray fluorescence analysis of sulfidation cinders confirmed the presence of the identified phases of mineralogical analysis, Figure 3.

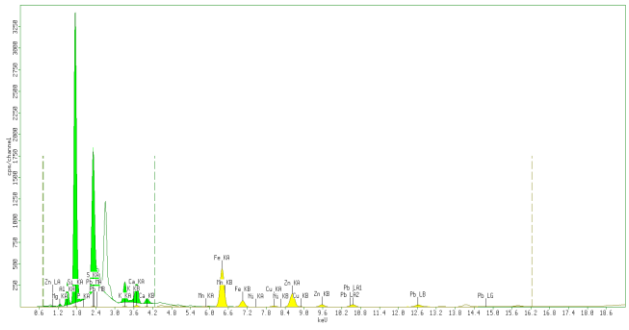

Figure 3 - Results of X-ray fluorescence analysis of sulfidation cinders

From the results of X-ray fluorescence analysis, it is clear that with increasing temperature the amount of sulfide decreases (the intensity of zinc peaks decreases), which is due to the excess of the rate of pyrite dissociation over the rate of sulfidation. The product of pyrite dissociation are pyrrhotites of composition $Fe_{0.62}S$ to $Fe_{0.9}S$, which have high magnetic properties. There are no zinc carbonate compounds, which indicates the complete decomposition of these compounds.

Mineralogical analysis of cyclone dust showed that they are 50-70% represented by pyrrhotite with sooty material, 3-4% undecomposed pyrite with limonite films, 15-37% carbonates and about 10% quartz. Sphalerite and other sulfides in the dust of the first two cyclones are present in the signs, and only in the third cyclone, their amount reaches 1-3%.

Pyrrhotite with sooty material is most concentrated in the second cyclone (67-68%). The carbonate content increases as the cyclones pass and in the third reaches 35-37%. On the contrary, the amount of quartz decreases and only traces are found in the third cyclone. In the first cyclone, hematite was found in the heavy fraction with a particle size of more than 0.05 mm, the origin of which can be attributed to both direct dust entrainment and oxidation of pyrrhotite.

The results of X-ray diffraction analysis of roasting dust showed the presence of pyrrhotite, hematite, magnetite, quartz and sphalerite in the dust, which confirms the data of mineralogical analysis.

The qualitative and quantitative characteristics of the roasting products presented according to mineralogical, X-ray diffraction and chemical phase analyzes allow us to conclude that sulfiding roasting of acidified lead-zinc ore together with pyrite concentrate proceeds most fully and efficiently at a temperature of 650 ºC and a pyrite:ore ratio of 1:1 and 2:1. As a result of heat treatment of ore under these conditions, almost complete destruction of non-ferrous metal carbonates is achieved, the opening of zinc intergrowths with pyrite and waste rock, an increase in grain size both in size and in connection with the components of the charge, deep sulfidization of oxide particles of non-ferrous metals and the conversion of iron into form magnetic pyrrhotite, which makes it possible to separate it from cinders using magnetic enrichment methods.

Thus, the large-scale laboratory studies carried out on the sulfidation roasting of lead-zinc ore in a fluidized bed furnace made it possible, based on the results of the balance of metals, their distribution

and the qualitative characteristics of the roasting products, to establish optimal conditions for conducting the sulfidation process.

Enrichment of roasting products

The results of previous studies [[11], [12], [13], [14], [15], [16], [17], [18]] and the study of the characteristics of roasting products showed that sulfides of non-ferrous metals obtained by sulfidation of oxides and carbonates have high hydrophobic properties, and pyrrhotite, a product of pyrite decomposition, has a significant magnetic susceptibility. All this predetermines further methods for processing sulfidation products. The preliminary removal of magnetic pyrrhotite into a separate product during magnetic enrichment will make it possible to obtain a commercial iron-containing product and zinc-enriched material for flotation processing.

Results of magnetic enrichment of cinders

The magnetic properties of the resulting firing products (cinder, dust) were studied on a KLY-2 cappameter (Czech Republic) with a sensitivity of 3-5·10^{-8} SI, which makes it possible to obtain magnetic susceptibility values characterizing the magnetic properties of the substance. The results of magnetic susceptibility measurements are graphically presented in Fig. 4.

Shown in Fig. 4. The dependences show that with increasing temperature, the magnetic susceptibility of the dissociation products of pyrite concentrate increases from 0.5 SI units at 650 ºC to 1.78 SI units at 750 ºC, and for cinders with an initial pyrite: ore ratio of 1:1 from 0, 3 SI units at 650 ºC to 0.98 SI units at 750 ºC.

The original pyrite concentrate and zinc-oligonite ore have a zero magnetic susceptibility value, and the roasting product of the original ore has a low magnetic susceptibility value, which ranges from 0.01-0.2 SI units when the temperature changes from 650 to 750 ºC [[18], [19], [20], [21], [22], [23], [24]].

The results obtained indicate that the magnetic susceptibility of roasting products depends on the completeness of pyrite dissociation. An increase in the value of magnetic susceptibility with increasing temperature can be associated both with a change in the composition of pyrrhotite and with an increase in the amount of pyrrhotite in the materials (curves 2,3,4) during the sulfidation of iron oxides. The magnetic susceptibility of roasting dusts for charges with pyrite:ore ratios of 1:1 and 2:1 is characterized by parabolic dependences with temperature changes.

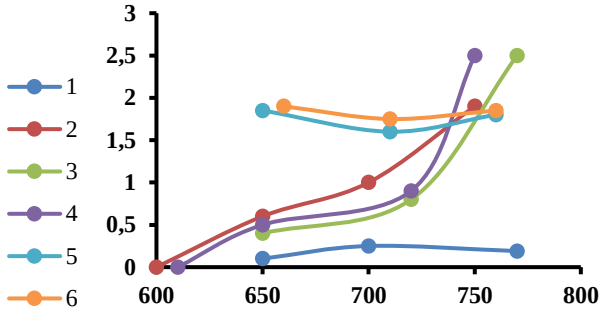

1 - pure ore cinder; 2 - cinder of pure pyrite concentrate; 3 - cinder 1:1; 4 - cinder 2:1; 5 - dust 1:1; 6 - dust 2:1

Thus, it has been established that sulfides of non-ferrous metals and waste rock have low magnetic susceptibility values compared to pyrrhotite. These properties of the components in the roasting products make it possible to separate them using magnetic separation and extract magnetic pyrrhotite into the magnetic fraction, and leave non-ferrous metal sulfides in the magnetic separation tailings.

Based on the above, sulfiding roasted cinders were subjected to wet magnetic separation at a magnetic field strength of 100-120 kA/m. Table 5 shows the results of magnetic separation for the extraction of iron into a magnetic product.

Table 5 - Results of magnetic separation of cinders

Product name	Experimental conditions		Magnetic fraction, iron extraction, %	Non-magnetic fraction, iron extraction, %
	◦C	Pyrite: ore ratio		
Cinder 1	650	1:1	88.4	11.6
		2:1	90.4	9.6
Cinder 2	700	1:1	91.4	8.6
		2:1	96.4	3.6
Cinder 3	750	1:1	96.6	3.4
		2:1	97.2	2.8
Cinder 4	650	1:1	91.7	8.3
		2:1	91.48	8.52
Cinder 5	650	1:1	90	10
		2:1	96	4

The presented results of magnetic separation show that in the selected range of magnetic field strength, more than 90 - 92% of the iron from roasting cinders is extracted into the magnetic product. It is noted that part of the iron present in the ore is also released into the magnetic product, because a small percentage of iron remains in the non-magnetic fraction compared to the original ore.

The results of spectral analysis of the magnetic and non-magnetic fractions (Table 6) showed that non-ferrous and rare metals are mainly concentrated in non-magnetic fractions.

Table 6 - Results of spectral analysis

Firing products	Contents of elements, %, 10^3									
	Zn	Pb	Cu	Mn	As	Ni	Sr	Ba	Ti	V
Cinder	1000	100	150	200	30	10	10	400	100	0
Magnetic fraction	300	60	100	200	20	10	10	150	100	2
Non-magnetic fraction	1000	200	300	400	100	5	30	500	200	4
	Contents of elements, %, 10^3									
Elements	Zr	Sb	Co	Mo	Cd	Bi	Ga	Tl	Au	Ag
Cinder	5	4	8.0	3.0	3.0	0.6	1.0	0.5	0.8	6.0
Magnetic fraction	5	4	10	2.0	2.5	0.3	1.0	0.3	0.8	5.0
Non-magnetic fraction	15	20	3.0	5.0	4.0	1.6	0.8	1.5	0.6	4.0

The results of spectral and chemical analyzes show that some of the zinc with a content of 0.2-0.3% is extracted into the magnetic fraction. Mineralogical analysis shows that zinc in the magnetic fraction is present in close contact with pyrrhotite. Apparently, this zinc was present in the original pyrite and remained in close association with it after firing.

The magnetic fraction by size is divided into a class of more than 0.05 -27% and a class of less than 0.05 mm - 33%. In the heavy fraction of the class greater than 0.65 mm, up to 5% of undecomposed pyrite and up to 3% of sphalerite were found. The main mass consists of sooty material with pyrrhotite composition $Fe_{0.855}S$, $Fe_{0.862}S$, $Fe_{0.877}S$, $Fe_{0.901}S$, $Fe_{0.911}S$, and in the class less than 0.05 mm, all material is represented by pyrrhotite, the composition of which is pyrrhotite $Fe_{0.855}S$, $Fe_{0.862}S$, $Fe_{0.877}S$, $Fe_{0.901}S$, $Fe_{0.911}S$. A fine-grained aggregate of quartz-mica composition is also extracted into the magnetic fraction.

The non-magnetic fraction is represented by rock fragments with fine dissemination of sulfides in the heavy fraction of 0.05 mm class, as well as free grains of sphalerite, chalcopyrite and minor galena, sooty material with pyrrhotite and pyrite in the form of cubic crystals are present. The gangue consists of fine-aggregate quartz-mica materials and carbonates, and grains of feldspars and quartz are observed. The extraction of zinc into the non-magnetic fraction was over 88 - 90%, and the extraction of lead was 100%.

Thus, magnetic separation makes it possible to sufficiently isolate magnetic pyrrhotite from roasting cinders and concentrate non-ferrous metals in a non-magnetic fraction for their extraction by flotation methods.

Development of a technological scheme for high-temperature sulfiding roasting of oxidized lead-zinc ore in a fluidized bed furnace

Based on the obtained results of processing lead-zinc ore of the Zhairem deposit with a zinc content of 2.5%, lead - 0.1% and the degree of zinc oxidation of more than 60%, a technology has been developed for activating, high-temperature, sulfiding roasting of this ore in a fluidized bed furnace using pyrite concentrate (with sulfur content - 45.15%) as a sulfidizer, Figure 5.

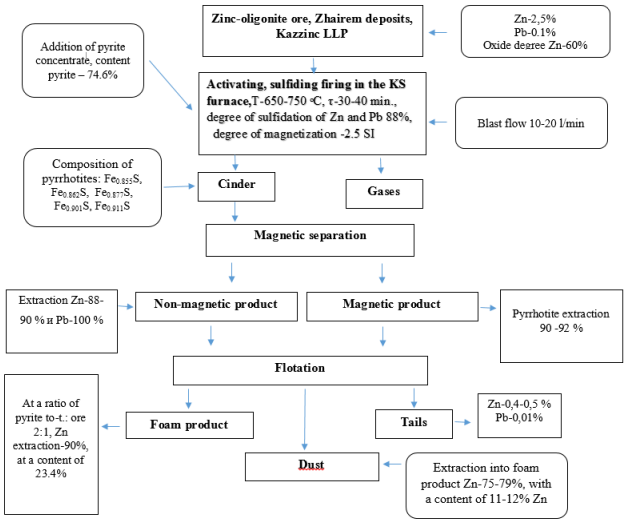

Figure 5 - Flow diagram of the technology for high-temperature sulfiding roasting of oxidized lead-zinc ore in a fluidized bed furnace

The results of electron microscopic analysis (Fig. 6) confirm the formation of lead sulfides; intermediate sulfidization products in the form of lead sulfate were also detected. The formation of sulfides begins from the surface of the initial phase and spreads into the particle. In Fig. Figure 6 shows

a micrograph of the formed sulfides and lead sulfate (≈ 630).

X-ray diffraction studies of sulfidization products show that intermediate lead sulfates are formed during the sulfidization process. It has been established that sulfidation proceeds according to the scheme PbO → PbO·$PbSO_4$ → $PbSO_4$ → PbS (activation scheme). The presence of the PbS phase is confirmed by the X-ray diffraction results, Figure 6 clearly shows the PbS phase highlighted in red (COD9008694) showing the most significant amplitude of the 2θ half-angle (2Theta: 26, 30, 43, 51.53.5). The established mechanism of decomposition during sulfidation has not been previously presented and confirmed by X-ray phase analysis in the literature.

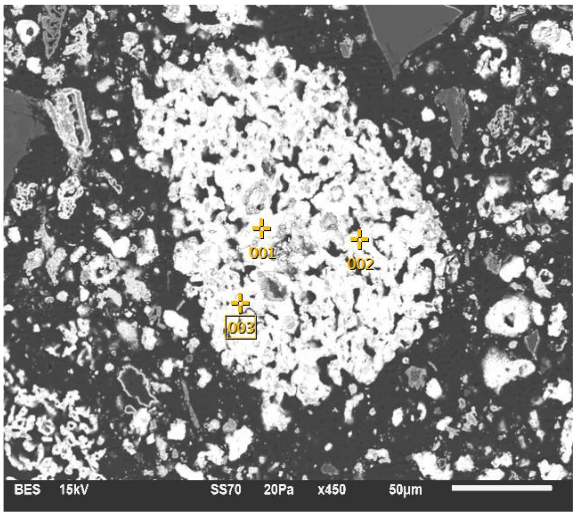

microphotograph:001 - PbS, 002 - $PbSO_4$, 003 – PbO

Figure 6 - Micrograph of lead sulfidization products (≈ 450)

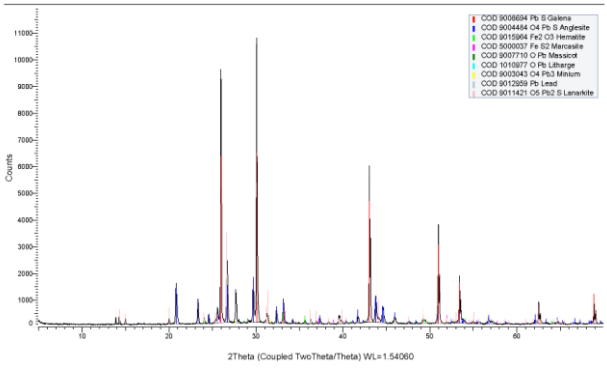

Figure 7 - X-ray results of lead sulfidization products

Thus, sulfidation roasting of lead-zinc flotation tailings with pyrite found in the tailings makes it possible to obtain lead and zinc sulfides similar in properties to natural sulfides, while pyrrhotites with pronounced magnetic properties of the composition are formed $Fe_{0.892}S$–$Fe_{0.869}S$ in the temperature range 600-800 ºC, which is confirmed by the results of X-ray phase analysis.

Development of a technological scheme for processing lead-zinc enrichment tailings

Figure 8 shows the developed technological scheme for processing lead-zinc tailings and middling products through sulfiding roasting in an environment with a limited amount of oxygen to obtain pyrrhotites with predicted properties. The results of enlarged tests are shown in the technological diagram, Fig. 8. Sulfidation firing was carried out in a fixed bed, in a tube furnace.

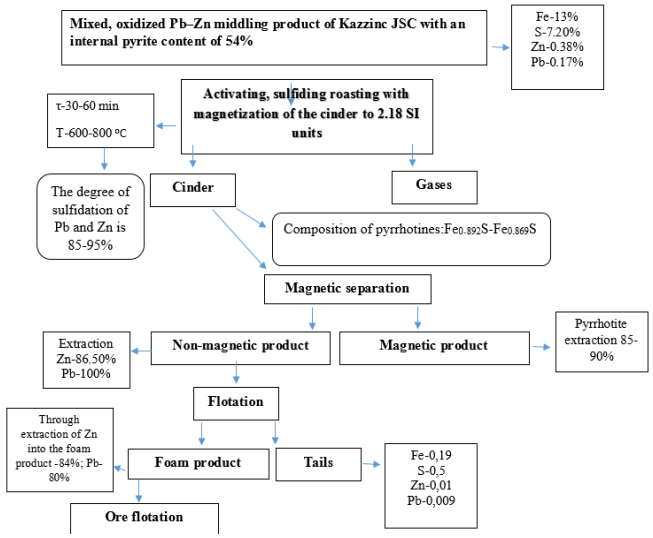

Figure 8 - Technological scheme for processing lead-zinc intermediate products of enrichment to obtain pyrrhotites with predicted properties

The economic effect of the processing technology for the complex processing of oxidized and mixed middling products enriched by sulfiding roasting with subsequent enrichment of the cinder is achieved through additional extraction of zinc from the middling product of lead flotation. A technical and economic calculation showed that with an annual production of 5,000 tons of concentrate, the payback period for the project will be 1.5 years.

Thus, the studies carried out on the activation of middlings by sulfidation roasting showed the effectiveness of the technology and the possibility of using it on an industrial scale; the results can be used in the design of a pilot plant.

Conclusion

It has been established that the sulfidation of lead oxides proceeds from the surface deep into the particle with the formation of a dense microporous sulfide layer, increasing the diffusion resistance, with the simultaneous enlargement of particles, according to the following mechanism: $PbO \rightarrow PbO*PbSO_4 \rightarrow PbSO_4 \rightarrow PbS$. At temperatures above 850 ºC, the process progresses according to the scheme: $PbO \rightarrow PbS$.

Thus, a hybrid technology has been developed for activating sulfiding roasting of zinc-containing and lead-containing industrial enrichment products in a fixed layer containing pyrite in its composition of at least 50-54%, used as a sulfidizer; Magnetic separation of cinders after heat treatment of middling products makes it possible to separate up to 70% of the iron in the form of pyrrhotite into the magnetic product, with the pyrrhotite content in the magnetic product being up to 98.2%. This technology for processing oxidized waste containing zinc and lead can be recommended for processing Kazakh and foreign technogenic deposits.

The proposed technology makes it possible to additionally extract zinc and lead from industrial products, significantly increasing the economic effect of production. The unit costs per 1 US dollar of commercial products using the proposed technology are lower than the unit costs of the existing technology, which is associated with the use of cheaper raw materials in the form of enrichment tailings and the production of pyrrhotites as additional commercial products.

Gratitude: This research was funded by the Science Committee of the Ministry of Science and Higher Education of the Republic of Kazakhstan (grant No. AP15473200).

Conflict of interest. On behalf of all the authors, the correspondent author declares that there is no conflict of interest.

Cite this article as: Chepushtanova TA, Merkibayev YS, Mamyrbayeva KK, Sarsenbekov T, Mishra B. Mechanism and technological results of sulfidation roasting of oxidized lead compounds. Kompleksnoe Ispolzovanie Mineralnogo Syra = Complex Use of Mineral Resources. 2025; 332(1):119-132. https://doi.org/10.31643/2025/6445.11

Тотыққан қорғасын қосылыстарын сульфидтеу арқылы күйдірудің механизмі және технологиялық нәтижелері

[1]Чепуштанова Т.А., [1*]Меркибаев Е.С., [1]Мамырбаева К.К., [1]Сарсенбеков Т., [2]Mishra B.

[1]Satbayev University, Алматы, Қазақстан
[2]Вустер политехникалық институты, Вустер, АҚШ

Мақала келді: *11 наурыз 2024*
Сараптамадан өтті: *9 сәуір 2024*
Қабылданды*: 16 сәуір 2024*

ТҮЙІНДЕМЕ

Жұмыста қорғасын-мырыш кендерін және өнеркәсіптік өнімдерді өңдеудің қолданыстағы технологияларына сыни талдау нәтижелері келтірілген. Зерттеудің өзектілігі – кендегі қорғасын мен мырыш мөлшерлерінің тез азаю жағдайында мырыш пен қорғасынды қосымша өндіруге бағытталған әдістерді әзірлеуде. Жұмыста сульфидтік күйдірудің термодинамикалық негіздемесі бойынша зерттеулер, кедей, қиын байытылатын қорғасын-мырыш кендері мен өнеркәсіптік өнімдерді қайнайтын қабаттағы пеште сульфидті күйдіріп алдын ала термиялық белсендіру арқылы өңдеу процесін интенсификациялау технологиясын әзірлеу нәтижелері берілген. $PbO \rightarrow PbO{\cdot}PbSO_4 \rightarrow PbSO_4 \rightarrow PbS$ схема бойынша тотыққан қорғасын қосылыстарының сульфидтену механизмі анықталған. Күйдіру өнімдерін физика-химиялық зерттеу нәтижелері, сонымен қатар өртенділерді магниттік байыту нәтижелері келтірілген. Өнеркәсіптік өнімдерді термиялық өңдеуден кейін өртенділерді магниттік бөлу нәтижелері пирротит түріндегі темірді 70% дейін магнитті өнімге бөлуге болатынын көрсетеді, ал магниттік өнімдегі пирротит мөлшері 98,2% дейін болады. Жұмыста қорғасын-мырышты өнеркәсіптік өнімдерді байыту кезінде болжамды қасиеттері бар пирротиттер алу үшін өңдеудің жаңа технологиялық схемасы ұсынылған.

Түйін сөздер: қорғасын, құрамында қорғасын бар қалдықтар, отқа төзімді кендер, сульфидтендіріп күйдіру, сұйық қабат пештері, сульфидтеу, пирит

Чепуштанова Татьяна Александровна	***Авторлар туралы мәліметтер:*** *Қауымдастырылған профессор, т.ғ.к., «Металлургиялық процестер, жылу техникасы және арнайы материалдар технологиясы» кафедрасының менгерушісі, Тау-кен металлургия институты, Сәтбаев университеті, Алматы, Қазақстан. Email: t.chepushtanova@satbayev.university*
Меркибаев Ерик Серикович	*Магистр, «Металлургиялық процестер, жылу техникасы және арнайы материалдар технологиясы» кафедрасының оқу зертханаларының меңгерушісі, Тау-кен металлургия институты, Сәтбаев Университеті, Алматы, Қазақстан. Email: y.merkibayev@satbayev.university*
Мамырбаева Кульзира Калдыбековна	*PhD докторы, «Металлургиялық процестер, жылу техникасы және арнайы материалдар технологиясы» кафедрасының қауымдастырылған профессоры, Тау-кен металлургия институты, Сәтбаев Университеті, Алматы, Қазақстан. Email: k.mamyrbayeva@satbayev.university*
Сарсенбеков Турар	*Докторант, «Металлургиялық процестер, жылу техникасы және арнайы материалдар технологиясы» кафедрасы, Тау-кен металлургия институты, Сәтбаев Университеті, Алматы, Қазақстан. Email: t.sarsenbekov@satbaev.university*
Brajendra Mishra	*Профессор және машина құрылысы және материалтану MPI директоры, Вустер политехникалық институты. АҚШ, Вустер. Email: bmishra@wpi.edu*

Механизм и технологические результаты сульфидирующего обжига окисленных соединений свинца

[1]Чепуштанова Т.А., [1*]Меркибаев Е.С., [1]Мамырбаева К.К., [1]Сарсенбеков Т., [2]Mishra B.

[1]Satbayev University, Алматы, Казахстан
[2]Вустерский политехнический институт, Вустер, США

Поступила: *11 марта 2024*
Рецензирование: *9 апреля 2024*
Принята в печать: *16 апреля 2024*

АННОТАЦИЯ

В работе представлены результаты критического анализа существующих технологий переработки свинцово-цинковых руд и промпродуктов, актуальность исследований заключается в разработке методов, направленных на дополнитиельное извлечение цинка и свинца в условиях стремительного снижения содержания свинца и цинка в рудах. В работе представлены исследования по термодинамическому обоснованию сульфидирующего обжига, результаты разработки технологии интенсификации процесса переработки бедных труднообогатимых комплексных свинцово-цинковых руд и промпродуктов за счет предварительной термической активации сульфидирующем обжигом в печи кипящего слоя. Установлен механизм сулфидирования окисленных соединений свинца по схеме: $PbO \rightarrow PbO{\cdot}PbSO_4 \rightarrow PbSO_4 \rightarrow PbS$. Представлены результаты по физико-химическому исследованию продуктов обжига, а также результаты магнитного обогащения огарков. Результаты магнитной сепарации огарков после термической обработки промпродуктов показывают, что возможно выделить в магнитный продукт до 70 % железа в виде пирротина, при этом содержание пирротина в магнитном продукте составляет до 98,2 %. В работе представлена новая технологическая схема переработки свинцово-цинковых промпродуктов обогащения с получением пирротинов прогнозируемых свойств.

Ключевые слова: свинец, свинецсодержащие отходы, труднообагатимые руды, сульфидизирующий обжиг, печи кипящего слоя, сульфидирование, пирит

Чепуштанова Татьяна Александровна	***Информация об авторах:*** *Ассоциированный профессор, кандидат технических наук, PhD доктор, заведующая кафедрой «Металлургические процессы, теплотехника и технология специальных материалов», Горно-металлургический институт, Satbayev University, Алматы, Казахстан. Email: t.chepushtanova@satbayev.university*
Меркибаев Ерик Серикович	*Магистр, заведующий учебными лабораториями кафедры «Металлургические процессы, теплотехника и технология специальных материалов», Горно-металлургический институт, Satbayev University, Алматы, Казахстан. Email: y.merkibayev@satbayev.university*
Мамырбаева Кульзира Калдыбековна	*PhD доктор, ассоциированный профессор кафедры «Металлургические процессы, теплотехника и технология специальных материалов», Горно-металлургический институт, Satbayev University, Алматы, Казахстан. Email: k.mamyrbayeva@satbayev.university*
Сарсенбеков Турар	*Докторант, Горно-металлургический институт, Satbayev University, Алматы, Казахстан. Email: t.sarsenbekov@satbaev.university*
Brajendra Mishra	*Профессор и директор MPI по машиностроению и материаловедению, Вустерский политехнический институт, США, Вустер. Email: bmishra@wpi.edu*

References

[1] Nowińska K, Adamczyk Z. Zinc and Lead Metallurgical Slags as a Potential Source of Metal Recovery: A Review. Materials. 2023; 16(23):7295. https://doi.org/10.3390/ma16237295

[2] Azevedo A, Oliveira HA, Rubio J. Treatment and water reuse of lead-zinc sulphide ore mill wastewaters by high rate dissolved air flotation. Minerals Engineering. 2018; 127:114-121.

[3] Turan MD, Altundoğan HS, Tümen F. Recovery of zinc and lead from zinc plant residue. Hydrometallurgy. 2004; 75:169-176.

[4] Luo X, Feng B, Wong C, Miao J, Ma B, Zhou H. The critical importance of pulp concentration on the flotation of galena from a low grade lead–zinc ore. J.Mater. Res. Technol. 2016; 5:131-135.

[5] Peng Y, Grano S, Fornasiero D, Ralston J. Control of grinding conditions in the flotation of galena and its separation from pyrite. Int J Miner Process. 2003; 70:67-82.

[6] Kostović M, Gligorić Z. Multi-criteria decision making for collector selection in the flotation of lead–zinc sulfide ore. Minerals Engineering. 2015; 74:142-149.

[7] Lei C, Yan B, Chen T, Xiao X. Recovery of metals from the roasted lead-zinc wastes by magnetizing roasting followed by magnetic separation. Journal of Cleaner Production. 2017; 158:73-80.

[8] He B, Tian X, Sun Y, Yang C, Zeng Y, Wang Y, Zhang S, Pi Z. Recovery of iron oxide concentrate from high-sulfur and low-grade pyrite cinder using an innovative beneficiating process. Hydrometallurgy. 2010; 104:241-246.

[9] Merkibayev Y, Panayotova M, Luganov V, Panayotov VA, Chepushtanova TA. Sulphidation roasting as means to recover zinc from oxidised ores (article) Comptes rendus de l'Acad´emie bulgare des Sciences. 2018; 71(8):1116-1123.

[10] Chepushtanova T, Merkibayev Y, Motovilov I, Polyakov K, Gostu S. Flotation studies of the middling product of lead-zinc ores with preliminary sulfidizing roasting of oxidized lead and zinc compounds (article). Kompleksnoe Ispolzovanie Mineralnogo Syra = Complex Use of Mineral Resources. 2022; 323(4):77-83.

[11] Chepushtanova TA, Merkibayev YS**,** Mishra B, Kuldeyev IE. Processing of the Zinc-Lead-Bearing Flotation Middlings by Sulfidizing Roasting with Pyrrhotites Production by Predicted Properties (article). Non-ferrous Metals. 2022; 2:15-24. https://doi.org/10.17580/nfm.2022.02.03

[12] Chepushtanova TA, Merkibayev YS, Baigenzhenov OS, Mishra B. Technology of high-temperature sulfidizing roasting of oxidized lead-zinc ore in a fluidized bed furnace (article). Non-ferrous Metals. 2023; 2:3-10. https://doi.org/10.17580/nfm.2023.01.01..

[13] Pat. 36282 RU. Cposob pererabotkı okıslennoı svıntsovo-tsınkovoı rýdy [Method for processing purified lead-zinc ore] . Chepushtanova TA, Merkibaev ES, Lyganov VA. Opubl. 30.06.2023. (in Russ.).

[14] Beisembaev BB, Kenzhaliev BK, Gorkin VI, Govyadovskaya O, Ignatiev MM. Glýbokaıa pererabotka svıntsovo-tsınkovyh rýd ı promprodýktov s polýcheniem prodýktsıı povyshennoı tovarnostı [Deep processing of lead-zinc products and industrial products with replenishment of higher-quality products]. Almaty, Bylym. 2002, 220. (in Russ.).

[15] Jumadilov T, Abilov Zh, Grazulevicius J, Zhunusbekova N, Kondaurov R, Agibayeva L, Akimov A. Mutual activation and sorption ability of rare cross-linked networks in intergel system based on polymethacrylic acid and poly-4-vinylpyridine hydrogels in relation to Lanthanum ions. Chemistry and Chemical Technology. 2017; 11(2):188-194.

[16] Hobzova R, Pradny M, Zhunusbekova NM, ...Guryca V, Michalek J. Bioactive support for cell cultivation and potential grafting. Part 1: Surface modification of 2-hydroxyethyl methacrylate hydrogels for avidin immobilization. E-Polymers. 2011; 043. https://doi.org/10.1515/epoly.2011.11.1.474

[17] Begentayev M, Nurpeisova M, Kuldiev E, Nurlybaev R, Bek U. Study of the influence of technological factors on the density and strength of ash-gas concrete. News of the National Academy of Sciences of the Republic of Kazakhstan, Series of Geology and Technical Sciences. 2024; 1(463):45-57.

[18] Aitkaliyeva G, Amitova A, Yelubay M, Vaičiukynienė D, Ismailova A, Ibraimbayeva G. Mineral Additives Based on Industrial Waste for Modifications of Bitumen Polymers. Journal of Sustainable Architecture and Civil Engineering. 2023; 1(32):196-204. https://doi.org/10.5755/j01.sace.32.1.32505

[19] Massakbayeva S, Aitkaliyeva G, Abdrakhmanova B, Yelubay M, Azat S. Evaluation of the properties of thermodifusion zinc coating of couplings of pump-compressor pipes produced by «KSP STEEL». News of the Academy of sciences of the Republic of Kazakhstan. Series of Geology and Technical Sciences. 2022; 6(456):106-117. https://doi.org/10.32014/2518-170X.242

[20] Aitkaliyeva G, Yelubay M, Ismailova A, Massakbayeva S, Baisariyeva A. Oil Sludge and Methods of Its Disposal. Polish Journal of Environmental Studies. 2022; 31(6):5563-5569. https://doi.org/10.15244/pjoes/152226

[21] Kenzhetaev Z, Togizov K, Abdraimova M, & Nurbekova M. Selecting the rational parameters for restoring filtration characteristics of ores during borehole mining of uranium depositst. Mining of Mineral Deposits. 2022; 16(3):1-10. https://doi.org/10.33271/mining16.03.001

[22] Togizov K, & Antonenko A. The structural tectonic position and predictive search criteria for the lead-zinc karst mineralisation (South Kazakhstan). SGEM International Multidisciplinary Scientific GeoConference EXPO Proceedings. 2020, 335-340. https://doi.org/10.5593/sgem2020/1.1/s01.042

[23] Bakhytuly N, Kenzhegulov A, Nurtanto M, Aliev A, & Kuldeev E. Microstructure and tribological study of TiAlCN and TiTaCN coatings . Kompleksnoe Ispolzovanie Mineralnogo Syra = Complex Use of Mineral Resources. 2023; 327(4):99-110. https://doi.org/10.31643/2023/6445.45

[24] Mamayeva A, Kenzhegulov A, Panichkin A, Kshibekova B, & Bakhytuly N. Deposition of carbonitride titanium coatings by magnetron sputtering and its effect on tribo-mechanical properties. Kompleksnoe Ispolzovanie Mineralnogo Syra = Complex Use of Mineral Resources. 2022; 321(2):65-78. https://doi.org/10.31643/2022/6445.19

МАЗМҰНЫ
СОДЕРЖАНИЕ
CONTENTS

Техникалық редакторлар:
Г.К. Қасымова, Н.М.Айтжанова, Т.И. Қожахметов

Компьютердегі макет:
Г.К. Қасымова

Дизайнер:
Г.К. Қасымова, Н.М.Айтжанова

Металлургия және кен байыту институты; Сәтбаев Университеті
050010, Қазақстан Республикасы, Алматы қаласы, Шевченко к-сі, 29/133

Жариялауға 16.04.2024 жылы қол қойылды

Технические редакторы:
Г.К. Касымова, Н.М. Айтжанова, Т.И. Кожахметов

Верстка на компьютере:
Г.К. Касымова

Дизайнер:
Г.К. Касымова, Н.М.Айтжанова

Институт металлургии и обогащения; Сатпаев Университет
050010, г. Алматы, Республика Казахстан. ул. Шевченко, 29/133

Подписано в печать 16.04.2024г.

Technical editors:
G.K. Kassymova, N.M. Aitzhanova, T.I. Kozhakhmetov

The layout on a computer:
G.K. Kassymova

Designer:
G.K. Kassymova, N.M. Aitzhanova

Institute of Metallurgy and Ore Benficiation; Satbayev University,
050010, Almaty city, the Republic of Kazakhstan. Shevchenko str., 29/133

Signed for publication on 16.04.2024